Evaluating the Performance of Fiber-Based Concrete Mixes for Various Applications

Project Leader: Krishneswar Ramineni

Team Members: Akash Ashok Tanshette, Nicole Arackal, Surya Congress, Nripojyoti Biswas

PI: Anand J. Puppala

Professor | A.P. and Florence Wiley Chair

Director – Center for Infrastructure Renewal

Closed Meeting

TAMU Site Proprietary

NSF IUCRC CICI TAMU SITE

NSF IUCRC CICI - IAB Fall 2023 Meeting

December 7th, 2023

TEXAS A&M UNIVERSITY
Zachry Department of Civil & Environmental Engineering

Presentation Outline

- Introduction
- Objectives
- Progress of Work
- Laboratory Testing
- Results
- Large Scale Laboratory Testing
- Summary

Introduction

- ❖ **Climate change and rising seawater levels → huge concerns for coastal areas**

- ❖ **Increase in intensity of storm surges → coastal areas are vulnerable**
  - ❑ **Coastal flooding**
  - ❑ **Shoreline erosion**
  - ❑ **Water pollution**
  - ❑ **High salinity of coastal waters**

A neighborhood in Port Arthur, Texas, flooded by Hurricane Harvey in 2017*[a]

Floods from Hurricane Ian, Naples, Florida, USA September 2022*[b]

*Source: SC National Guard [a] , City of Naples FL Police Department [b]

Introduction

❖ Sandbags are used as barriers to control the destructive behavior of flooding

❖ Limitations of the current methods

- ❑ Handling and logistical issues
- ❑ Long-term performance of sandbags
- ❑ Limited resources

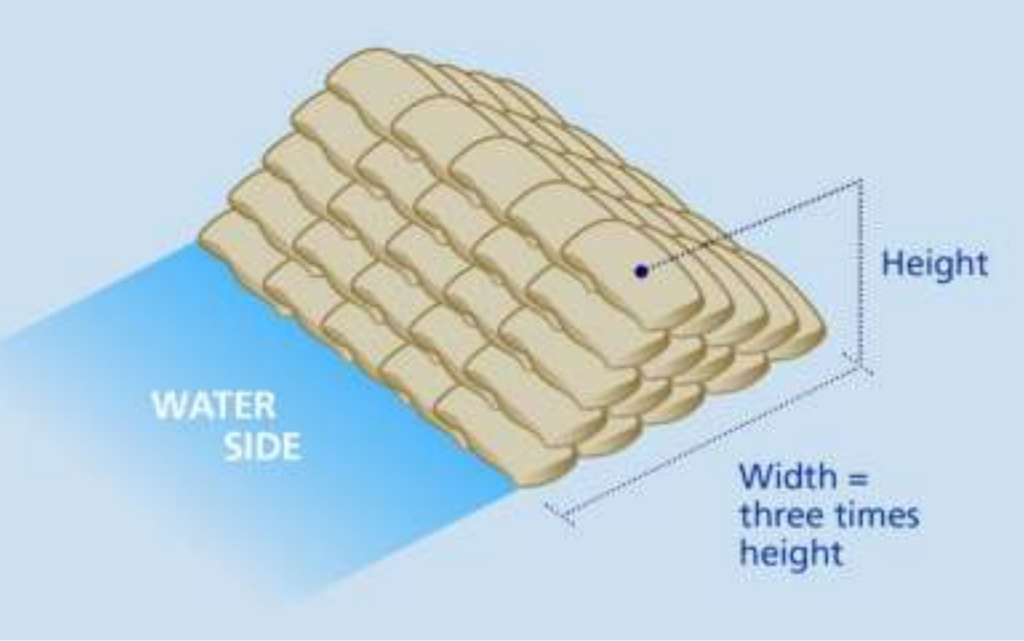

*Source: www.zurich.com

Typical schematic of sandbagging method*

❖ Objective

- ❑ To develop optimized fiber-based concrete mixes to address the flooding and erosion-related waterways and coastal infrastructure problems caused due to climate change

Progress of Work

Task List

- ❖ **Characterization of materials**
- ❖ **Wetting and Drying studies**
  - ❑ **Potable water (4°C, 20°C and 40°C)**
  - ❑ **Seawater (4°C and 20°C)**
- ❖ **Permeability studies**
- ❖ **Strength studies**
- ❖ **Laboratory-scale large box studies**

Last IUCRC meeting 5th Dec 2022

IUCRC meeting 8th May 2023

IUCRC meeting 7th Dec 2023

Laboratory Testing

Concrete mix proportion

Percentage	60%	50%	40%	30%	No fiber
Proportions	1:3:3:10.5	1:3:3:7	1:3:3:4.67	1:3:3:3	1:3:3:0
Cement (g)	86.3	107.8	129.4	151.0	215.7
Sand (g)	322.1	402.6	483.0	563.6	805.2
Pea Gravel (g)	296.2	370.3	444.2	518.4	740.6
Fiber (g)	135.9	113.2	90.6	67.9	0

*Note - Proportions A:B:C:D = Cement: Fine aggregate: Coarse aggregate: Fibers

Concrete mix constituents

Concrete mixes after five wetting and drying cycles at 20 C

Large Scale Laboratory Testing

- A large box with dimensions of 3 x 1 x 2 ft was constructed for testing
- Two sizes of geotextile bags with dimensions 12”×12”×4” and 12”×6”×4” are filled with fiber mix (1:3:3:3) and sand as a control.
- Test setup was used to perform
  - Wetting and Drying studies at room temperature under potable and saltwater conditions
  - Permeability studies

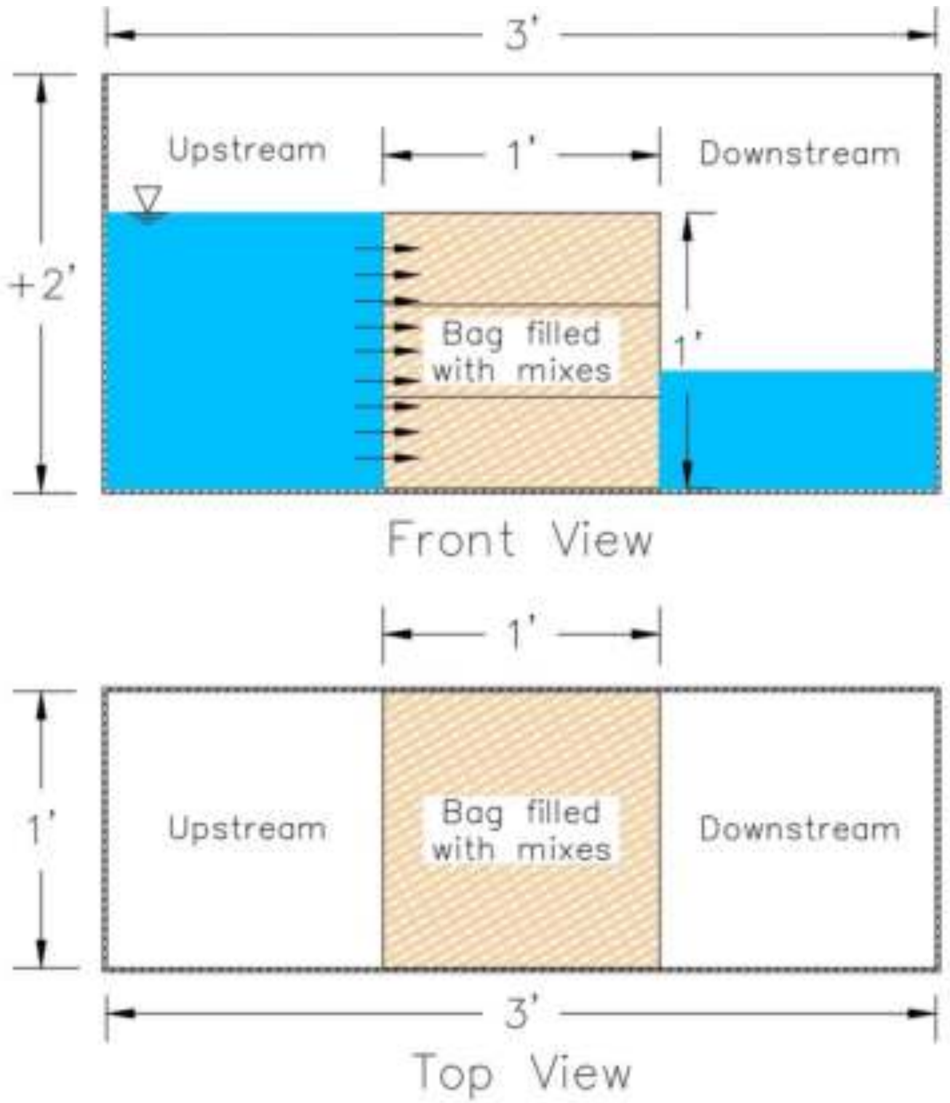

Schematic diagram of large box

Large Scale Laboratory Testing : Construction steps

Bag preparation

Large box setup

Stacking arrangement of bags


Absorption testing


Flow rate testing

Results – Large Scale Testing: Wetting and Drying (Potable Water)

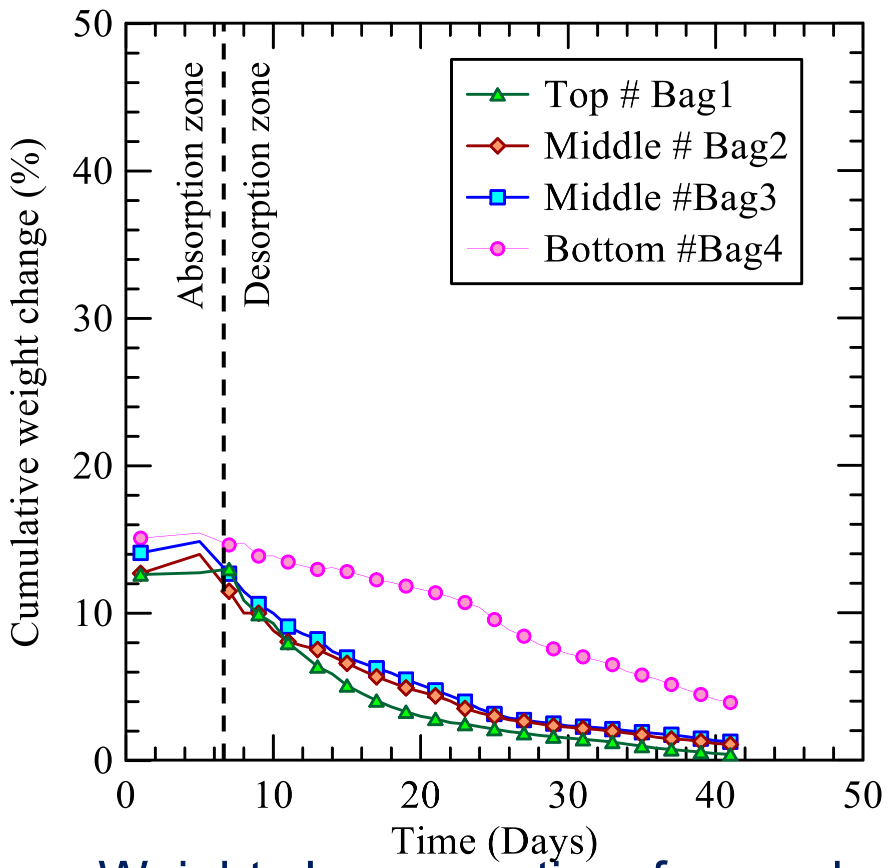

Weight change vs time for sand

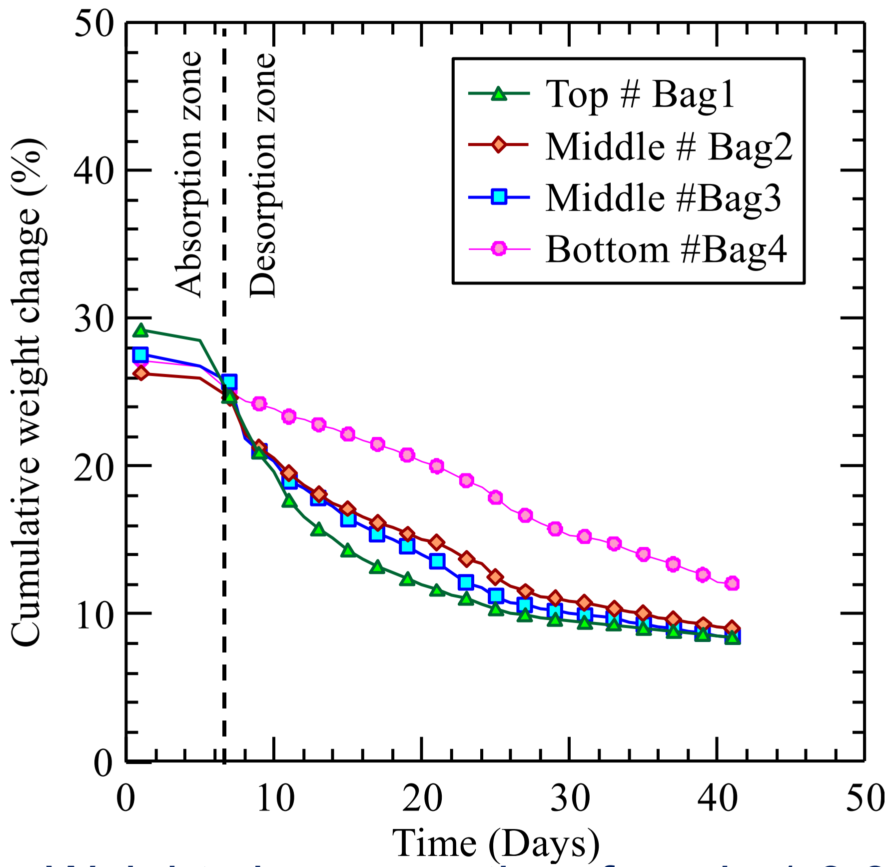

Weight change vs time for mix 1:3:3:3

- ❖ **Fiber mix → Weight change due to wetting and drying increased**
- ❖ **Similar weight change trend was observed during drying in both fiber mix and sand filled bags with respect to bag position**

Results – Large Scale Testing: Wetting and Drying (Saltwater)

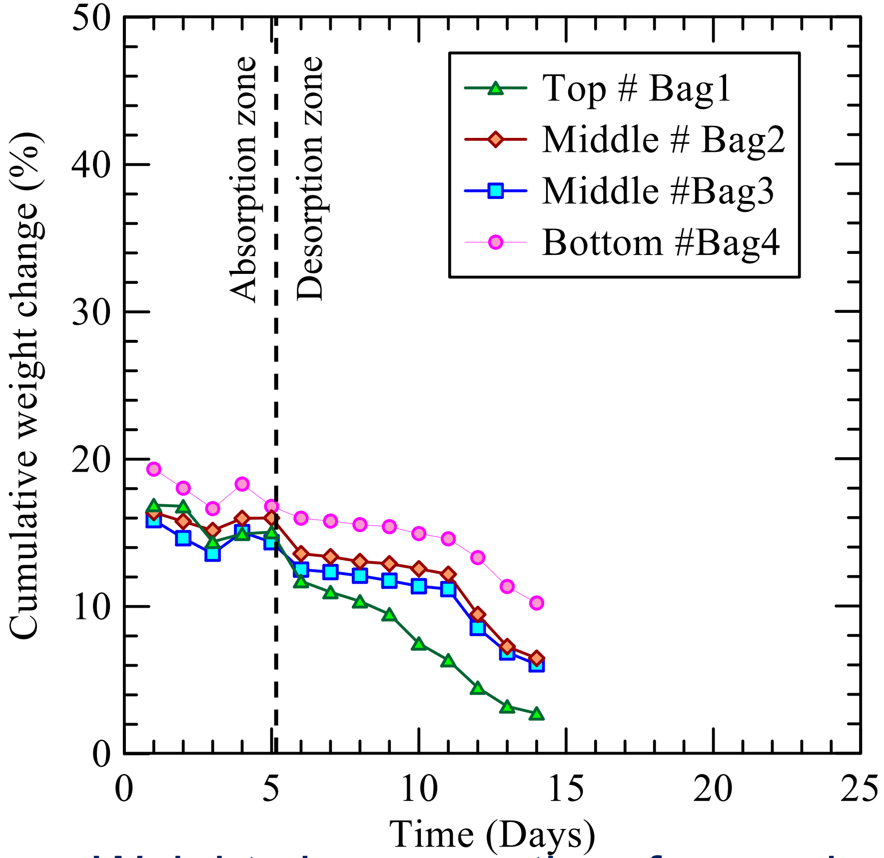

Weight change vs time for sand

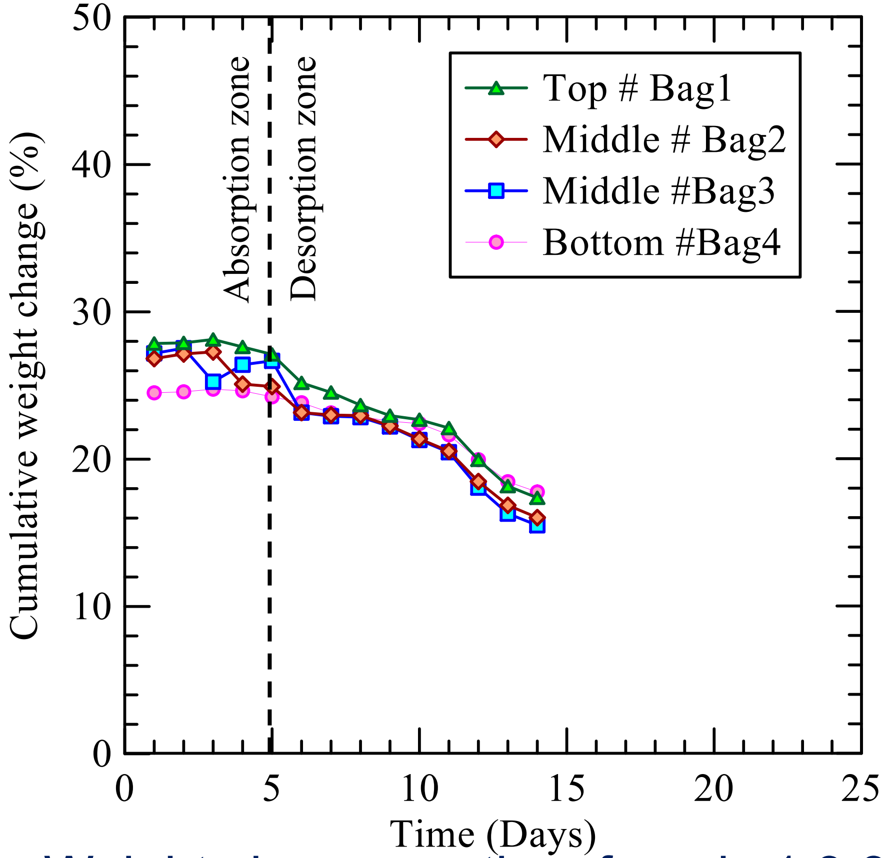

Weight change vs time for mix 1:3:3:3

- **Fiber mix → Weight change due to wetting and drying increased**
- **No effect of bag position was found in fiber mix whereas sandbag has some effect with bag position.**

Results – Large Scale Testing

- Sand mix - flow rate = 0.65 gal/min & Mix 1:3:3:3 - flow rate = 0.21 gal/min
- Mix 1:3:3:3 has ↓ flow rate due to presence of cement hardening leading to drop in void and fibers water absorption.
- Mix 1:3:3:3 shows ↑ rate of weight change due to absorption of fiber
- Top and middle bags show similar trends for cumulative weight change
- Bottom bag for both materials shows ↓ rate of cumulative weight change due to ↑ amount entrapped moisture in voids and exposure conditions as compared to bags above.

Summary

- Fiber mixes experienced higher water absorption and desorption (A & D) compared to control mixture
  - No fiber mix - 1:3:3:0 – Lowest A & D in all testing environments
  - Fiber mix - 1:3:3:10.5 – Highest A & D in all testing environments
- Percent fiber in mixes increases water absorption and desorption
- The coefficient of permeability of fiber mixes ranged between 7.5 to 9.2 x 10^{-5} ft/sec
- No fiber mix has better strength properties compared to fiber mixes
- In large scale testing fiber mix bag performed better in terms of wetting and drying compared to sand filled bags in both potable and saltwater conditions.

Center for Integration of Composites into Infrastructure

Application of Geofoam in Thermal Encapsulation of Foundations

Project Leader: Hiramani R. Chimauriya

Team: Clay Caldwell, Gustavo Hernandez Martin, Surya Congress, Nripojyoti Biswas

PI: Anand J. Puppala
Professor | A.P. and Florence Wiley Chair
Director – Center for Infrastructure Renewal

Closed Meeting

TAMU Site Proprietary

NSF IUCRC CICI TAMU SITE
NSF IUCRC CICI - IAB Fall 2023 Meeting

Dec. 7-8, 2023

THERMAFOAM LLC

TEXAS A&M UNIVERSITY
Zachry Department of Civil & Environmental Engineering

Presentation Outline

- ❑ Introduction
- ❑ Test Methodology
- ❑ Control Test (Baseline)
- ❑ Previous GBF & GAF Tests
- ❑ R-130 Geofoam Around Footing (GAF) Tests
  - GAF-8 in. R-130 Test
  - Indoor Temperature: Control vs GAF
- ❑ Numerical Simulations
- ❑ Conclusions
- ❑ Future Work

Introduction

- Temperature fluctuations inside the dwellings typically occur from advection, diffusion and radiation at foundation superstructure joints
- About 15% of all heat loss in a home is through floors or basements
- Thermal Encapsulation using Geofoam
  - Research Plan
  - Laboratory Testing Setups

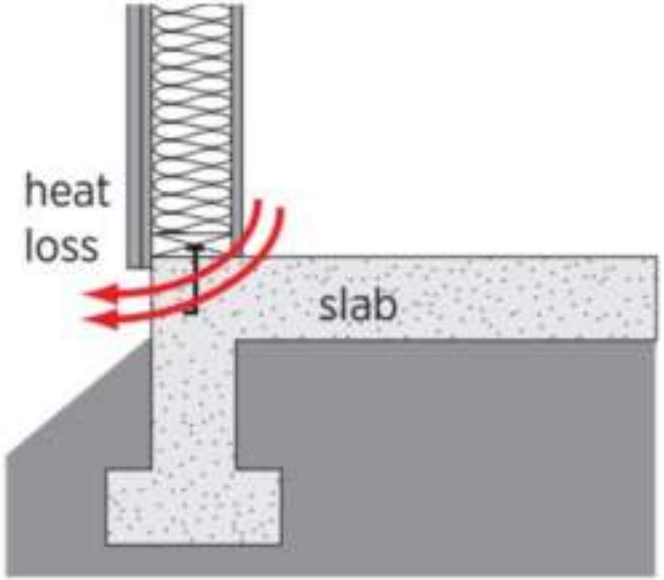

Heat loss

The stack effect

Source: EPA, US DOE (2011, 2012)

Test Methodology

Control Tests (Baseline)

*GBF Geofoam-R-250 (8, 4, and 2 in. thick)

*GAF Geofoam-R-250 (8, 4, and 2 in. thick)

GAF-2 in. Geofoam-R-130

COMSOL Modeling of Laboratory Tests

Initial Setup

Final Setup

*GBF: Geofoam Below Foundation
GAF: Geofoam Around Foundation

TEXAS A&M UNIVERSITY
Zachry Department of Civil & Environmental Engineering

Control Test (Baseline)

- "Bands" of temperature zones
- Slab-soil interface locations – coldest
- Bottom of the test box – warmest
- Indoor over 2˚C warmer – loss of heat to soil is cooling the slab

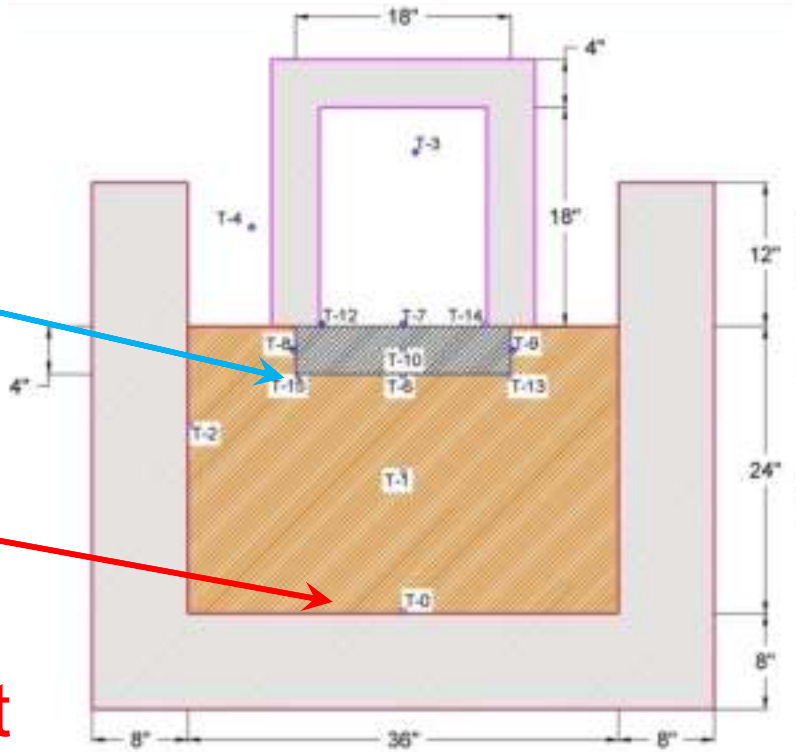

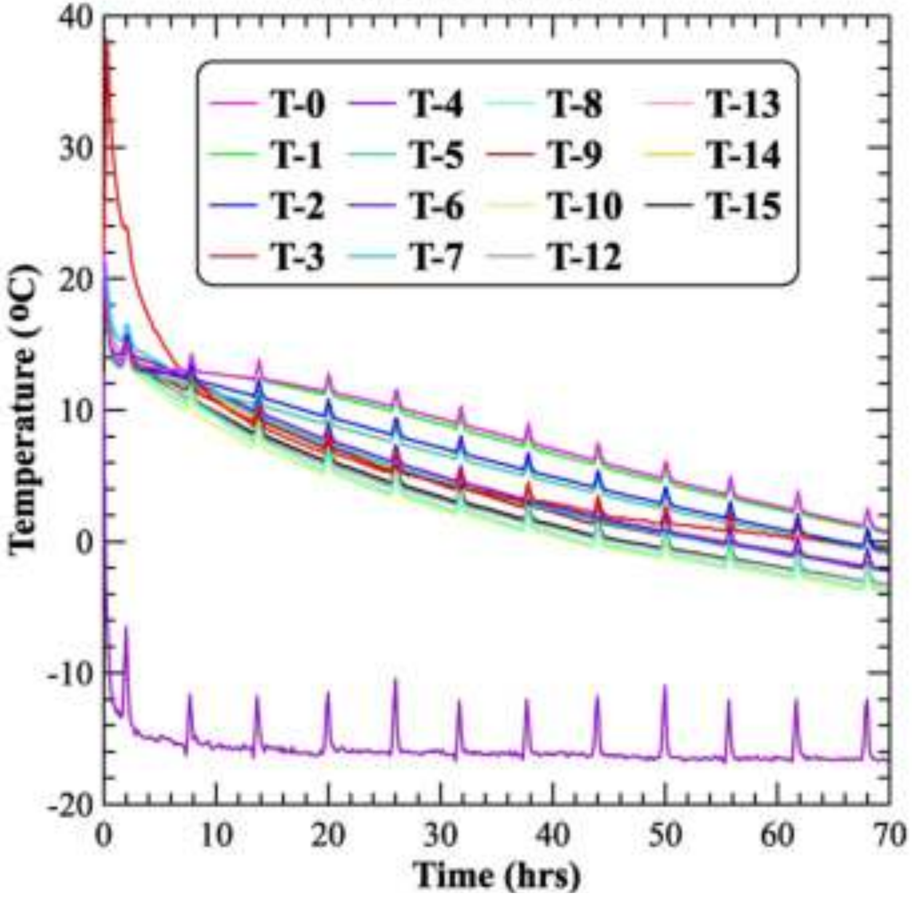

GBF & GAF R-250 Tests

- ❑Tests performed using R-250 grade geofoam
- ❑GAF configurations significantly outperform all GBF tests
- ❑GAF sections had >8˚C warmer indoor temperature than GBF sections and >10˚C warmer than Control section
- ❑Not much difference in performance for thicker insulation ➡ 2 in. GAF most efficient

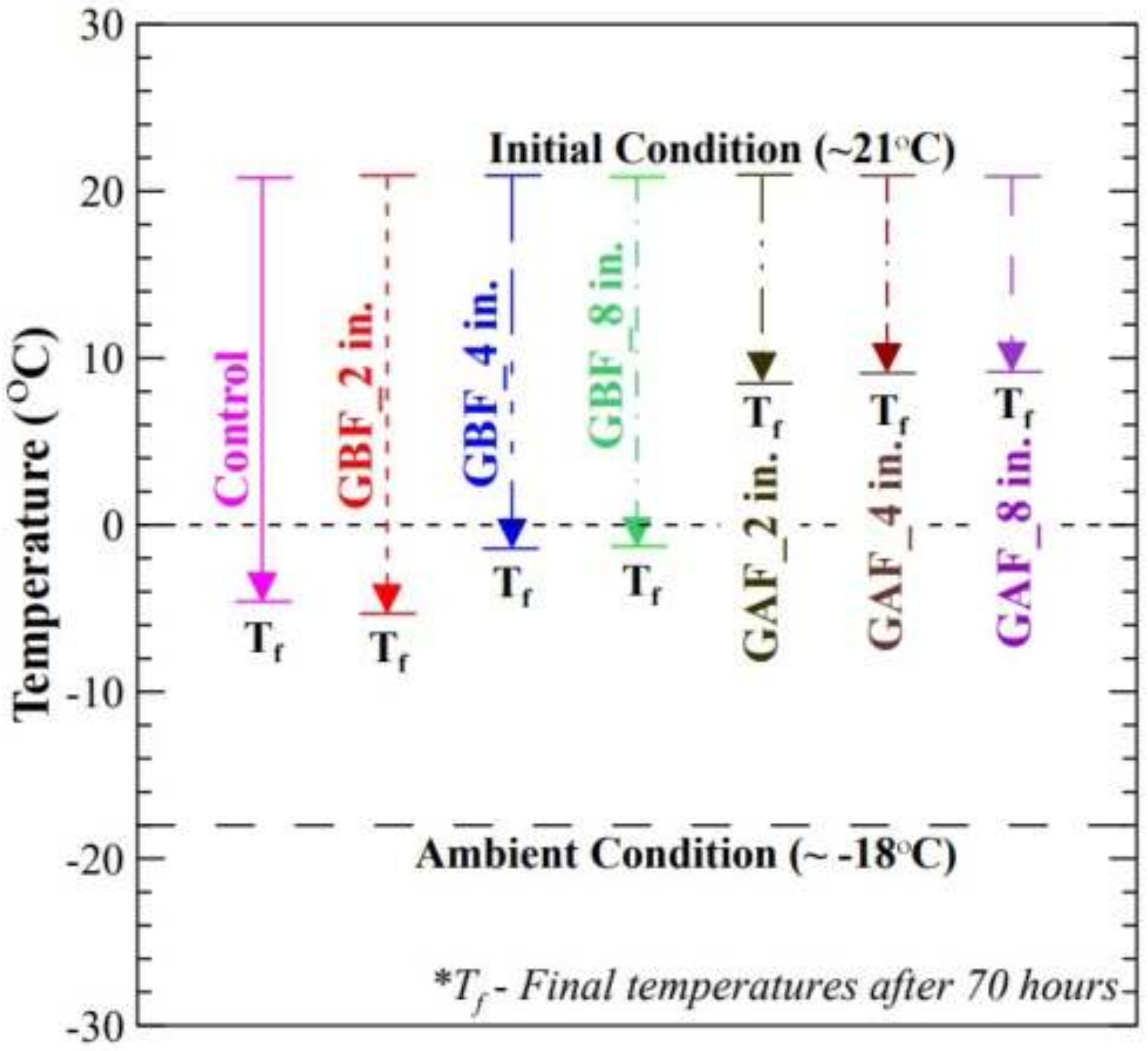

GAF-8 in. R-130 Test

- Temperature fluctuations between zones significantly reduced
- Significantly warmer indoor temperature compared to control test (>7 ˚C) warmer
- Increased temperature observed within the slab and superstructure – reduced heat loss
- Side walls – coldest

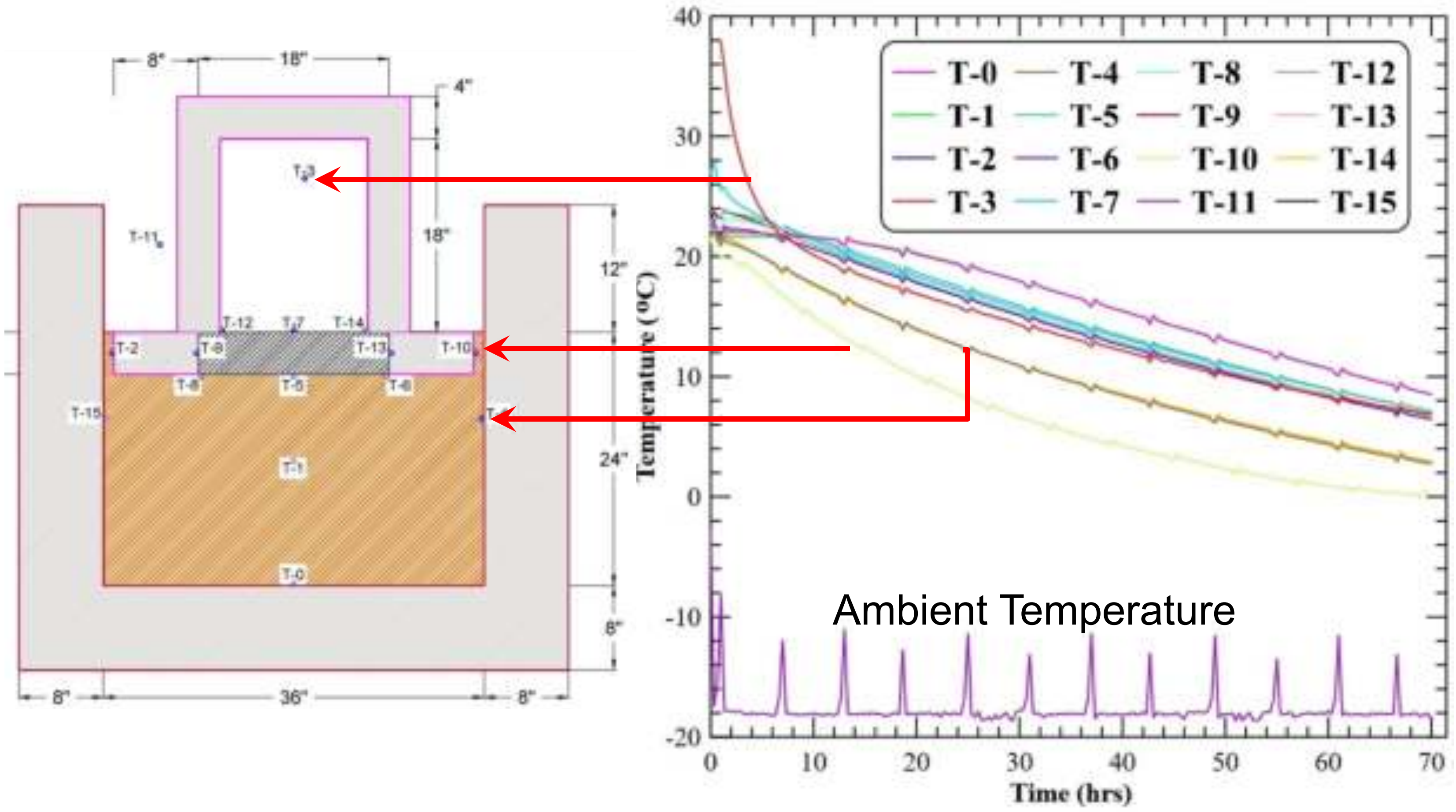

TEXAS A&M UNIVERSITY
Zachry Department of Civil & Environmental Engineering

Indoor Temperature: Control vs GAF

- Similar trend of reduced heat loss observed in all 3 GAF tests
- Lower R-values led to cooler indoor temperatures
  - R-250 sections > 1.5 ˚C warmer than R-130 section
- 8 in. thick R-130 geofoam may be less efficient than 2 in. and 8 in. thick R-250 geofoam
- Warmer temperatures with higher R-values regardless of thickness

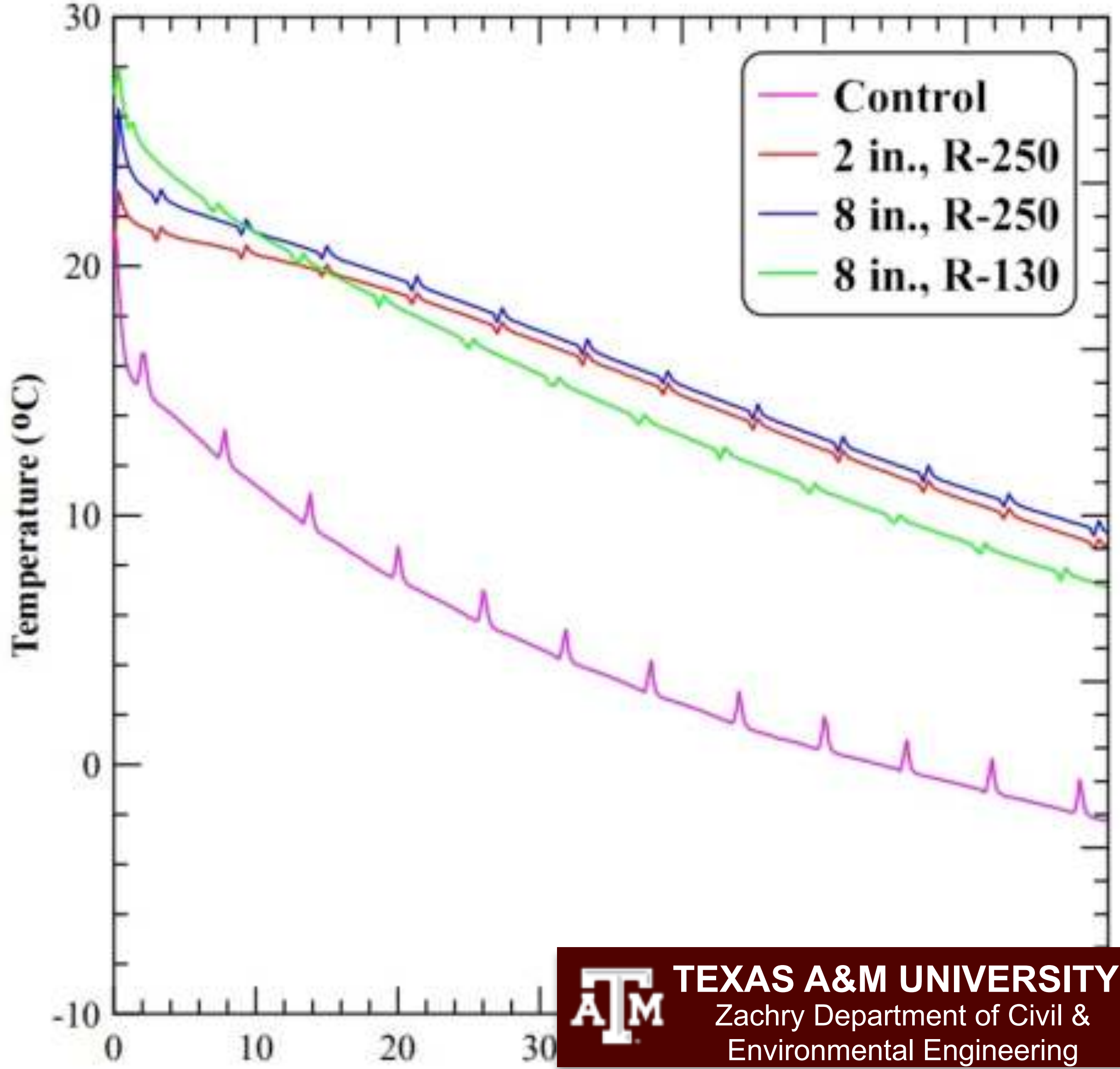

Numerical Simulations

- COMSOL simulations to explore wider parameters
- Model verified using control tests (previous meetings)
- Model performance compared with GAF tests

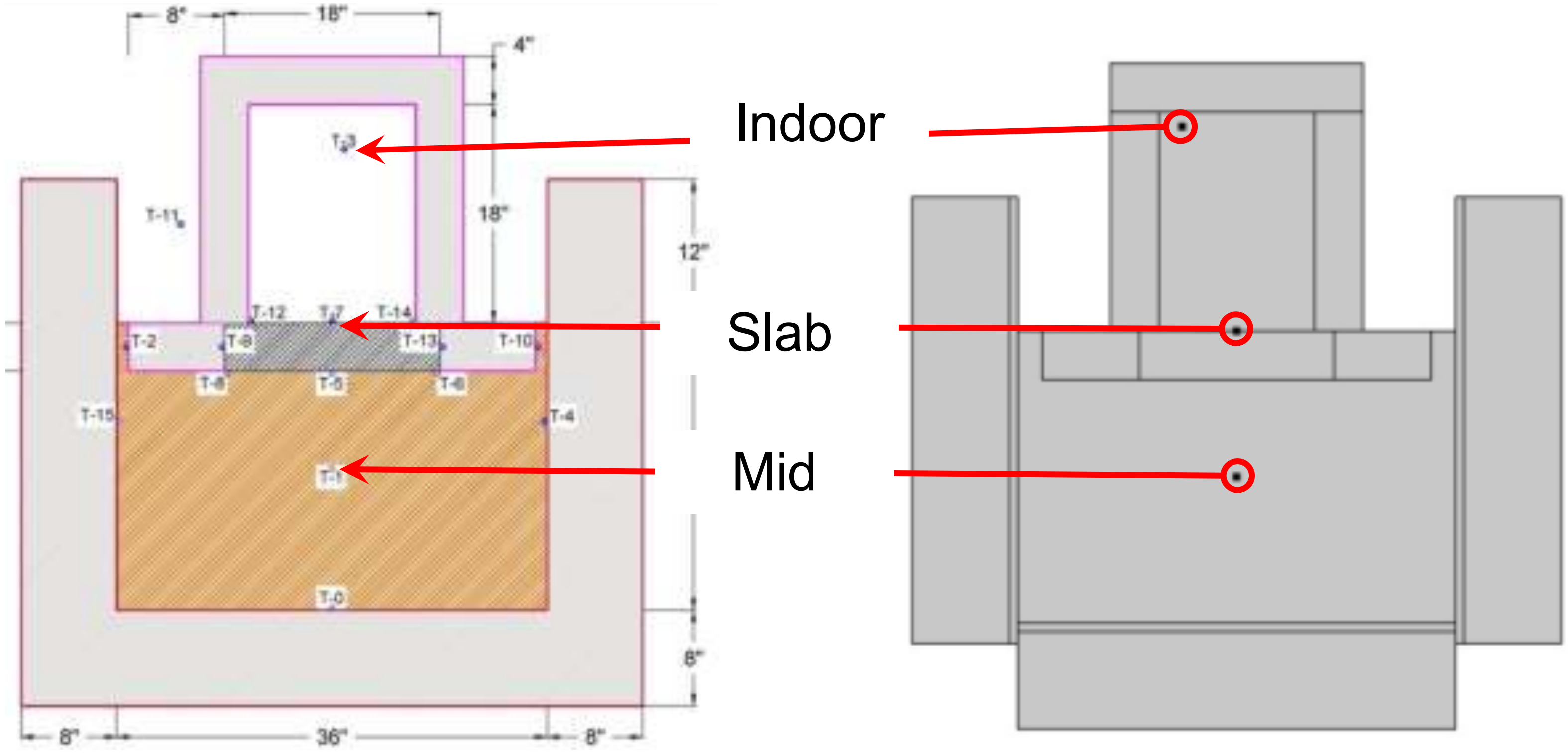

Lab Schematic

Numerical Model

Numerical Simulations

- ❑Temperature variation at 3 locations (indoor air, top of slab, and middle of soil layer) compared
- ❑Model shows fairly good agreement with test results
- ❑Initial period of sharp temperature drop not represented in the model
- ❑Difference in measured vs. simulated values within than ±2 °C after the initial period

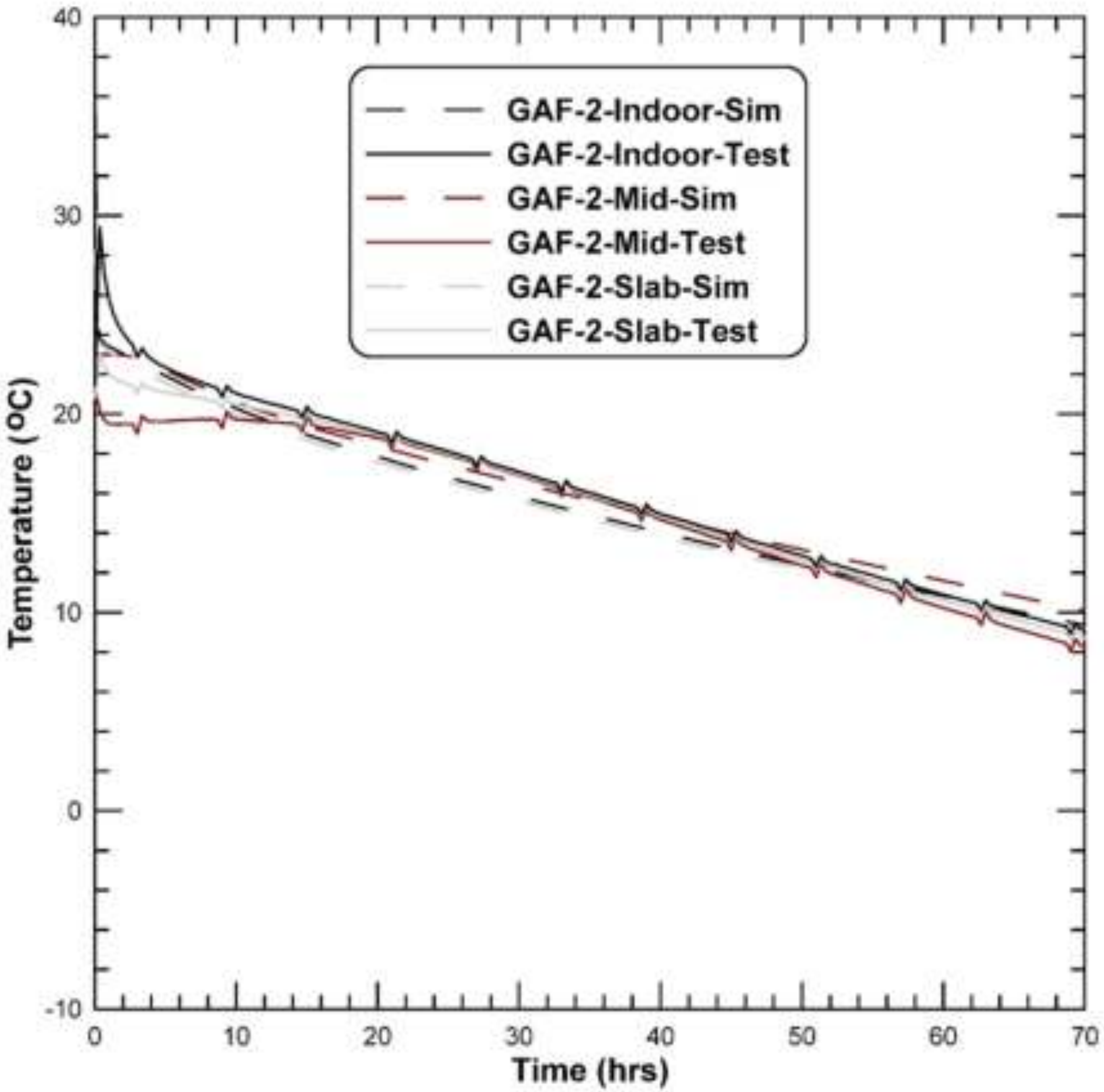

Conclusions

- Thinner insulation with higher R-value performs better than thicker insulation with lower R-value
  - GAF-2 in. thick R-250 outperforms GAF-8 in. thick R-130
- Better performance of GAF → Heat lost to ambient air controlling factor
- Thermal properties and insulation configuration have more influence than thickness of geofoam
- 2 in. thick R-250 under GAF configuration could be an efficient option
- Numerical simulation of the lab tests showed good agreement with test data, less than ± 2 °C deviations in predictions observed

Future Works

- Repeat lab tests for other grades of geofoam
- Use numerical simulation to further study system performance and perform parametric studies to account for boundary effects

Design and Testing of IFI Geosynthetic Products

Project (Leader): Krishneswar Ramineni

Team: Md Ashrafuzzaman Khan, Aditya Deshmukh, Avinash Gonnabathula, Godfred Akwaa

PI: Anand J. Puppala
Professor | A.P. and Florence Wiley Chair
Director – Center for Infrastructure Renewal

Closed Meeting

TAMU Site Proprietary

NSF IUCRC CICI TAMU SITE
NSF IUCRC CICI - IAB Fall 2023 Meeting

December 7th, 2023

TEXAS A&M UNIVERSITY
Zachry Department of Civil & Environmental Engineering

Presentation Outline

- Background
- Objectives
- Scope of the Work
- Pavement Section Details
- Field Studies
- Laboratory Studies
- Numerical Studies
- Summary
- Future Work

Introduction

- Pavements over poor subgrade → low bearing capacity, construction issues
- Modern ground improvement → geosynthetic system (geogrid + geocell)
- Field application status → visual inspection showed improved performance
- Design with geosynthetic system → no specific guidelines
- Load carrying mechanism → need to investigate
- Layer performance → need to determine layer coefficients

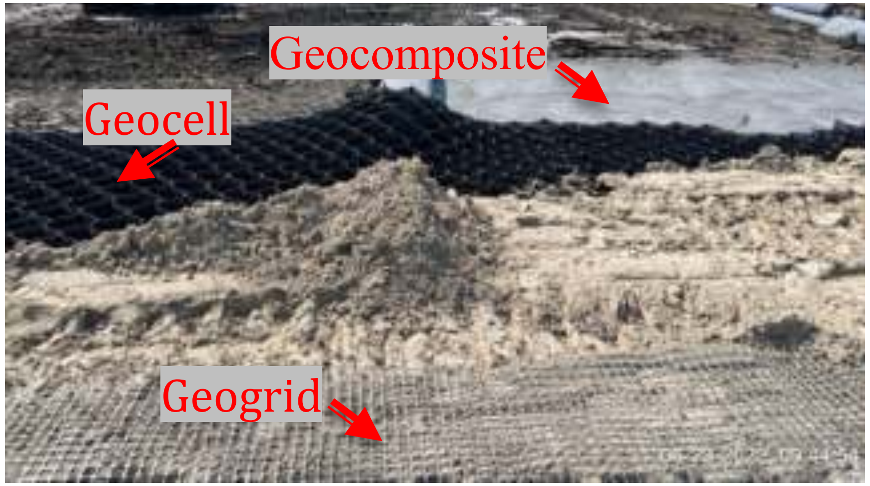

Objectives

The objectives of the current study are:

- Phase 1 Part 1 Objective I : Performing repeated load tests on geosynthetic reinforced base layers built on different weak subgrades (12-inch base sections)
- Phase 1 Part 2 Objective II: Development of various design charts and methods for IFI, Inc Geosynthetic Products based on Phase 1 Part 1 results
- Phase 1 Part 3 Objective III: Perform non-destructive tests on geosynthetic reinforced unpaved sections and develop numerical model to determine the stiffness properties of different pavement layers in the field.
- Phase 2 Part 1 Objective IV: Performing repeated load tests on geogrid reinforced base layers built on different weak subgrades (6-inch base sections)
- Phase 2 Part 2 Objective V: Development of various design charts and methods for IFI, Inc Geogrids Products based on Phase 1 Part 1 and Phase 2 Part 1 results

Scope of The Work

Following tasks are performed to fulfill objective in Phase 1 Part 3

- ❑Task 1.1: Performing Dynamic Cone Penetration (DCP) test → field (to determine the effectiveness of geocell)
- ❑Task 1.2: Performing Light Weight Deflectometer (LWD) tests → lab and field (determine layer stiffness)
- ❑Task 1.3: Performing Variable Energy Dynamic Cone Penetration VE-DCP → lab and field (development of correlations)
- ❑Task 2.1: Numerical model → FE-based Model
- ❑Task 2.2: Parametric study → effect of material types and geometry

Pavement Section Details

- ❑ Total length of the haul road ≈ 5 miles
- ❑ Approximate daily truck traffic ≈ 500
- ❑ Test section under investigation:
  - ➢ No reinforcement – 1 section
  - ➢ Lime treated subgrade + unreinforced base – 1 section
  - ➢ Untreated subgrade + reinforced base – 7 section

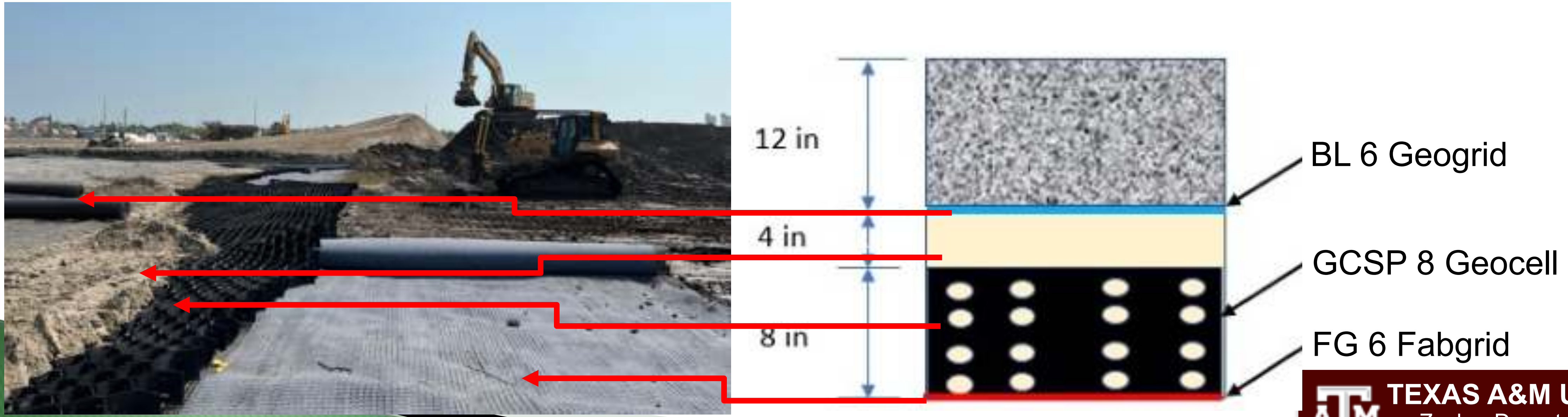

Field Studies: DCP Testing

Field Testing Plan

- Reinforced road – 1, 3, 4, 6-9 (7)
- Unreinforced road – 5 (1)
- New construction site – 2 (1)

Location of Field Testing located in coastal Louisiana

S.N.	ID	Road Name & Description	Tests
1	R_A(12)	Road A with 12-inch base	3 LWD + 1 DCP + 1 PDCP
	R_A(10)	Road A with 10-inch base	3 LWD
	R_A(6)	Road A with 6-inch base	3 LWD
	R_P	Parking Lot (12-inch base + 12-inch sand + stabilized subgrade)	3 LWD + 2 DCP + 2 PDCP
2	E1	Bottom of base layer	1 LWD + 1 DCP + 1 PDCP
	E2	Top of base layer	1 LWD
	E3	Top of subgrade	4 DCP + 4 PDCP
3	R_1b	Road 1	3 LWD
4	R_Da	Road D	3 LWD
5	R_X	Unknown Road	3 LWD
6	R_5a	Road 5	3 LWD
7	R_1a	Road 1	3 LWD
8	R_Ca	Road C	3 LWD
9	R_3a	Road 3	3 LWD

Field Studies: DCP Testing

Evaluation of foundation soil

- ❑Average CBR values of the prepared subgrade → 0.8
- ❑Soil shear strength → 3.5 psi < 4.0 psi (very soft soil)

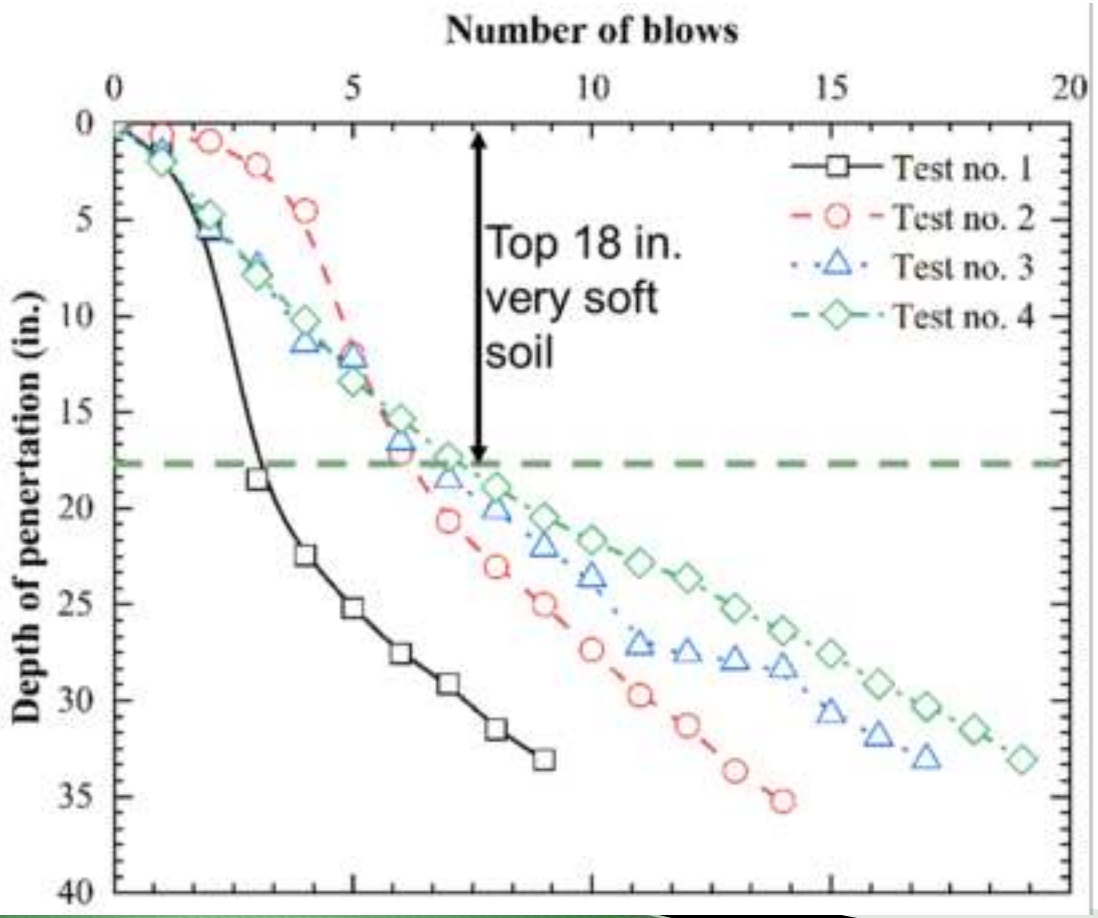

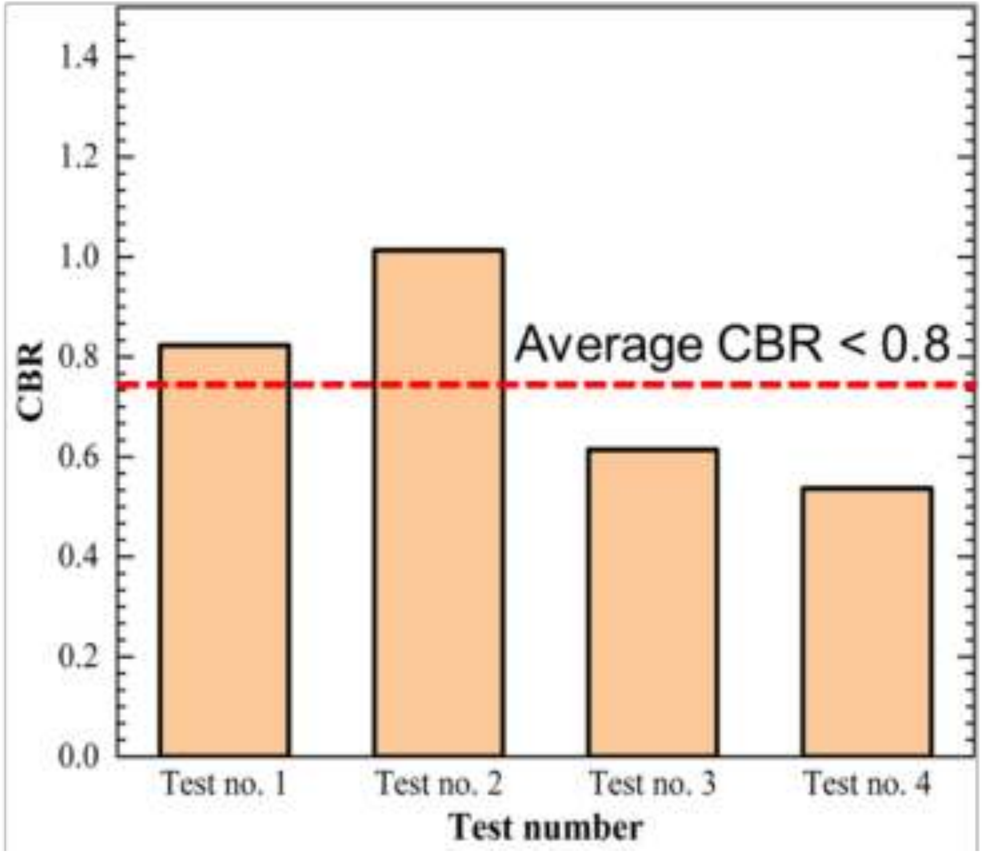

Field Studies: DCP Testing

Evaluation of base and subgrade layer

- ❑ Test section quality → consistent
- ❑ Base layer → DPI index = 12.5 mm/blow → CBR = $292/(12.5^{1.12}) = 17.2$
- ❑ Subgrade layer CBR = $292/(85^{1.12}) = 2.0$

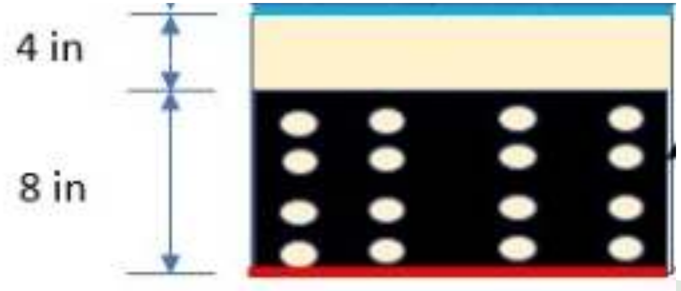

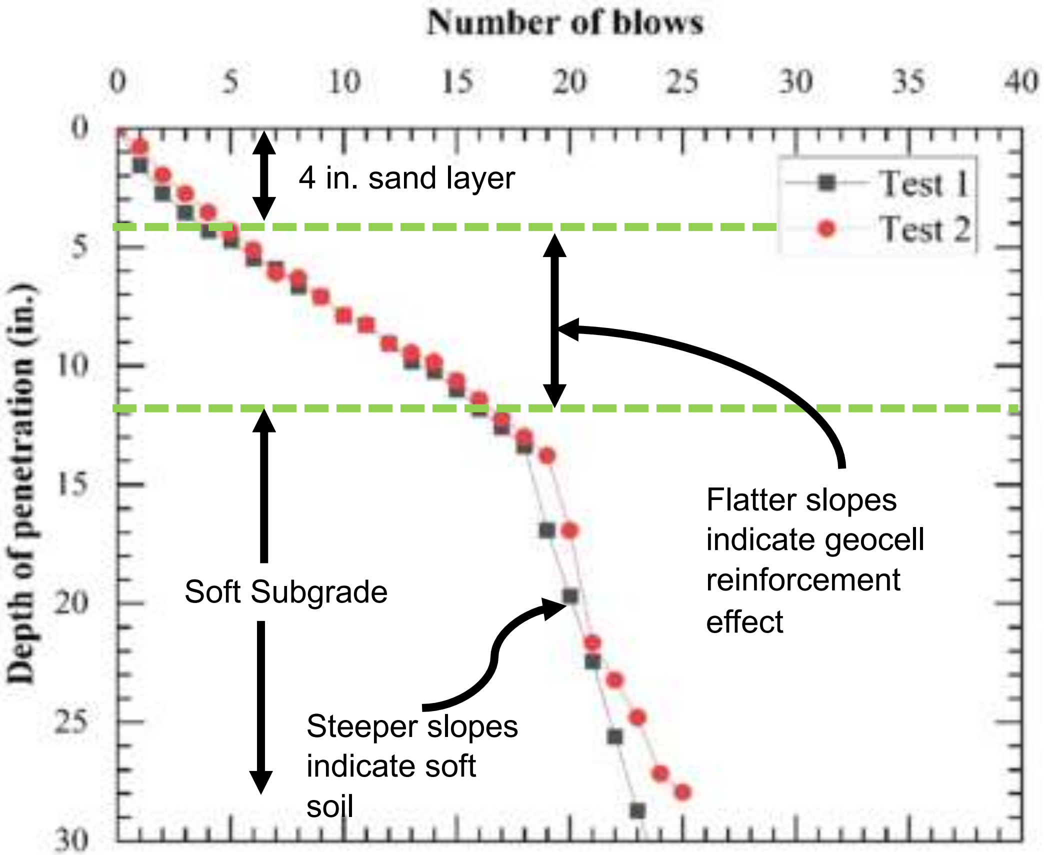

Field Studies: LWD Testing

Surface Modulus

- ❑Reinforced section surface modulus = 14.2 ksi
- ❑Reinforced section showed 1.5 to 3.6 times improvement of stiffness

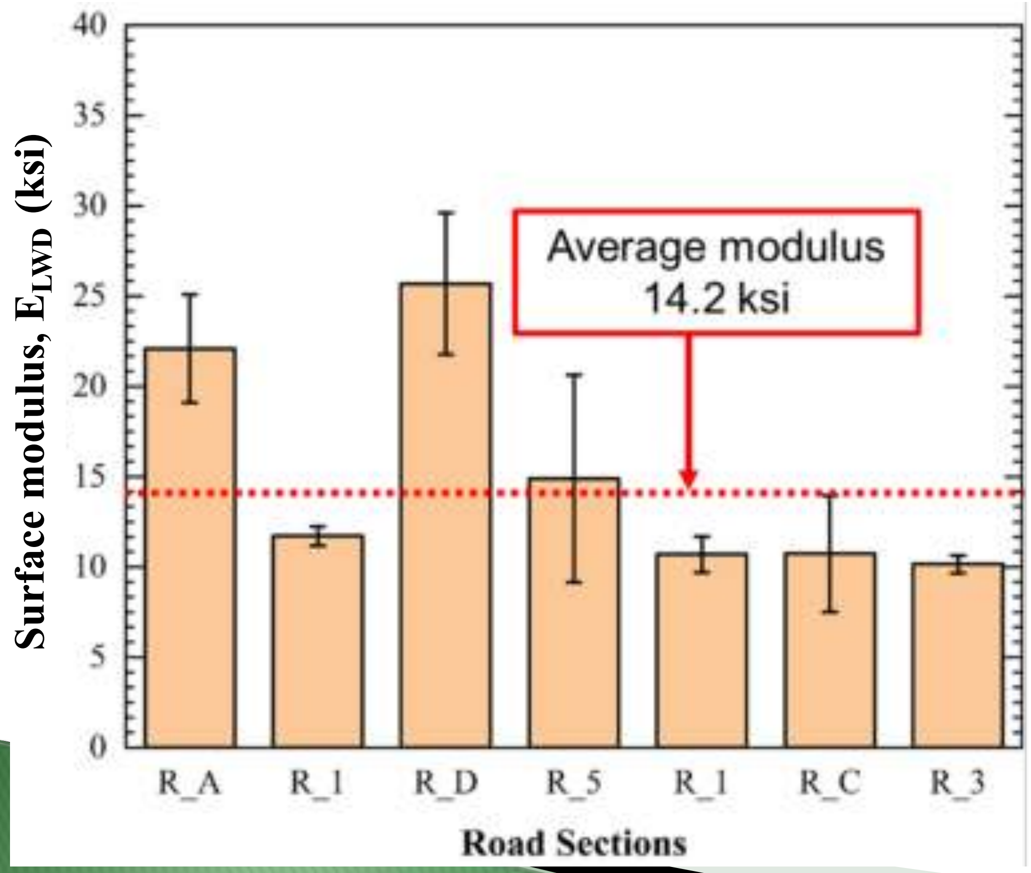

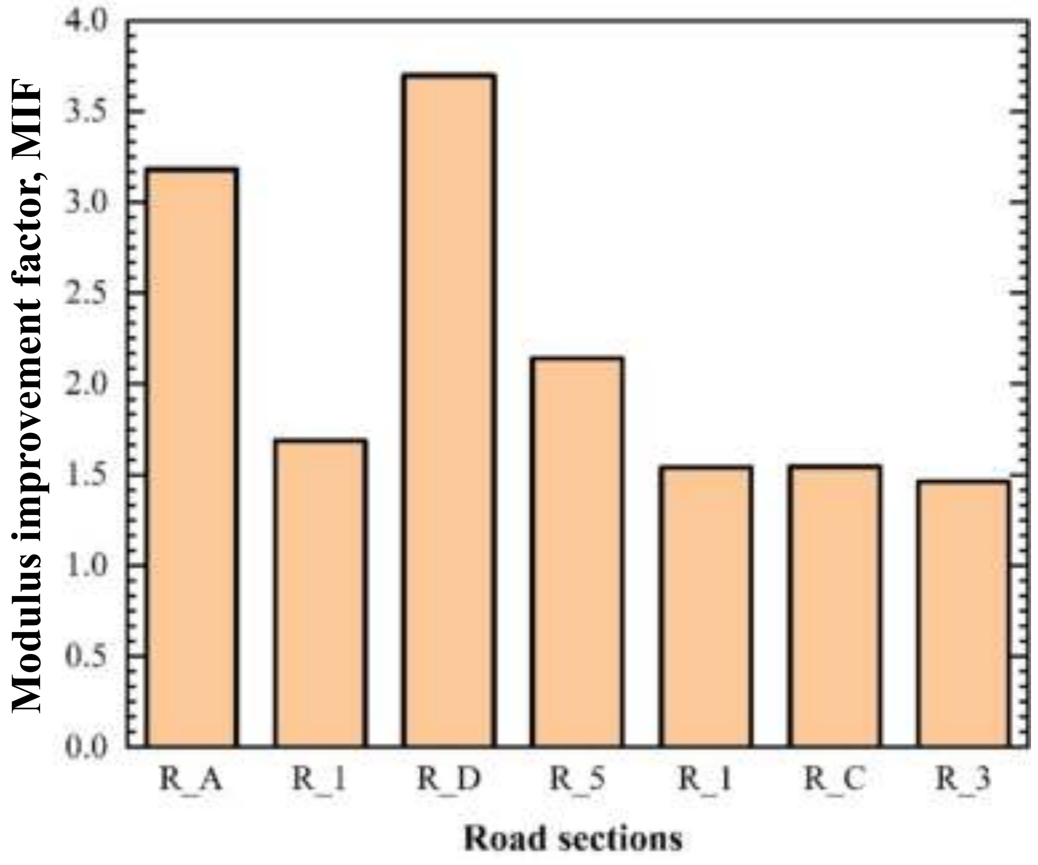

Field Studies: VE-DCP Testing

Evaluation of Subgrade layer

- Dry density = 90 to 110 pcf

Evaluation of base layer

- Inclusion of geocell enhanced the layer stiffness by 1.6 times
- Maximum tip resistance was observed near at a depth of two-third height of the geocell layer
- FG6 enhanced the tip resistance beyond the depth of the geocell layer

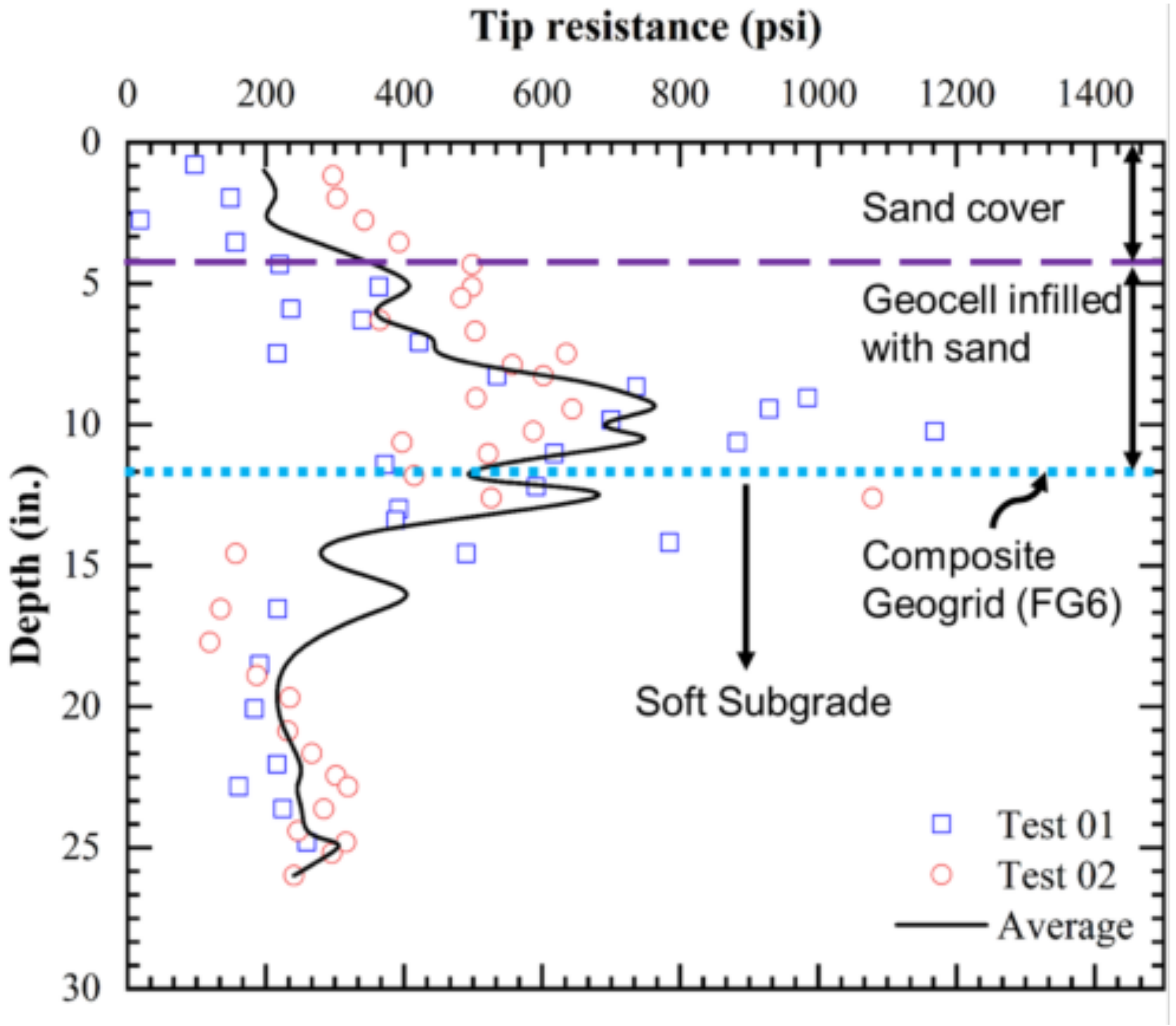

Laboratory studies: VE-DCP Testing

VE-DCP laboratory tests

- ❑ Tip resistance was maximum near the geogrid location
- ❑ Enhanced tip resistance was observed for the layer beneath the reinforcement

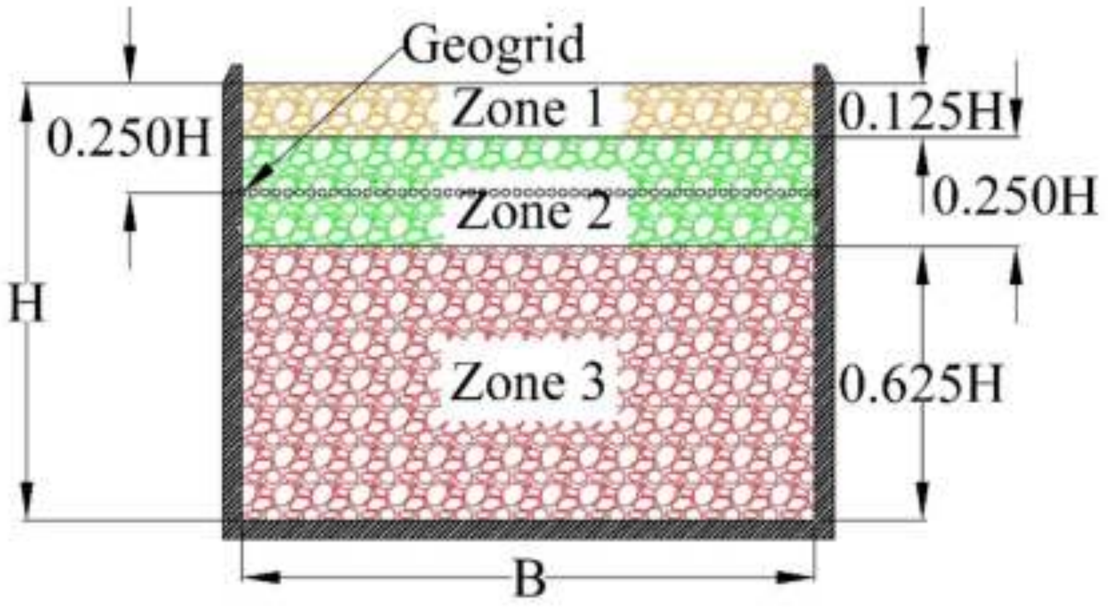

Different zones of the composite section in CBR mold

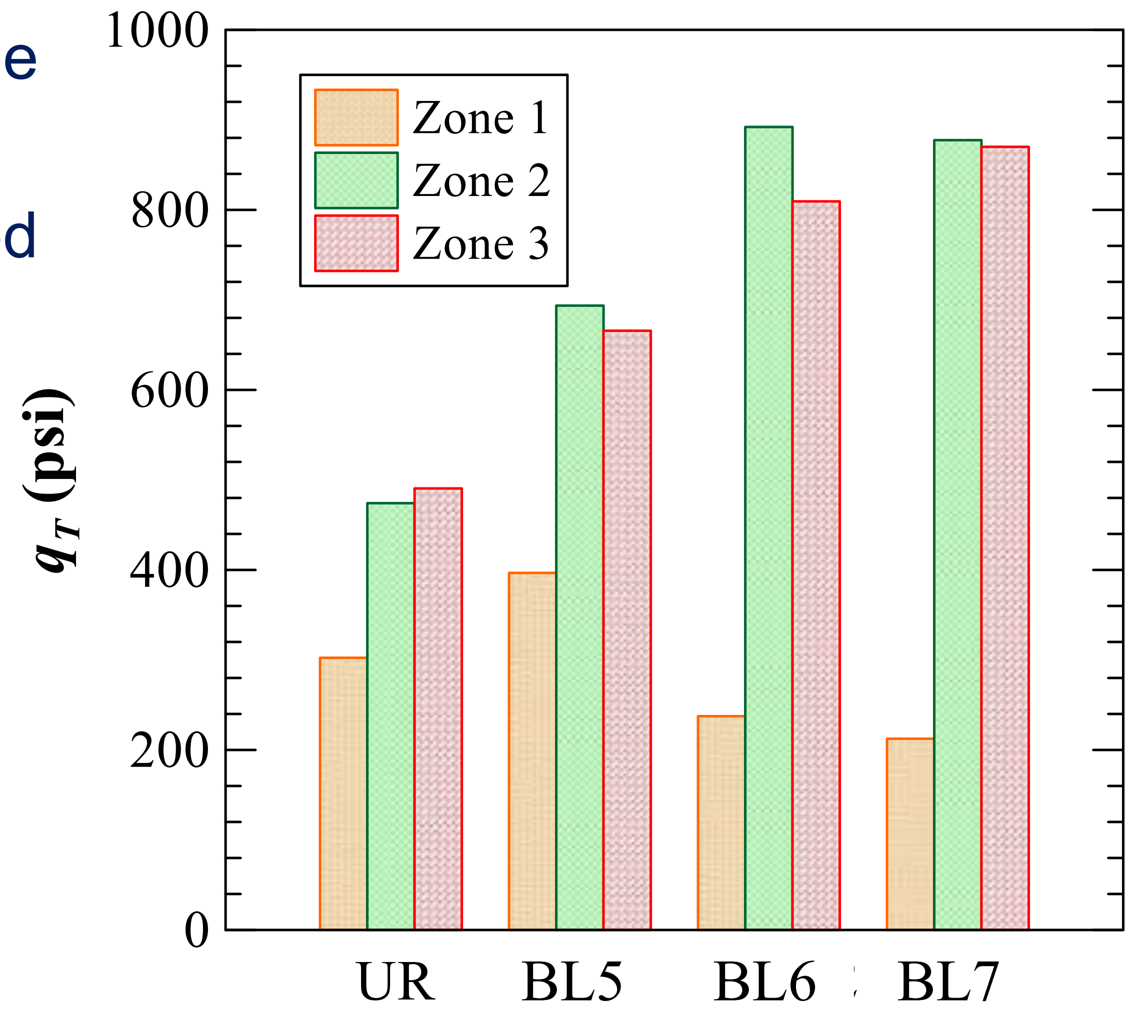

Average tip resistance in different zones in the test sections

Laboratory studies

Lab correlation

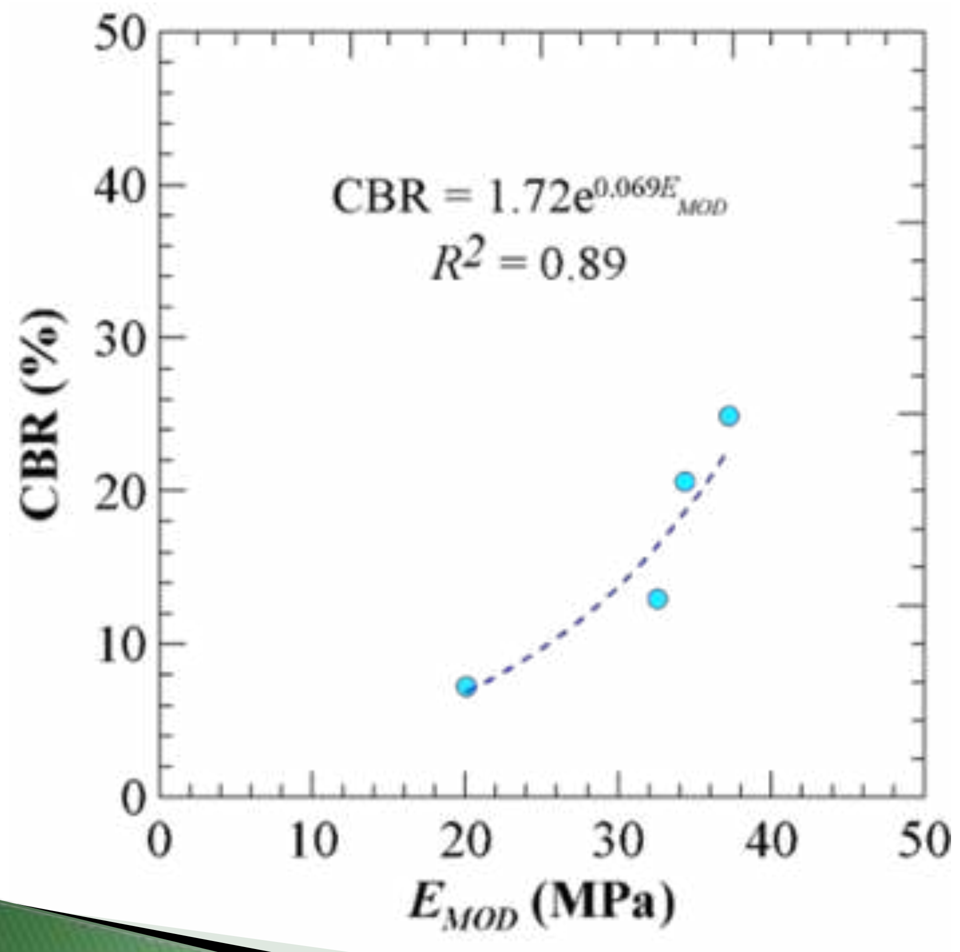

CBR and Elastic modulus of test sections

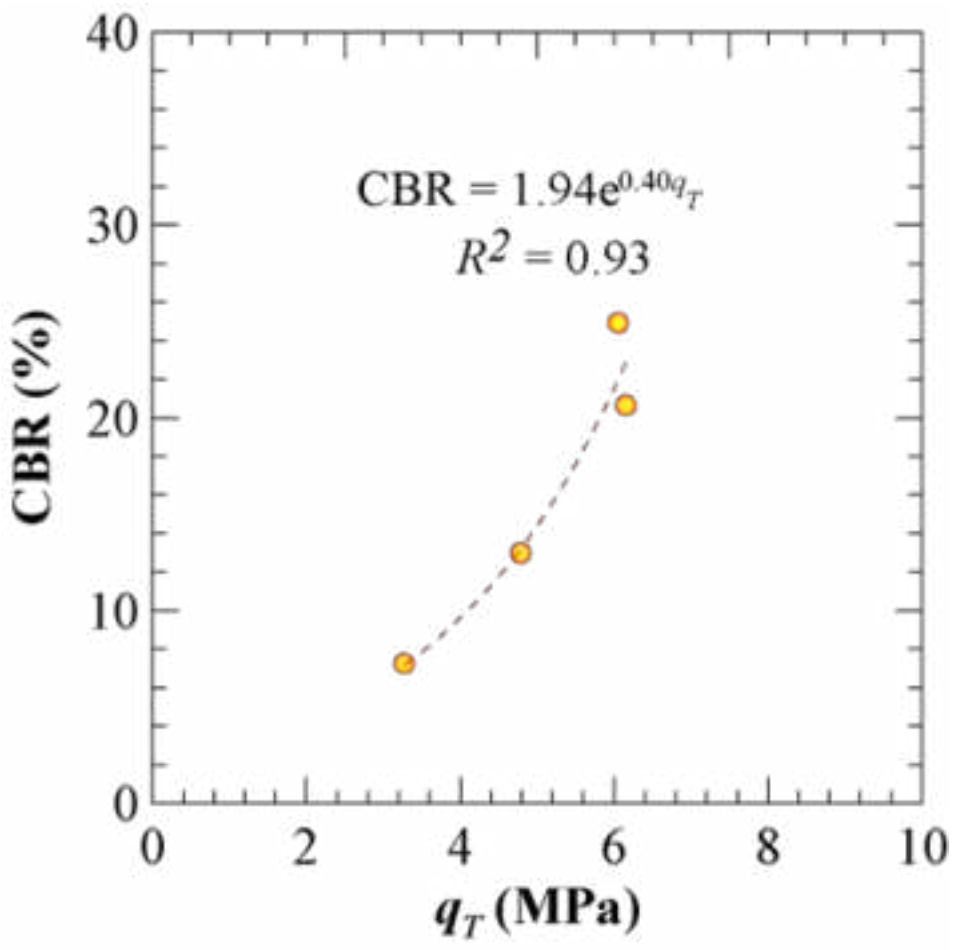

CBR and tip resistances near geogrid layer (Zone-2)

Task 2.1 Numerical Modeling

Numerical model and workflow diagram

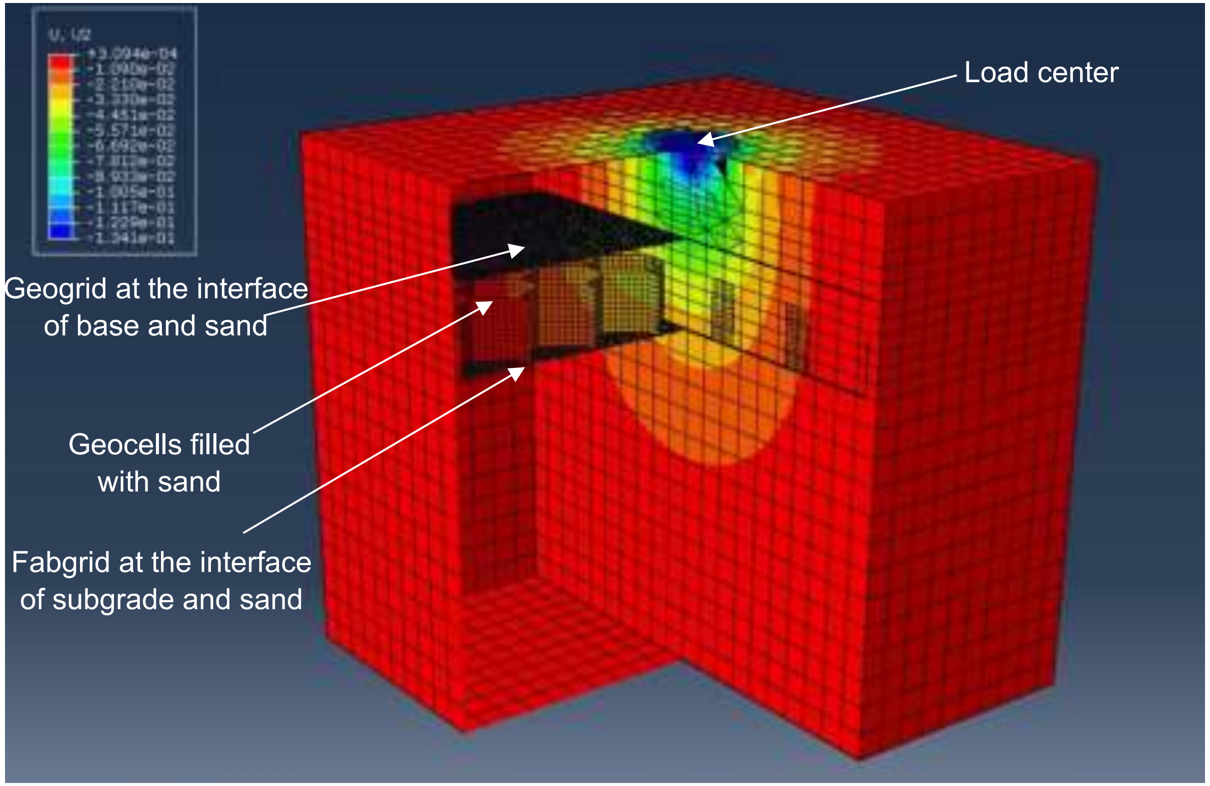

Deformation profile of a FEM based geocell-geogrid reinforced pavement section model cross section

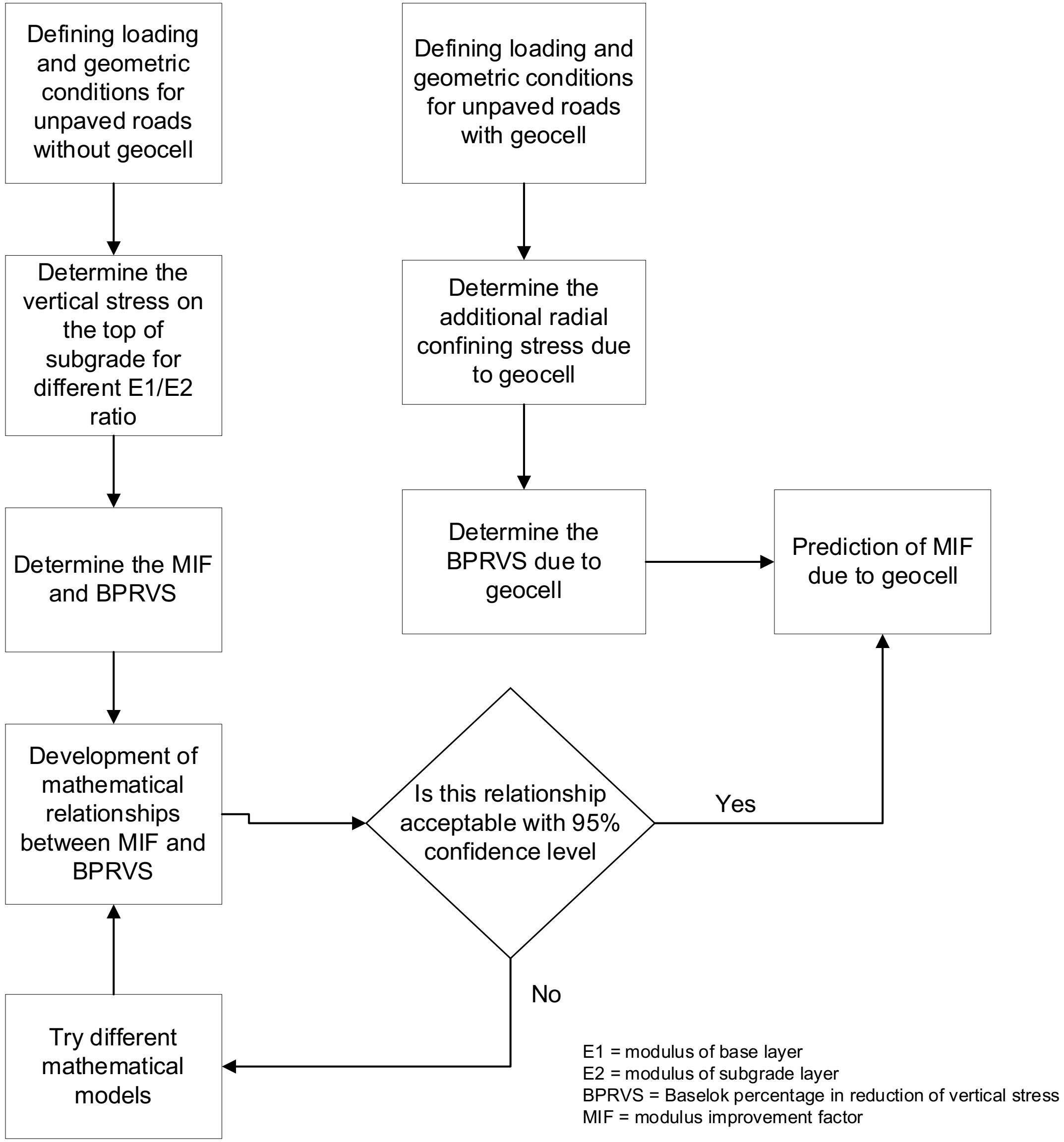

Flowchart used for the development of the proposed method

Task 2.1 Numerical Modeling

Vertical stress distribution & improvement factor

$$BPRVS_i = \frac{\sigma_{aj} - \sigma_{ai}}{\sigma_{aj}} \times 100\ \%$$

$$MIF_i = \frac{m_i}{m_j}$$

j = 1 to 6;

i = (j + 1) to 10;

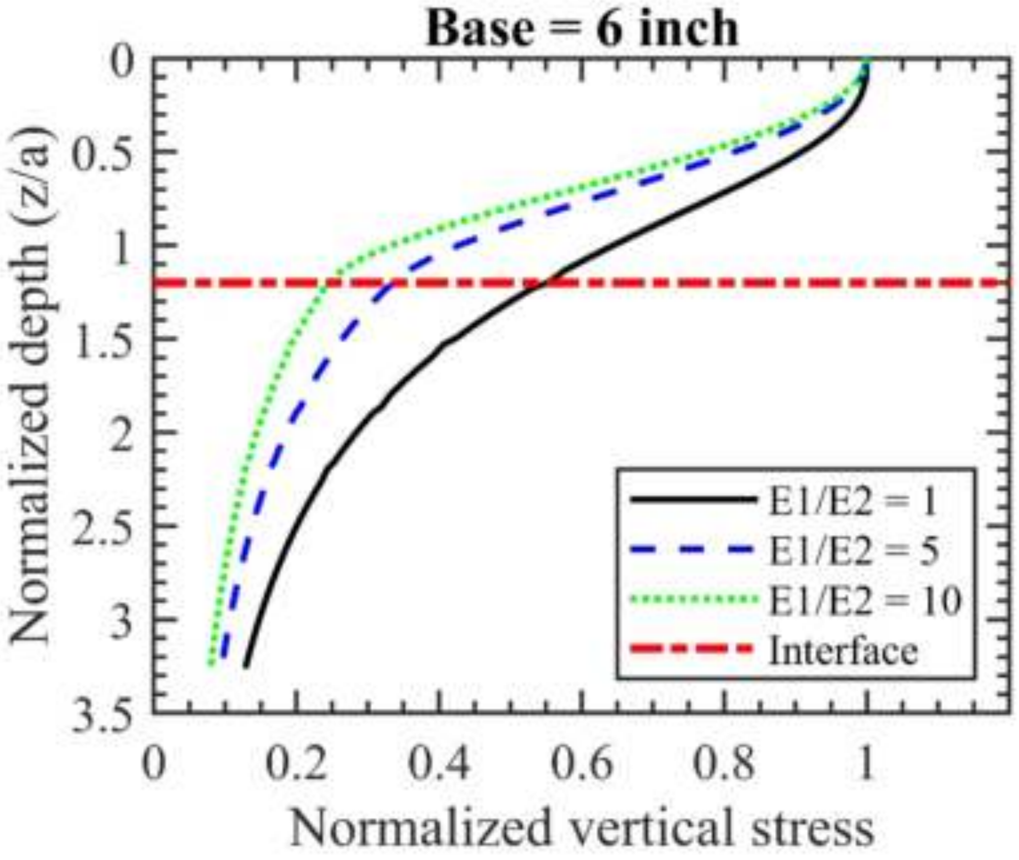

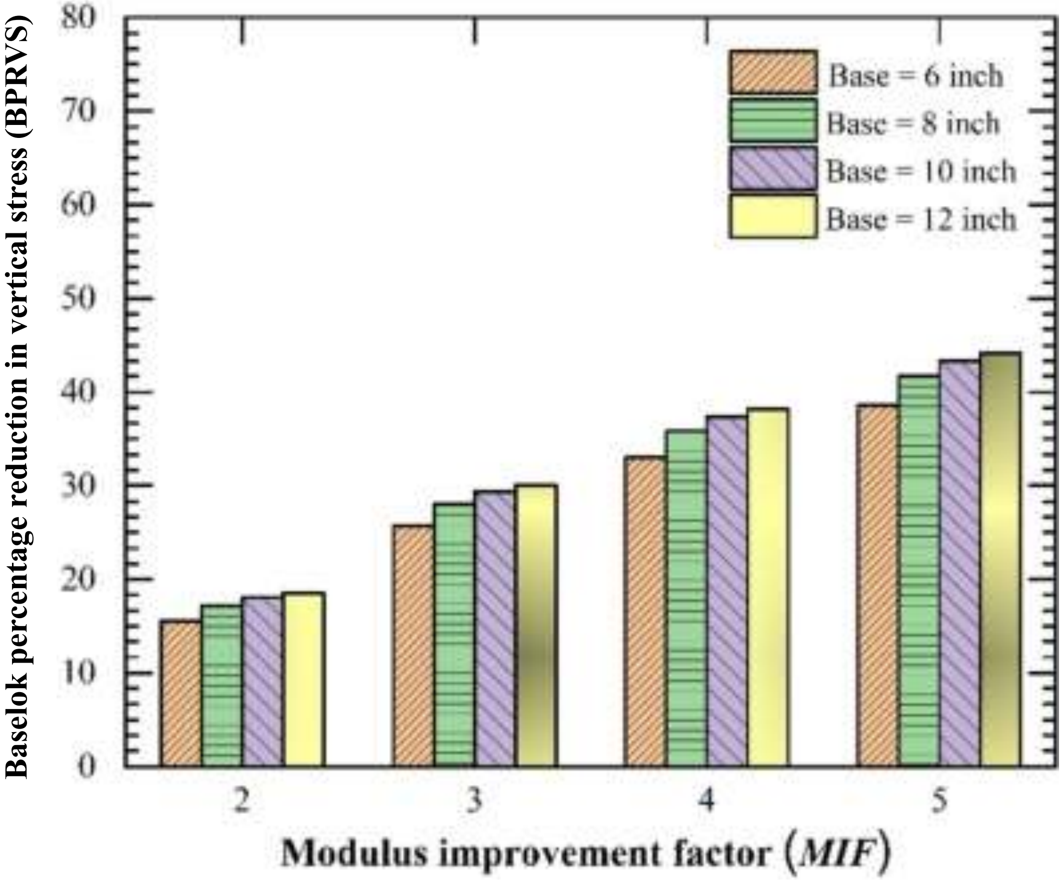

Task 2.1 Numerical Modeling

Correlation between geocell properties with improvement factor

$$\Delta\sigma_3 = \frac{2M}{d}\frac{\epsilon_r}{1-\epsilon_a}$$

$$\varepsilon_r = \frac{1-\sqrt{(1-\varepsilon_a)}}{\sqrt{(1-\varepsilon_a)}}$$

$$\varepsilon_r = 0.553\varepsilon_a$$

$$\Delta\sigma_3 = \frac{1.1M}{d}\frac{\varepsilon_a}{1-\varepsilon_a}$$

$$S = 2\pi r(h_g)\tan(\delta)\,\Delta\sigma_3$$

$$q_r = \frac{1.1Mh_g}{r^2}\tan(\delta)\frac{\varepsilon_a}{1-\varepsilon_a}$$

$$BPRVS = \frac{1.1Mh_g}{r^2 * \sigma_A}\tan(\delta)\frac{\varepsilon_a}{1-\epsilon a} \text{ x } 100\%$$

$$MIF = 0.566*\exp\left[\frac{5.17Mh}{r^2 * \sigma A}\tan(\delta)\frac{\varepsilon_a}{1-\varepsilon_a}\right]$$

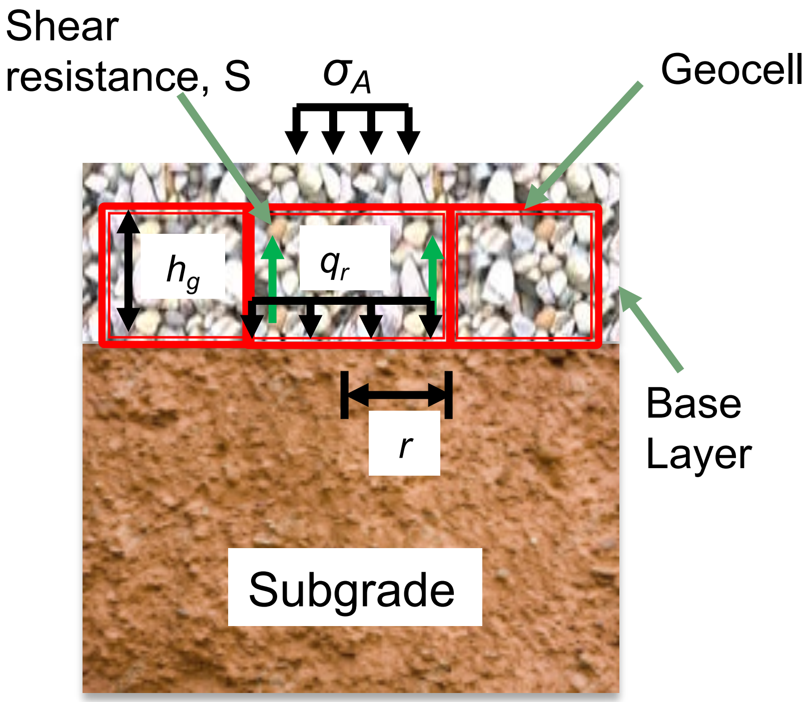

$$h_{base} = \frac{R}{\sqrt{\dfrac{1}{\left(1-\dfrac{N_c C_u + \dfrac{1.1Mh_g}{r^2}\tan(\delta)\dfrac{\varepsilon_a}{1-\varepsilon_a}}{p}\right)}}}$$

$\Delta\sigma_3$ = additional confining stress provided by geocell
M = stiffness per unit length of the geocell
ϵ_a and ϵ_r = the axial and radial strain acting within the infill material
δ =interface friction angle between geocell wall and infill material

Task 2.2: Parametric Study

Proposed Method

- ❑Considers geocell stiffness
- ❑Applicable when infill material with higher friction angle
- ❑Different aspect ratio (geocell height to dimeter ratio) was considered

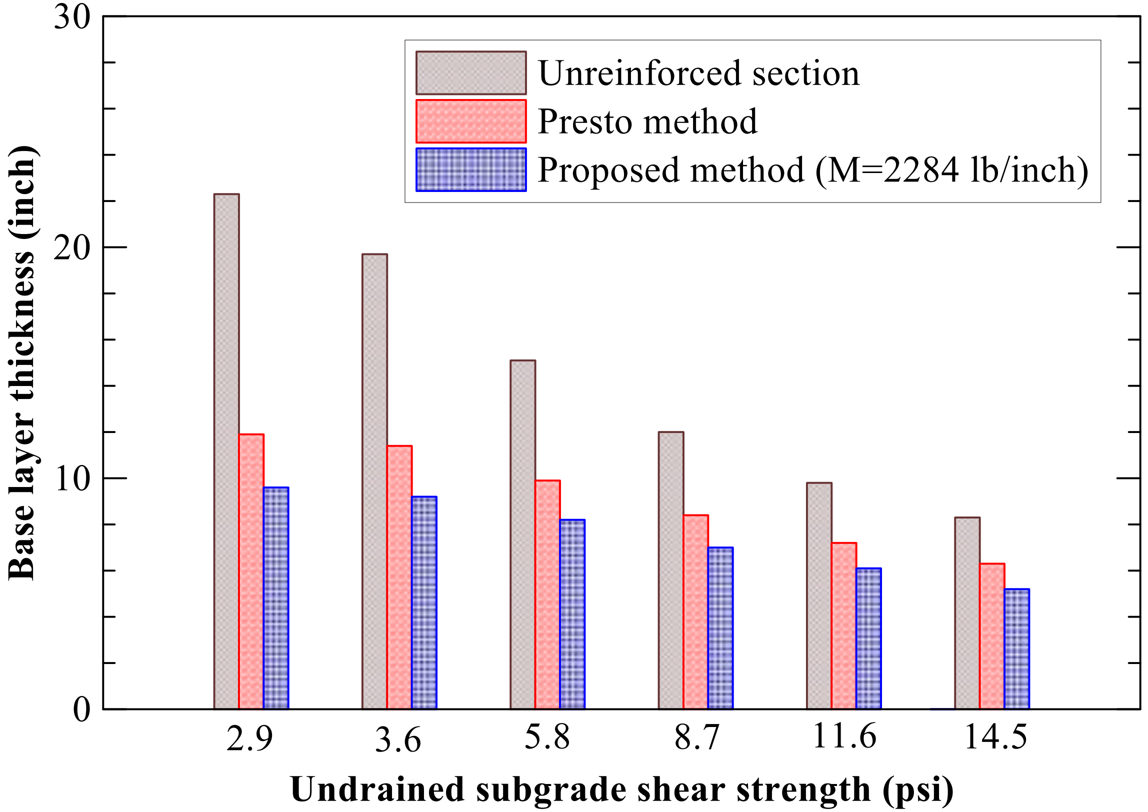

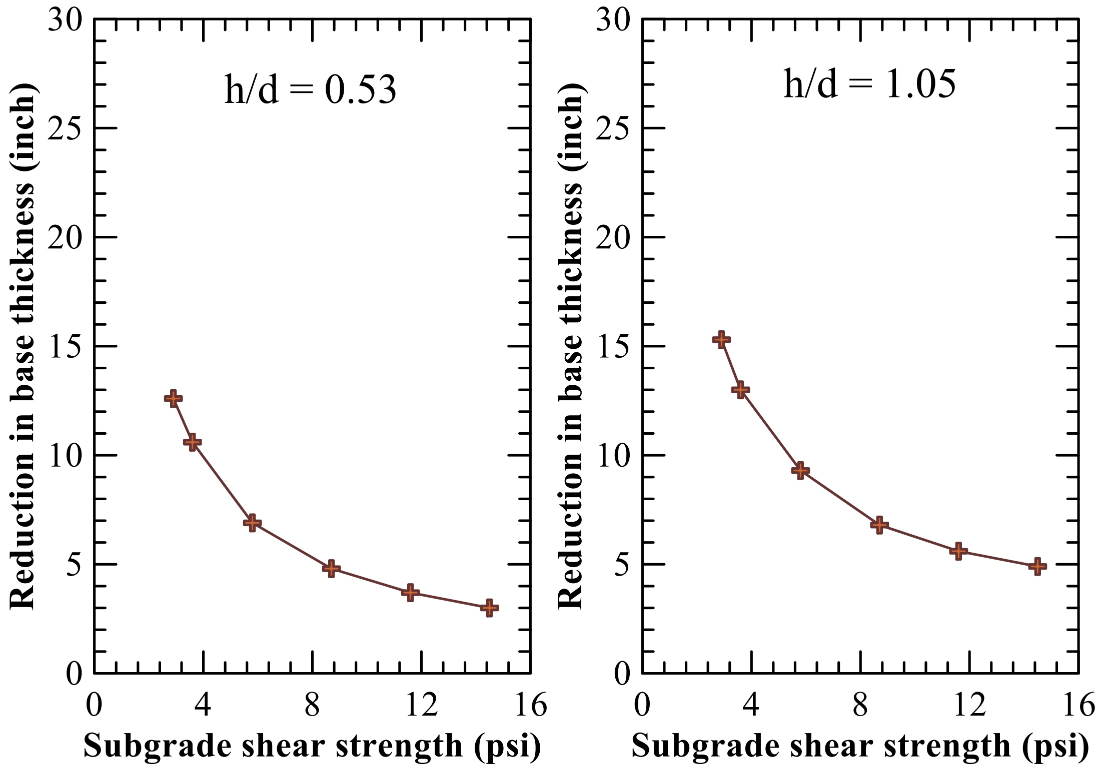

Summary

- ❑DCP tests indicated that average subgrade CBR < 1 (very soft foundation soil)
- ❑CBR for geocell reinforced base layer was 17.2
- ❑Geosynthetic reinforcement also enhanced the subgrade stiffness by 2.5 times
- ❑LWD studies showed relative modulus improvement with the geosynthetic system were 1.5 to 3.6 times compared with the unreinforced
- ❑VE-DCP showed very soft layer up to a depth of 18 inch
- ❑Tip resistance and surface modulus was correlated with CBR results for future usage
- ❑Numerical model was developed, and the model predicted that vertical stress on top of the subgrade layer ↓ with the ↑modular ratios
- ❑ An analytical model was proposed that consider the effect of geocell wall stiffness, infill material and geometry of geocell

Future Works

- Continue laboratory large scale repeated load tests for 6-inch base configuration
- Develop design charts based on laboratory large scale repeated load tests

Performance of pavement sections with H_2Ri geosynthetics

Project Leader: Nripojyoti Biswas

Team members: Avinash Gonnabathula, Krishneswar Ramineni and Gustavo Hernandez Martin

PI: Anand J. Puppala

Professor | A.P. and Florence Wiley Chair

Director – Center for Infrastructure Renewal

Closed Meeting

TAMU Site Proprietary

NSF IUCRC CICI TAMU SITE

NSF IUCRC CICI - IAB Fall 2023 Meeting

December 7-8, 2023

TEXAS A&M UNIVERSITY

Zachry Department of Civil & Environmental Engineering

Presentation Outline

- Introduction
- Task Plan
- Field Test Sections
- Life Cycle Analysis
  - Life Cycle Cost Analysis
  - Sustainability Analysis
- Summary

Introduction

❖ **Objective**

- ❑ **Evaluate the feasibility/efficiency of using H_2Ri geosynthetic for improving drainage and strength of pavement sections built on high-plastic expansive soil**

❖ **Field Studies indicated efficacy of application**

❖ **Laboratory studies**

- ❑ **Control Section**
- ❑ **Reinforced Sections**

Control Section

Reinforced Section

Task Plan

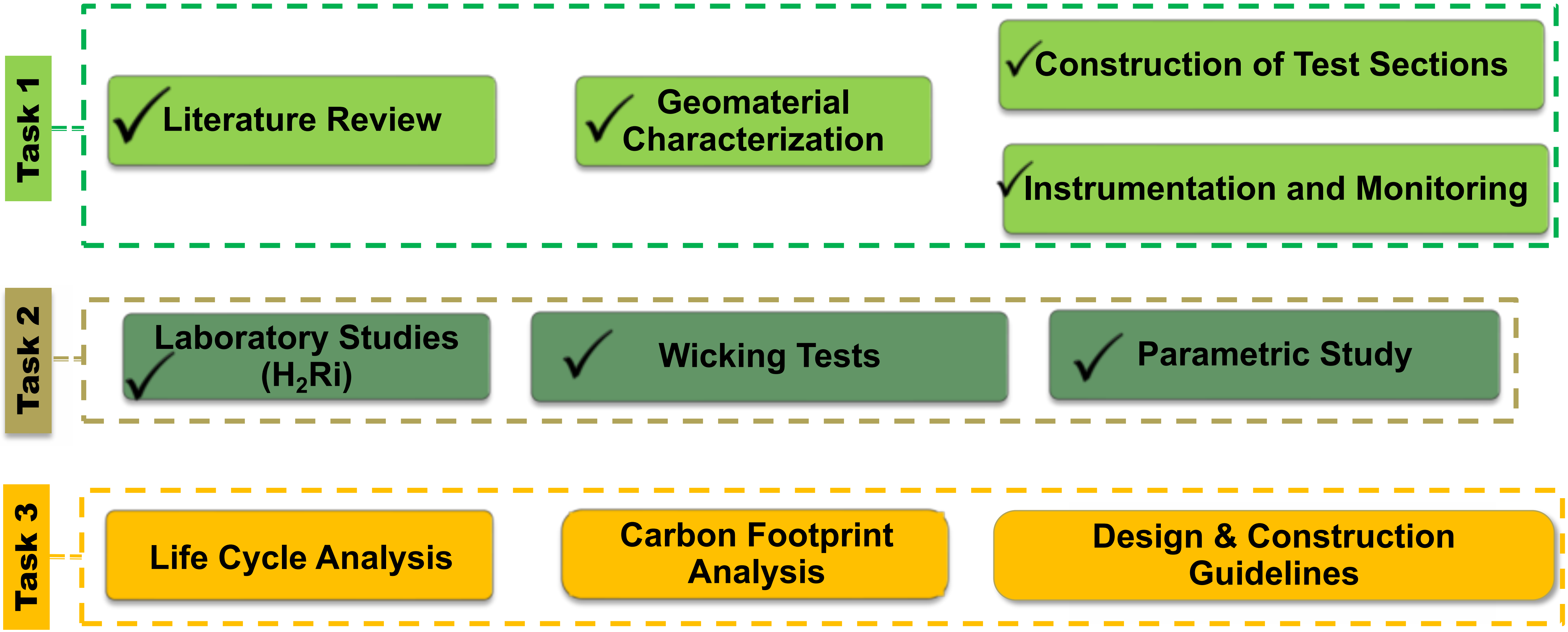
Task 1
✓Literature Review
✓Geomaterial Characterization
✓Construction of Test Sections
✓Instrumentation and Monitoring
Task 2
✓Laboratory Studies (H_2Ri)
✓Wicking Tests
✓Parametric Study
Task 3
Life Cycle Analysis
Carbon Footprint Analysis
Design & Construction Guidelines

Field Test Sections

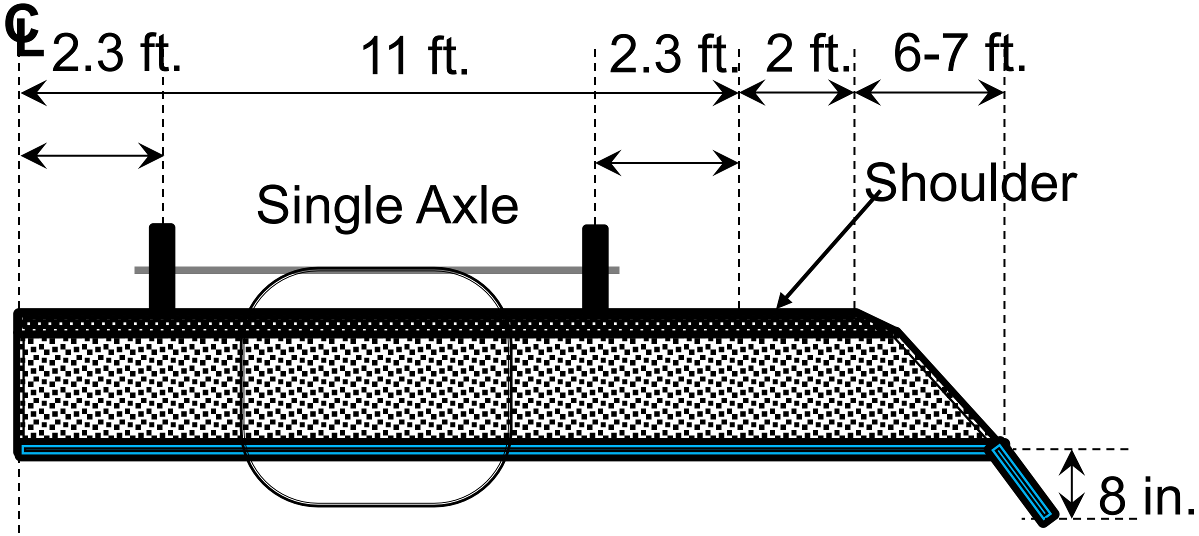

AC – Asphalt Concrete RAP - Reclaimed Asphalt Pavement Aggregates FB - Flex Base
EPC - Earth Pressure Cells SAA - Shape Array Sensors

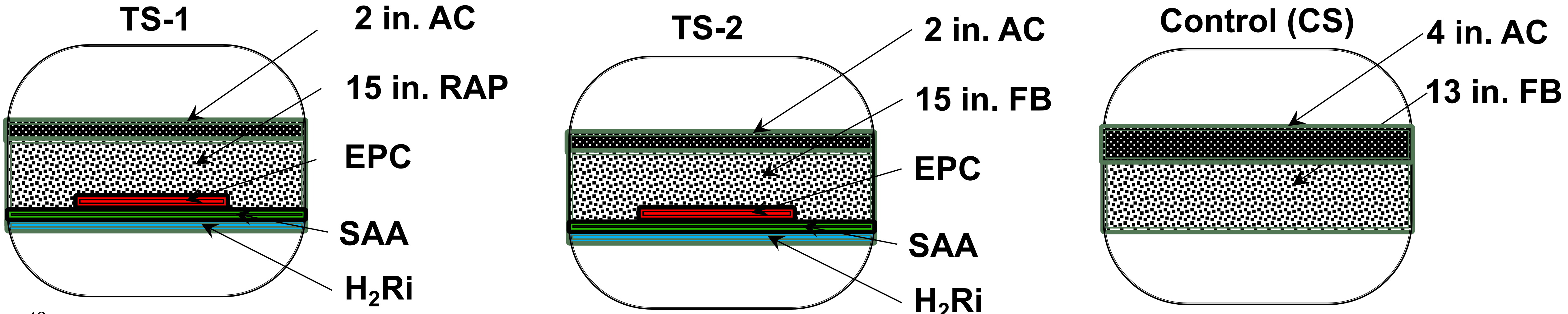

Life Cycle Analysis

Combined Assessment Framework (Das 2018)

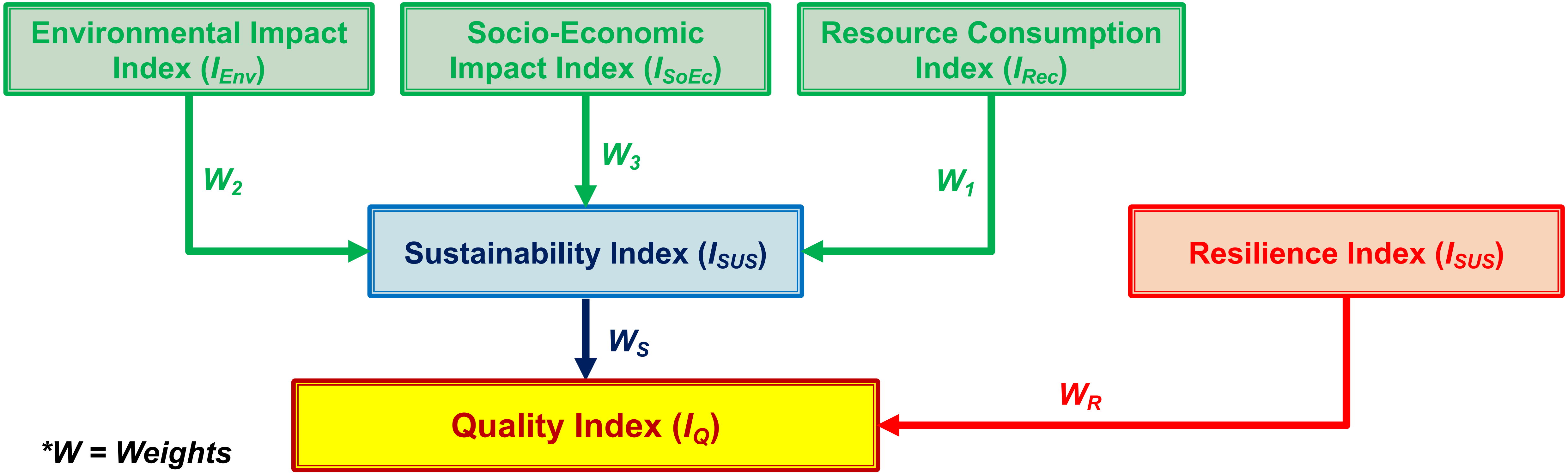

***W = Weights**

$$*\sum W = 1$$

$$I_{SUS} = W_1 \times I_{Env} + W_2 \times I_{SoEc} + W_3 \times I_{Rec}$$

$$I_Q = W_s \times I_{SUS} + W_R \times I_{Res}$$

Lower value indicates better alternative

Research Flow

- Boundary condition is considered as cradle to gate + transportation to site
- Construction machinery costs and impacts are assumed to be uniform across all sections
- The database costs are market costs for the products
- Cost and Impact analysis was done per meter length of road
- Sustainability analysis for environmental impact was performed using OpenLCA
- ReCiPe 2016 Midpoint method was used for calculation
  - Factors → Climate change, human toxicity, resource depletion, ecosystem quality

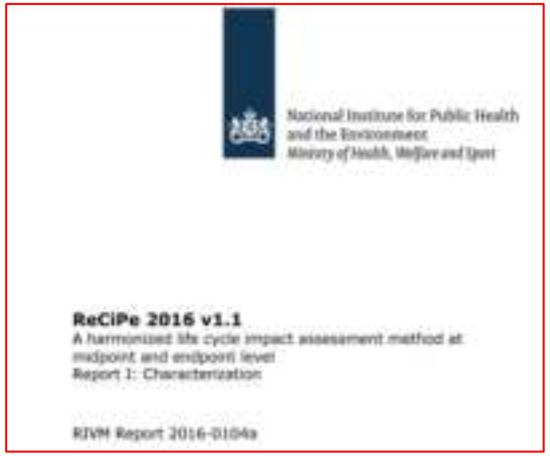
National Institute for Public Health
and the Environment
Ministry of Health, Welfare and Sport

ReCiPe 2016 v1.1
A harmonized life cycle impact assessment method at midpoint and endpoint level
Report 1: Characterization

RIVM Report 2016-0104a

LCA Analyses Boundary

Boundary: Cradle to Gate + Transportation to site

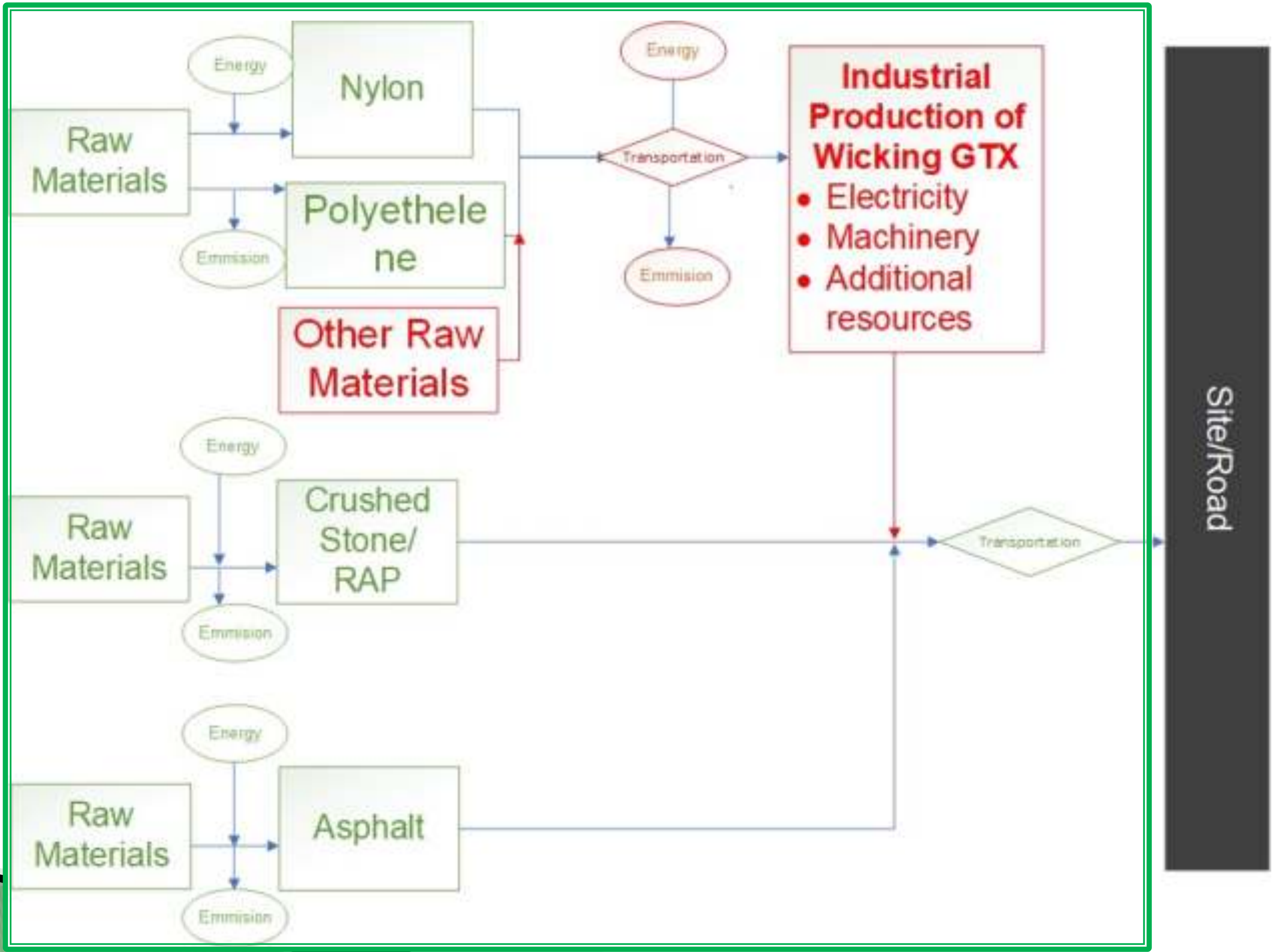

Sustainability Analysis – Test Parameters

$$I_{Rec} = w_{1a} \times E_{E\,(material\ production)} + w_{1b} \times E_{E\,(Transportation)}$$

$$I_{Env} = w_{2a} \times Water_{TOX} + w_{2b} \times Water_{EUT} + w_{2c} \times GW_P + w_{2d} \times Carc_{TOX} + w_{2e} \times N - Carc_{TOX}$$

$$I_{SoEc} = w_3 \times C$$

Where,
w_i = Weight factors
E_E = Embodied Energy;
$Water_{TOX}$ = Freshwater Ecotoxicity
$Water_{EUT}$ = Freshwater Eutrophication
GW_P = Global Warming Potential
$Carc_{TOX}$ = Human Carcinogenic Toxicity
N-$Carc_{TOX}$ = Human Non-Carcinogenic Toxicity
C = Cost of the materials

Test ID	A	B	C
Section ID	TS-1	TS-2	Control
Section Parameters	15 in. RAP + 2 in. AC + H_2Ri gtx	15 in. FB + 2 in. AC + H_2Ri gtx	13 in. FB + 4 in. AC
Section Length	3.3 m	3.3 m	3.3 m
Section Width	15 ft.	15 ft.	15 ft.

Flow of Materials (Test Section-1)

❖ **Software output flow for RAP + GTX section construction**

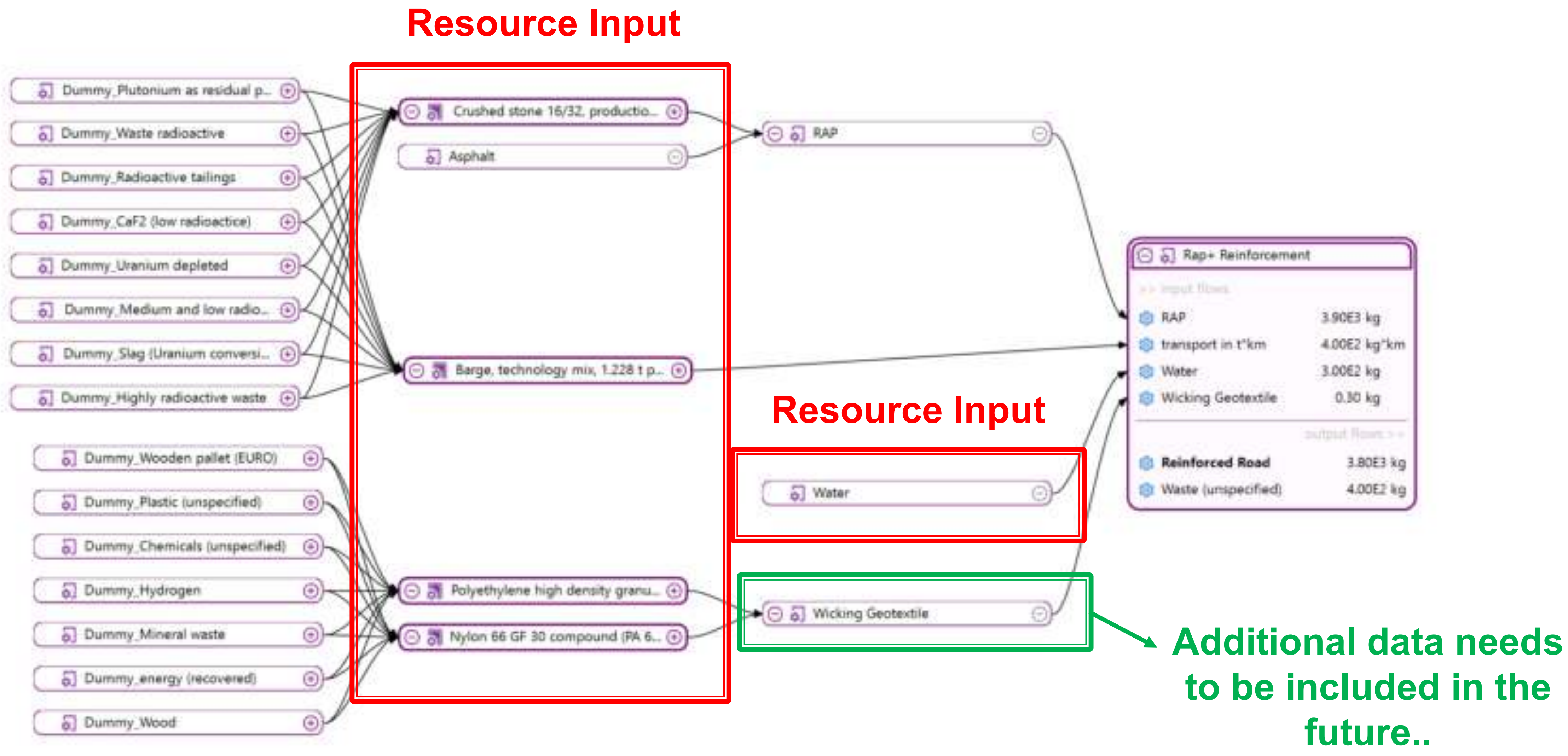

Flow of Materials (Test Section-2)

❖ **Software output flow for FB + GTX section construction**

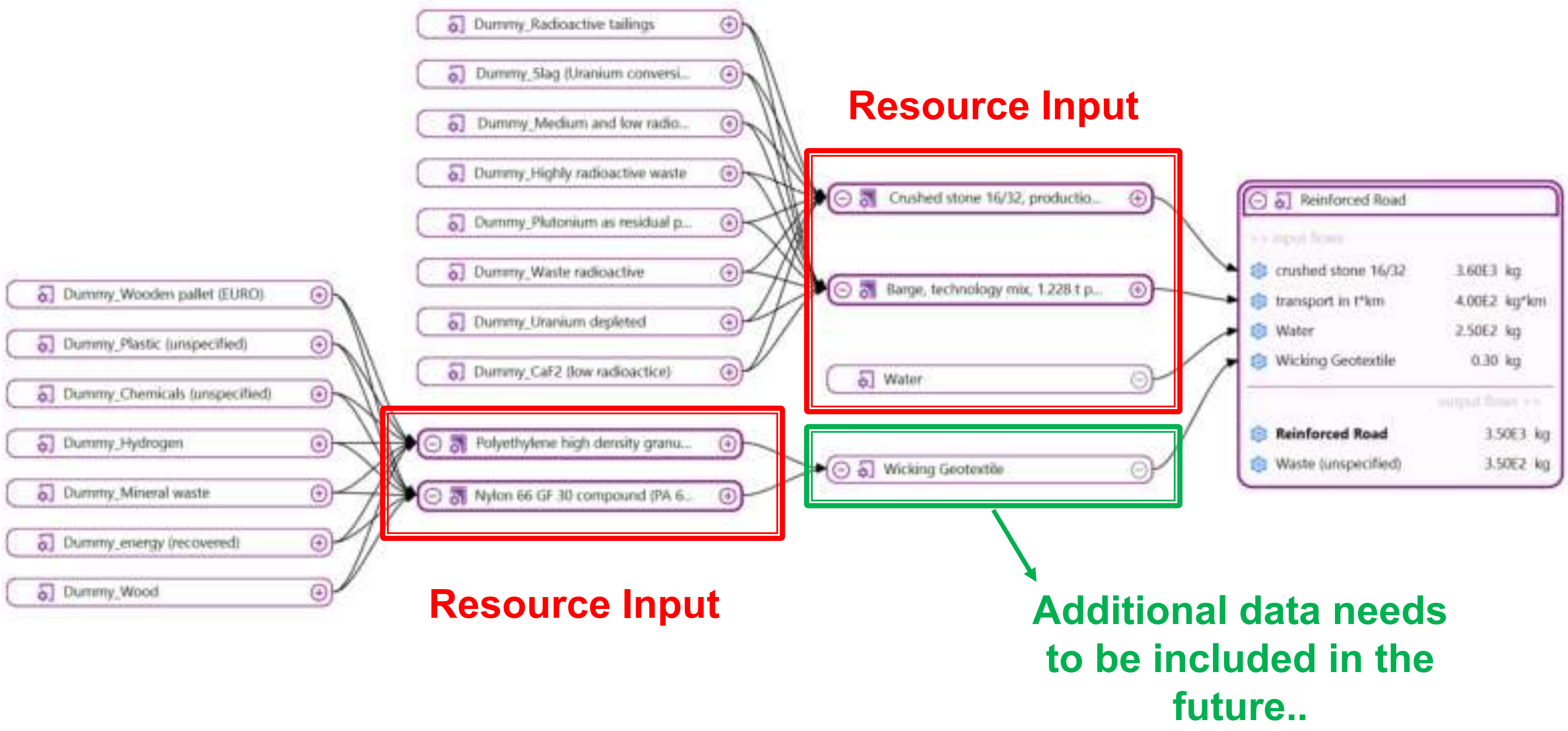

Flow of Materials (Control Section)

❖ Software output flow for unreinforced section construction

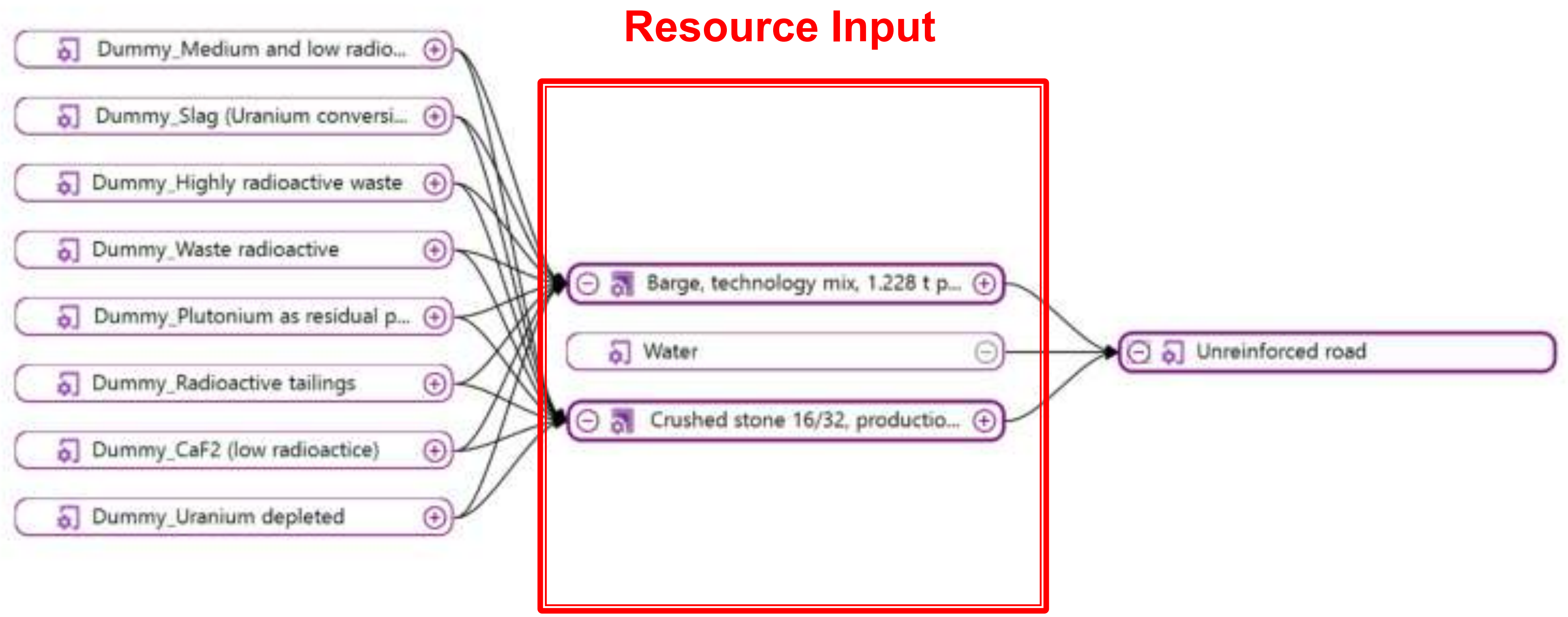

Sustainability Analysis – Embodied Energy

Energy Category	A	B	C
Energy from Coal (MJ)	347	356	325
Energy from Gas (MJ)	430	440	397
Energy from Oil (MJ)	291	295	264
Others (MJ)	2490	2520	3725
Total Embodied Energy	**3557**	**3611**	**4711**

❖ **Traditional Pavement Section has higher Embodied Energy as compared to Reinforced Section**

Sustainability Analysis – Environmental Impact

Environmental Impact Category	A	B	C
Freshwater ecotoxicity (kg 1,4-DCB)	0.01	0.01	0.001
Freshwater eutrophication (kg P eq)	0.0001	0.0001	0.0001
Global warming (kg CO2 eq)	**165.30**	**167.26**	**212.2**
Human carcinogenic toxicity (kg 1,4-DCB)	0.04	0.04	0.05
Human non-carcinogenic toxicity (kg 1,4-DCB)	4.92	5.04	5.62

- **Traditional Pavement Section has higher kg eq. of CO_2 emission as compared to Reinforced Section**

Life Cycle Cost Analysis

Database for Cost Calculation

Material	Unit weight		Cost (USD)		Transportation (miles)
RAP	122	pcf	$27	per ton	20
FB	135	pcf	$48.50	per ton	20
GTX	1.2	kg/m^2	$4,900*	15'x300' roll	250
AC	145	pcf	$80	per ton	20

Data Source: Sustainable pavement with geocell reinforced reclaimed-asphalt-pavement (RAP) base layer - Khan and Puppala

* - From web-resources of the manufacturer

Life Cycle Cost Analysis Impact

Material	A	B	C
Asphalt	48.76	48.76	97.52
Flex Base		159.16	184
RAP	80.13	-	-
Sub Grade	17.48	17.48	17.48
Geotextile	55.2	55.2	-
Total (USD)	**201.5**	**280.6**	**299**

❖ **RAP with wicking geotextile has lower cost until system boundary**

Summary

- A comprehensive Life Cycle Cost Analysis (LCCA) for the H2Ri geotextile was developed (cradle-to-gate + Construction)
- Sustainability assessment indicates the overall embodied energy and GHG emissions are more in RAP + GTX section although the cost is less.
- Sustainability assessment indicates GHG emissions during production of geotextile and cost of geotextile are major factors affecting sustainability benefits of the project
- Future benefits could be realized with the inclusion of Resiliency Function

Future Works

- Need to develop a comprehensive Life Cycle Cost Analysis (LCCA) for the H2Ri geotextile (cradle-to-gate + End-of-life)
- Large Scale Testing is to be performed.

CICI IAB Meeting, Fall 2023

December 7 and 8, 2023

News and Accomplishments

West Virginia University

NC STATE UNIVERSITY

TEXAS A&M UNIVERSITY

UNIVERSITY OF MIAMI

News and Accomplishments

- Published over 10 new papers in refereed journals, numerous articles, conferences…
- Lunch and learn professional program.
- Initiating collaboration with LOWE Art museum.
- Participation to numerous conferences, most notably: ACI Fall Convention (Boston, MA)

News and Accomplishments

SEAHIVE – Sustainable Estuarine and Marine Revetment (NCHRP)

- Coral reefs function as submerged breakwaters reducing wave action and providing flood-reduction benefits for coastal communities.
- Synergy of ideal application for composites.
- Significant traction form DOT – demo in Miami Beach
- Large volume opportunity.

News and Accomplishments

- A. Nanni, 100th ACI President. Follow: **#ACI100President**

News and Accomplishments

UNIVERSITY OF MIAMI

- The American Composites Manufacturers Association recognized Antonio Nanni with the **Academic Pioneer Award** at CAMX Atlanta 2023.

News and Accomplishments

UNIVERSITY OF MIAMI

<u>ASTM D30.10 – CICI synergistic work:</u>

- ASTM D8505 – New FRP bar specification approved.
- Increase of 25% of membership participation
- More than 10 new work items in the pipe line, nearly doubling the ASYM documents relevant to Composites for Civil Structures.

This international standard was developed in accordance with internationally recognized principles on standardization established in the Decision on Principles for the Development of International Standards, Guides and Recommendations issued by the World Trade Organization Technical Barriers to Trade (TBT) Committee.

Designation: D8505/D8505M – 23

Standard Specification for Basalt and Glass Fiber Reinforced Polymer (FRP) Bars for Concrete Reinforcement[1]

This standard is issued under the fixed designation D8505/D8505M; the number immediately following the designation indicates the year of original adoption or, in the case of revision, the year of last revision. A number in parentheses indicates the year of last reapproval. A superscript epsilon (ε) indicates an editorial change since the last revision or reapproval.

1. Scope

1.1 This specification covers basalt and glass fiber reinforced polymer (BFRP and GFRP, respectively) bars, provided in straight (longitudinal) cut lengths, of solid round cross-section, and having a surface enhancement for internal concrete reinforcement applications. Bars covered by this specification shall meet the requirements for geometric, material, mechanical, and physical properties as described herein.

1.2 Subsection 1.6 defines the type of FRP bars that are out of the scope of this specification.

1.6.2 Bars made from fibers other than glass or basalt.

1.6.3 Bars having no external surface enhancement (that is, plain or smooth bars, or dowels).

1.6.4 Bars with geometries other than solid, round cross sections.

1.6.5 Pre-manufactured grids and gratings made with FRP materials.

1.6.6 Bent bars (that is, bars that are not made of straight, continuous lengths).

News and Accomplishments

UNIVERSITY OF MIAMI

- Structures and Materials Inspection Body (SMIB)
- ISO 17020 Accredited Inspection Body
- Focus on composites and RC

IAS INTERNATIONAL ACCREDITATION SERVICE

CERTIFICATE OF ACCREDITATION

This is to attest that

UNIVERSITY OF MIAMI
STRUCTURES AND MATERIALS INSPECTION BODY
1251 MEMORIAL DRIVE, MCARTHUR ENGINEERING BUILDING 108
CORAL GABLES, FLORIDA 33146

Inspection Agency AA-829 (Type C)

has met the requirements of AC98, *IAS Accreditation Criteria for Inspection Agencies*, and has demonstrated compliance with ISO/IEC Standard 17020:2012, *Conformity assessment - Requirements for the operation of various types of bodies performing inspection*. This organization is accredited to provide the services specified in the scope of accreditation.

Effective date: Month Day, Year

IAS ACCREDITED

President

News and Accomplishments

Renewing our commitment…

- Structures and Materials Laboratory (SML) re-assessment
- Renewed ISO 17025 Accredited Testing Laboratory (TL-478), celebrating our **11th Anniversary**
- Material, durability, structural testing

Center for Integration of Composites into Infrastructure

IAB Meeting, Fall 2023

#1 Using Machine Learning and Artificial Intelligence to Implement FRP in Infrastructure: Areas of Opportunity

Civil Engineering

Computer Science

Antonio Nanni

Cited by		VIEW ALL
	All	Since 2018
Citations	28037	12542
h-index	83	56
i10-index	411	254

Cited by		
	All	Since 2018
Citations	1031	1031
h-index	19	19
i10-index	31	31

Seyedali Mirjalili

Cited by		
	All	Since 2018
Citations	88545	84507
h-index	100	100
i10-index	351	343

Francisco De Caso

Cited by		VIEW ALL
	All	Since 2018
Citations	612	480
h-index	9	9
i10-index	9	9

AI ❤ Concrete

Yelena Yesha

Cited by		VIEW ALL
	All	Since 2018
Citations	6708	1033
h-index	38	17
i10-index	100	31

Metaheuristic algorithm?

- *Heuristic* (from an old Greek word *heuriskein*):

  "*the art of discovering new strategies (rules) to solve problems*"

- *Meta* (a Greek word):

  "*upper level methodology*"

- *Metaheuristic*:

"*Upper level general methodologies that can be used as guiding strategies in designing underlying heuristics to solve specific optimization problems*"

- ***Exploration*** **vs.** ***Exploitation***
  - Exploration of the search space (*Diversification*) and Exploitation of the best solutions found (*Intensification*)
  - Good solutions are clue for promising regions

In intensification, the promising regions are explored more thoroughly in the hope to find better solutions

In diversification, non-explored regions must be visited to be sure that all regions of the search space are evenly explored and to avoid from local optima traps

Cuckoo Search and SPO

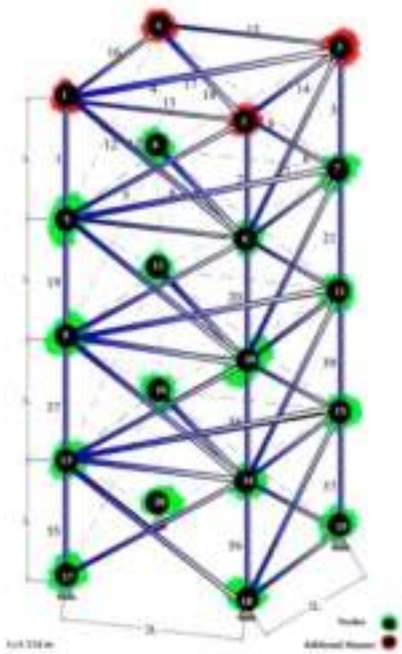

Materials	GFRP		CFRP		STEEL	
Member Group	SPO	CSSPO	SPO	CSSPO	SPO	CSSPO
1 (A_1-A_4) cm^2	13.3972	4.7702	1.4932	1.4932	1.4932	1.1560
2 (A_5-A_{12}) cm^2	9.4481	9.9981	3.4486	3.4486	3.4486	2.6751
3 (A_{13}-A_{16}) cm^2	0.6450	0.6450	0.6450	0.6450	0.6450	0.6450
4 (A_{17}-A_{18}) cm^2	0.6724	0.7181	0.6450	0.6450	0.6450	0.6450
5 (A_{19}-A_{22}) cm^2	12.0096	10.5253	3.4111	3.4111	3.4111	2.6876
6 (A_{23}-A_{30}) cm^2	11.3740	10.0562	3.5042	3.5042	3.5042	2.6555
7 (A_{31}-A_{34}) cm^2	0.6450	0.6450	0.6450	0.6450	0.6450	0.6450
8 (A_{35}-A_{36}) cm^2	0.6450	0.6450	0.6450	0.6450	0.6450	0.6453
9 (A_{37}-A_{40}) cm^2	13.6289	16.9763	5.7274	5.7274	5.7274	4.2783
10 (A_{41}-A_{48}) cm^2	8.6208	10.0865	3.5086	3.5086	3.5086	2.6824
11 (A_{49}-A_{52}) cm^2	0.6450	0.6450	0.6450	0.6450	0.6450	0.6450
12 (A_{53}-A_{54}) cm^2	0.6450	0.6450	0.6450	0.6450	0.6450	0.6452
13 (A_{55}-A_{58}) cm^2	20.0000	20.0000	7.3112	7.3112	7.3112	5.6892
14 (A_{59}-A_{66}) cm^2	11.2354	9.9604	3.4397	3.4397	3.4397	2.7112
15 (A_{67}-A_{70}) cm^2	0.6450	0.6450	0.6450	0.6450	0.6450	0.6450
16 (A_{71}-A_{72}) cm^2	0.6450	0.6450	0.6450	0.6450	0.6450	0.6450
Best weight (kg)	236.0334	227.2641	103.4361	94.8585	356.0184	337.7553
Average weight (kg)	268.0583	227.3044	129.3833	94.8953	472.1857	337.8333
Standard deviation	23.0932	0.0311	18.6853	0.0271	65.8768	0.0600
No. Analyses	19,100	6900	6800	4900	4150	4050

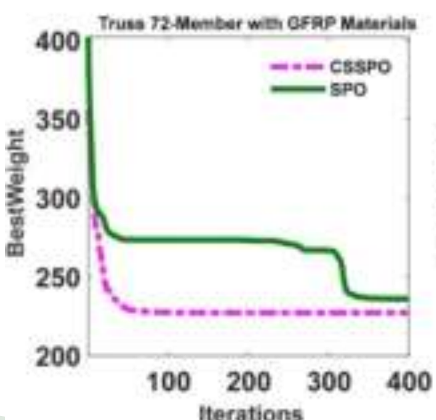

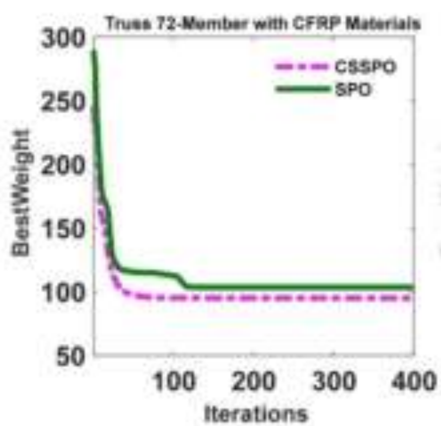

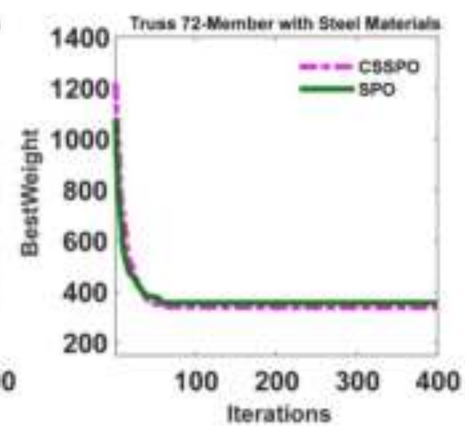

Predicting the flexural strength of 3D printed fiber-reinforced concrete (3DP-FRC) using efficient training of artificial neural networks with the meta-heuristic

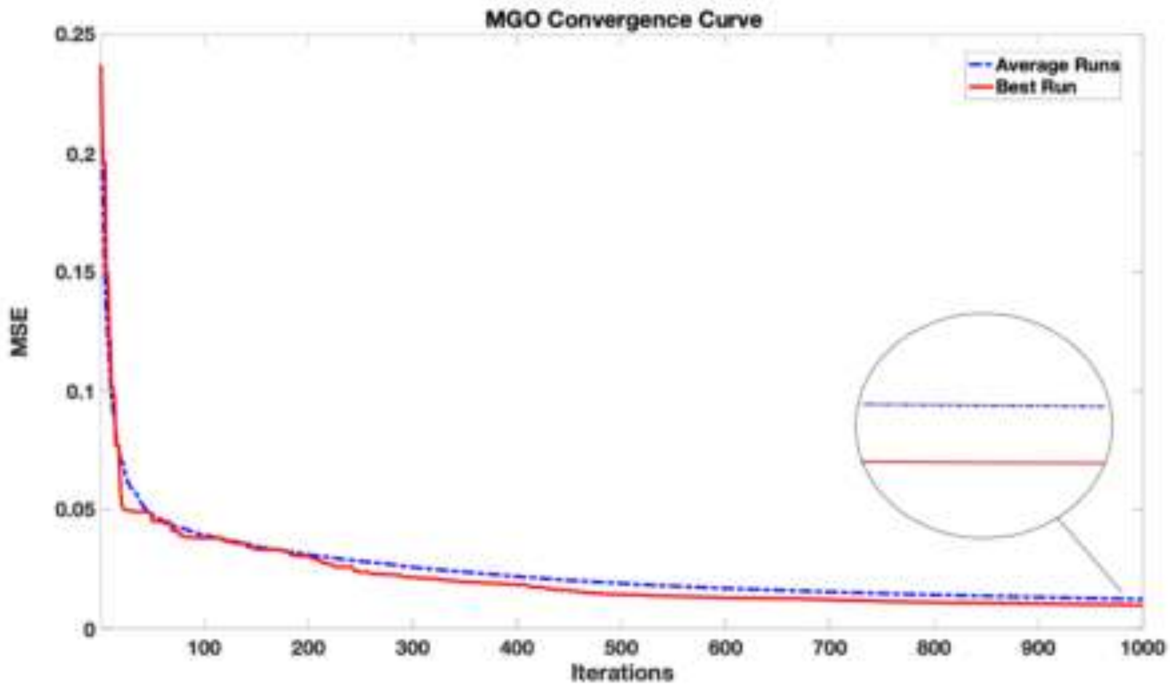

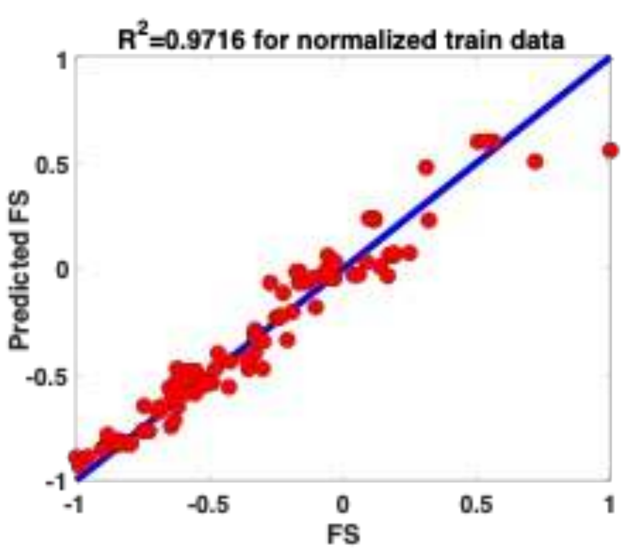
R^2=0.9716 for normalized train data
Predicted FS
FS

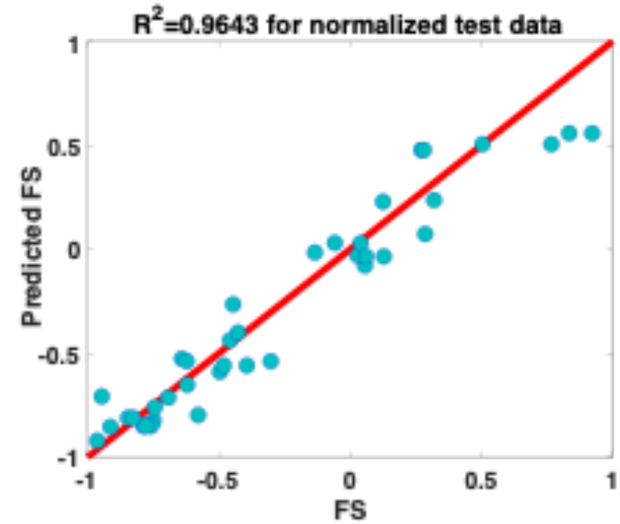
R^2=0.9643 for normalized test data
Predicted FS
FS

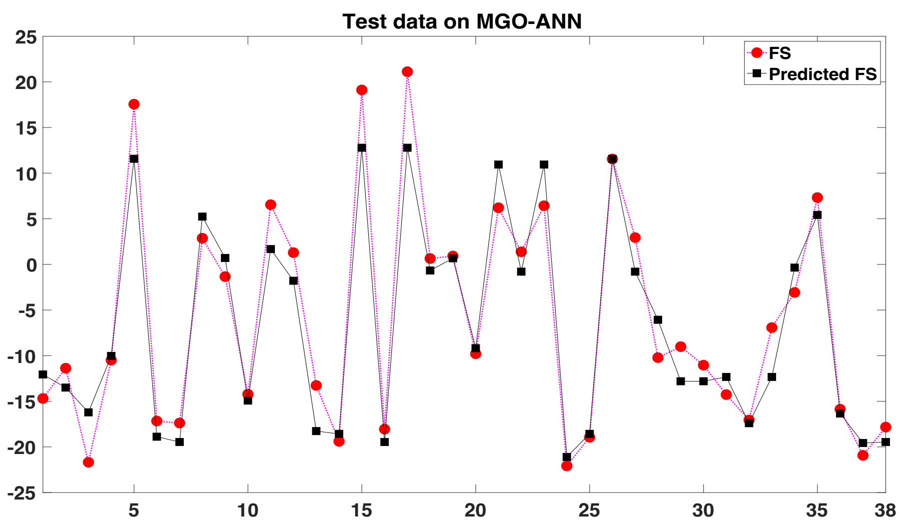
Test data on MGO-ANN
FS
Predicted FS

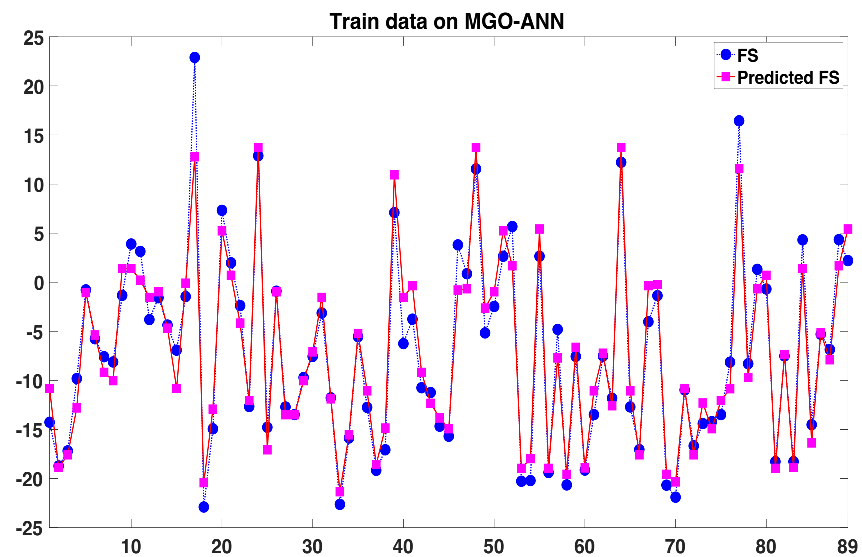
Train data on MGO-ANN
FS
Predicted FS

GUI

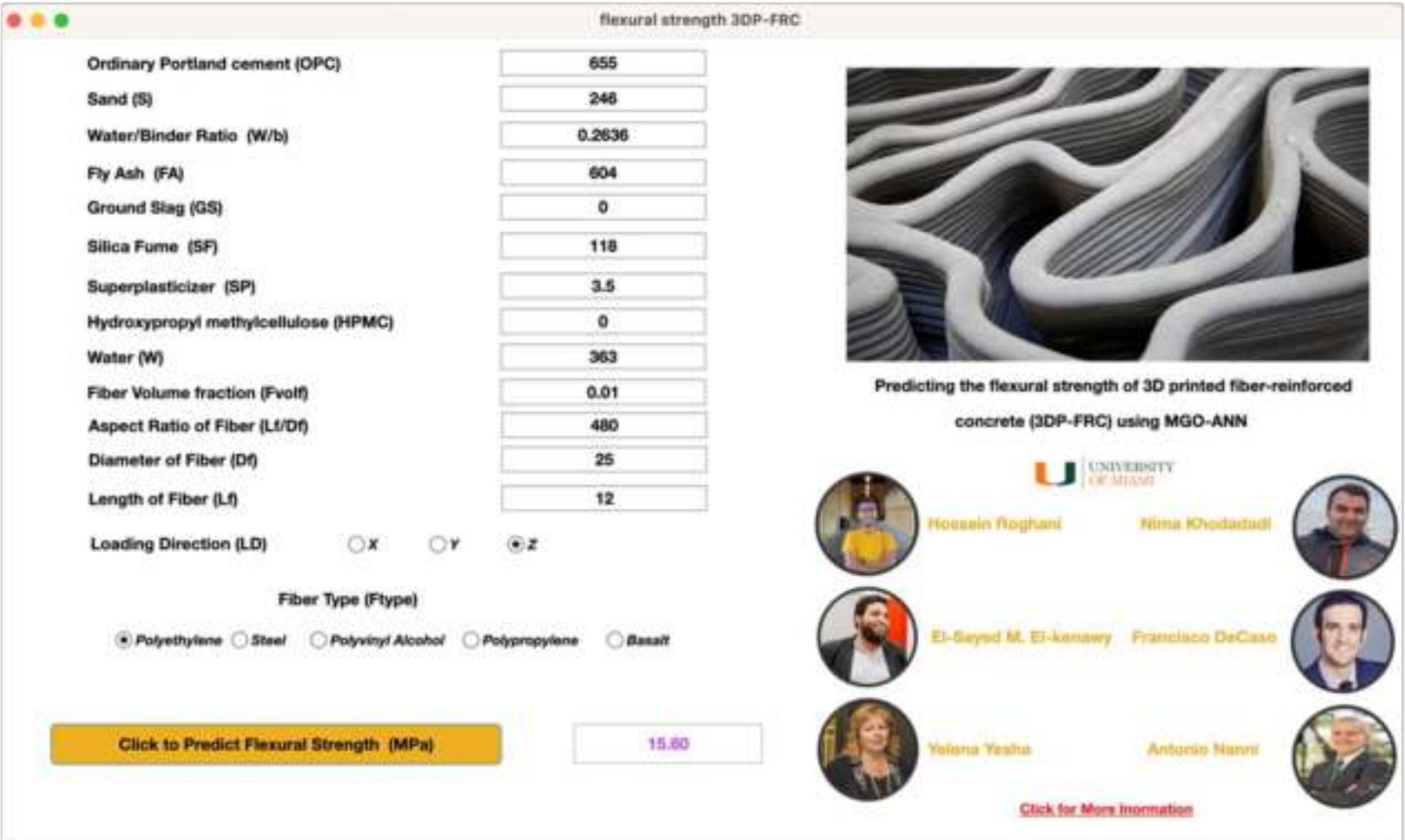

flexural strength 3DP-FRC
Ordinary Portland cement (OPC)
655
Sand (S)
246
Water/Binder Ratio (W/b)
0.2636
Fly Ash (FA)
604
Ground Slag (GS)
0
Silica Fume (SF)
118
Superplasticizer (SP)
3.5
Hydroxypropyl methylcellulose (HPMC)
0
Water (W)
363
Fiber Volume fraction (Fvolf)
0.01
Aspect Ratio of Fiber (Lf/Df)
480
Diameter of Fiber (Df)
25
Length of Fiber (Lf)
12
Loading Direction (LD)
X
Y
Z
Fiber Type (Ftype)
Polyethylene
Steel
Polyvinyl Alcohol
Polypropylene
Basalt
Click to Predict Flexural Strength (MPa)
15.60
Predicting the flexural strength of 3D printed fiber-reinforced concrete (3DP-FRC) using MGO-ANN
Hossain Roghani
Nima Khodadadi
El-Sayed M. El-kenawy
Francisco DeCaso
Yelena Yesha
Antonio Nanni
Click for More Inormation

Data-Driven PSO-CatBoost Machine Learning Model to Predict the Compressive Strength of CFRP- Confined Circular Concrete Specimens

INTRODUCTION

FRP-Confined Concrete

- Rising interest in using FRP in the construction sector.
- Significant amount of experimental and analytical research.
- Lateral confinement of concrete columns increases ductility and strength.
- Enhances the durability and service life concrete elements.
- Two major categories of research: 1) experimental investigations; and 2) analytical investigations (model development)

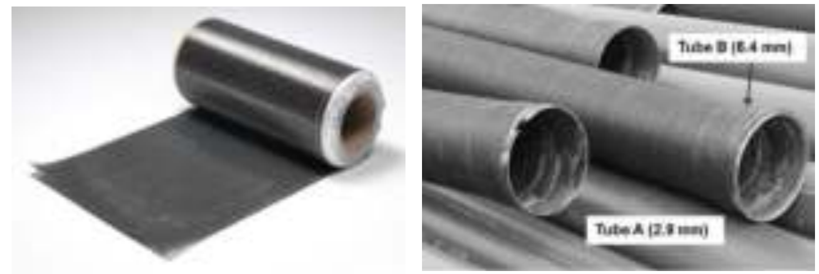

Fig.1. CFRP wrap[1] and filament wound FRP tubes[2].

Fig.2. CFRP-wrapped Columns for bridge retrofitting[3,4].

[1] FRP Carbon Fibre Reinforcing Systems | Strong-Tie | Together we're helping build safer stronger structures (strongtie.com.au).
[2] Ahmed, A. A., & Masmoudi, R. (2018). Journal of Composites Science, 2(4), 57.
[3]ctech-carbon-wrap-frp-Columns-bridge-Retrofitting-concrete | CTech-LLC

CONSTRUCTION OF MODEL

Particle Swarm Optimization-

Categorical Boosting (PSO-CatBoost)

- Gradient Boosted Decision Trees (GBDTs), an ensemble method based on decision trees.
- This study is focused on one of the GBDT variations, namely Categorical Boosting (CatBoost), which is improved to generate a prediction model.

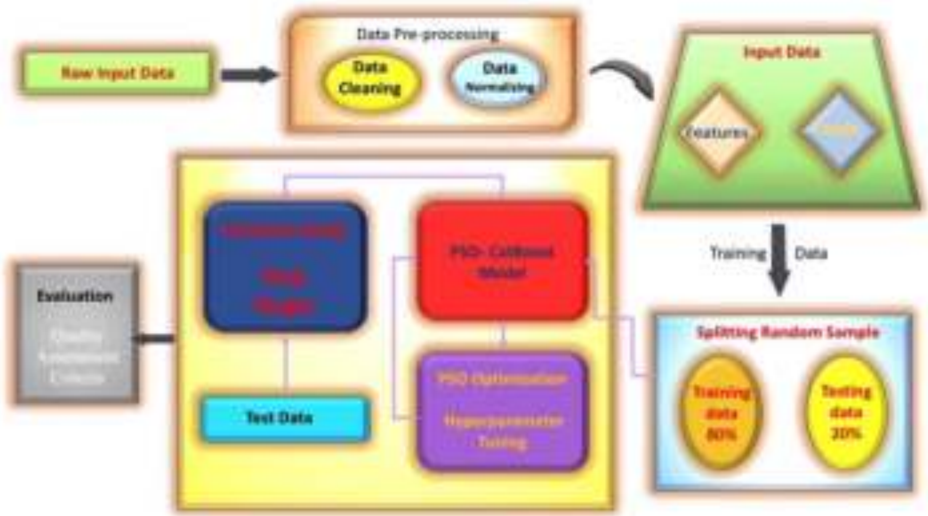

Fig.9. The architectural detail PSO-CatBoost Model.

RESULTS AND DISCUSSION

Predicted Vs. Observed (training data)

- Training data and the prediction model exhibit exceptional congruence.
- High degree of overlap indicates the model's ability to accurately reflect and predict the underlying patterns.
- Error margins for the training data indicate a high level of accuracy (most errors are less than 0.025).
- High R-squared value of 0.9898, signifying a strong relationship between independent and dependent variables.

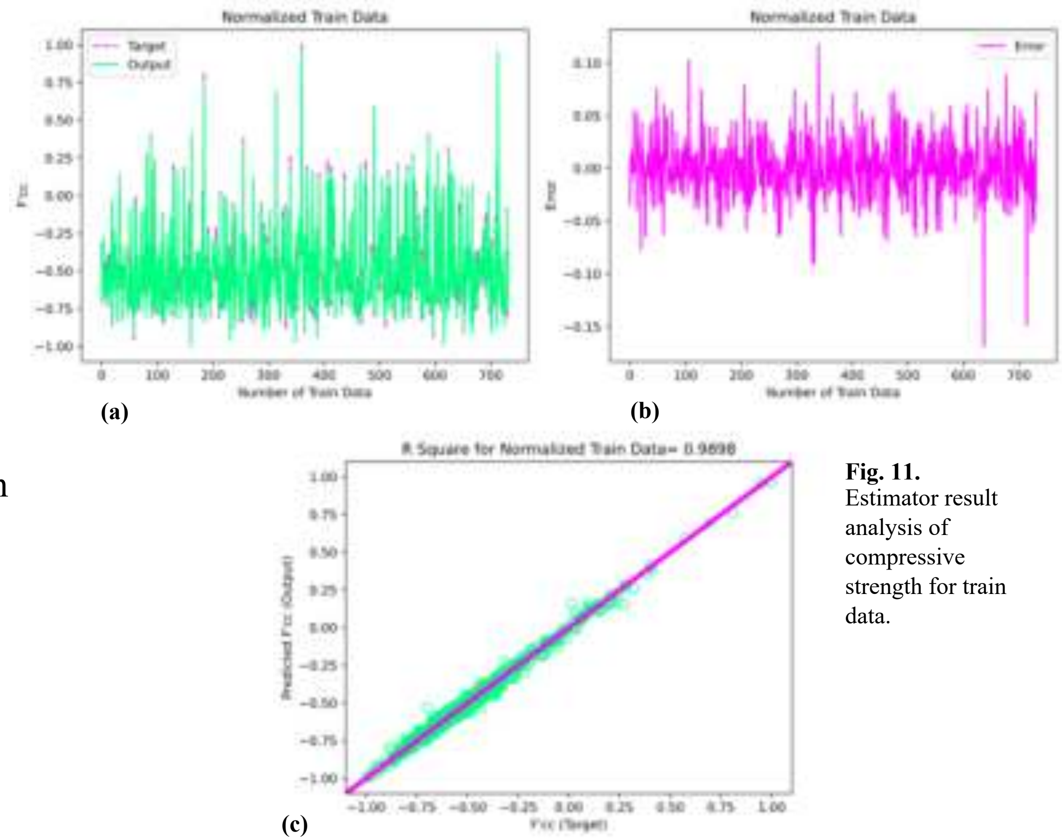

Fig. 11. Estimator result analysis of compressive strength for train data.

RESULTS AND DISCUSSION

Predicted Vs. Observed (test data)

- Test data closely matches the target or desired output (model has been effectively trained and is able to generalize well to unseen data).
- Model is not overfitting to the training data.
- Error is evaluated by comparing predicted outcomes with actual data.
- R-squared value of 0.9572 obtained for the test data.

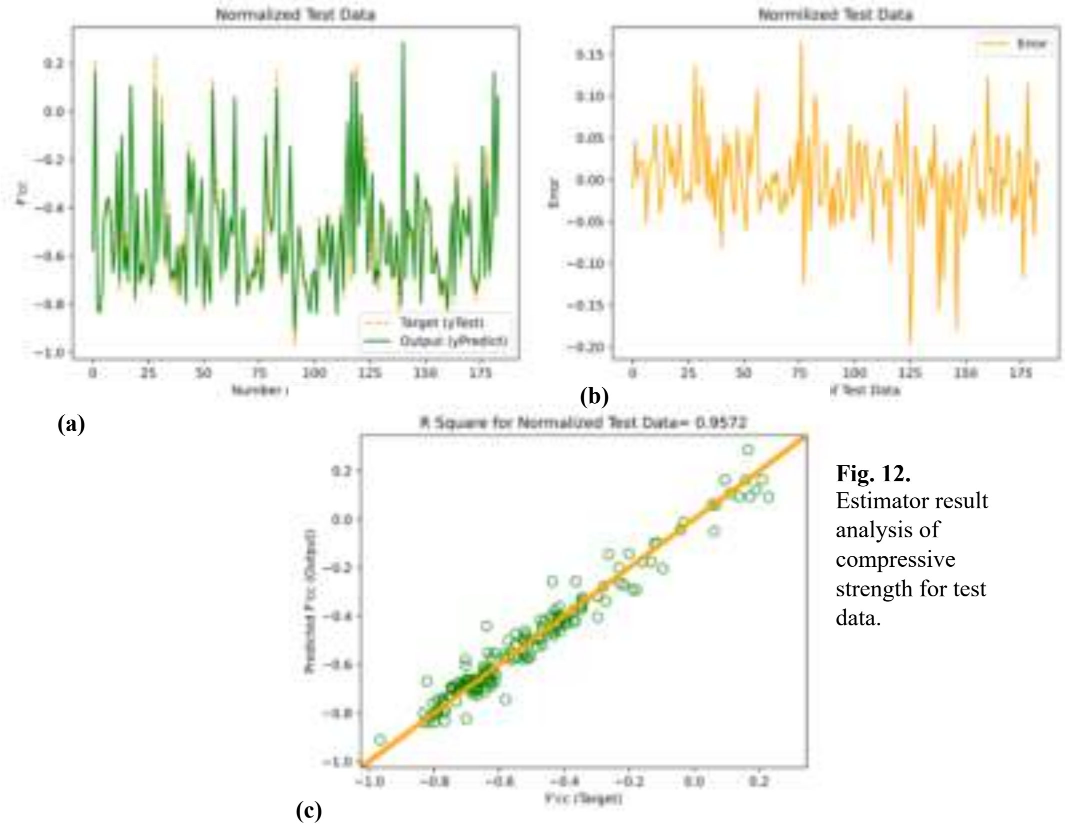

Fig. 12. Estimator result analysis of compressive strength for test data.

RESULTS AND DISCUSSION

Visualize Model Outcomes

- Scatter plot Figure 13a. visualizes the differences between the predicted and actual values.
- Figure 13b. show patterns in the model's residuals.
- R-squared value of 0.9847 obtained and represented in Figure 9c.
- Line of correlation very closely resembled the ideal scenario of y = x (high degree of accuracy in predictions).

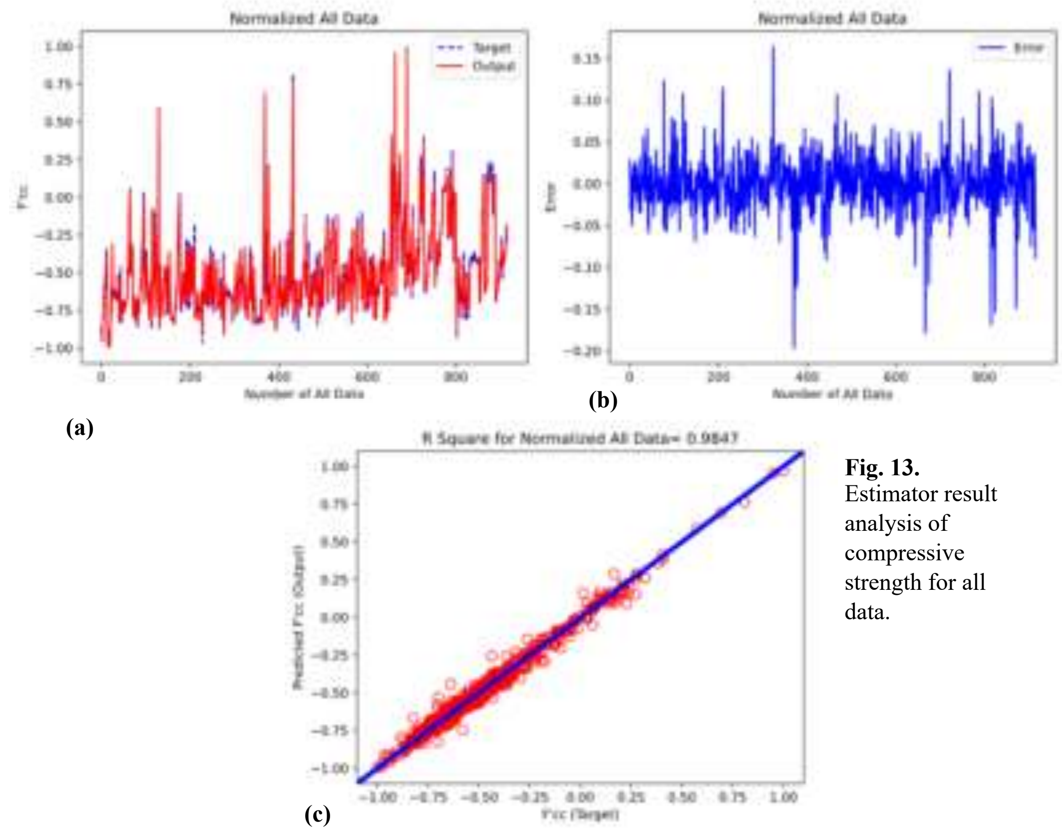

(a) (b) (c)

Fig. 13. Estimator result analysis of compressive strength for all data.

RESULTS AND DISCUSSION

Comparison of Models

- Proposed model compared with Mandal et al., Karbhari et al. and Lilliston and Jolly.
- PSO-CatBoost model shows much better performance.

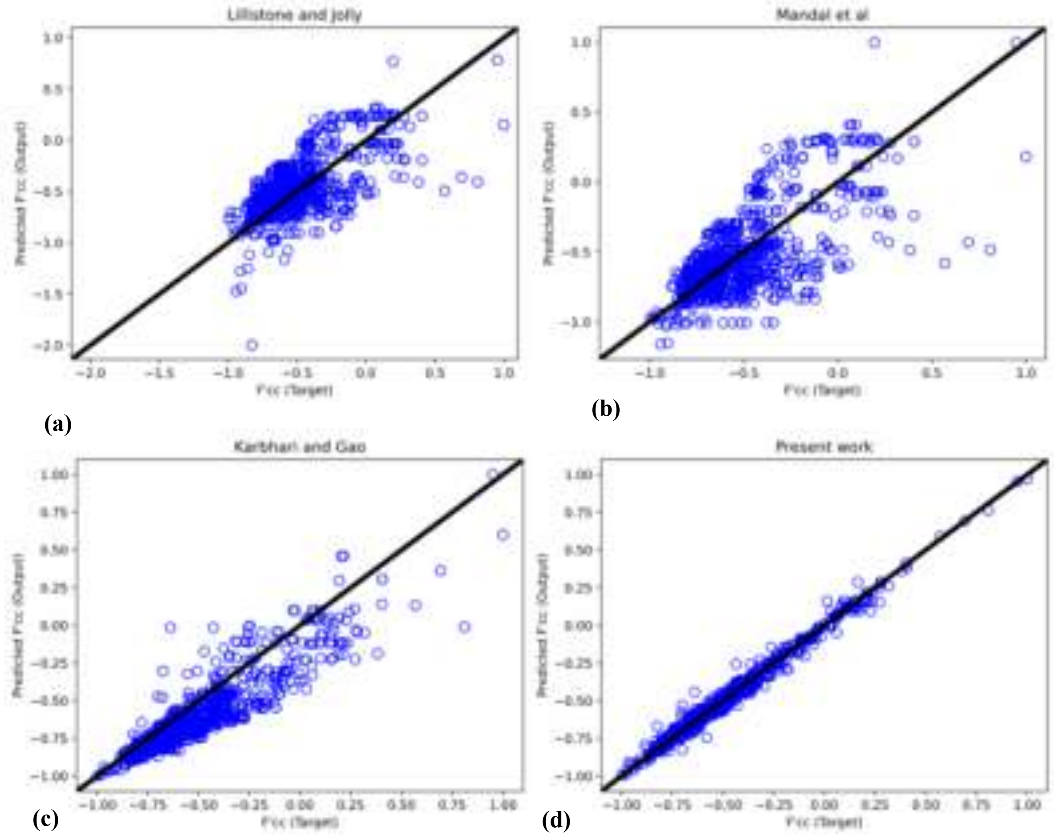

Fig. 15. Comparison of present work with other methods.

RESULTS AND DISCUSSION

Comparison of Models

- PSO-CatBoost predicts quite accurately and outperforms other models.
- Proposed model obtains an RMSE of 0.0347, an MSE of 0.0012, and an MAE of 0.0250.
- These values are noticeably lower than those for empirical equations.
- R-squared value of the proposed model is noticeably higher than those for empirical equations.

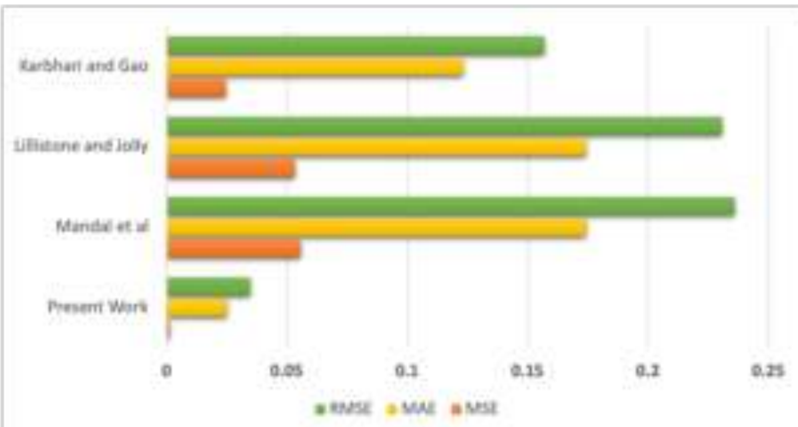

Fig. 16. Comparing RMSE, MAE, and MSE metrics for all data with all models.

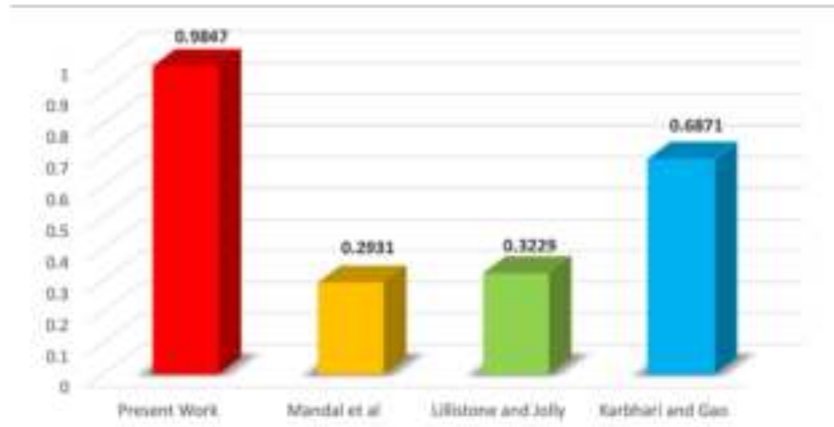

Fig. 17. Comparing R-Squared metric for all data with all models.

RESULTS AND DISCUSSION

Taylor Diagram

- R-squared, RMSD, and SD of the patterns are represented in Taylor diagram.
- Proposed model performs better than other models in most cases (greater correlation coefficient, smaller standard deviation, and lower RMSE).

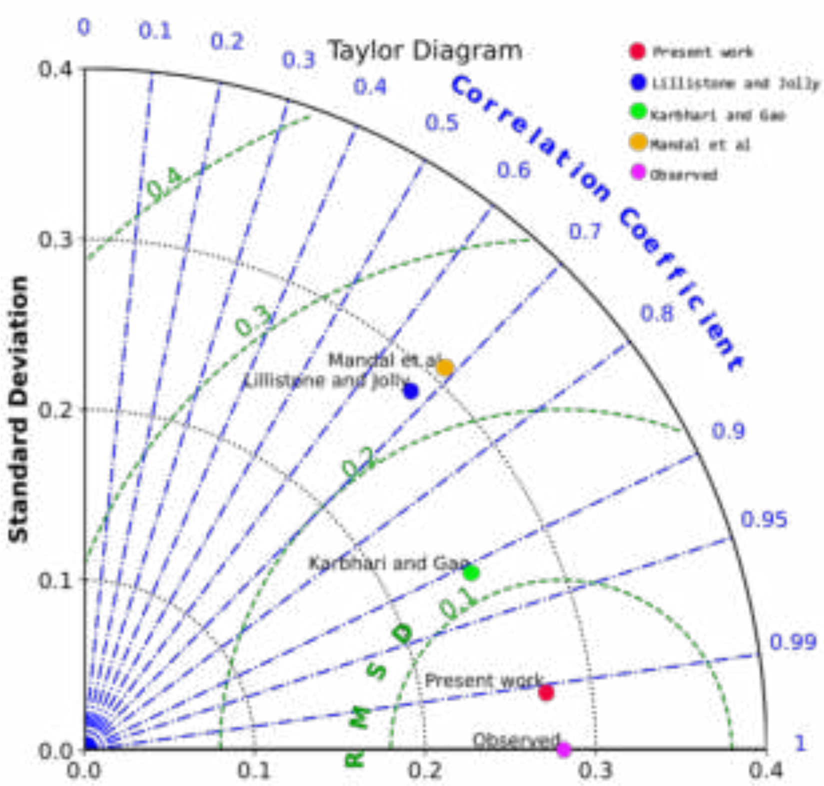

Fig. 18. Taylor Diagram.

Applied Computing and Intelligence
https://www.aimspress.com/journal/aci

Applied Computing and Intelligence
3 (2): 116–144
DOI: 10.3934/aci.2023007
Received: 23 May 2023
Revised: 21 September 2023
Accepted: 26 September 2023
Published: 07 October 2023

Research article

The Mountain Gazelle Optimizer for truss structures optimization

Nima Khodadadi[1,*], El-Sayed M. El-Kenawy[2], Francisco De Caso[1], Amal H. Alharbi[3], Doaa Sami Khafaga[3] and Antonio Nanni[1]

[1] Department of Civil and Architectural Engineering, University of Miami, Coral Gables, FL, USA; nima.khodadadi@miami.edu, fdecaso@miami.edu, nanni@miami.edu
[2] Department of Communications and Electronics, Delta Higher Institute of Engineering and Technology, Mansoura 35111, Egypt; skenawy@ieee.org
[3] Department of Computer Sciences, College of Computer and Information Sciences, Princess Nourah bint Abdulrahman University, P.O. Box 84428, Riyadh 11671, Saudi Arabia; ahalharbi@pnu.edu.sa, dskhafga@pnu.edu.sa

Decision Analytics Journal

A comparison performance analysis of eight meta-heuristic algorithms for optimal design of truss structures with static constraints

Nima Khodadadi, Ayhike Özyüksel Çiftçioğlu, Seyedali Mirjalili, Antonio Nanni

buildings

MDPI

Article

Optimizing Truss Structures Using Composite Materials under Natural Frequency Constraints with a New Hybrid Algorithm Based on Cuckoo Search and Stochastic Paint Optimizer (CSSPO)

Nima Khodadadi *, Ehsan Harati, Francisco De Caso and Antonio Nanni

Presentations at ACI

Meta-Heuristic Optimization: Effective Machine Learning Techniques for Concrete Structures

Presented By: Nima Khodadadi
Affiliation: University of Miami
Description: A fundamental aspect of nature-based systems is the ability to optimize. Similarly, since ancient times humans have had a tenancy to naturally focus on optimizing their activities making them more feasible, economical, functional, and practical. Analogously in structural engineering design "structural optimization" is a simulation-driven design technique that identifies and explores high-potential designs, while also rejecting low- potential ones early in the design phase, aiming to solve problems of structural design. However, such optimization methods have not been widely used in the design of concrete structures. This is in part be due to the design and construction of concrete structures involves complex processes, and optimization techniques face serious challenges. Nevertheless, modern meta-heuristic methods of optimization, can provide higher-level procedures or heuristic designed to find, generate, tune, or select a heuristic (partial search algorithm) that may provide a sufficiently good solution to an optimization problem or a machine learning problem. In Machine Learning, historical data is used to teach and train the system developed, in order to be able to better predict future behavior. In meta-heuristic approaches, the need to have historical data is not necessary. Instead, the system generates random data and uses them to find an optimal solution that satisfies all the constraints. This iterative process continues until the algorithm reaches a defined criteria. Meta-heuristic algorithms are traditionally used in non-deterministic polynomial-time based problems, where for a given time and effort obtaining a "good" solution is preferred to an "optimum" one. To this end, meta-heuristic algorithms help select the optimal parameters for machine learning and deep learning techniques to train and improve the model's performance. Concrete structures optimization often aims to minimize costs, including those related to concrete material and reinforcement.

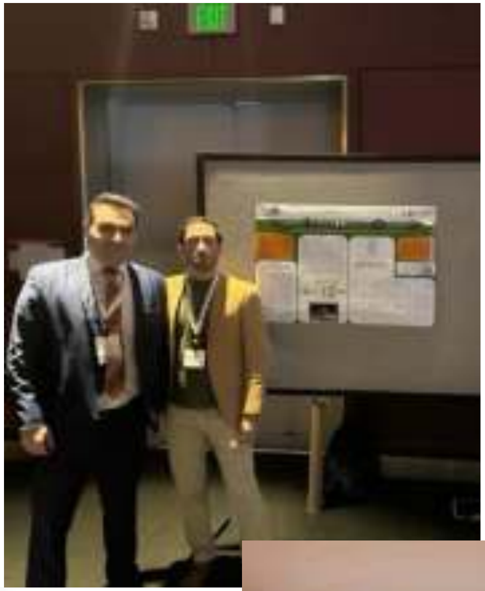

PSO-CatBoost Machine Learning Model to Predict the Compressive Strength of CFRP- Confined Circular Concrete Columns

Presented By: Nima Khodadadi
Affiliation: University of Miami
Description: In the last two decades, extensive experimental research has been conducted to understand the behavior of Fiber-Reinforced Polymer (FRP)-confined concrete columns. This paper presents a novel model based on Particle Swarm Optimization (PSO) and the CatBoost algorithm (PSO-CatBoost) to predict the ultimate compressive strength of Carbon FRP (CFRP) confined circular concrete columns. A comprehensive database was compiled from 1503 test results across 98 studies published between 1991 and mid-2023 with different features. This data was used to create training and test sets for model validation using criteria such as mean square error, root mean square error, and correlation coefficient. The deep analysis revealed crucial insights into significant parameters affecting FRP-confined concrete behavior. It is shown that the predictions of the proposed model are in close agreement with the test results, and the model provides improved predictions of the ultimate conditions of FRP-confined concrete compared to any of the existing models.

Under Review

- 1. Data-Driven PSO-CatBoost Machine Learning Model to Predict the Compressive Strength of CFRP-Confined Circular Concrete Specimens

2. Predicting the flexural strength of 3D printed fiber-reinforced concrete (3DP-FRC) using efficient training of artificial neural networks with the meta-heuristic algorithm

3. Modeling the compressive strength of geopolymer recycled aggregate concrete using ensemble machine learning

4. Fiber-Reinforced Polymer (FRP) in Concrete: A Comprehensive Survey

NEWS AND EVENTS
COLLEGE OF ENGINEERING

Miami Engineering Doctoral Student Receives National Science Foundation INTERN Award

Nima Khodadadi wants to use AI and machine learning to make concrete more sustainable.

Nima Khodadadi, Ph.D. civil engineering doctoral student at the University of Miami College of Engineering. (Photo: Eva Hart/University of Miami)

UNIVERSITY OF MIAMI
GRADUATE SCHOOL

September 21, 2023

Nima Khodadadi
VIA e-mail
nimakhodadadi@miami.edu

Dear Nima,

Congratulations! I am pleased to inform you that you are the recipient of the **Wulkan Family American Public Transportation Foundation Endowed Scholarship** for the 2023-2024 academic year in the amount of $2,500.

This scholarship may be used to offset your Fall 2023 and/or Spring 2024 tuition balances, be applied toward the mandatory student fees, and/or be used to support you presenting at a scholarly conference in Fall 2023 or Spring 2024. If you accept this award, we will then discuss with you how you intend to use the award within these limits. You must maintain full-time enrollment in Fall 2023 and Spring 2024 to receive the scholarship.

Please indicate your acceptance of this offer by signing and returning this letter to me no later than Friday, **September 29, 2023.** You may e-mail me a signed copy of this letter to pabril@law.miami.edu (with cc to Ana Pineda and Sabrina Mendoza at apineda@miami.edu and sabrinamendoza@miami.edu respectively).

Please also review the enclosed "Consent to Release of Personally Identifiable Information." The Donor, Mr. Wulkan, would like to receive information on the recipient of the scholarship. The Graduate School would also like to announce you as the recipient of this scholarship. If you agree to signing the Consent form, please return it along with the signed offer letter.

Sincerely,

Patricia Sanchez Abril, J.D.
Interim Dean of the Graduate School

Contact me

Center for Integration of Composites into Infrastructure

Thank U

NSF

FICEM

Center for Integration of Composites into Infrastructure

IAB Meeting, Fall 2023

#1 Using Machine Learning and Artificial Intelligence to Implement FRP in Infrastructure: Areas and Opportunity

L.I.F.E. forms

Center for Integration of Composites into Infrastructure

IAB Meeting, Spring 2023

#2 Composites for infrastructure Applications: Areas of Improvement in the ACI 440.11 Code

Composites for infrastructure Applications: Areas of Improvement in the ACI 440.11 Code

Research Group

Zahid Hussain
Graduate Student

Antonio Nanni
Professor and Chair

Objective

Areas of improvement in the ACI 440.11 Code;
Possible modifications

- Development length equation
  - Bond strength
  - Stirrup's confinement
  - Suggested updates
- Punching shear equation
  - ACI 440.11 shear equation (Background)
  - Suggested modifications

Development Length Equation

ACI 440.11

$$l_d = \frac{d_b\left(\frac{f_{fr}}{0.083\sqrt{f_c'}} - 340\right)\omega_t}{13.6 + \frac{c_b}{d_b}}$$

ACI 318-19

$$l_d = d_b \frac{f_y}{1.1\lambda\sqrt{f_c'}} \frac{\omega_t \omega_e \omega_s}{\left(\frac{c_b + K_{tr}}{d_b}\right)}$$

$$K_{tr} = \frac{40A_{tr}}{s d_b}$$

$$\frac{c_b + K_{tr}}{d_b} \leq 2.5 d_b$$

$l_d =$	Development length of a bar in tension, mm
$d_b =$	Diameter of bar, mm
$f_{fr} =$	Stress in the bar, MPa
$f_c' =$	Concrete compressive strength in MPa
$c_b =$	Lesser of: (a) the distance from center of a bar to nearest concrete surface, & (b) one-half the center-to-center spacing of bars being developed, mm
$\lambda =$	Modification factor based on type of concrete
$K_{tr} =$	Transverse reinforcement index, mm
$\omega_t \omega_e \omega_s =$	Modification factors based on reinforcement location, coating, & size

Development Length Equation

8 Beams without stirrups

8 Beams with stirrups at 100 mm, and 200 mm c/c.

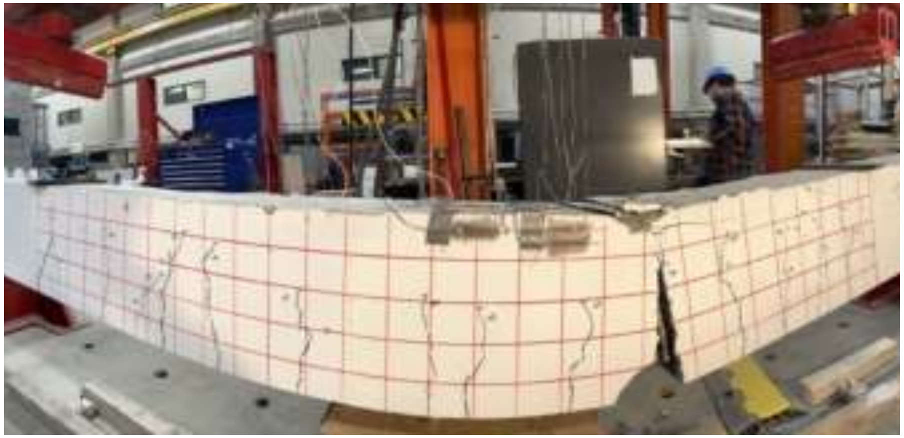

Experimental results

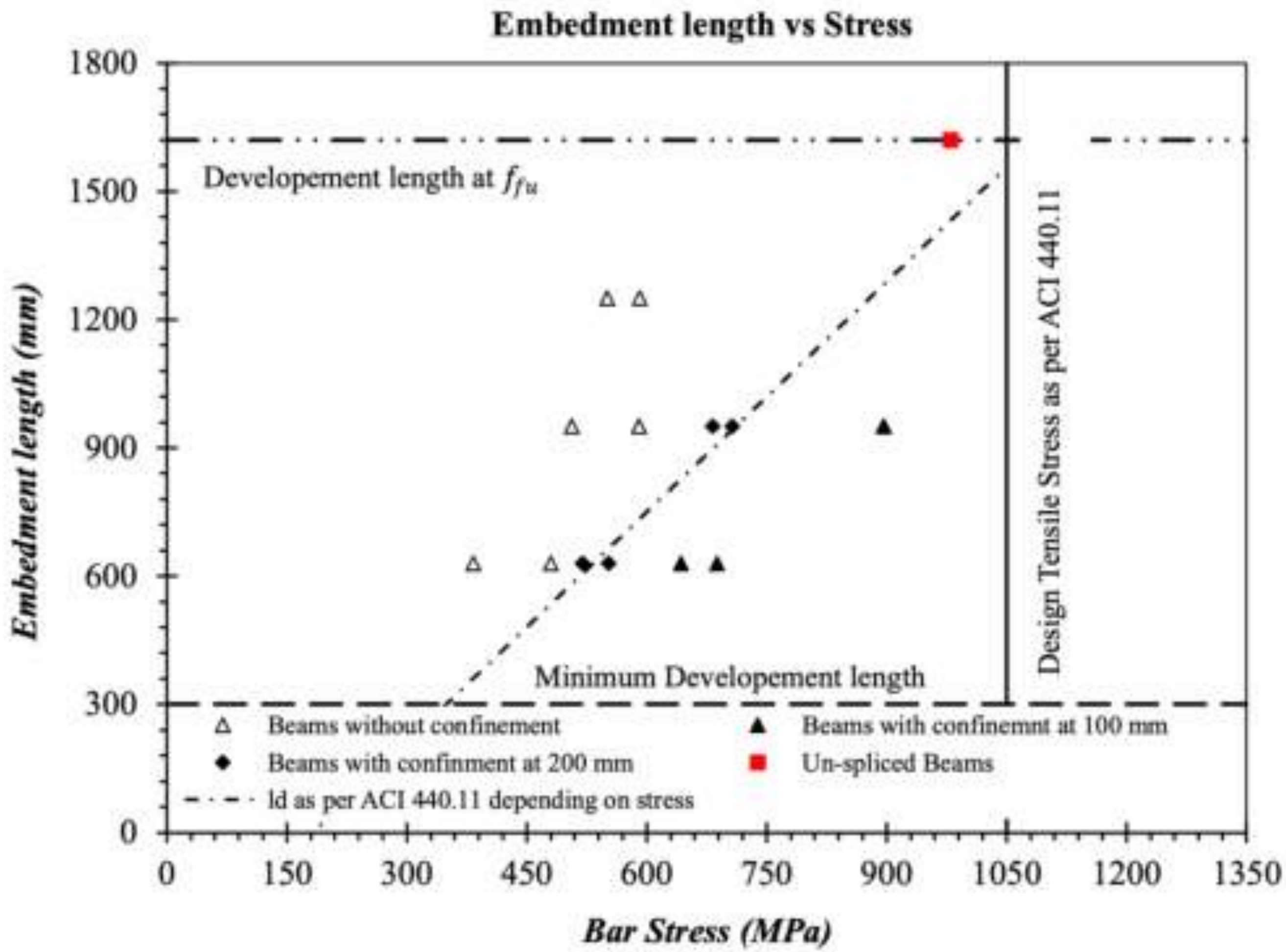

Results and suggestions

Effect of stirrups on bond strength

- ❖ Increased stress at failure
- ❖ Decreased slip
- ❖ Increased bond strength

Suggestions

❖ $K_{tr} = f_R \frac{A_{tr} f_{yt}}{s d_b}$ => $f_R = 0.11$

Taking sand coated bars as reference, a single factor could be adopted in the code as minimum, & for better performing bars manufacturer's data could be adopted.

Punching Shear Equation in ACI 440.11

$$v_c = 0.83\lambda_s k_{cr}\sqrt{f_c'}$$ (i) Ospina et al. 2003

$$v_c = 0.13\lambda_s\sqrt{f_c'}$$ (ii) Nanni et al. 2014

v_c =	Stress corresponding to nominal two-way shear strength provided by concrete, MPa
λ_s =	Size effect factor
k_{cr} =	Ratio of elastic cracked transformed neutral axis depth to effective depth
f_c' =	Concrete compressive strength, MPa

Punching Shear Equation in ACI 440.11

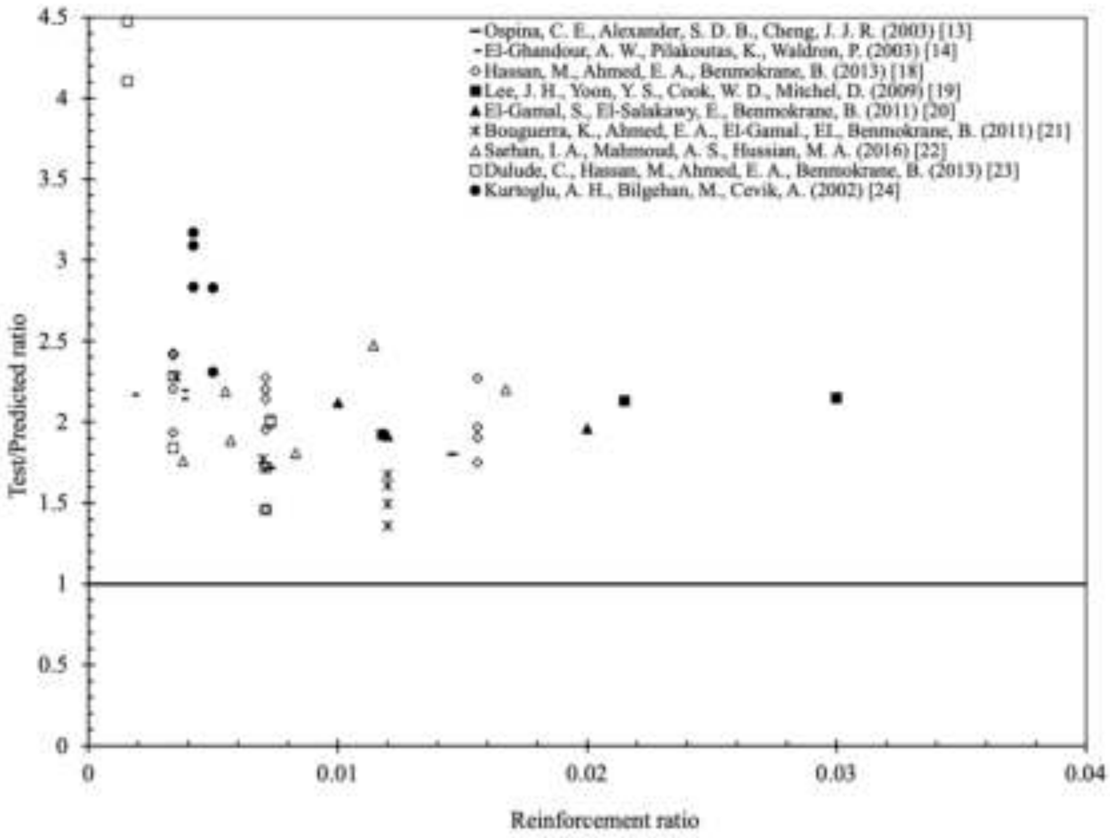

- 51 GFRP-RC slabs
- Test-to-predicted ratio 1.8
- Standard deviation 0.35
- Coefficient of variation 20%

Proposed Modifications

$$v_c = 0.17\lambda_s\sqrt{f_c'}$$

v_c =	Stress corresponding to nominal two-way shear strength provided by concrete, MPa
λ_s=	Size effect factor
f_c'=	Concrete compressive strength in MPa

- 51 GFRP-RC slabs
- Test-to-predicted ratio 1.3
- Standard deviation 0.26
- Coefficient of variation 20%

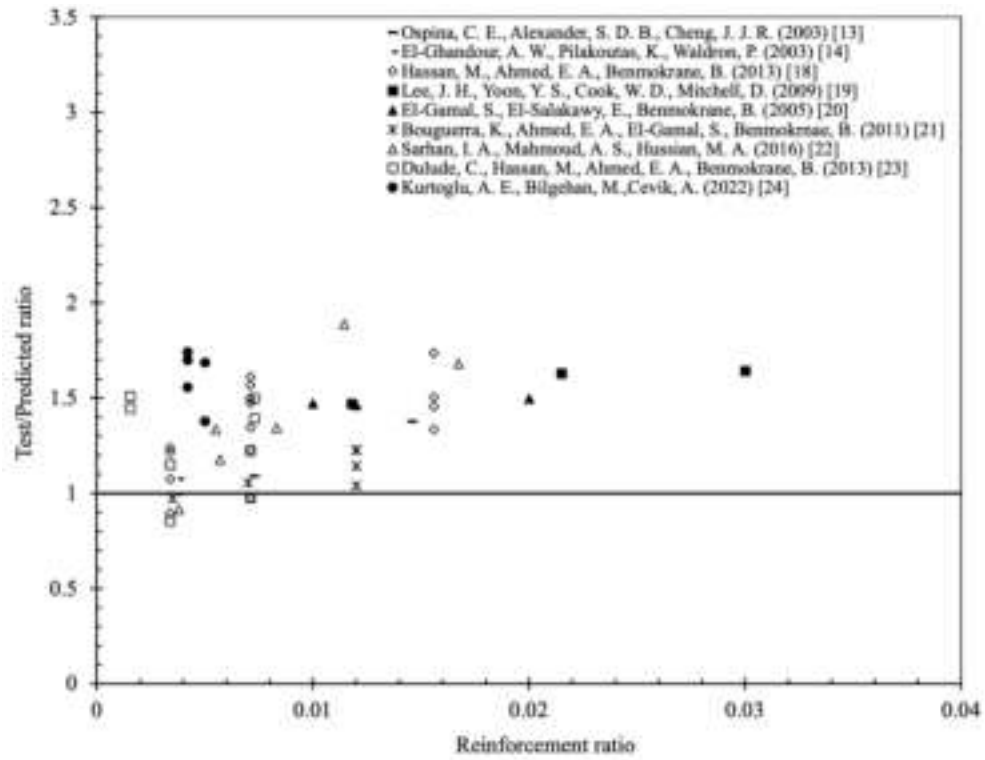

Center for Integration of Composites into Infrastructure

IAB Meeting, Fall 2023

#2 Composites for infrastructure Applications: Design optimization of GFRP-RC footings

L.I.F.E. forms

Center for Integration of Composites into Infrastructure

IAB Meeting, Fall 2023

#3 Solutions for the Implementation of Composites Through Experimental Testing and Design:

Part A: Push-off Test

Part B: Compressive behavior of GFRP bars

PART A: Push-off Test

Research Group

Camilo Vega
Graduate Student

Amin Mirdarsoltany
Graduate Student

Antonio Nanni
Professor and Chair

Francisco De Caso
Principal Scientist

Objective

- Experimentally determine the contribution of GFRP bars to the mechanism of shear transfer by using the push-off test. Propose a model representing this behavior.

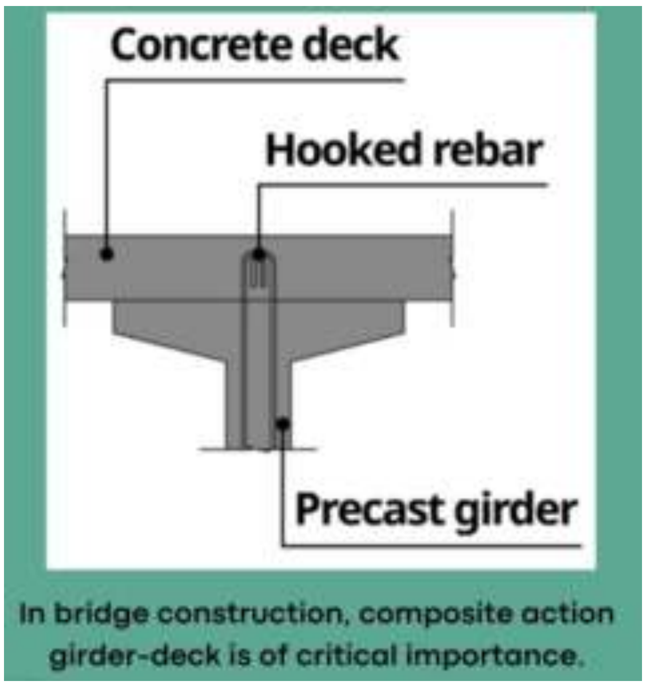

Application:
Use of GFRP for shear transfer mechanism in prestressed concrete bridge girders

Among critical applications is where a PC girder has GFRP auxiliary reinforcement.

Methodology

- Phase 1: Three groups of specimens were constructed monolithically; without reinforcement, steel stirrups and GFRP stirrups.

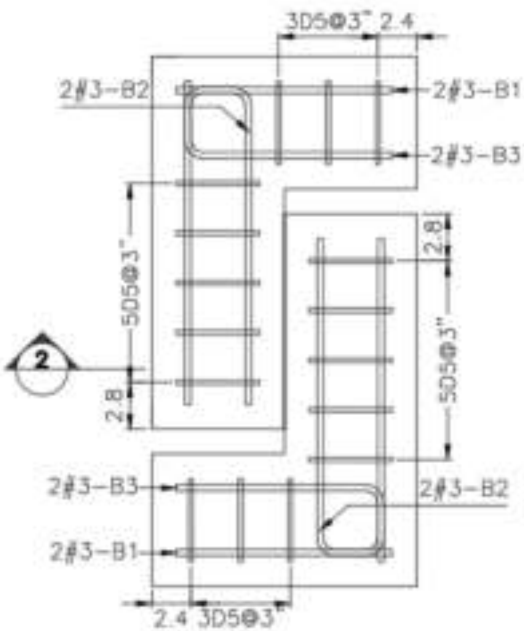

Push-Off Specimen without reinforcement crossing the shear plane

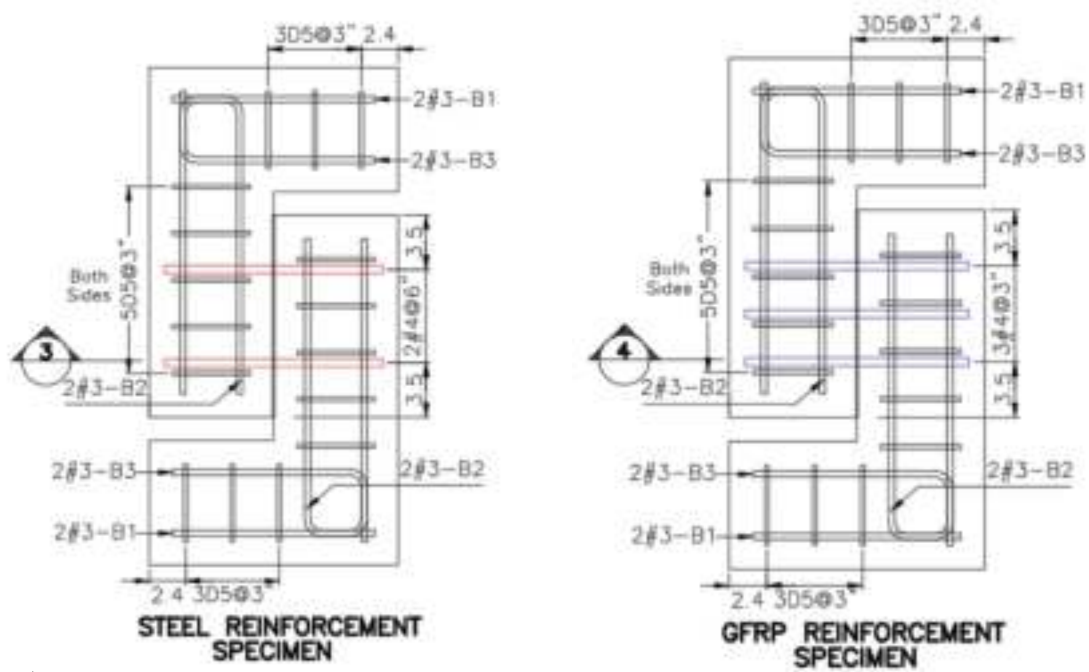

Push-Off specimen with reinforcement crossing the shear plane

Methodology

- Phase 2: Additional specimens were constructed with a different reinforcement ratio and in two stages to consider a cold joint condition.

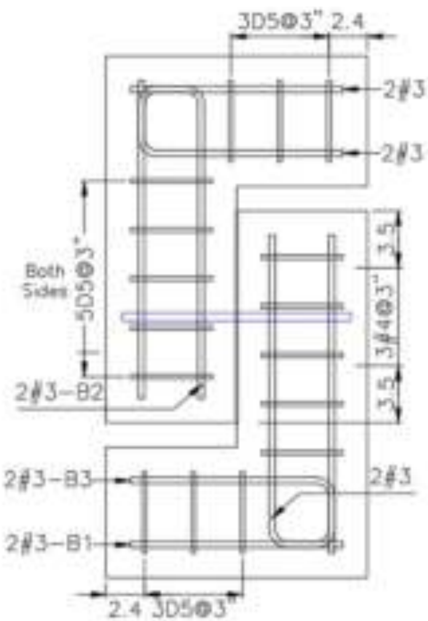

Monolithically and different ρ_f

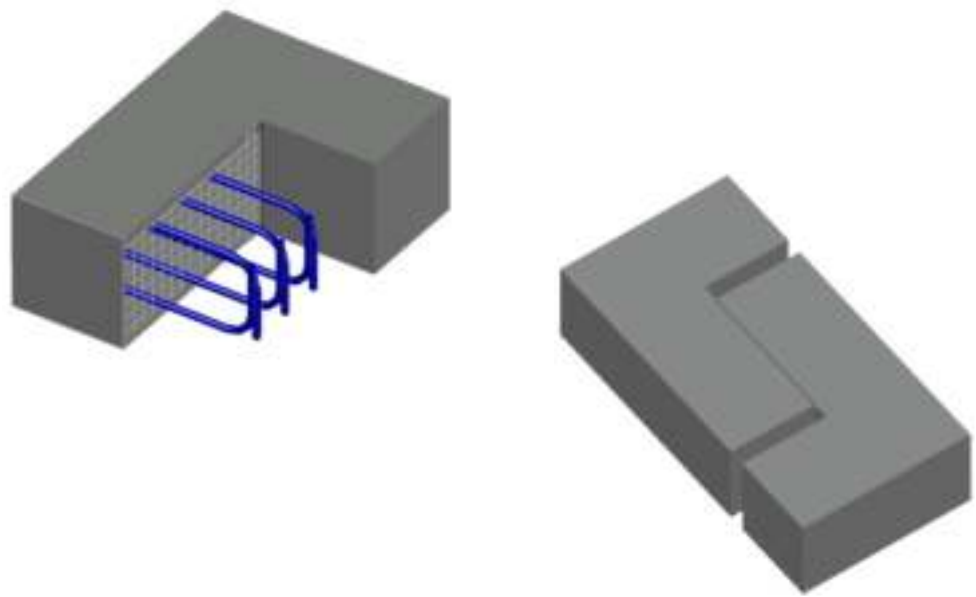

Specimens with cold joint condition

Push-off test set-up

Results

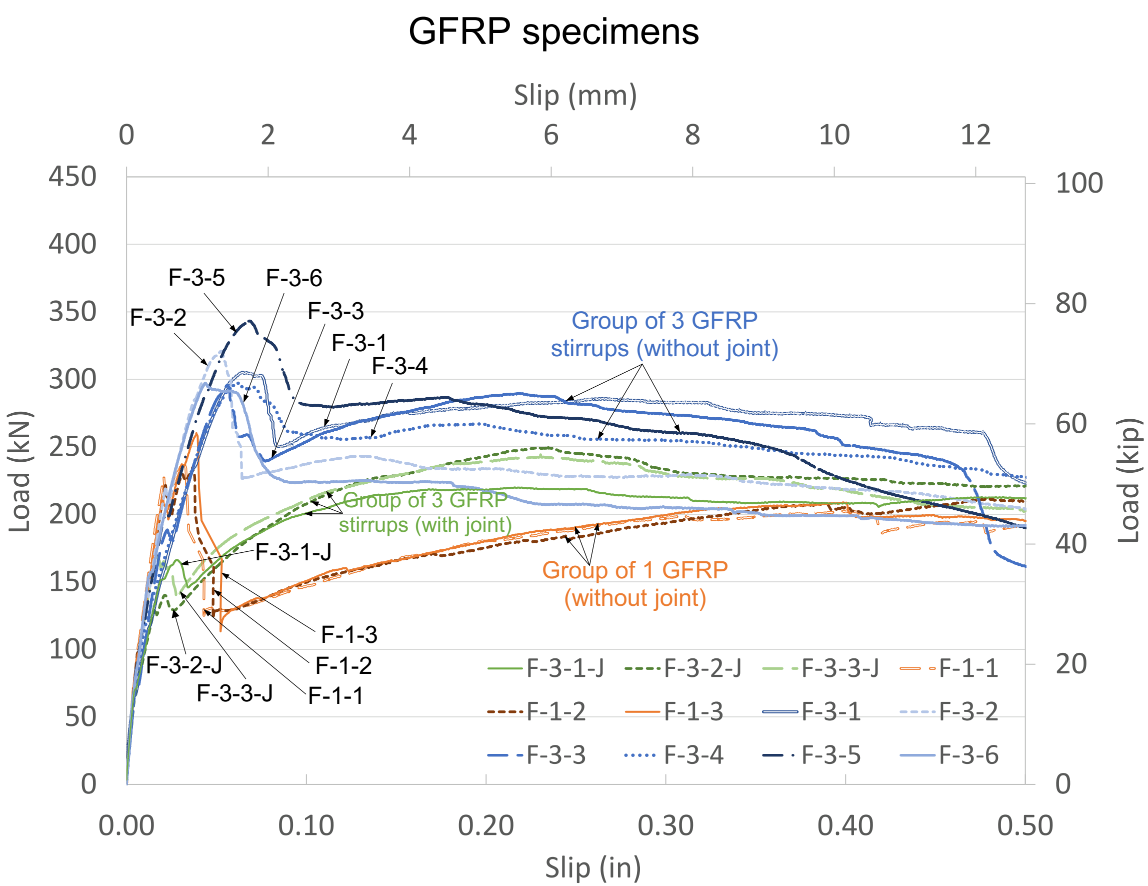

GFRP specimens
Slip (mm)
Load (kN)
Load (kip)
Slip (in)
Group of 3 GFRP stirrups (without joint)
Group of 3 GFRP stirrups (with joint)
Group of 1 GFRP (without joint)
F-3-5
F-3-6
F-3-2
F-3-3
F-3-1
F-3-4
F-3-1-J
F-1-3
F-1-2
F-3-2-J
F-3-3-J
F-1-1
F-3-1-J F-3-2-J F-3-3-J F-1-1
F-1-2 F-1-3 F-3-1 F-3-2
F-3-3 F-3-4 F-3-5 F-3-6

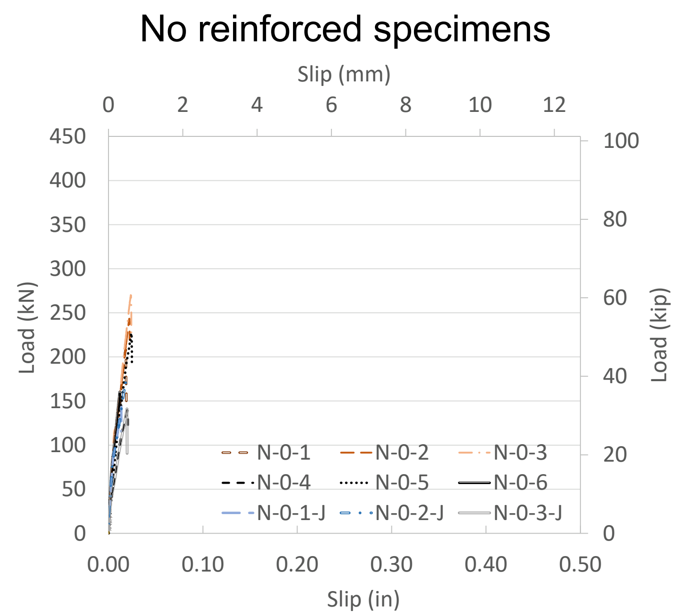

No reinforced specimens
Slip (mm)
Load (kN)
Load (kip)
Slip (in)
N-0-1 N-0-2 N-0-3
N-0-4 N-0-5 N-0-6
N-0-1-J N-0-2-J N-0-3-J

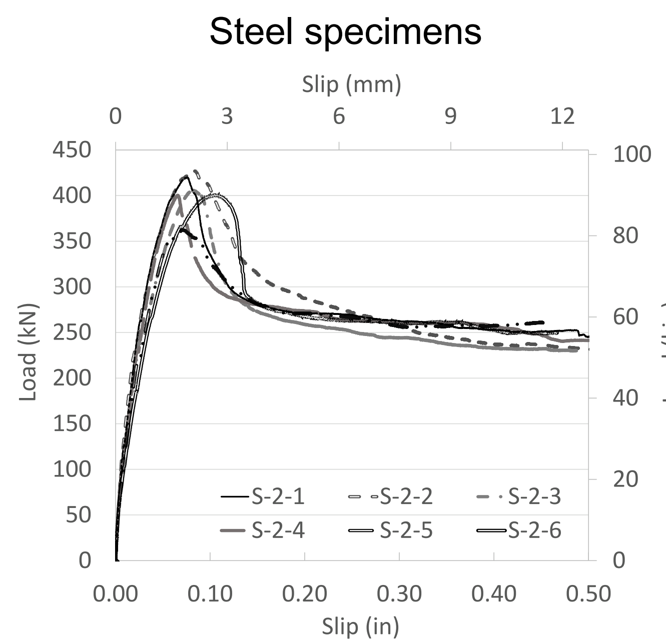

Steel specimens
Slip (mm)
Load (kN)
Load (kip)
Slip (in)
S-2-1 S-2-2 S-2-3
S-2-4 S-2-5 S-2-6

Failure Modes

- Either steel or GFRP (monolithically or cold joint), the contribution to the interface shear resistance and avoidance of sudden failure were significant.
- The typical mode of failure happened at the shear interface.
- Concrete spalling was noticed in certain specimens
- There were no instances of complete rupture of the bar cross-section.

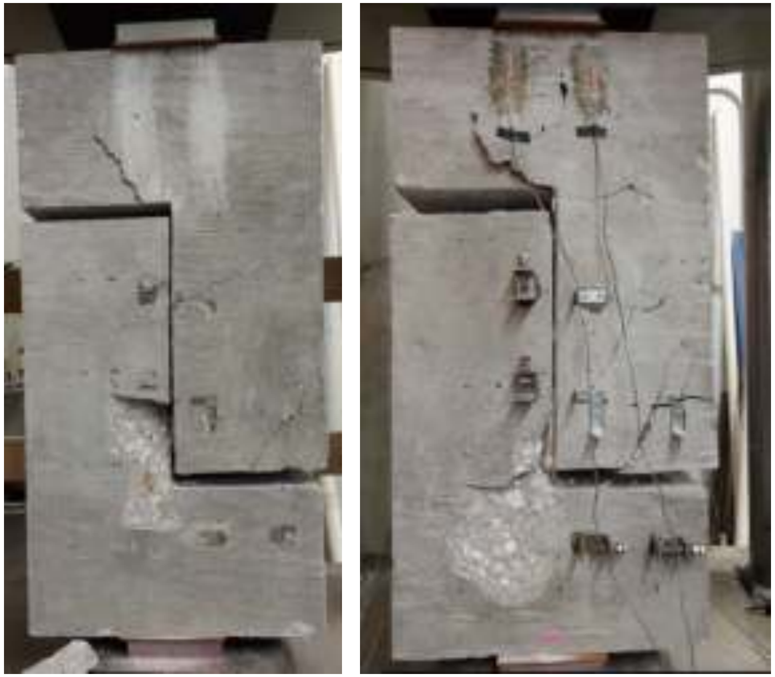

Typical failure mode

Future Directions

<u>Use of data collected from push-off specimens</u>

Propose a mathematical model to enhance the understanding of the variables involved in the shear transfer mechanism at the interface when using GFRP.

Multivariate linear regression model

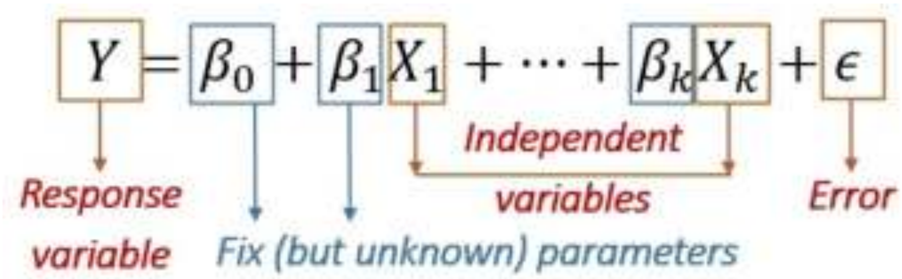

PART B: Compressive behavior of GFRP bars

Research Group

Mohammadamin
Mirdarsoltany
Graduate Student

Nima Khodadadi
Graduate Student

Hossein Roghani
Graduate Student

Antonio Nanni
Professor and Chair

Importance of evaluating compressive behavior of the FRP bars

Lack of standard test method for obtaining compressive behavior of FRP bars

Cause

- Divergencies between compressive test results
- Neglecting their contribution to designing compressive members

Some issues from previous proposed test setups in literature

- **Complicated** → Use of grout within steel tubes for placing FRP bars → Steel tube cannot be used again for another sample.
- **Edges of the samples were not parallel** → Causing buckling during the applying compressive load.
- **Approach to apply the load** → No specific procedure to apply the load on the center of the FRP bars.
- **Capturing the real behavior of FRP bars in compression** → Effect of steel tube's stiffness on the compressive behavior of FRP bars.

Proposed test method

- **Easy-to-use** → Plastic plugs replaced the grout in steel tubes
- **Parallel edges** → Using a special method for cutting the samples
- **Approach to apply the load** → Proposed test setup applies the load at the center of the sample
- **Capturing the real behavior of FRP bars in compression** → Using plastic plugs in steel tubes to minimize the effect of the steel stiffness on the compressive behavior of the bars.

Proposed test method

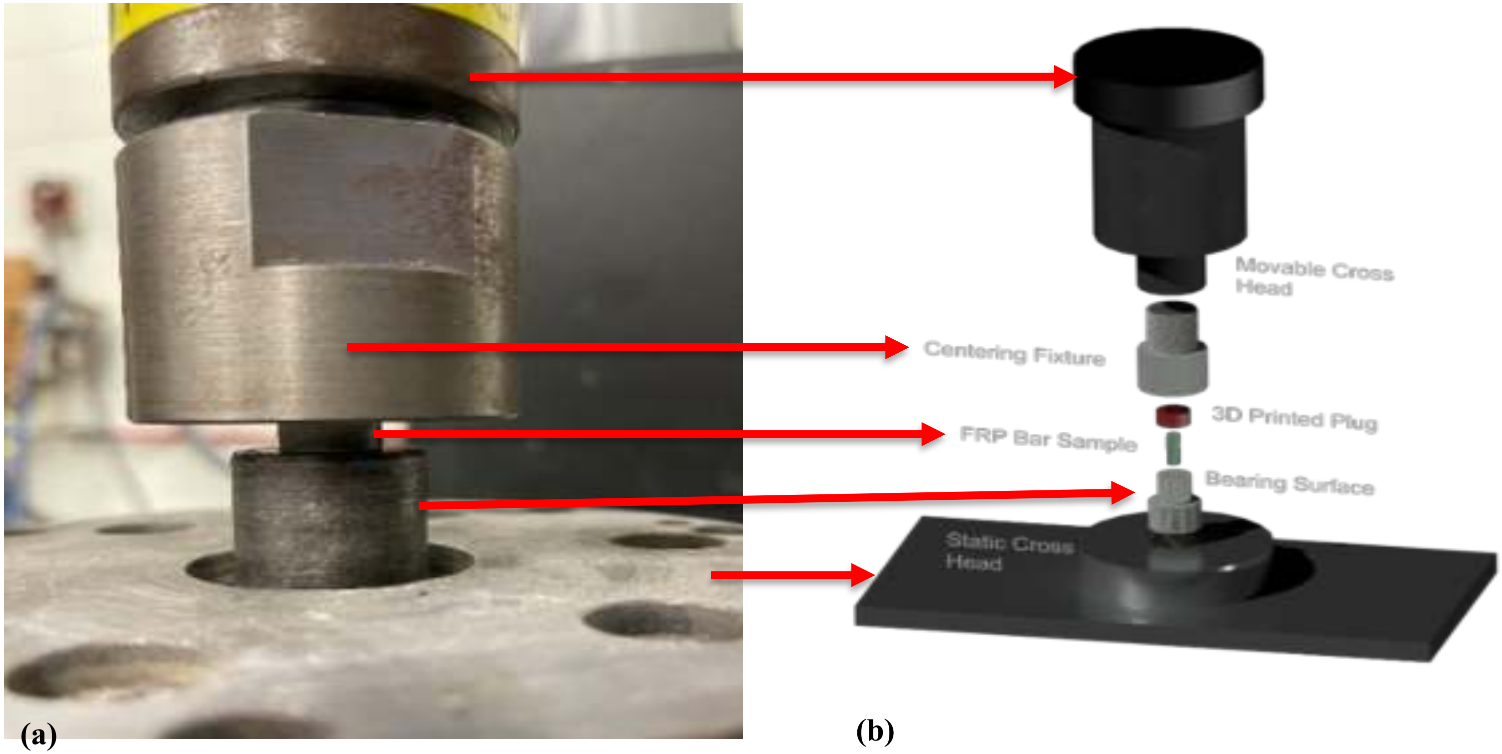

Compressive strength test setup: (a) actual test setup; and (b) schematic overview of test setup.

Investigated Parameters

- **Length-to-diameter ratio** → Length-to-diameter ratios of 2 and 4
- **Cutting approaches**→ Chop saw (CS) and Diamond blade wet saw (DWS)
- **Plug materials**→ Polylactic acid (PLA) and Thermoplastic Polyurethane (TPU)
- **GFRP bars manufacturer**→ Two different GFRP bars (G1 and G2) from different manufacturers were used

Results

Specimen ID	Type of Plug	Length-to-diameter ratio	Cutting type	Average compressive strength	Average tensile to compressive strength
G1-T-P-4-CS	PLA	4	CS	612.8	1.7
G1-T-P-4-DWS			DWS	847.2	1.2
G2-T-P-4-CS			CS	474.4	2.4
G1-T-P-2-CS		2		705.7	1.5
G1-T-P-2-DWS			DWS	851.4	1.2
G2-T-P-2-CS			CS	530	2.1
G2-T-P-2-DWS			DWS	730	1.6
G1-L-P-2-CS			CS	532.6	2
G2-L-P-2-CS				417.3	2.7
G1-L-T-2-CS	TPU			511.6	2
G2-L-T-2-CS				395.2	2.9

Results

Specimen ID	Type of Plug	Length-to-diameter ratio	Cutting type	Average compressive strength	Average tensile to compressive strength
G1-T-P-4-CS	PLA	4	CS	612.8	1.7
G1-T-P-4-DWS			DWS	847.2	1.2
G2-T-P-4-CS			CS	474.4	2.4
G1-T-P-2-CS		2		705.7	1.5
G1-T-P-2-DWS			DWS	851.4	1.2
G2-T-P-2-CS			CS	530	2.1
G2-T-P-2-DWS			DWS	730	1.6
G1-L-P-2-CS			CS	532.6	2
G2-L-P-2-CS				417.3	2.7
G1-L-T-2-CS	TPU			511.6	2
G2-L-T-2-CS				395.2	2.9

The average compressive strength of the samples with PLA is higher than samples with TPU.

Reasons

- The stiffness of PLA materials is higher than TPU.
- TPU materials are deformable and don't prevent the sample from changing their position while the load is applied.

Results

Specimen ID	Type of Plug	Length-to-diameter ratio	Cutting type	Average compressive strength	Average tensile to compressive strength
G1-T-P-4-CS	PLA	4	CS	612.8	1.7
G1-T-P-4-DWS			DWS	847.2	1.2
G2-T-P-4-CS			CS	474.4	2.4
G1-T-P-2-CS		2		705.7	1.5
G1-T-P-2-DWS			DWS	851.4	1.2
G2-T-P-2-CS			CS	530	2.1
G2-T-P-2-DWS			DWS	730	1.6
G1-L-P-2-CS			CS	532.6	2
G2-L-P-2-CS				417.3	2.7
G1-L-T-2-CS	TPU			511.6	2
G2-L-T-2-CS				395.2	2.9

The average compressive strength of the samples with DWS cutting is higher than samples with CS cutting.

Reasons

- As opposed to CS, cutted edges by DWS were completely parallel → Applying the load on the surface of the bars uniformly.

Results

Specimen ID	Type of Plug	Length-to-diameter ratio	Cutting type	Average compressive strength	Average tensile to compressive strength
G1-T-P-4-CS	PLA	4	CS	612.8	1.7
G1-T-P-4-DWS			DWS	847.2	1.2
G2-T-P-4-CS			CS	474.4	2.4
G1-T-P-2-CS		2		705.7	1.5
G1-T-P-2-DWS			DWS	851.4	1.2
G2-T-P-2-CS			CS	530	2.1
G2-T-P-2-DWS			DWS	730	1.6
G1-L-P-2-CS			CS	532.6	2
G2-L-P-2-CS				417.3	2.7
G1-L-T-2-CS	TPU			511.6	2
G2-L-T-2-CS				395.2	2.9

The average compressive strength of the samples with length-to-diameter ratio of 2 were higher than samples with length-to-diameter ratio of 4.

Reasons

- As opposed to CS, cutted edges by DWS were completely parallel → Applying the load on the surface of the bars uniformly.

Compressive elastic modulus of G1 bar

- The surface of the G2 bars was not smooth.
- Cross-section of the bars was not a perfect circle.

Surface profile of G2 bar.

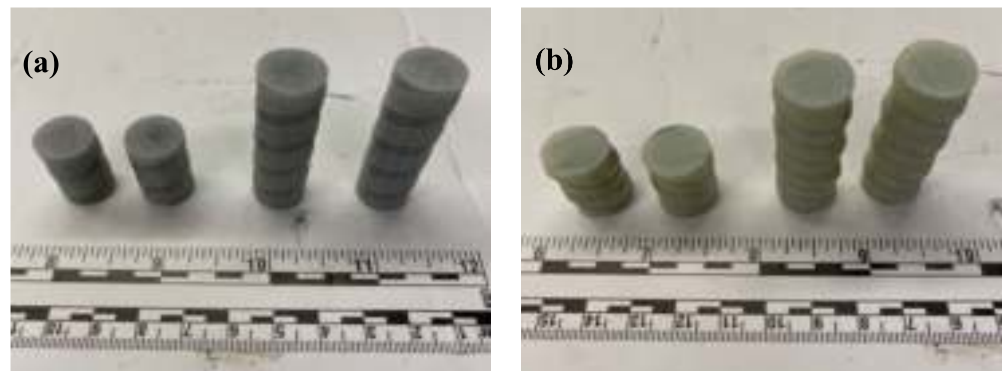

Tested GFRP bars: (a) G1 coupons; and (b) G2 coupons.

UNIVERSITY OF MIAMI
NC STATE UNIVERSITY

Compressive elastic modulus of G1 bar

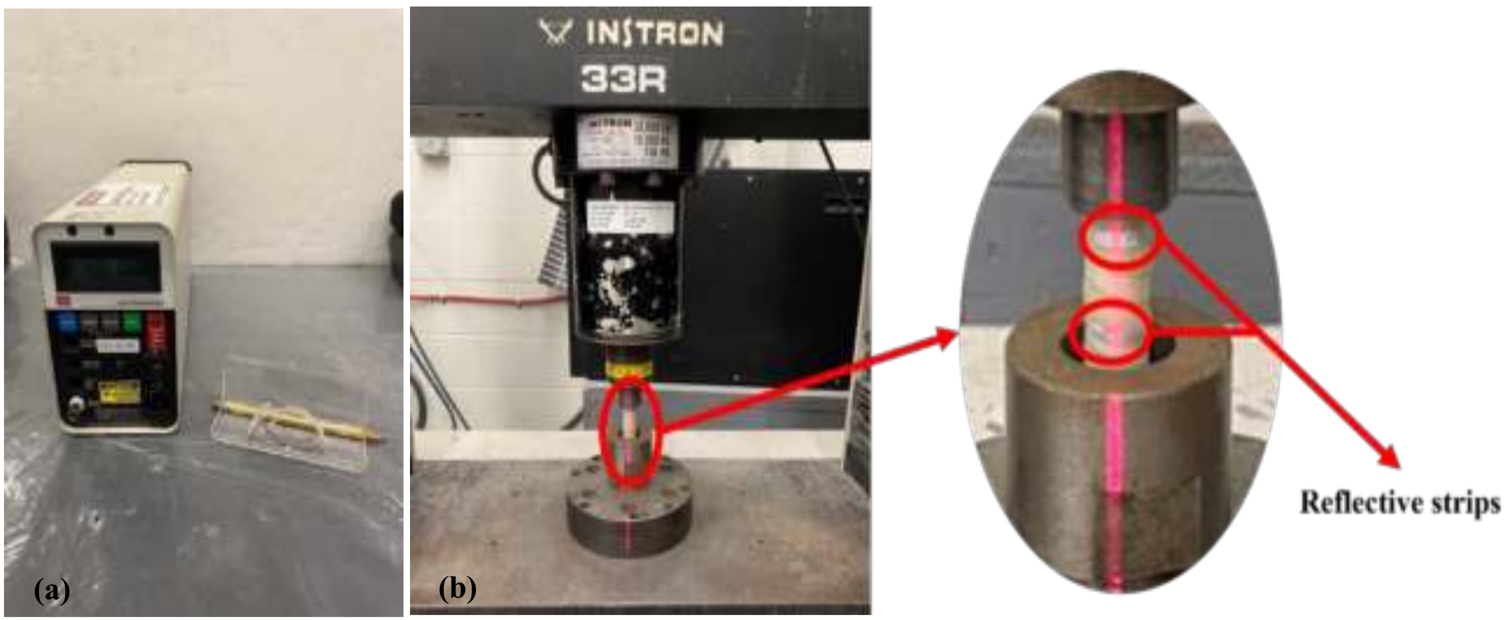

Laser extensometer for strain measurements: (a) device and reflective strips; and (b) setup.

Compressive elastic modulus of G1 bar

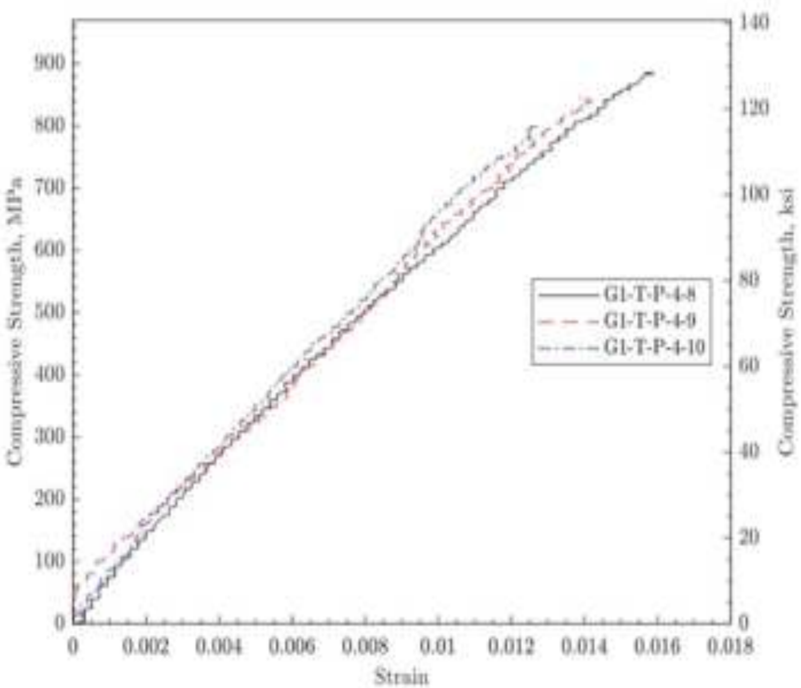

Stress-strain curves of G1 coupons.

ID	Tensile elastic modulus (E_t) GPa	Compressive elastic modulus (E_c) GGa	Average (E_c) GPa
G1-T-P-4-8	58.7	57.1	58.7
G1-T-P-4-9		57.0	
G1-T-P-4-10		62.1	

The compressive elastic modulus of tested FRP bars is **similar** to their tensile elastic modulus.

UNIVERSITY OF MIAMI NC STATE UNIVERSITY

Investigating the crack initiation via Micro-computed thermography

Applying the load on G1 bars in three different stages

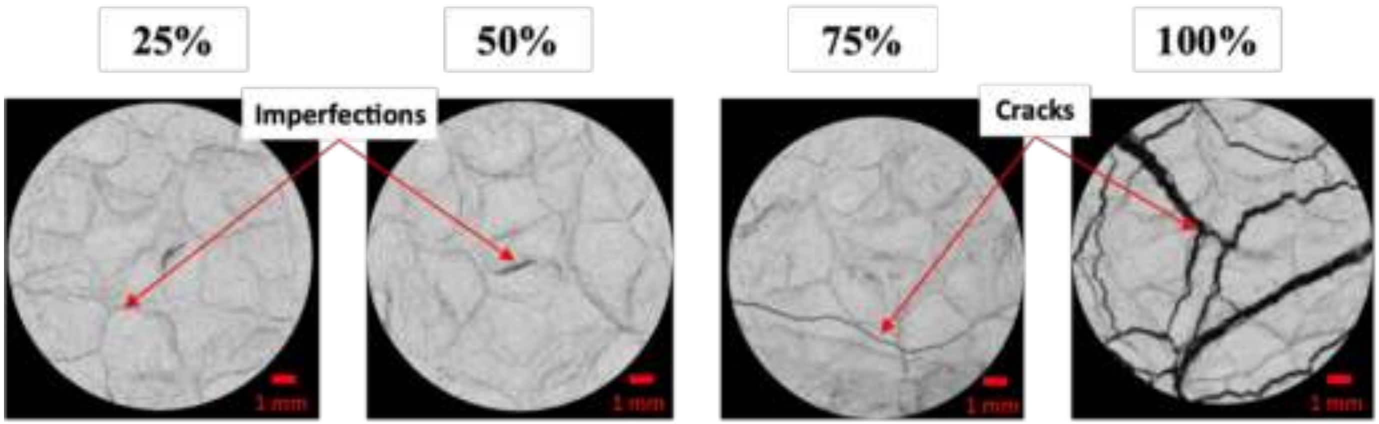

Investigating the crack initiation via Micro-computed thermography

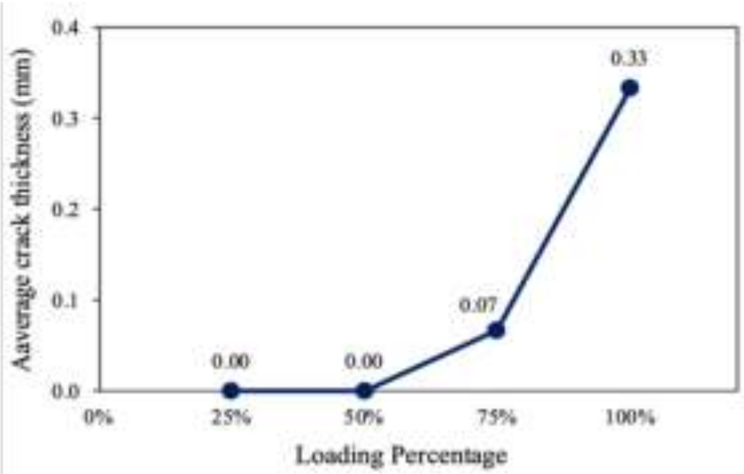

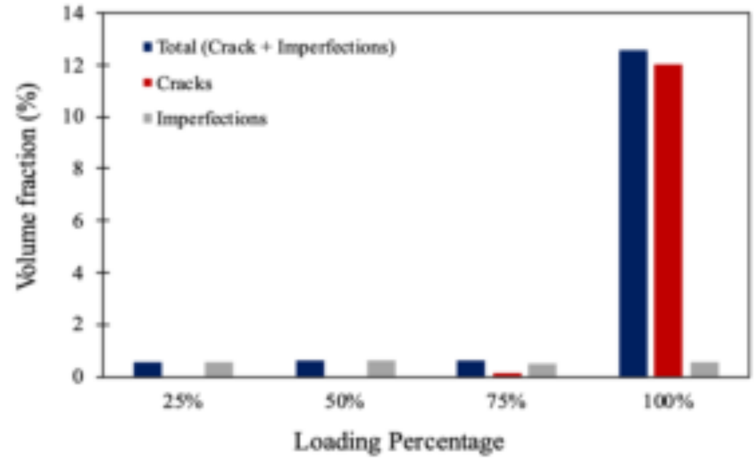

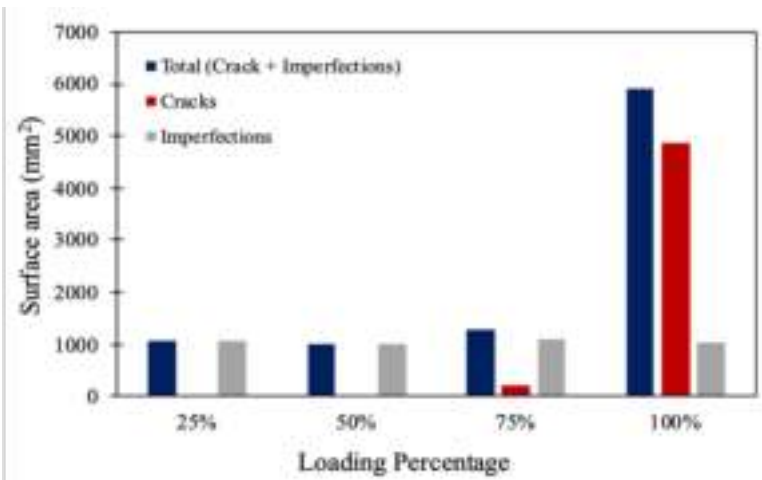

Most cracks develop in the 75%-100% range.

Conclusion

1- The compressive strength of GFRP bars is considerable, and neglecting it in designing procedures for compressive members, such as columns, is a conservative practice.

2- Increasing the length-to-diameter ratio reduces the ultimate compressive strength.

3- Using PLA plugs instead of TPU ones increases the compressive strength of the FRP bars.

4- Cutting surfaces must be in a way that creates two parallel surfaces to apply the load uniformly.

5- The obtained elastic modulus for G1 bars in compression showed that this value equals the tensile elastic modulus (58.7 MPa).

6- Micro-CT scans revealed that the majority of the damage develops after reaching 75% of the ultimate capacity and propagates into inter-connected crack plates.

Center for Integration of Composites into Infrastructure

IAB Meeting, Fall 2023

#3 Solutions for the Implementation of Composites Through Experimental Testing and Design:
Part A: Push-off Test
Part B: Compressive behavior of GFRP bars

L.I.F.E. forms

Center for Integration of Composites into Infrastructure

IAB Meeting, Fall 2023

#4 Propelling the use of FRP Composites with Meaningful Codes and Guidelines:

Part A: Guide for Field Inspection

Part B: Use of profilometry to standardize FRP surface enhancement

Part C: Guideline for FRP Composite Mesh in Concrete

Part A: Guide for Field Inspection

Research Group

Jesús D. Ortiz
Graduate Student

Ehsan Harati
Graduate Student

Antonio Nanni
Professor and Chair

- A project together with the Florida International University (**FIU**) and the Federal Highway Administration (**FHWA**)

Part A: Guide for Field Inspection

- **Inspection methods** and codification of damages have been in use for a long time for conventional steel and reinforced concrete bridges.
- Standardized and unified methodology or guide for inspection and damage detection of **concrete bridge elements** reinforced or strengthened with fiber reinforced polymer (FRP) does not exist.
- Lack of **clear guidelines** and effective methods for condition assessment of FRP reinforced/strengthened concrete (FRP-RSC) elements could have negatively affected the proliferation of its use.

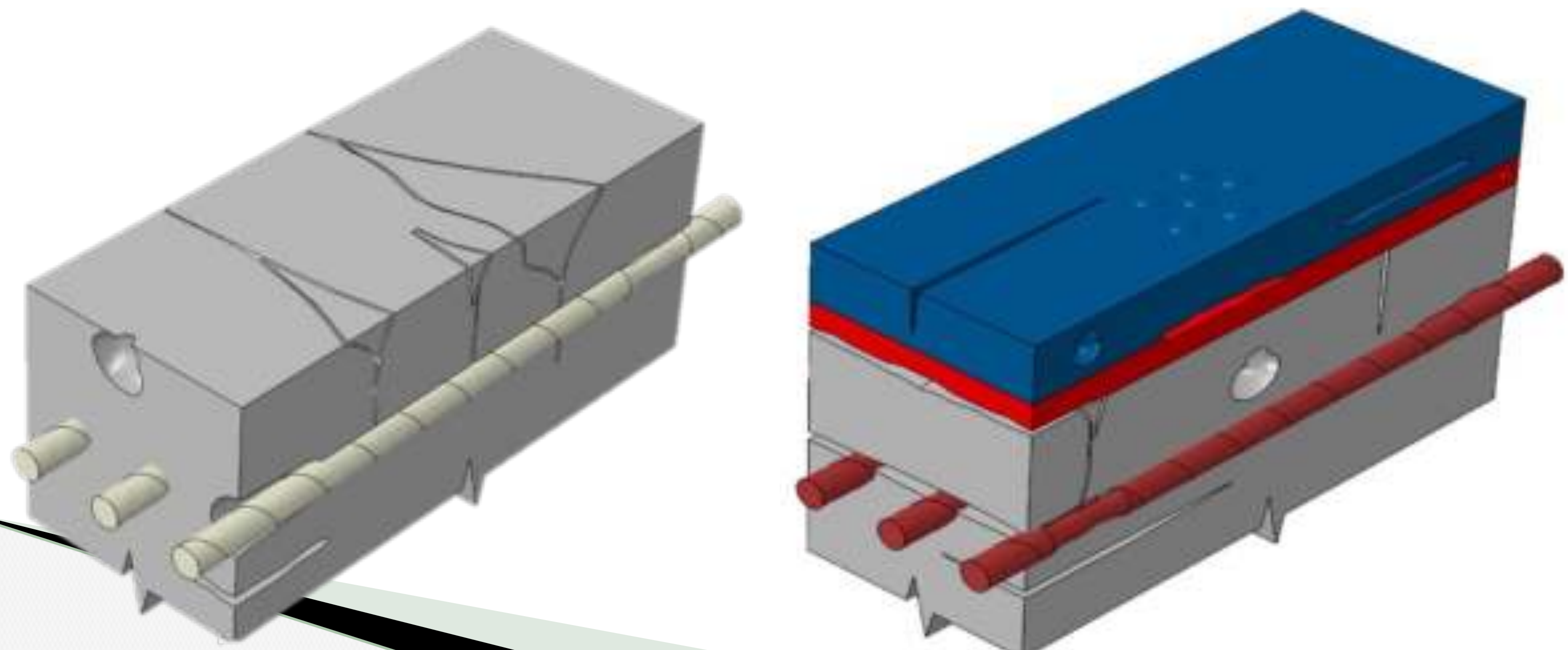

Approach and Industrial Relevance

To Recognize the common/potential defects of FRP-reinforced/strengthened concrete elements in bridge structures.

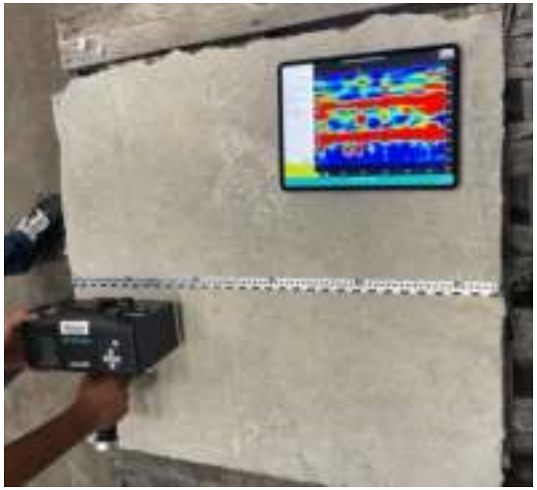

To Assess the potential and appropriate use of available NDT techniques.

To Develop the framework of a unified and uniform guide for Inspection and Coding assessment of in-service FRP-RSC bridge elements

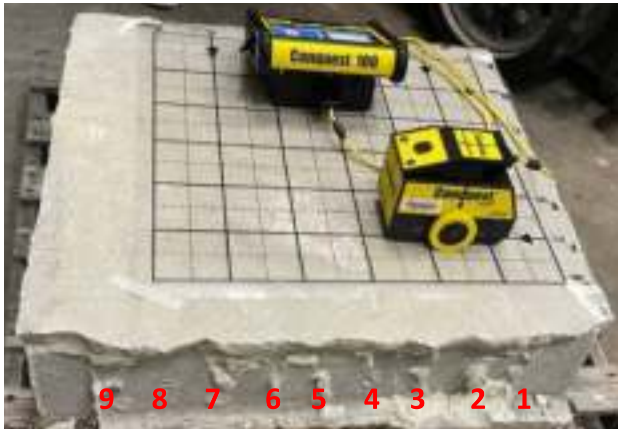

Observed and Expected Damage and Defects

Defect Categories	Defect Locations	Defects
Defects Intrinsic to FRP Composites (Defects in FRP Reinforcing Bars, Strands)	A. FRP Reinforcement	1. Loss of Cross-sectional Property (Other Potential Defects: Voids at Fiber-Matrix Interface, Wrinkling, Blistering, Fiber-Matrix Debonding, Delamination Between Composite Layers, Fiber Exposure, Scratches, Cracks, Discoloration)
Defects in the Interface	B. Concrete-FRP Reinforcement Interface	2. Debonding (Others Potential Defects: Slippage, Anchorage Failure)
Defects in Concrete	C. Concrete	3. Cracks 4. Voids 5. Delamination

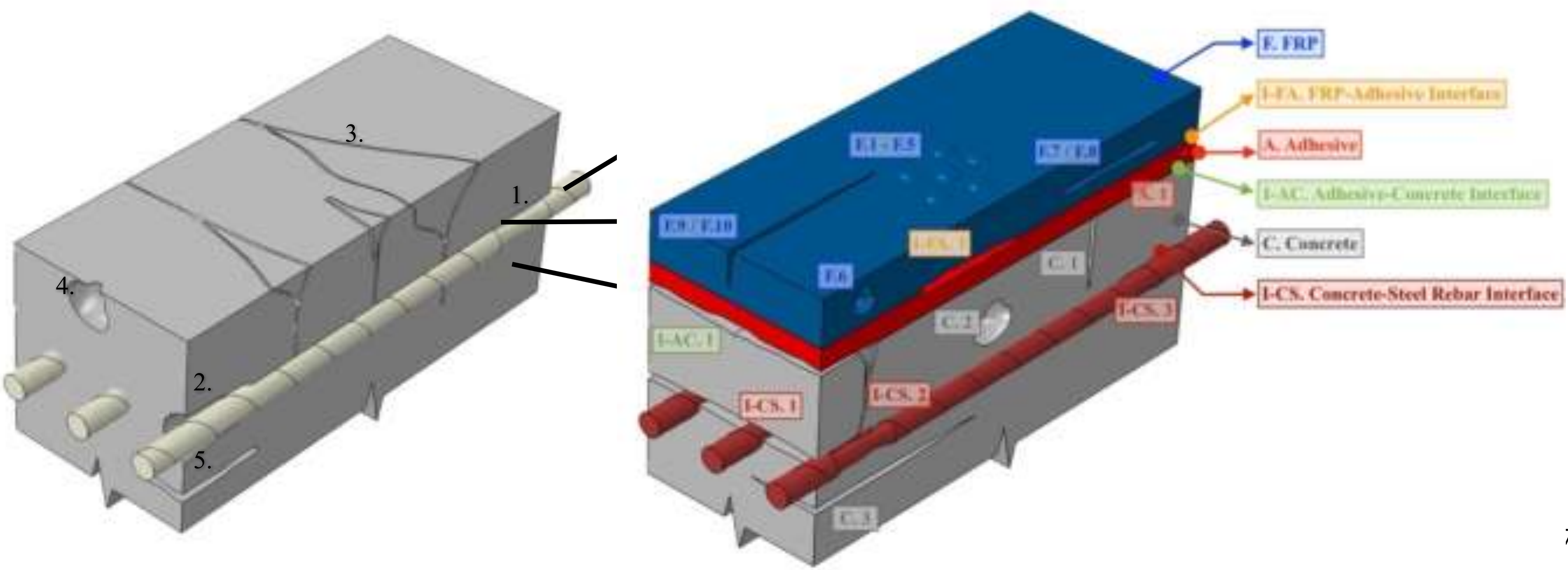

Experimental Work

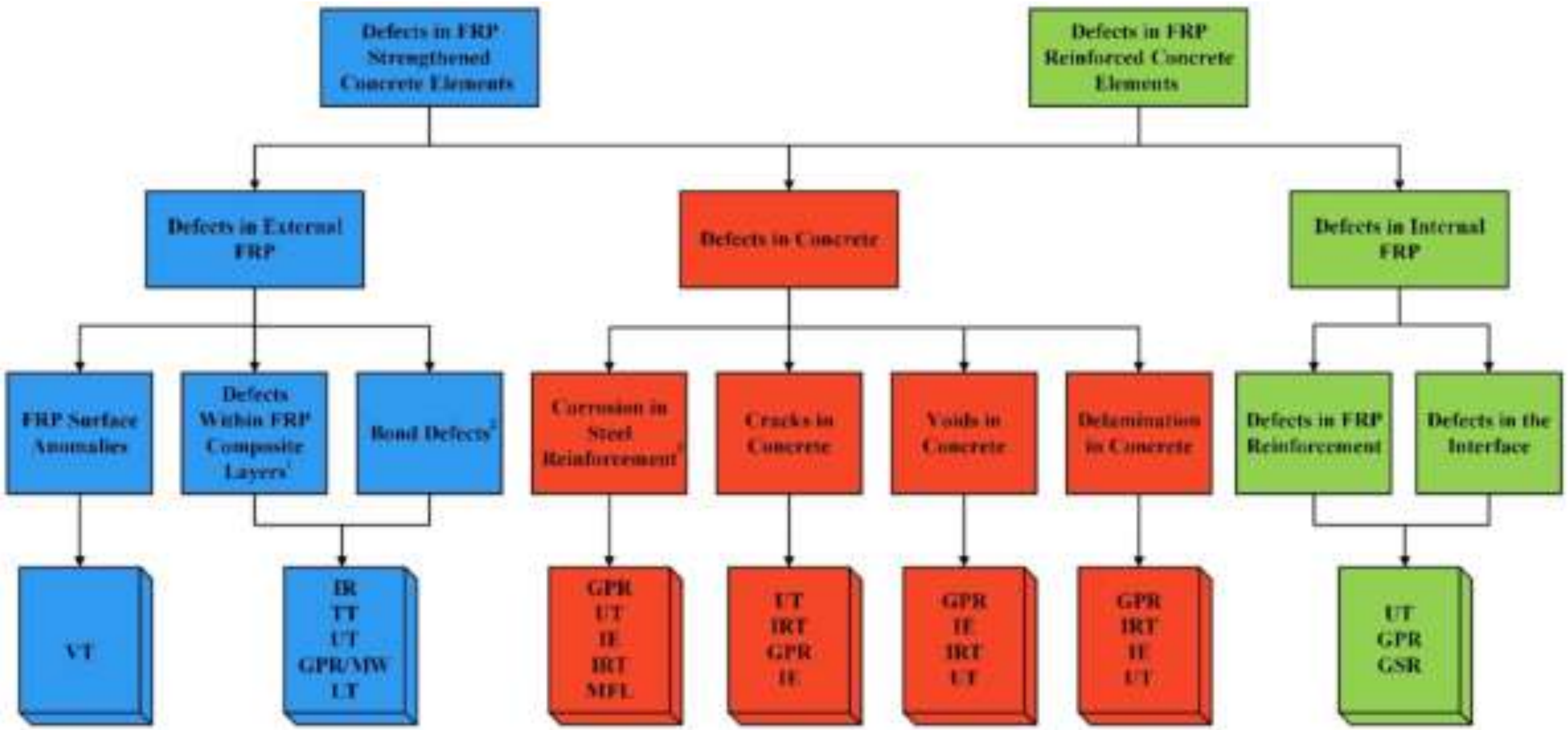

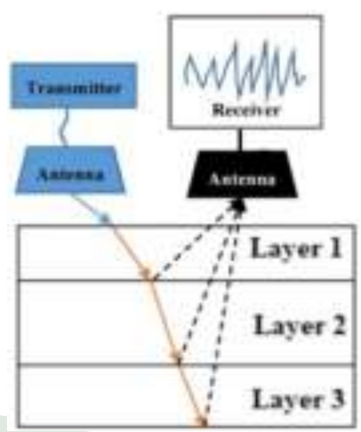

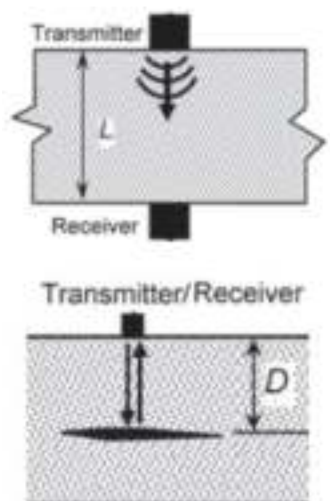

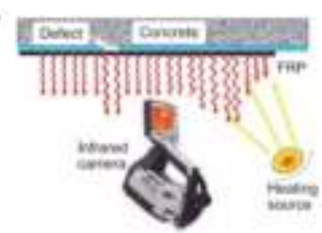

Experimental Work

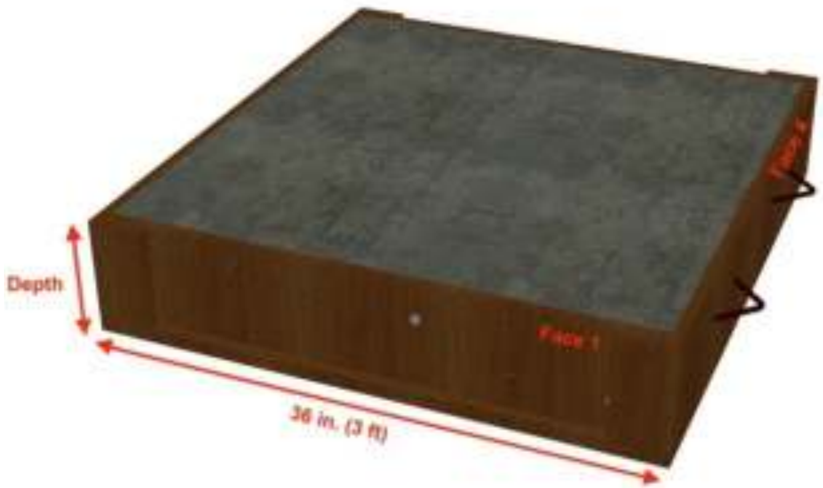

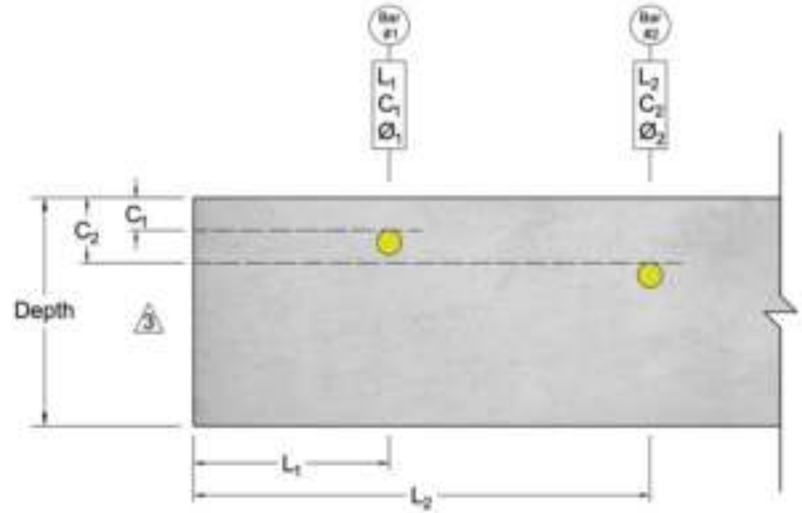

Preliminary Conclusions

- **IR**, **GPR**, or **UT/PAU** can be employed for quantitative defect assessment within the FRP composite or between the FRP and concrete. Suspected void areas can be further investigated using tap testing or IR.
- **GPR** could not detect defects or damages introduced into the externally applied CFRP and the internal targets beneath the CFRP layer due to its conductive nature. PAU exhibited relatively better performance in inspecting the external application of FRP. Other NDT techniques, including VT, TT, and IR, were also found to be quite effective in detecting defects and damages on externally applied FRP.
- **GPR** could detect damages in GFRP bars, CFRP strands, steel bars and all the internal damages introduced in concrete. It was not able to detect damages in BFRP bars in the experimental setup considered in this study, but there is a possibility that higher frequency GPR device might have been able to detect damages in BFRP bars which will be investigated in future studies.
- **PAU** showed limitations in its capability to detect damages in GFRP and BFRP bars but performed well in detecting damages in CFRP strands, steel bar and concrete.

- A project together with the Florida International University (**FIU**) and the Federal Highway Administration (**FHWA**)

Part B: Design and Selection of FRP Pultruded Elements

Research Group

Ehsan Harati
Graduate Student

Alvaro Ruiz Emparanza
Postdoctoral Associate

Francisco De Caso
Principal Scientist

Antonio Nanni
Professor and Chair

UNIVERSITY OF MIAMI

NEX An ACI Center of Excellence for Nonmetallic Building Materials

What are FRP pultruded structural shapes?

What are FRP pultruded Structural shapes?

Summarized Timeline of the Development of Pultrusion

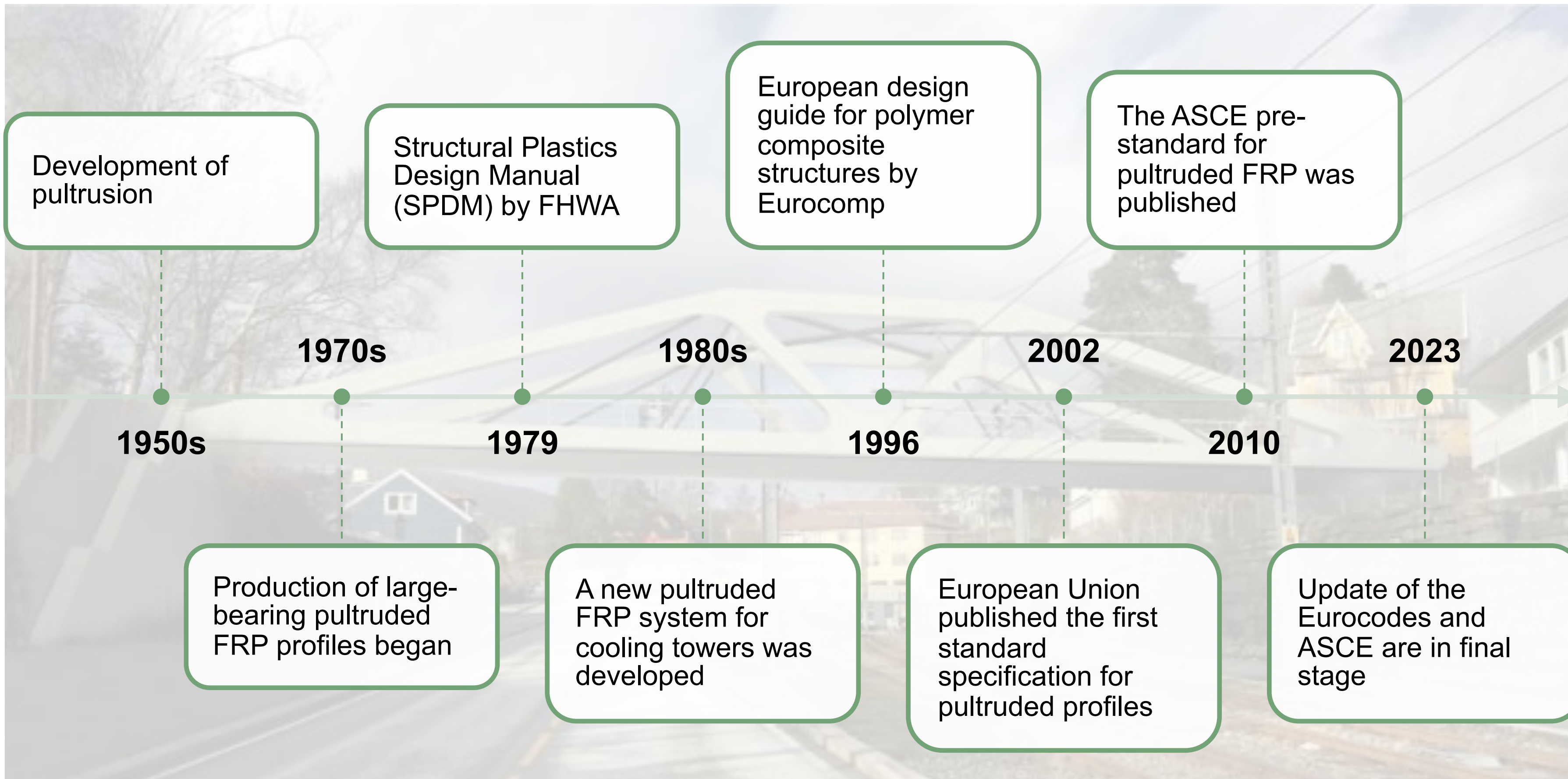

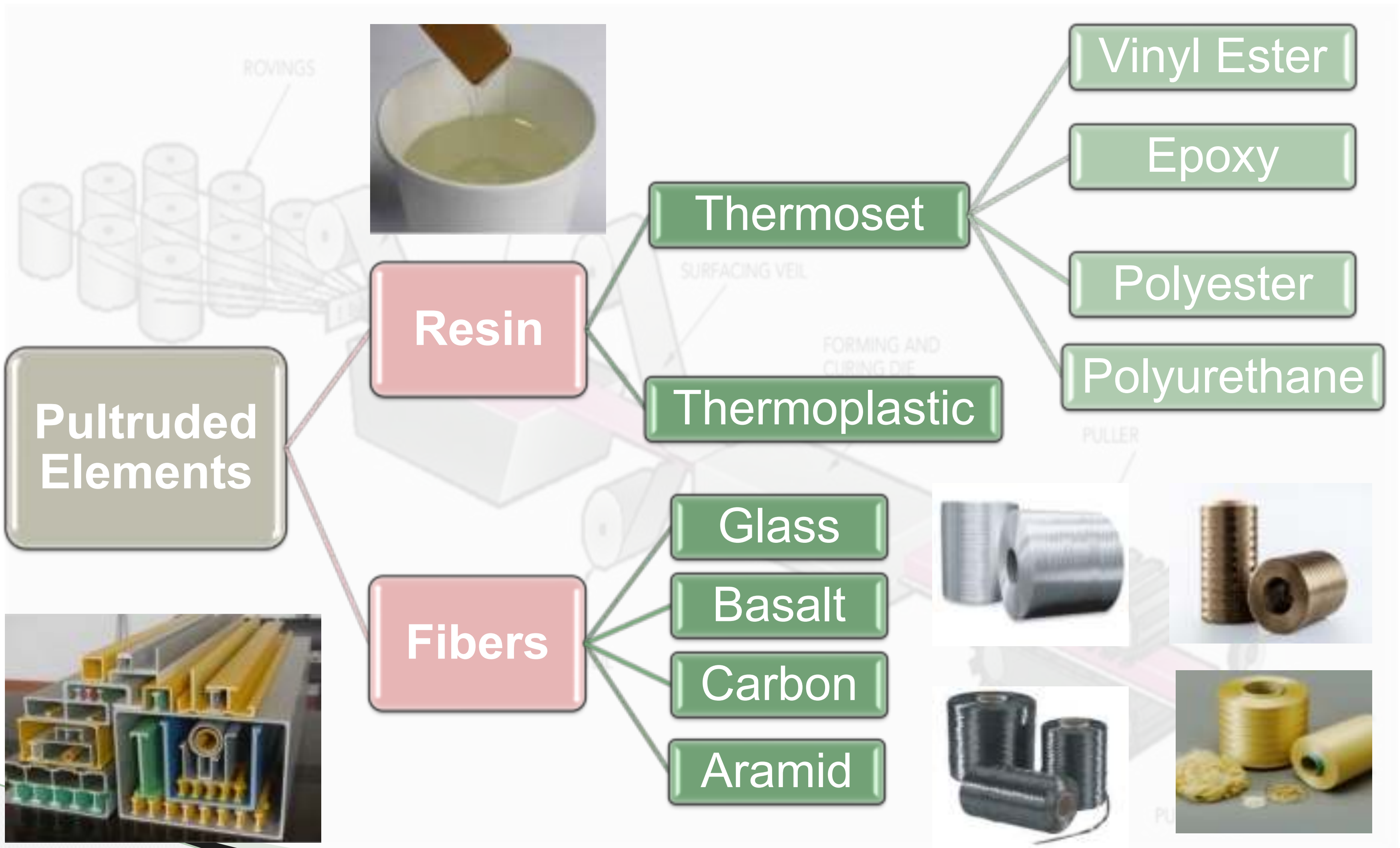
Pultruded Elements
Resin
Fibers
Thermoset
Thermoplastic
Vinyl Ester
Epoxy
Polyester
Polyurethane
Glass
Basalt
Carbon
Aramid

Structural shapes, ladder rails, window profiles, wind turbine blade spars, and gratings are a few of the major pultrusion applications

Relevant codes, Standards, and Guidelines

- ASCE-(2010)
- ASCE-74-(2023)
- EUROCODE-(2022)
- Design Guides

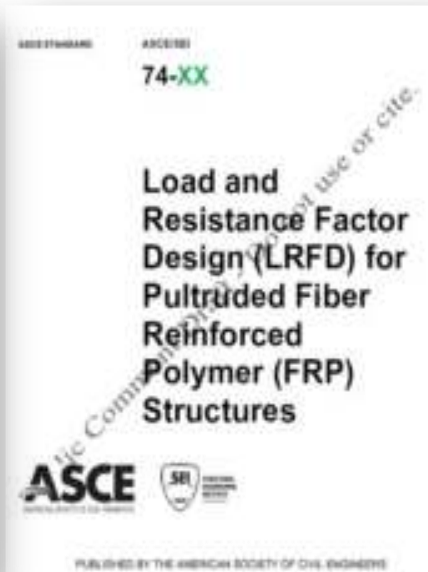

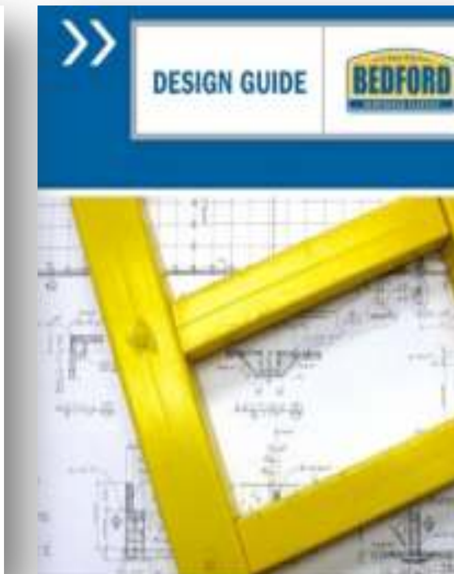

ASCE-74

1. General Provision
2. Design Requirements
3. Design of Tension Members
4. Design of Compression Members
5. Design of Members for Flexural & Shear
6. Design of Members Under Combined Forces & Torsion
7. Design of Plates and Built-up-Members
8. Design of Bolted Connection
9. Seismic Design Requirements

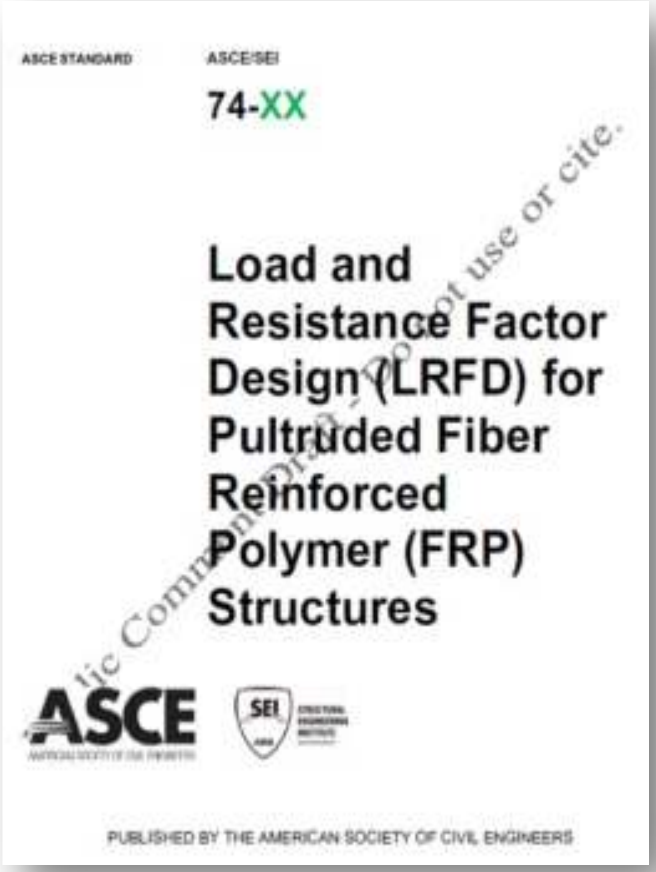

87

EUROCODE

1. Basis od Design
2. Materials
3. Durability
4. Structural Analysis
5. Ultimate limit states
6. Serviceability limit states
7. Fatigue
8. Detailing
9. Connections and joints

Pultruded Connection

ASCE-74

1. General Provision
2. Design Requirements
3. Design of Tension Members
4. Design of Compression Members
5. Design of Members for Flexural & Shear
6. Design of Members Under Combined Forces & Torsion
7. Design of Plates and Built-up-Members
8. Design of Bolted Connection
9. Seismic Design Requirements

AISC 360-22

1. General Provision
2. Design Requirements
3. Design For Stability
4. Design of Members for Tension
5. Design of Members for Compression
6. Design of Members for Flexural
7. Design of Members for Shear
8. Design of Members for Combined Forces & Torsion
9. Design of Composite Members
10. Design of Bolted Connection

Failure Modes of Pultruded Bolted Connection

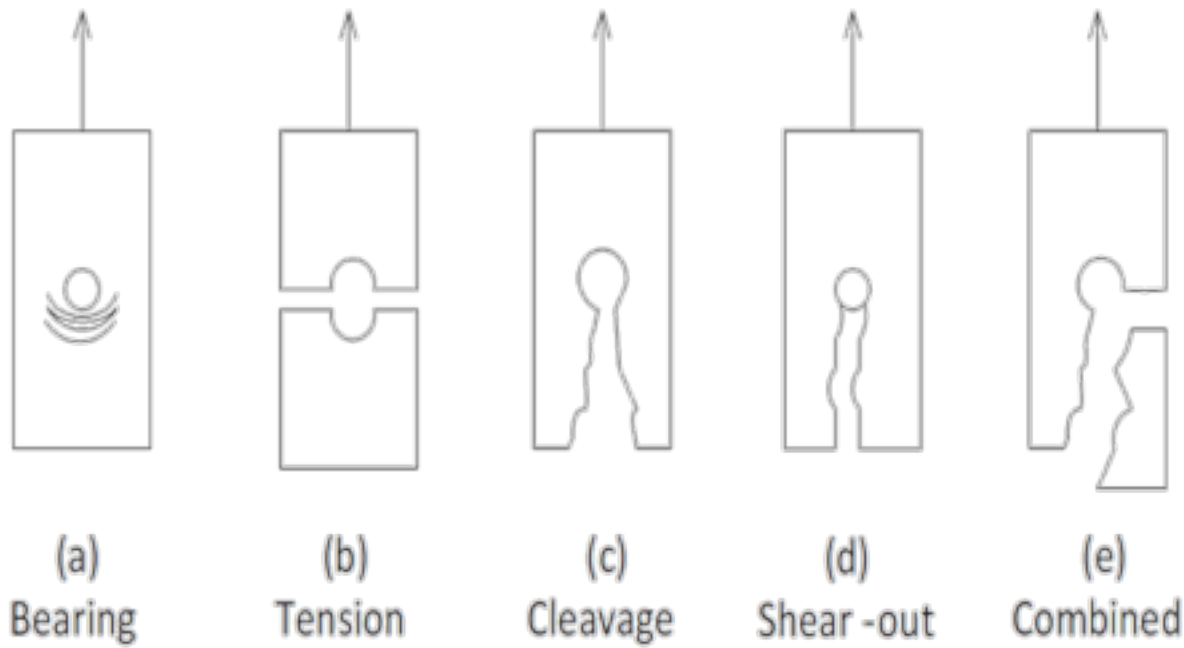

90

FRP Pultruded Connection

- **Block-shear failure**

AISC 360-22	ASCE-74	EUROCODE
$R_n = 0.60F_u A_{nv} + U_{bs} F_u A_{nt}$	$R_{bs} = 0.5\left(A_{ns}\, F_{sh} + A_{nt}\, F_L^t\right)$	$N_{bs,Rd} = 0{,}5\left(A_{ns} \cdot f_{xy,v,d} + A_{nt} \cdot f_{t,t,d}\right)$

- **Shear-out failure**

AISC 360-22	ASCE-74	EUROCODE
NOT APPLICABLE	$R_{sh} = 1.4\left(e_1 - \frac{d_n}{2} + s\right) t\, F_{sh}$	$V_{so,1,Rd} = 1{,}5\left(e_1 - 0{,}5d_0\right) \cdot t \cdot f_{xy,v,d}$

References

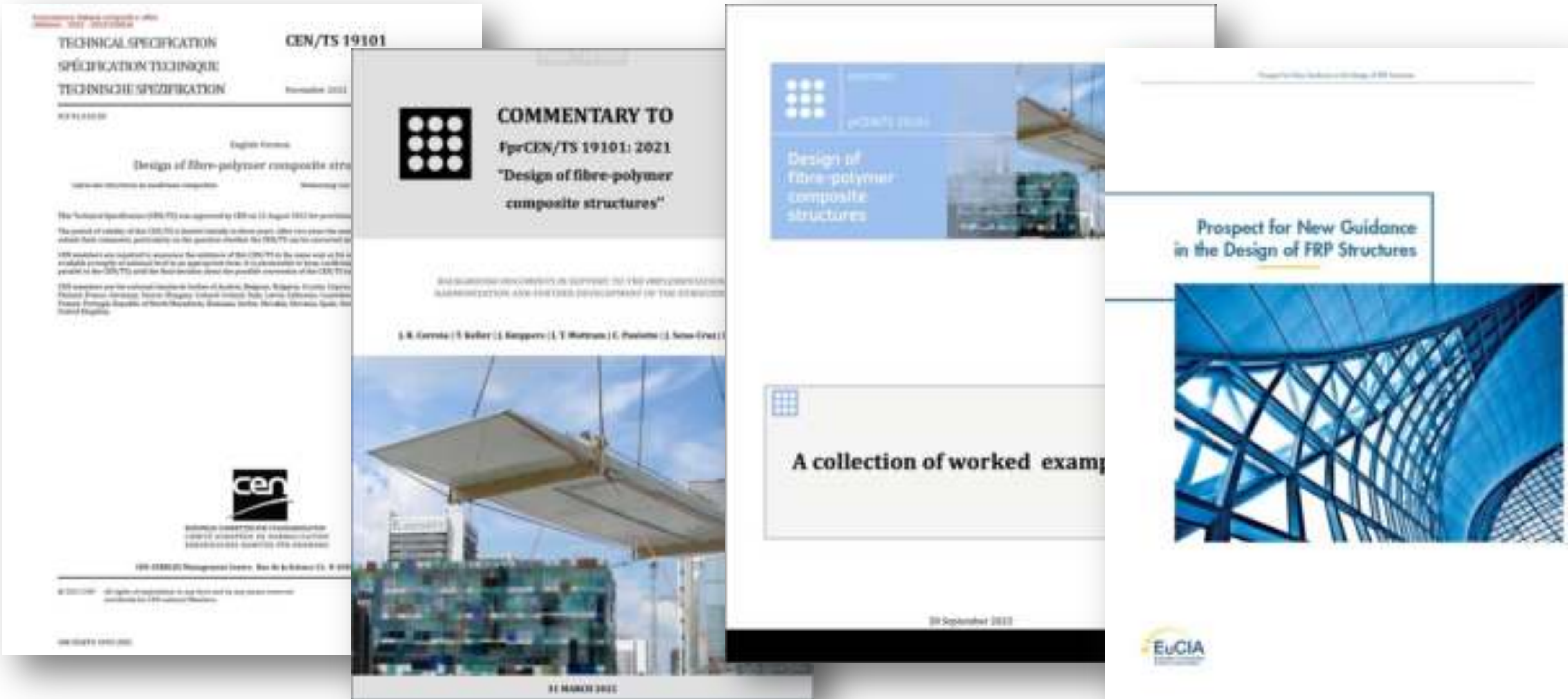
TECHNICAL SPECIFICATION
SPÉCIFICATION TECHNIQUE
TECHNISCHE SPEZIFIKATION
CEN/TS 19101
COMMENTARY TO
FprCEN/TS 19101: 2021
"Design of fibre-polymer
composite structures"
Design of
fibre-polymer
composite
structures
A collection of worked examp
Prospect for New Guidance
in the Design of FRP Structures
EuCIA

References


Pre-Standard for
Load & Resistance Factor
Design (LRFD) of Pultruded
Fiber Reinforced Polymer (FRP)
Structures
(Final)
ASCE STANDARD
ASCE/SEI
74-XX
Load an
Resistar
Design (
Pultrude
Reinforc
Polymer (FRP)
Structures
ASCE
PUBLISHED BY THE AMERICAN SOCIETY OF CIVIL ENGINEERS
Design Guide for
FRP Composite
Connections
ASCE Manuals and Reports on
Engineering Practice No. 102
ASCE
FRP COMPOSITE STI
THEORY, FUNDAMENTALS,
HOTA V. S. GANGA
WORAPHOT PRACHA
CRC Press
Composites
for
CONSTRUCTION
Structural Design with FRP Materials
Reinforced
Concrete with
FRP Bars
Mechanics and Design
Antonio Nanni
Antonio De Luca
Hany Jawaheri Zadeh
CRC Press

Where is the GAP? Education....

1. Design Guide
2. Design Aids:
   charts, tables, software
3. Worked Examples


Table 6-2 (continued)
Available Strength for Members Subject to Axial, Shear, Flexural and Combined Forces
W-Shapes
W12

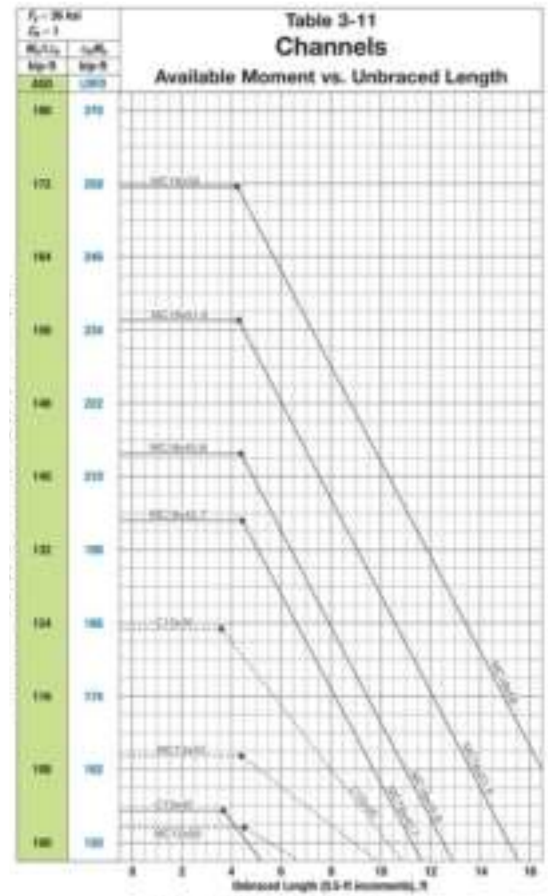

Part C: Guideline for FRP Composite Mesh in Concrete

Research Group

Hossein Roghani
Ph.D. Candidate

Alvaro Ruiz Emparanza
Postdoctoral Associate

Francisco De Caso
Principal Scientist

Antonio Nanni
Professor and Chair

UNIVERSITY OF MIAMI

NEX An ACI Center of Excellence for Nonmetallic Building Materials

Part C: Guideline for FRP Composite Mesh in Concrete

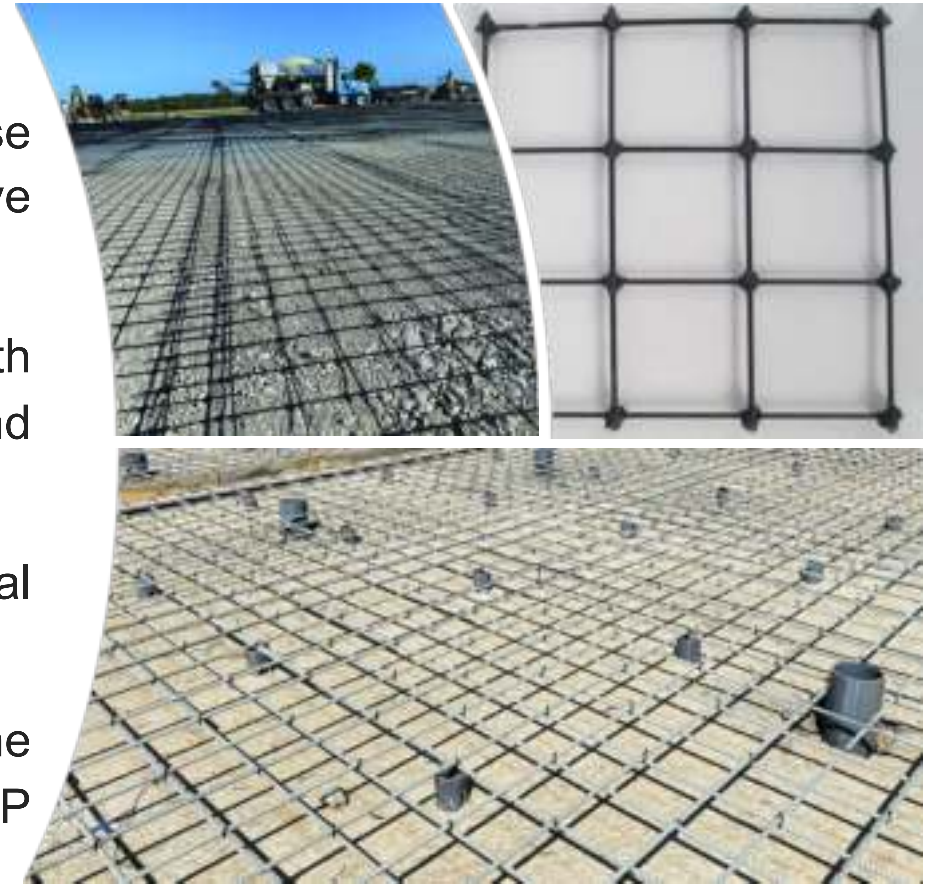

- Develop a comprehensive, concise document offering an extensive overview.
- Beyond available literature, provide with an understanding of potentials and benefits.
- Explore the applications, practical implementation, and constructability.
- Case studies to demonstrate the effectiveness and performance of FRP mesh.

Project Phases

Phase 1 — Data gathering and contact manufacturers

Phase 2 — Literature review and document development

Phase 3 — Document finalization and review

Background

FRP composite mesh can be a promising alternative:

1. Repair/Rehabilitation/Strengthening
- ❖ Reinforced concrete
- ❖ Unreinforced masonry
2. Internal Reinforcement
- ❖ Specialized applications: insulated wall panel product, skatepark, shotcrete, etc.
- ❖ Conventional applications: Slab-on-ground, sidewalk, pool, etc.

Fig. 1. Repair/rehabilitation/strengthening.

Fig. 2. Specialized applications.

Fig. 3. Internal reinforcement.

FRP Mesh Component

This document addresses FRP meshes with the following characteristics:

1. Fibers: Glass, Carbon, and Basalt.
2. Resin: Epoxy, Vinyl Ester, Polyester and Isophthalic Polyester
3. Classification:

❖ Grid Type Mesh (smaller spacing)

❖ Wire type Mesh (larger Spacing)

❖ Bar Type Mesh

4. Manufacturing

❖ Pultrusion

❖ Weaving

❖ Alternative manufacturing techniques: knitting, Laminating, and welding/bonding, 3D printing, molding, hybrid

Fig. 4. Fiber types.

Key Attributes

- Corrosion Resistance and Durability
- Lightweight
- High Strength-to-Weight Ratio
- Flexibility and Adaptability
- Electrical and Thermal Insulation
- Non-Magnetic
- Anisotropy and Dimensional Stability
- Sustainability
- Mesh Layout

Fig. 5. GFRP mesh for slab-on-ground.

Testing Methods

Mechanical Properties:

- Tensile Strength and Young's Modulus: ASTM D7205, ASTM D5035, ASTM D3039, ASTM D638
- Flexural Strength and Modulus: ASTM D790
- Mean Shear Strength of Mesh Intersection: ASTM A1064
- Shrinkage Cracking: ASTM C1579
- Shear Strength: ASTM D7617, ASTM D4255, ASTM D7078
- Interlaminar Shear Strength: ASTM D4475, ASTM D2344
- Bond Strength: ASTM D7913
- Compressive Strength: ASTM D695
- Creep and Relaxation: ASTM D2990

Physical Properties:

- Density: ASTM D792, ASTM D5261
- Width: ASTM D3774
- Moisture absorption: ASTM D570

Durability and Environmental Performance:

- Aging and Durability: ASTM D7705, ASTM D2244, ASTM D5870

Fire Performance:

- Flammability and Fire Resistance: ASTM E84, ASTM D2584, ASTM E1354

Thermal Properties:

- Thermal Conductivity: ASTM E1952
- Dimensional Stability: ASTM D696

Electrical Properties:

- Electrical Conductivity or Resistivity: ASTM D257

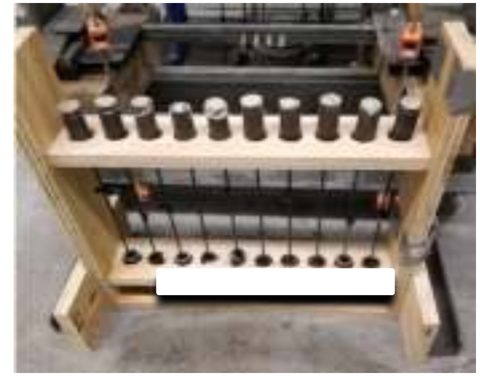

Fig. 1. Mesh potting.

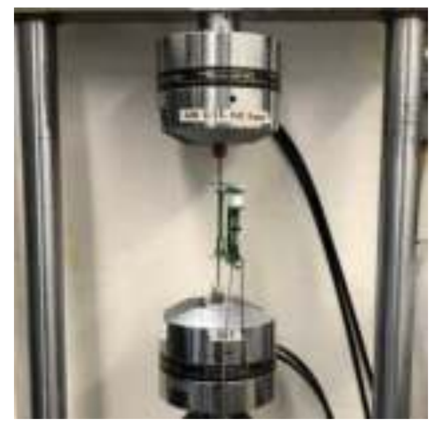

Fig. 1. Tensile test set-up.

Fig. 1. Representative failure mode of tensile tests.

How the project may be transformative and/or benefit society?

- Realization of potential economic advantages
- Address knowledge- and practice-gap that exists across all stakeholders .
- Advantageous for all manufacturers of FRP who produce mesh or grid

Center for Integration of Composites into Infrastructure

IAB Meeting, Fall 2023

#4 Propelling the use of FRP Composites with Meaningful Codes and Guidelines:

Part A: Guide for Field Inspection

Part B: Use of profilometry to standardize FRP surface enhancement

Part C: Guideline for FRP Composite Mesh in Concrete

Center for Integration of Composites into Infrastructure

Project #9: Enhancing Load Capacity of FRP Pedestrian Bridges

December 7-8, 2023

Sponsor: Bedford Reinforced Plastics, Inc.

By:
P.V. Vijay, Ph.D., P.E.
Hota V.S. GangaRao, Ph.D., P.E.
Chao Zhang, Ph.D.

Constructed Facilities Center
Wadsworth Department of Civil and Environmental Engineering
Statler College of Engineering and Mineral Resources

Introduction

- ❑ GFRP are strong/stiff, rust proof, light weight, durable, easy to transport/construct, economical and are the future of construction.
- ❑ GFRP pedestrian bridges tested at WVU-CEE/CFC lab using C-channels, box sections, WF beams, and metal/FRP connectors.
- ❑ Truss-bridge elements consisted of:
  - ❖ top & bottom-chord members (including splice plates)
  - ❖ diagonal web members/vertical posts/sloped web members
  - ❖ transverse beams/longitudinal beams
  - ❖ outriggers
  - ❖ horizontal braces
  - ❖ Wood decks
- ❑ Exploring ways to improve individual member and load capacity.
- ❑ Deflections, bridge strains, and associated safety assessment.

Component Testing

- Experimental values
  - Compression: 2.9 ksi (96“ long specimen) – 22.2 ksi (24“ long specimen)
  - Bending: 42.3 ksi – 61.6 ksi

3-Point Bending of 3”×3”×0.5” specimen (84” span)

2.5”×2.5”×0.5” specimen (24” long in compression)

Buckling of 3.0”×3.0”×0.5” square tube (84” long)

Component Testing: C-Channel Sections

- Weak-axis bending: 37.1 ksi – 49.2 ksi

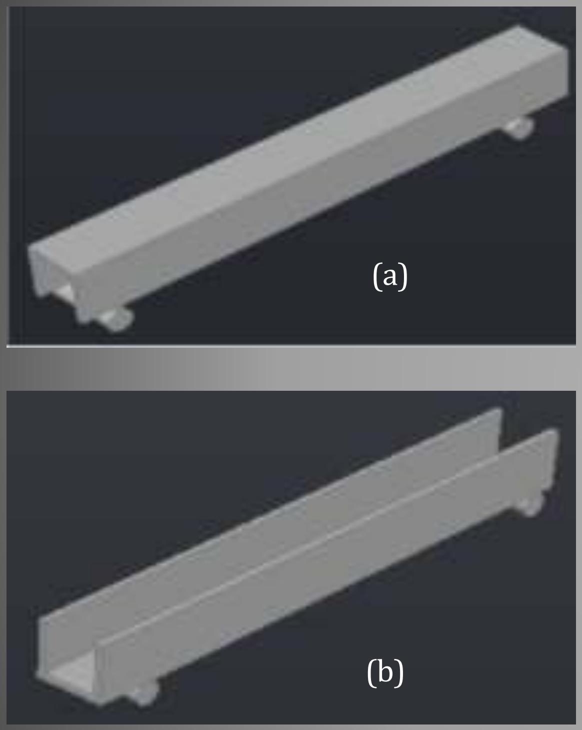

Channel (weak axis) bending: (a) flanges on supports and (b) web on supports

3-Point Bending of 10”×2.75”×0.5” channel (web on supports), span=72”

Component Testing: Back-to-back C-Channels

- Average maximum stress:
  - Strong-axis bending: 12.5 ksi – 15.2 ksi
  - Axial compression: 3.15 ksi – 5.125 ksi

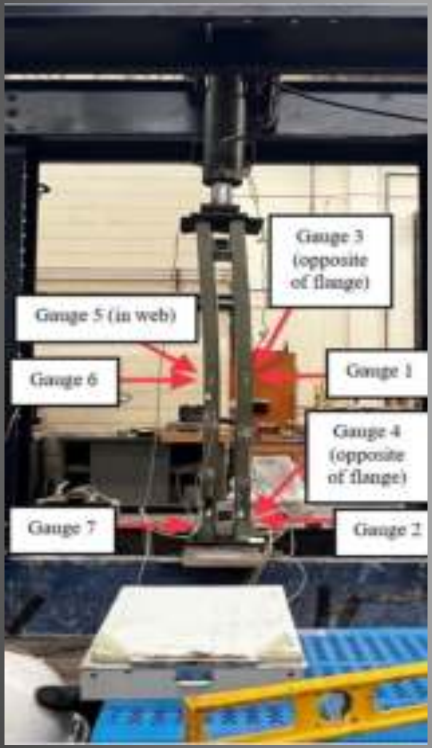

Locations of gauges for 8”×2.125”×0.375” & 10”×2.75”×0.5” double Channels

10”×2.75”×0.5” Back-to-back channels: lateral torsional effects under bending

Bridge Testing

- ❑ Truss bridges were subjected to different loading schemes
- ❑ Only vibration test shown below

Raw data — FFT → Natural Frequency

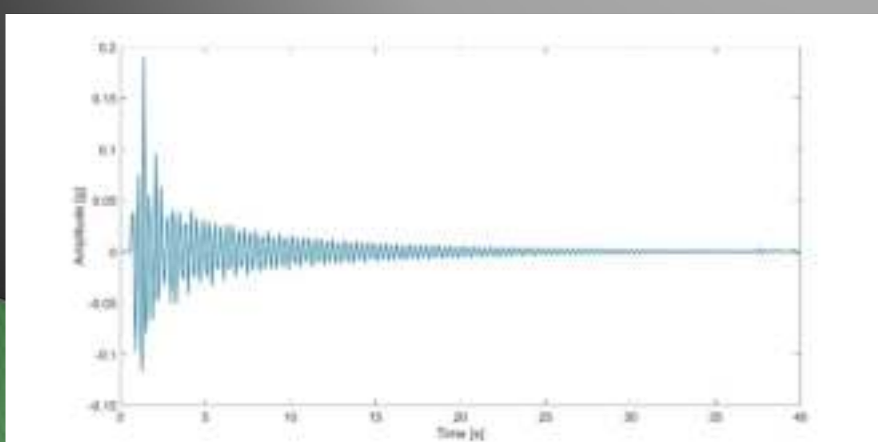

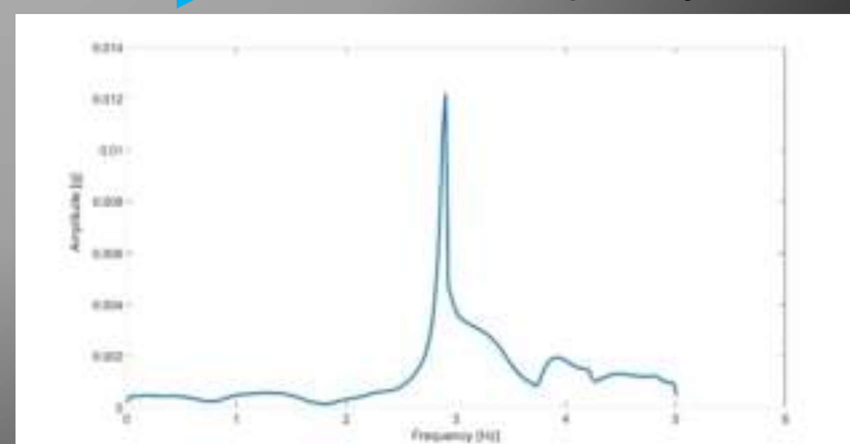

Brief Summary

- Behavior was similar to other truss type FRP bridges previously discussed under H5, UDL, Equestrian, lateral and bridge excitation testing.
  - Majority of members exhibiting strain values below 2000 to 3000 micro-strains. Very few members exhibiting above 3000 micro-strains.
- Deflections of the members being consistent with the lower FRP stiffness and the limits such as span/500 or higher need further consideration.
- Some of the vertical frequencies being around 3 Hz and 4.4 to 5 Hz (horizontal and Transverse) may need further consideration.

Project Name: Enhancing Load Capacity of FRP Pedestrian Bridges

Project Number: WVU-9

Project #10
Multiscale simulation of protective composite jacketing for tank cars

Masoud Mohammadi, PhD Candidate (GRA)
Dr. Eduardo M. Sosa, Task Leader

Department of Mechanical, Materials, and Aerospace Engineering

Presented at the CICI Industrial Advisory Board (IAB)
Fall 2023 Meeting, December 7th - 8th-, 2023

WestVirginiaUniversity

Center for Integration of Composites into Infrastructure

Problem: Tank Car Failure

Canada, 2013 [1]

Ohio, 2023 [2]

West Virginia, 2015 [3]

Canada, 2013 [1]

[1] Austen I. Canada Saw a Deadly Derailment. A Decade Later, Little Has Changed. NYTimes 2023.
[2] NTSB Issues Investigative Update on Ohio Train Derailment.
[3] West Virginia Oil Train Derailment Renews Concerns About Aging Rails. NBC News 2015.

Consequences

Reported Consequences:

- **Spills and Leaks:** Hazardous and chemical material.
- **Water Contamination:** A threat to ecosystems and human health.
- **Fire and Explosions:** Spill of flammable, corrosive or explosive materials.
- **Evacuations:** Disrupt to communities and large economic losses.
- **Injuries and Fatalities:** Injuries or fatalities in the vicinity of the accident.

Proposed Solution

- A protective composite jacket for tank cars to prevent failure by puncture.
- Experimental work jointly carried out by CEE, MAE and ChE Departments.

Focus of this study:

- Finite element simulations of the composite jacket under low-velocity impacts.

Experimental Prototype

18-layer layup

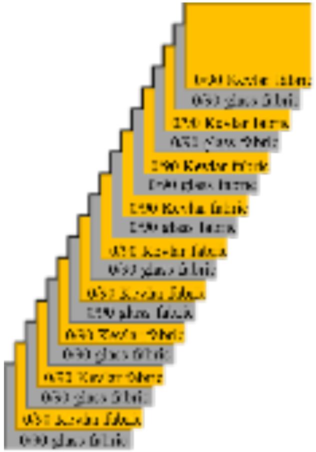

Lay-up configuration and stacking sequence

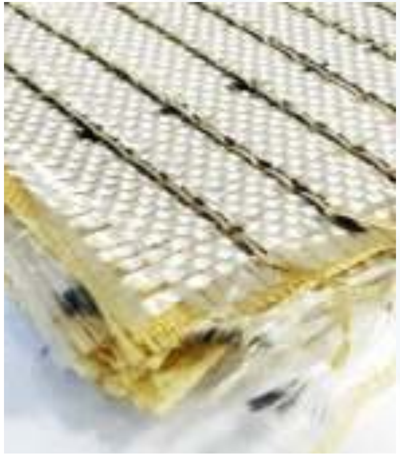

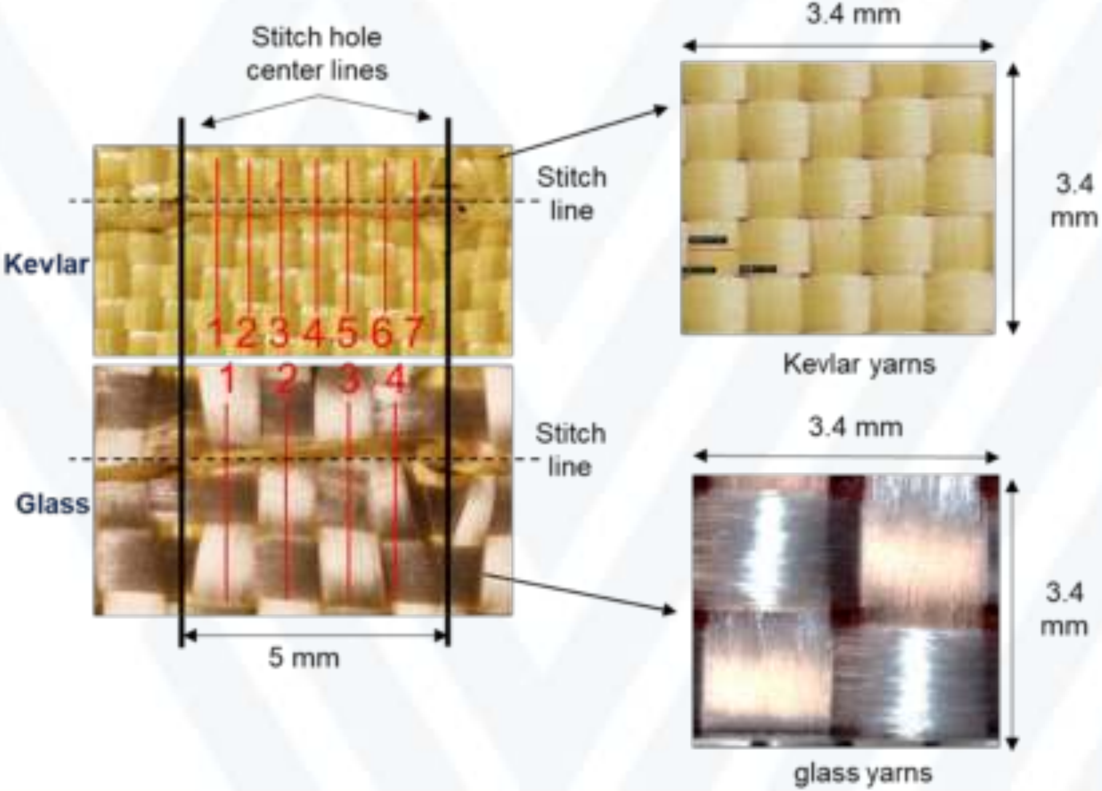

Multiscale Simulation Strategy

Scale Levels of Finite Element Simulation:

HMP: Homogenized Mechanical Properties

Microscale

HMP of single layer composites

Mesoscale

HMP of stitched composite

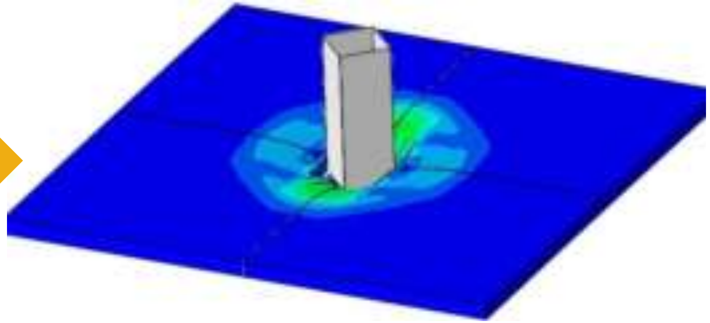

Macroscale

First Homogenization

Second Homogenization

Process under investigation:
Low-velocity impact
6.0-9.0 m/s, or ~25-30 km/h [3].

Multiscale Analysis Flow

[3] Razali N, Sultan M, Mustapha F, Yidris N, Ishak M (2014).

Microscale: Geometry of RVE*

Woven yarns

+

Surrounding
Epoxy resin

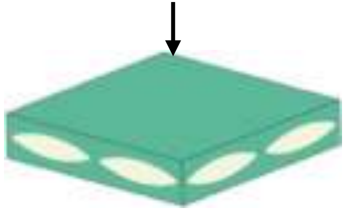

Microscale RVE

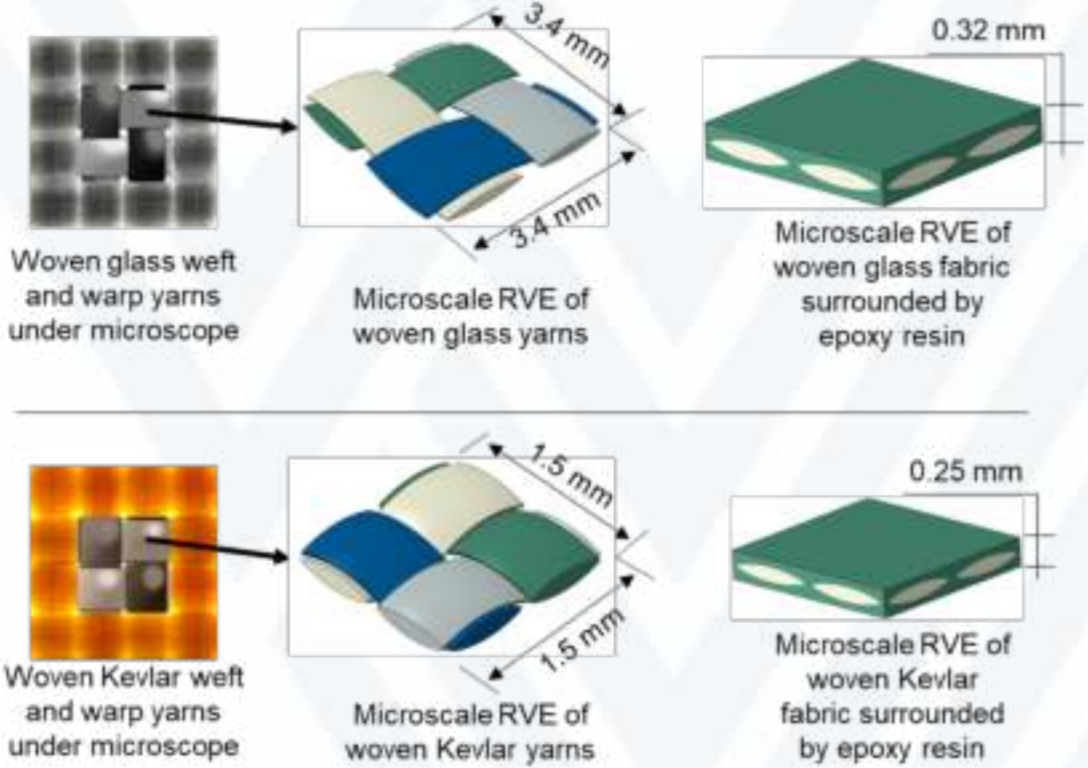

RVE*: Representative Volume Element - the smallest unite of a periodic structure.

Microscale: Homogenization

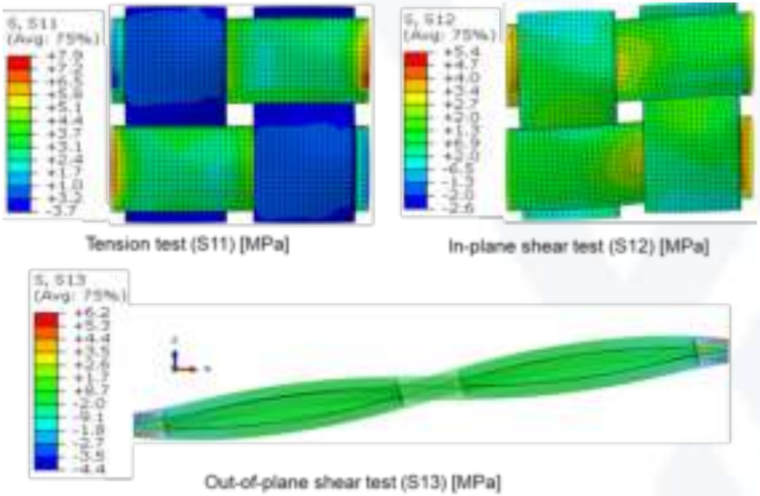

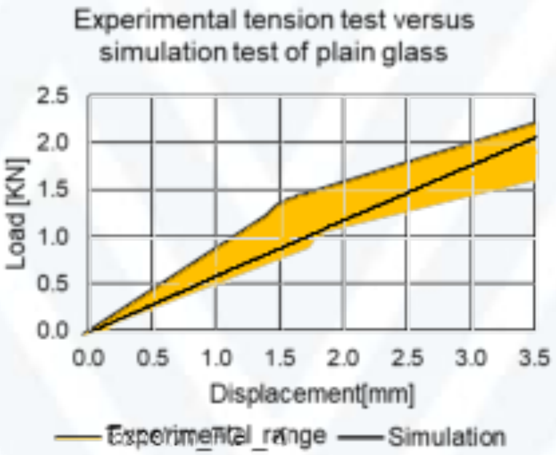

Microscale: Damage Model, Single Layer

Simulation of damage propagation in a single layer Glass/epoxy composite

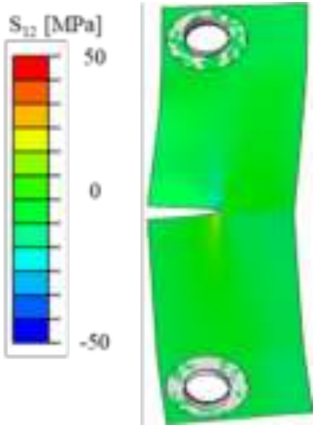

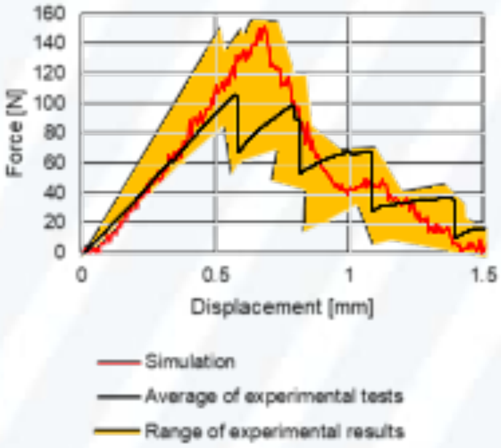

Experimental fracture test of a single layer Glass/epoxy composite based on ASTM standard [1]

Experimental results vs. numerical results

[1] ASTM E1922/E1922M (Last Updated: Jun 01, 2022).

Mesoscale: Features and Components

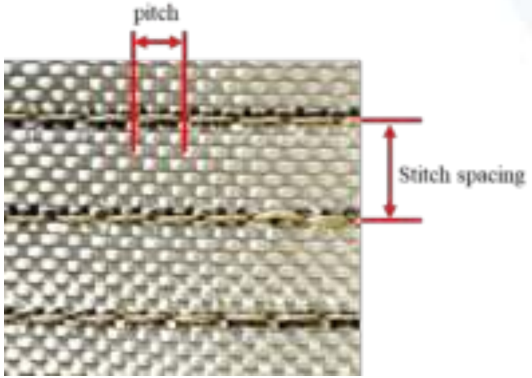

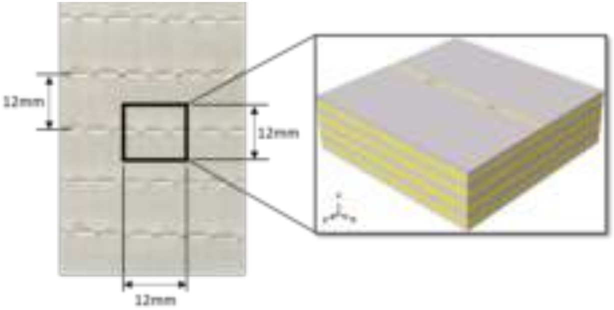

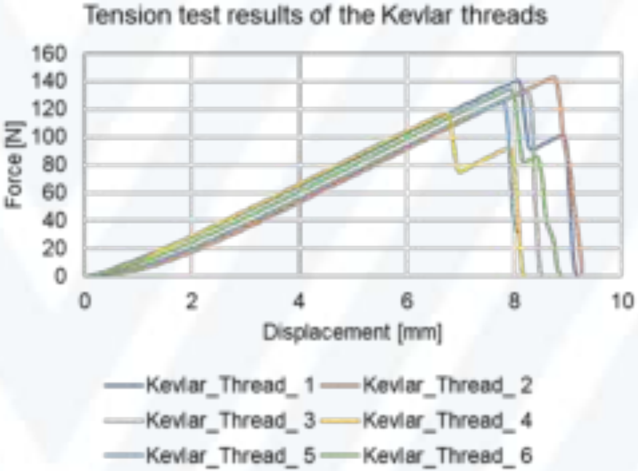

Tension test of Kevlar thread based on ASTM standard [1]

[1] ASTM D7269/D7269M-17. "Standard Test Methods for Tensile Testing of Aramid Yarns." (2017).

Mesoscale: Simulation of Stitches

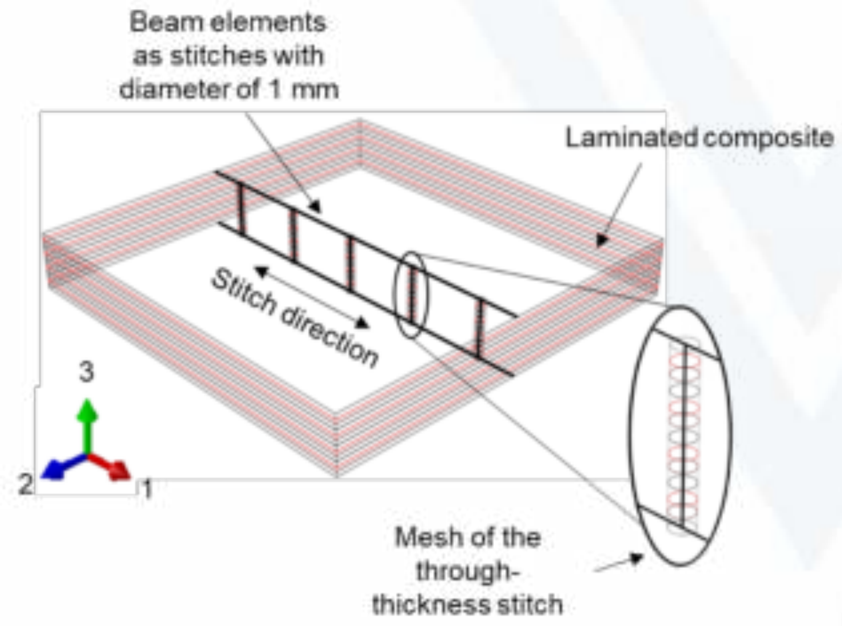

beam elements (B31) for stitches

18-L composite with stitch spacing of 12 mm

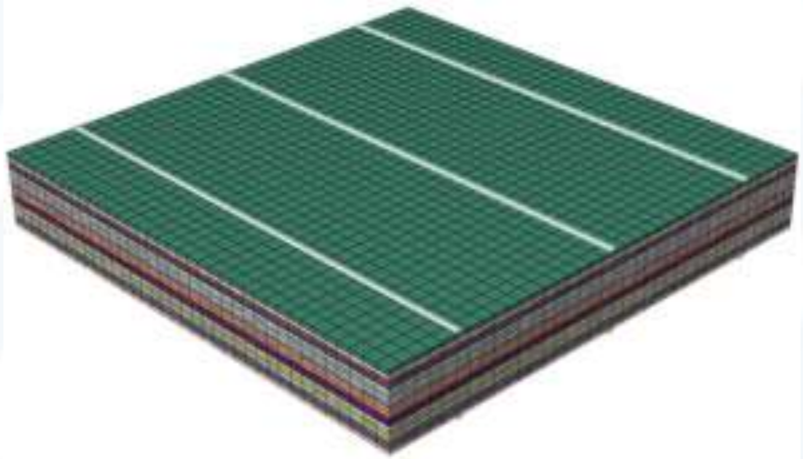

Hexahedral elements (C3D8R) with approximate size of 1 mm for composite layers

Mesoscale: Delamination

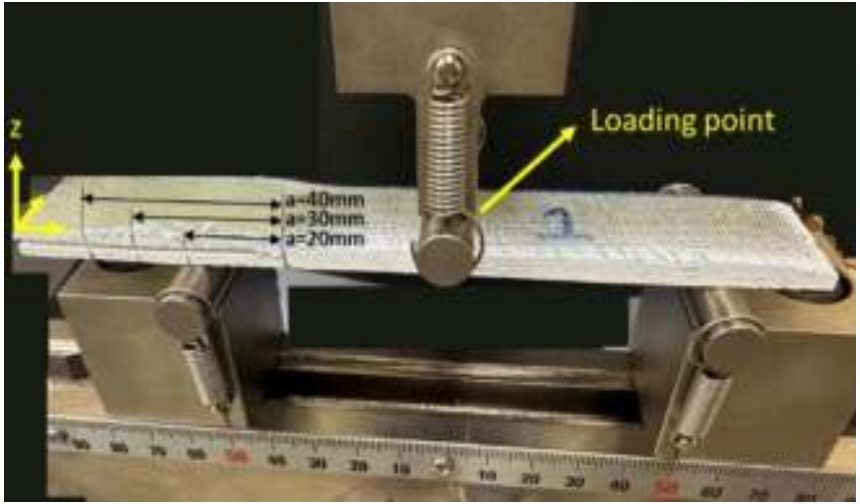

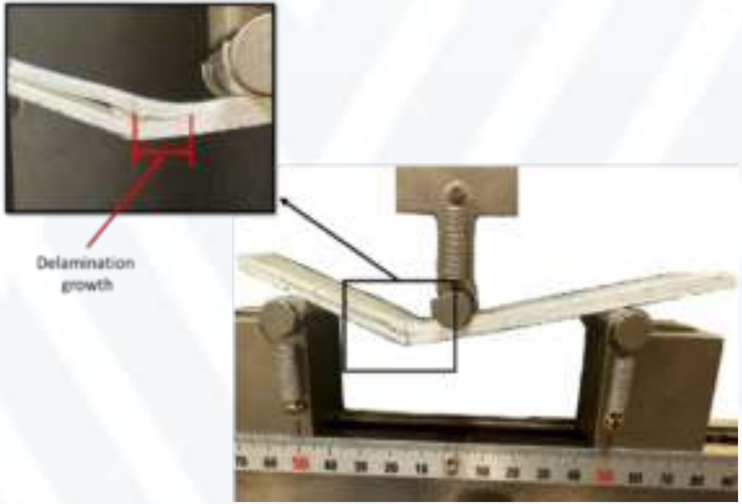

Mode II interlaminar fracture toughness [1]: $G_{IIc} = \dfrac{3mP_{Max}^2 a_0^2}{2B}$

[1] ASTM D7905/D7905M (Last Updated: Nov 06, 2019).

Mesoscale: Delamination

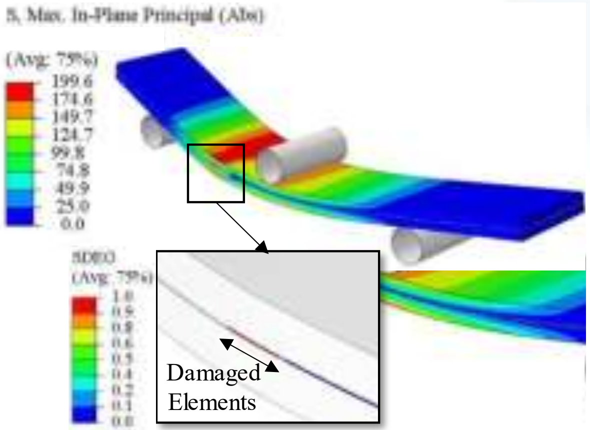

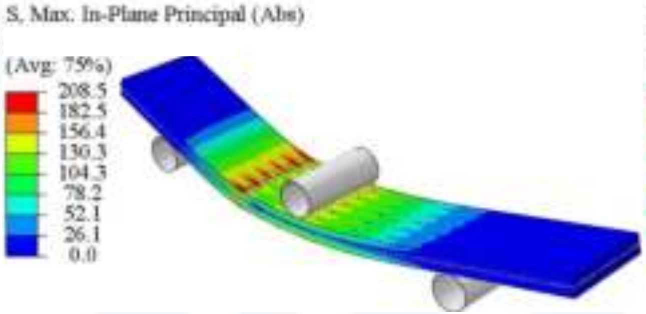

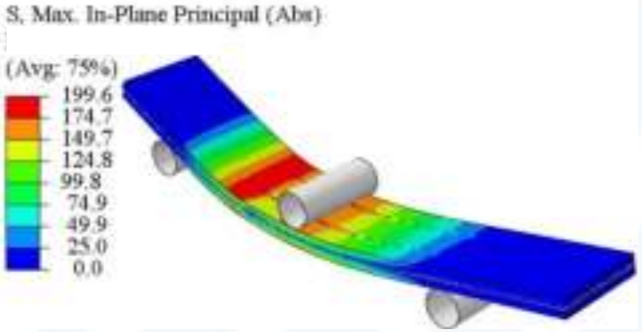

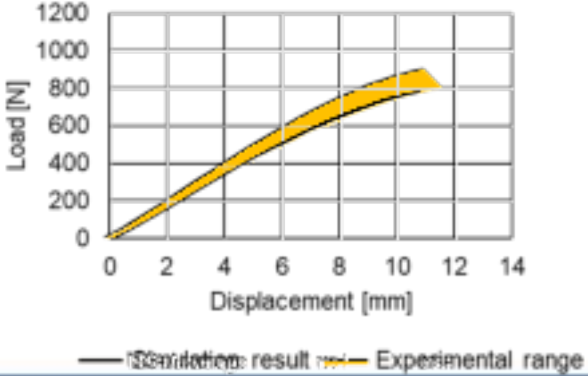

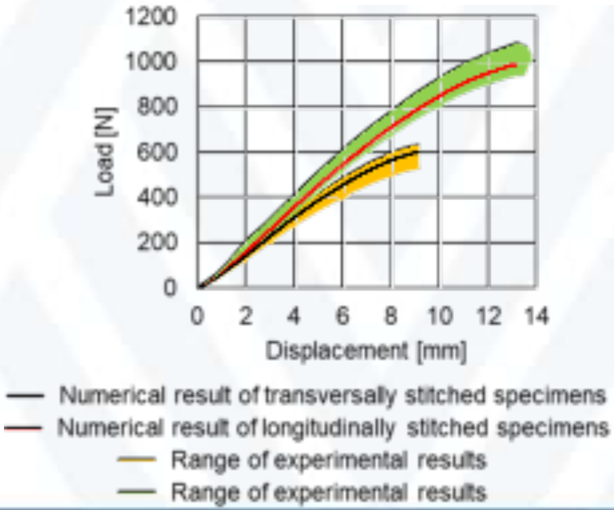

Macroscale: Experimental Controlled Impact

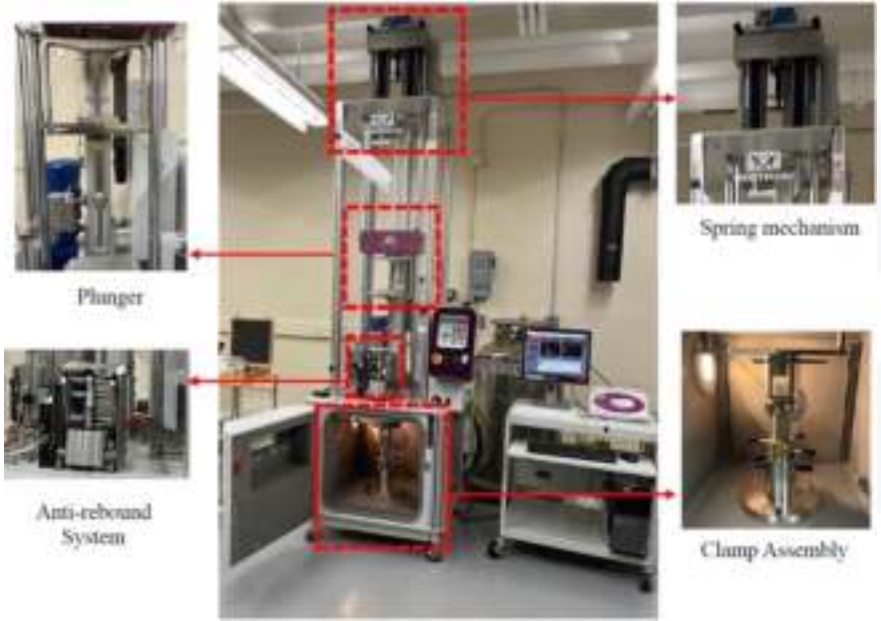

Low-velocity impact setup [1]

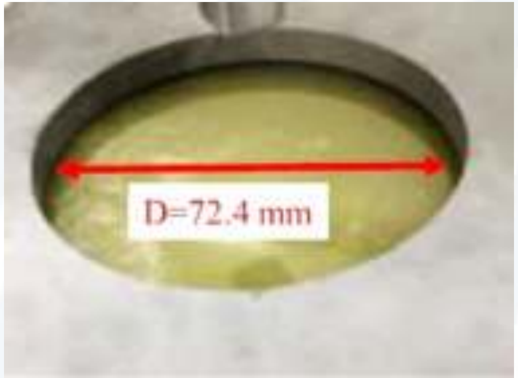

Exposed area [1]

Square cross-section steel Impactor
17.8 x 17.8 mm [1]

[1] Bhandari L (2023).

Macroscale: FE Low-Velocity Impact

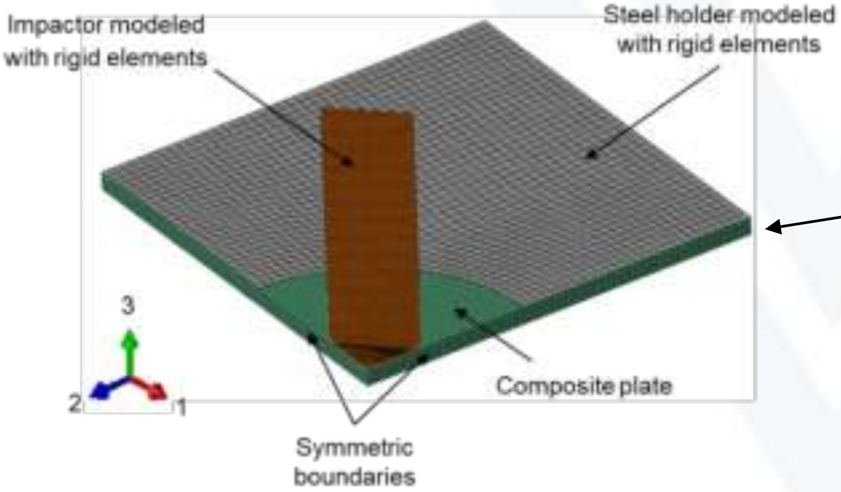

31684 linear hexahedral elements (C3D8R)
With homogenized material properties (HMP)
of stitched material from mesoscale RVE:

Homogenized properties of the mesoscale RVE of the stitched composite.	
Total thickness of RVE [mm]	3.68
Density [g/cm^3]	2.05
E_1 [MPa]	8407
E_2 [MPa]	7036
E_3 [MPa]	3518
ν_{12}	0.1
ν_{13}	0.11
ν_{23}	0.11
G_{12} [MPa]	1342
G_{13} [MPa]	268
G_{23} [MPa]	190
Tensile strength (US_1) [MPa]	473
Tensile strength (US_2) [MPa]	368
Tensile strength (US_3) [MPa]	200
in-plane shear strength (US_{12}) [MPa]	229
Out-of-plane shear strength (US_{13}) [MPa]	200
Out-of-plane shear strength (US_{23}) [MPa]	138

Macroscale Inputs:
-ROC (Radius of Curvature)
-DOEA (Diameter of Exposed Area)
-Impact velocity
-Shape of impactor
-Size of impactor

Macroscale Outputs
-Energy absorption
-Weight
-Force-Displacement

Mesoscale: Combination of Models

Integration of microscale HMP, damage model, delamination model, and stitch model under low-velocity impact (Top view).

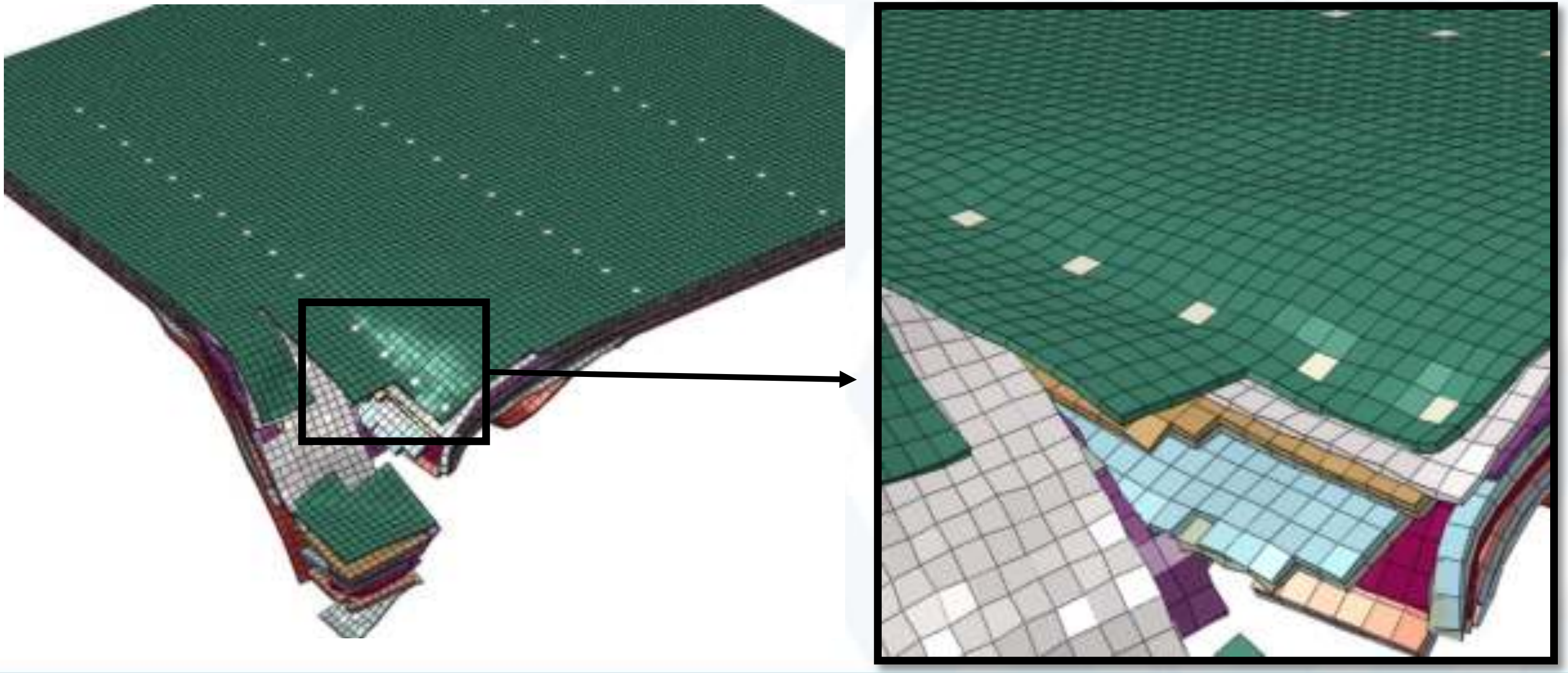

Mesoscale: Simulation of Stitches

Bottom view

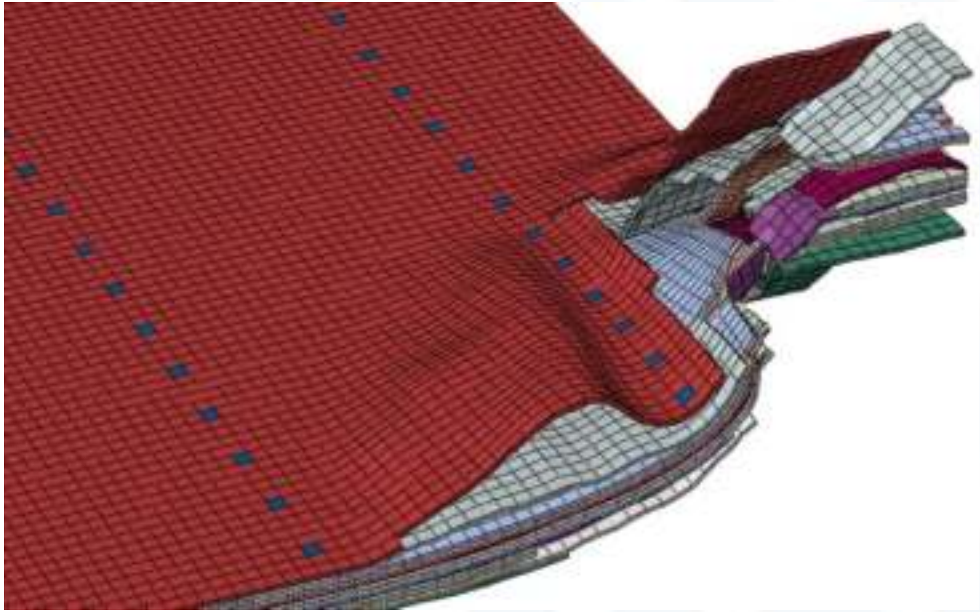

Simulation Results

Implementation of FEM-Based System

The composite jacket under low velocity impact

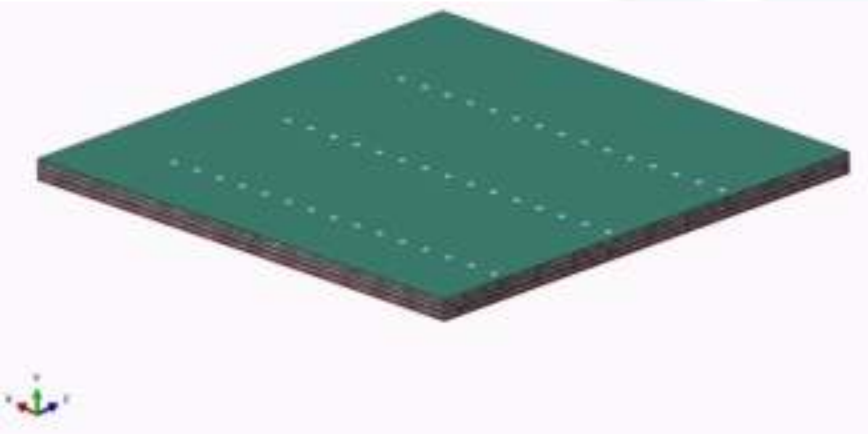

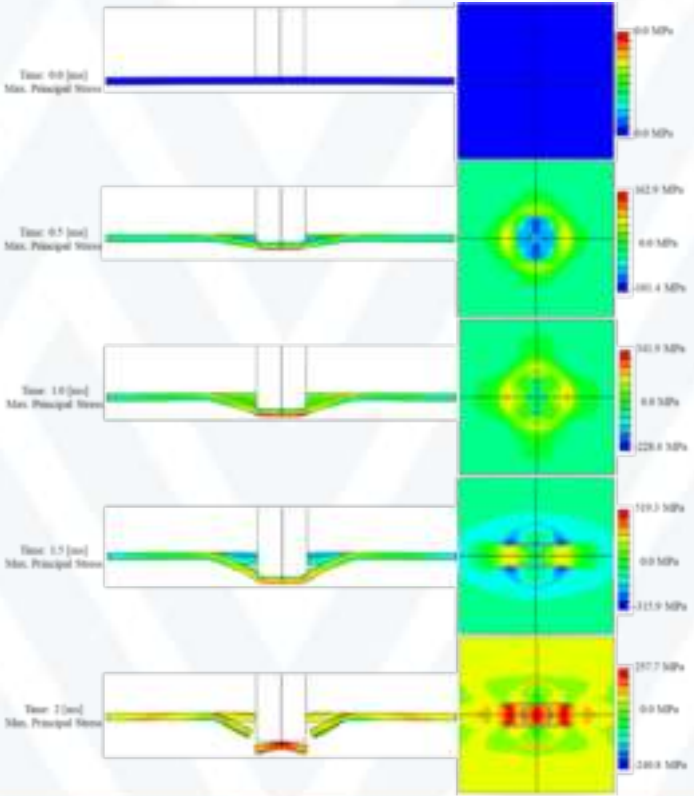

Validation with Experiments

Flat panel
12L: [G,K,G,G,K,G,G,K,G,G,K,G]
Orientation: [0,0,0,0,0,0,0,0,0,0,0,0]
Stitch Spacing: 25 mm
Loading rate: 7600 mm/s (Low-velocity impact)

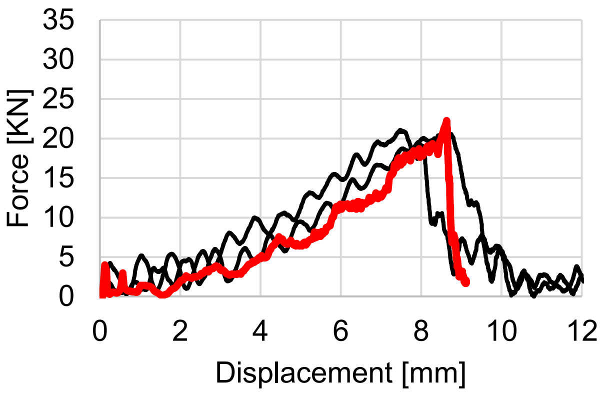

Experimental tests results
Simulation results

Flat panel
18L: [G,KG,K,G,K,G,K,G,K,G,K,G,K,G,K,G,K]
Orientation: [0,0,0,0,0,0,0,45,0,45,0,0,0,0,0,0,0,0]
Stitch Spacing: 12 mm
Loading rate: 7600 mm/s (Low-velocity impact)

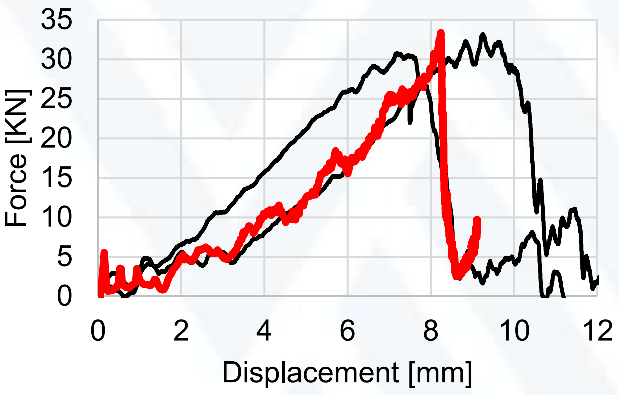

Experimental tests results
Simulation results

Curved panel
18L: [G,KG,K,G,K,G,K,G,K,G,K,G,K,G,K,G,K]
Orientation: [0,0,0,0,0,0,0,0,0,0,0,0,0,0,0,0,0,0]
Stitch Spacing: Un-stitched
Loading rate: 7600 mm/s (Low-velocity impact)

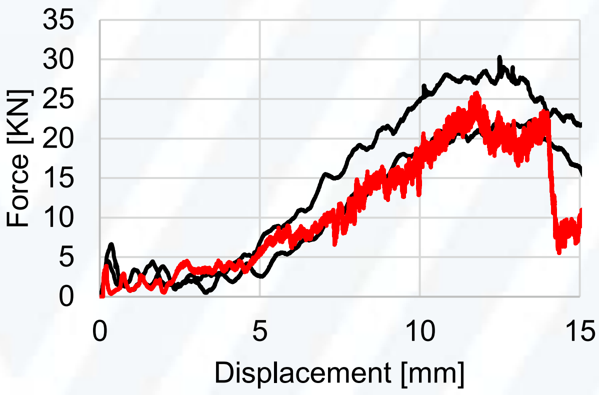

Experimental tests results
Simulation results

Validation

Curved panel upon foam and steel
18L: [G,KG,K,G,K,G,K,G,K,G,K,G,K,G,K,G,K]
Orientation: [0,0,0,0,0,0,0,0,0,0,0,0,0,0,0,0,0,0]
Stitch Spacing: 12 mm
Loading rate: 7600 mm/s (Low-velocity impact)

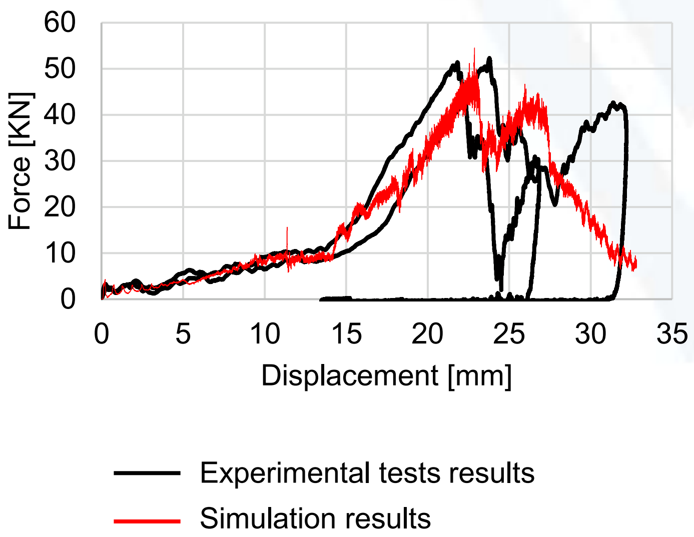

Curved panel upon foam and steel
18L: [G,KG,K,G,K,G,K,G,K,G,K,G,K,G,K,G,K]
Orientation: [0,0,0,0,0,0,0,0,0,0,0,0,0,0,0,0,0,0]
Stitch Spacing: 12 mm
Loading rate: 0.02 mm/s (Quasi-Static)

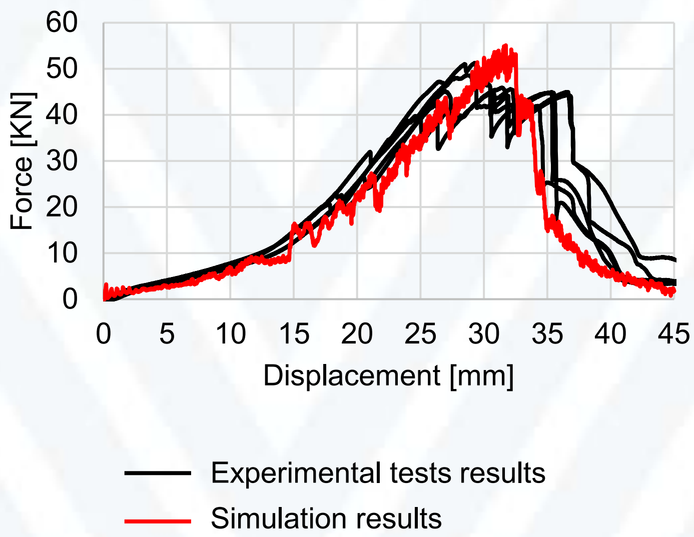

Thank you!

West Virginia University

Center for Integration of Composites into Infrastructure

Industrial Advisory Board (IAB) Meeting

Dec 7, 2023

Project #11: Evaluation of Fire Protection Methods for Composite Utility Structures

Ray Liang, Siddhant Sitoula, Chao Zhang, Hota GangaRao & Rakesh Gupta

Need and Industrial Relevance

- Sponsored by Electric Power Research Institute (EPRI)
- FRP poles have been receiving keen attention from utility companies due to their inherent advantages over wood, steel and concrete poles, especially for mountainous terrain.
- However, frequent wildfires pose a threat to these FRP composite poles without fire protection mechanisms.
- A better understanding on how FRP composite utility poles respond to wildfires is needed.

Overall Objectives

To better understand the performance of GFRP composite under fire and its implication to FRP composite utility structures when exposed to wildfire related thermal stresses, WVU team:

- Reviewed on fire performance of FRP composites
- Developed a flame exposure test method
- Evaluated strength reduction under fire exposure for poles and crossarms
- **Reviewed strategies to enhance the fire performance of FRP poles**
- **Evaluated wildfire protection methods**
- FRP wraps to restore the capacity of post-fire FRP poles and crossarms

Simulating Wildfires

Wildfires are uncontrolled burning of vegetation in uninhabited and wildland-urban interface areas ignited due to many natural and human causes (85%).

- Temperature range, heat flux, exposure time
- Ground fires, surface fires and crown fires
- Wildfire behavior is complex

Air temperature as the fire front approaches and various stages of burning [Mueller et al., 2018]

- Typical fire duration is 45-60 sec
- Typical fire temp peak below 1000 C
- Moderate: 30 to < 90 sec
- Severe: 90-120 sec
- Extreme 121 to 180 sec

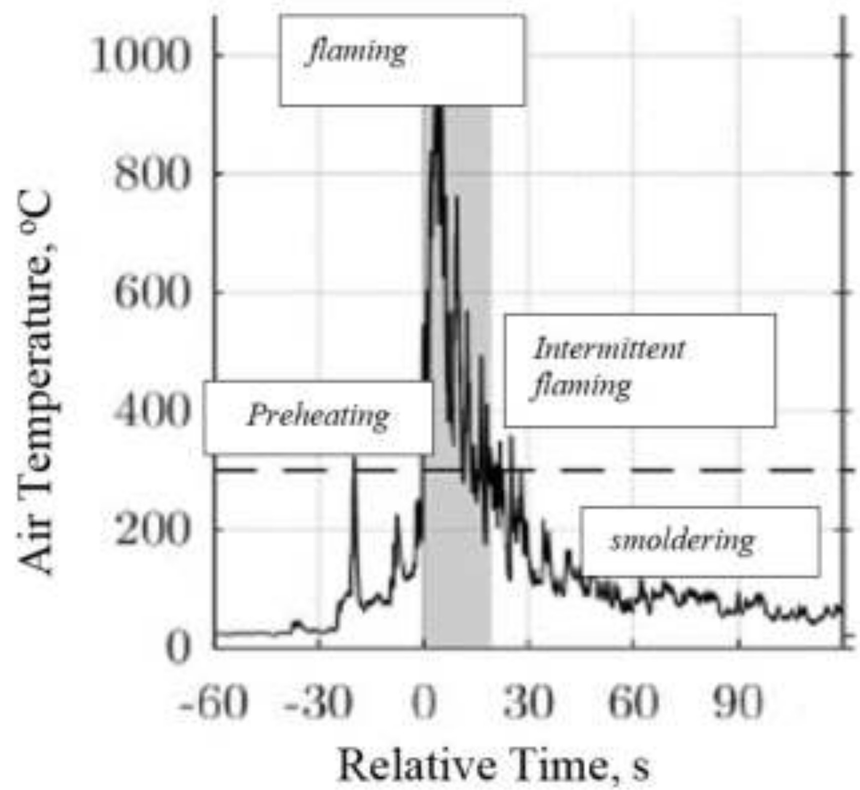

Fire Exposure ~1000C, 1-2-3 minutes

Sample Temperature Profile of the Flame
Impacting the Surface of the Pole Samples for 2 min Duration

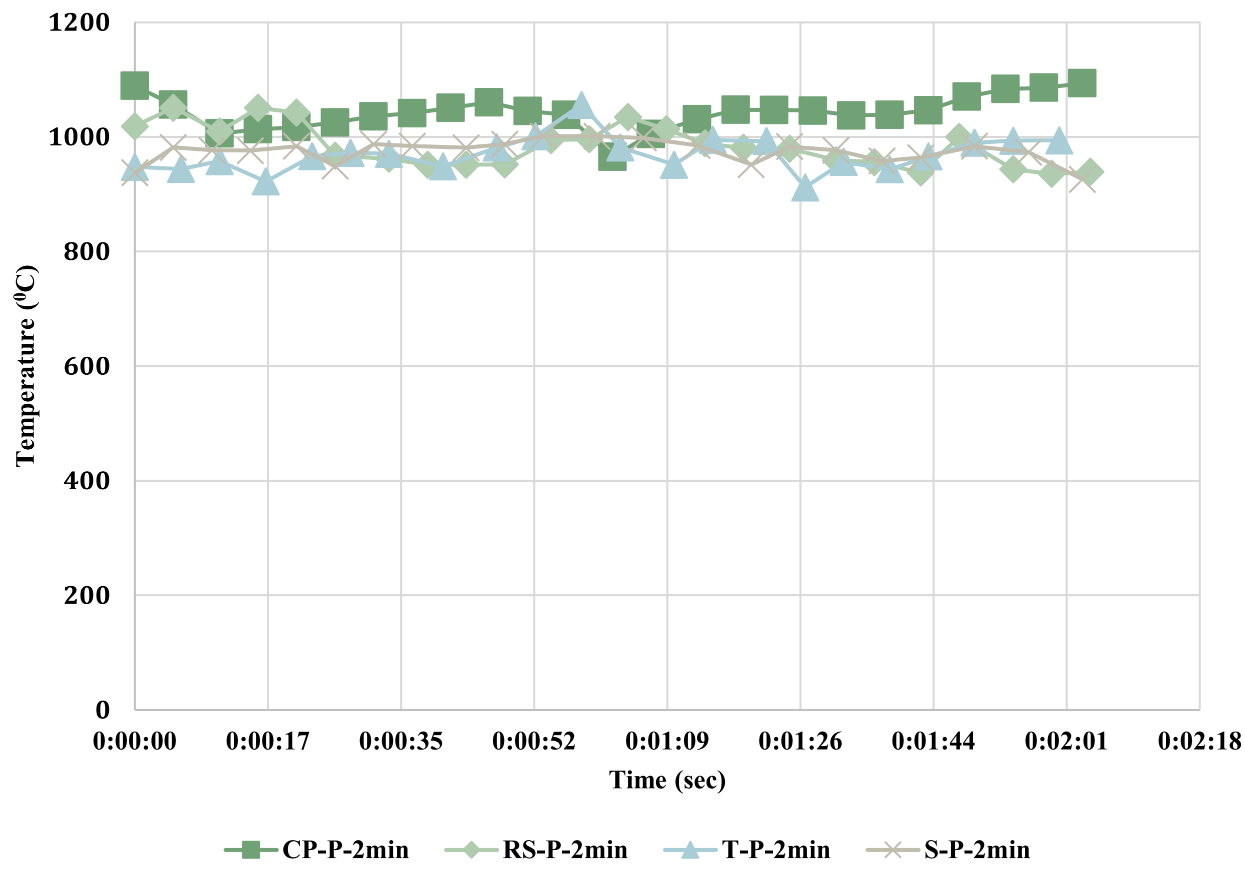

Samples

- Poles from 4 manufacturers
- Crossarms from 6 manufacturers



Application of Intumescent Coating




Poles with Protective Sleeve


RS Pole with Sleeve

CP Pole with Sleeve

Mechanical Test-setup

- ASTM D790-17 for the bending test
- ASTM D2334-16 for the short beam shear test

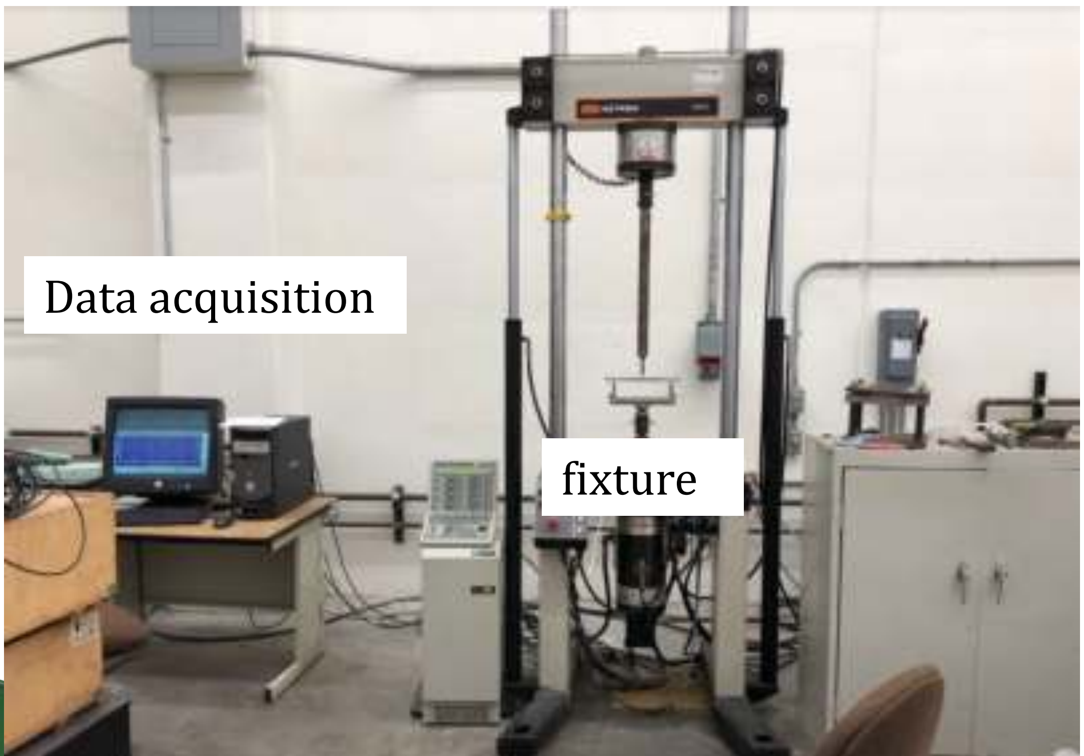

$\frac{L}{d}$=16 for bending test

$\frac{L}{d}$=4 for short beam shear test

L= Span length of specimen
d= thickness of the sample

Number of bending Tests: 229
Number of shear Tests : 99
A total number of Mech Tests: 328

Mechanical Test-setup

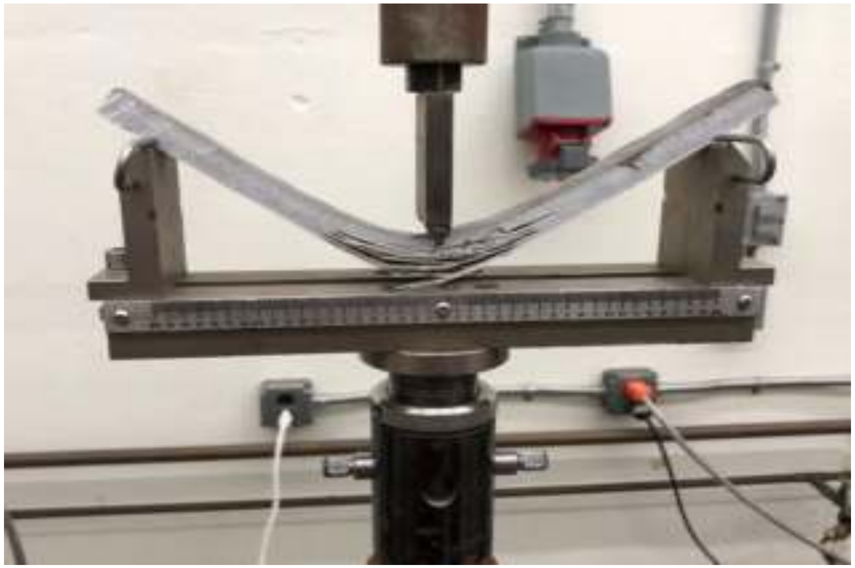

Three-point bending test on a sample

Short-beam shear test on a sample

- Tests were conducted by applying load on both unburnt and burnt sections/surfaces of the specimens.
- Bending and short-beam shear tests were conducted for poles.
- Only bending tests were conducted for cross-arms.

Bending strength retention percentage for uncoated (left) and coated (right) poles when load is applied on the burnt side of specimen

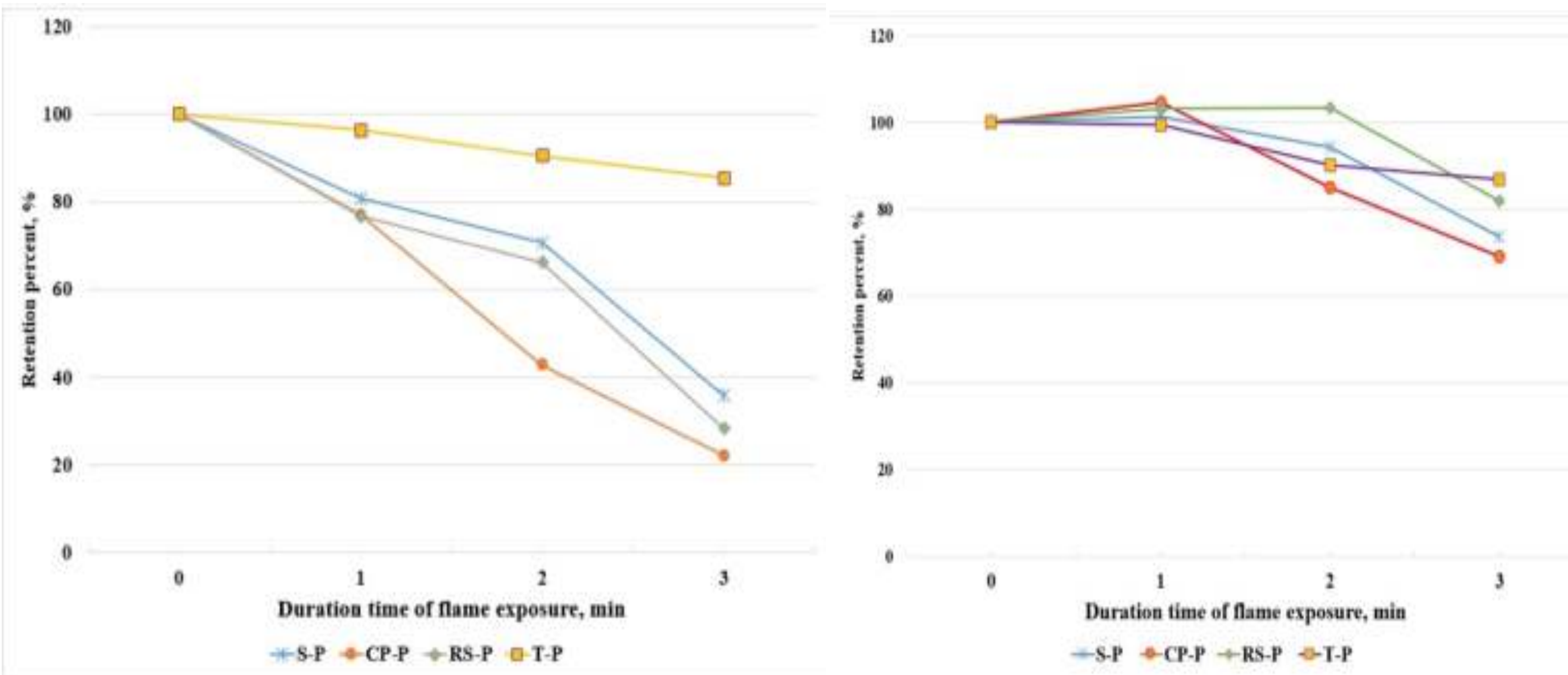

Shear strength retention percentage for uncoated (left) and coated (right) poles when load is applied on the unburnt side of specimen

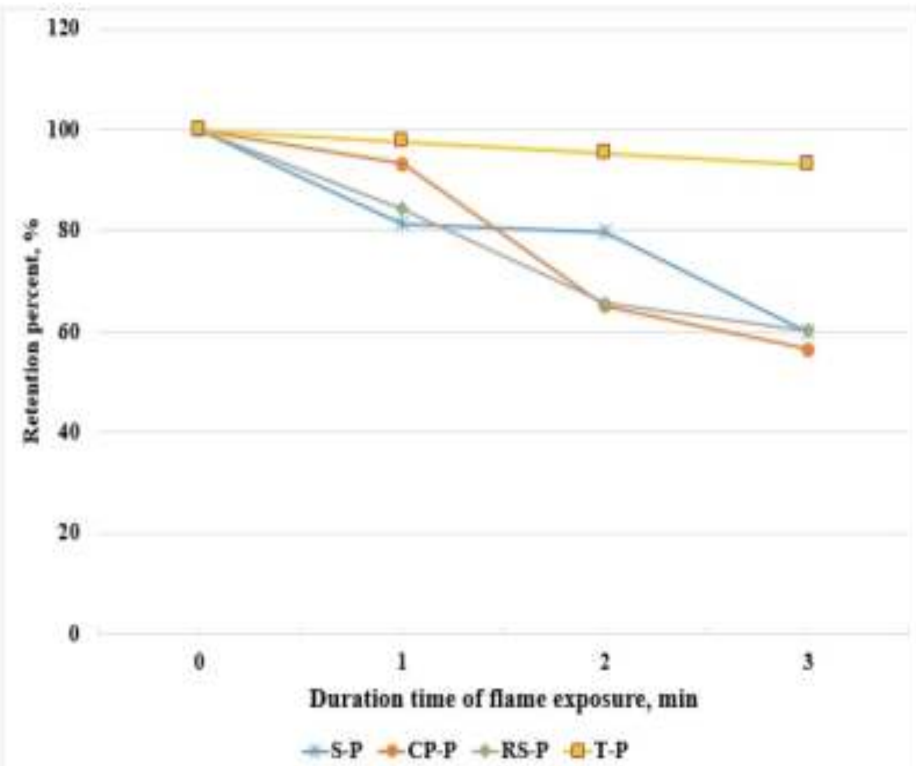

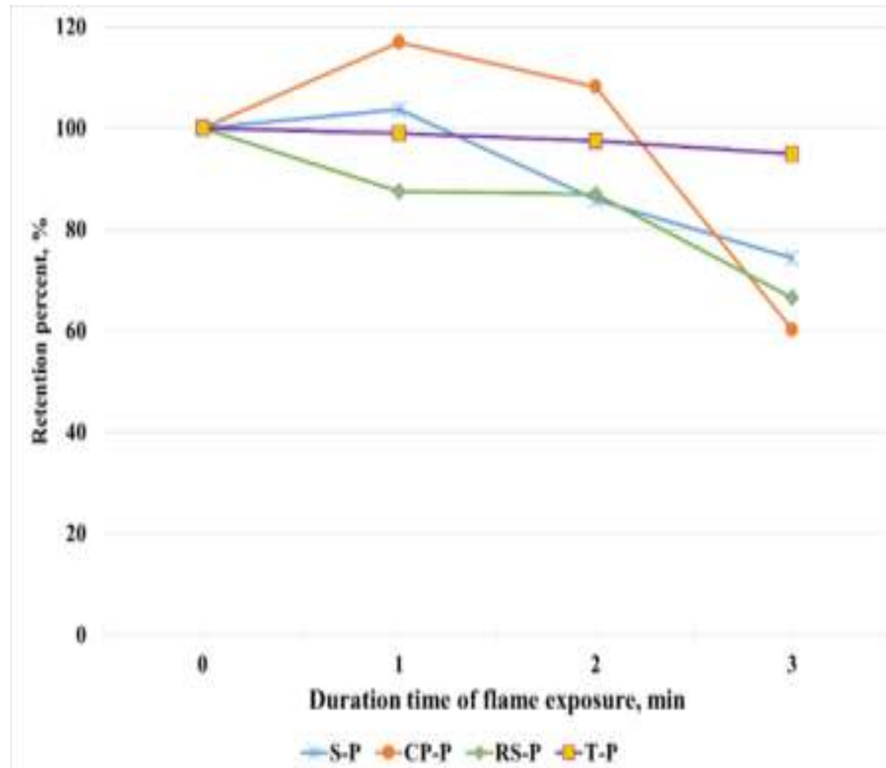

Comparison of bending strength of uncoated and coated CP crossarm samples

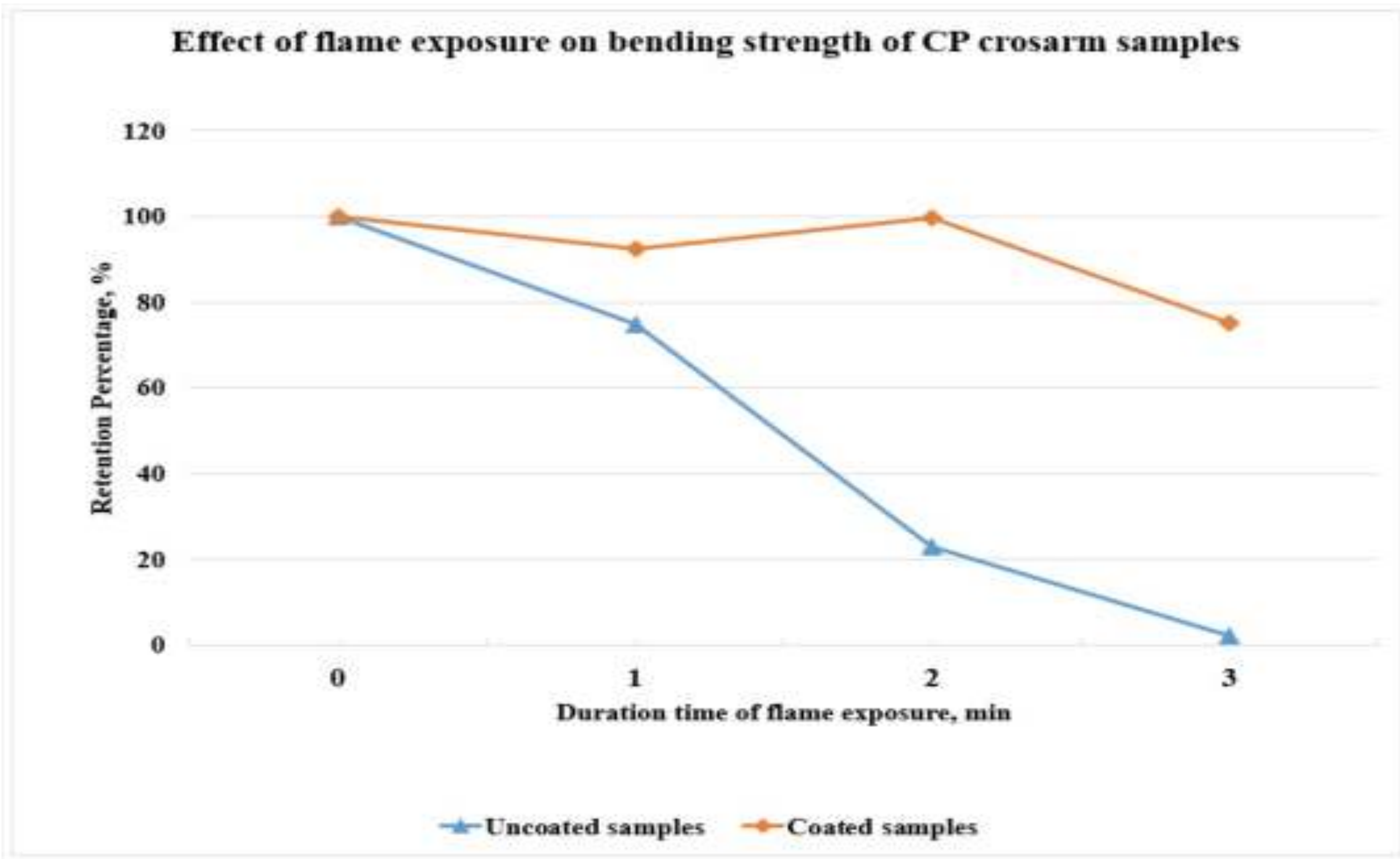

Comparison of bending strength of uncoated vs coated vs sleeved RS composite pole

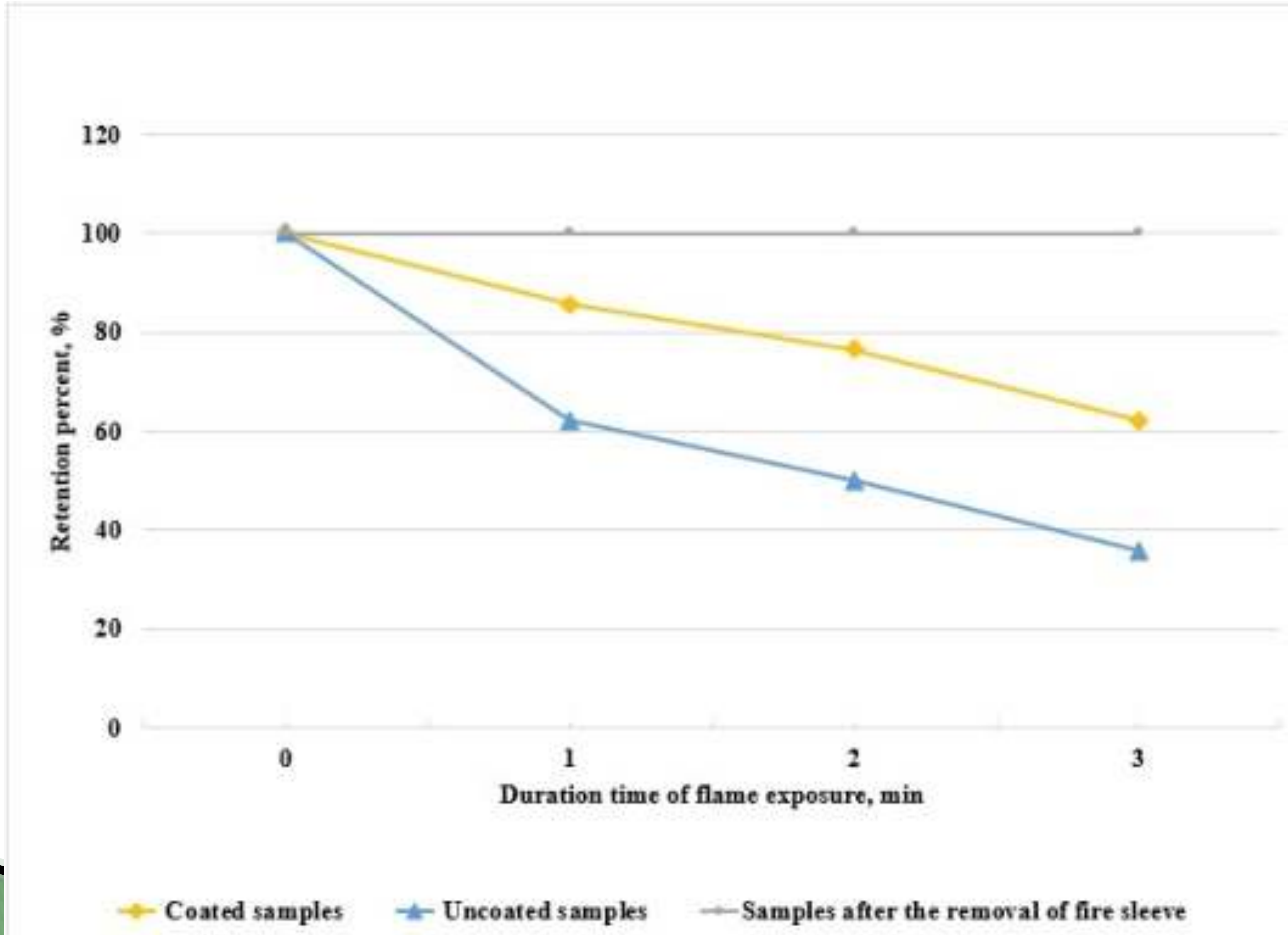

Comparison of bending strength of uncoated vs coated vs sleeved CP composite pole

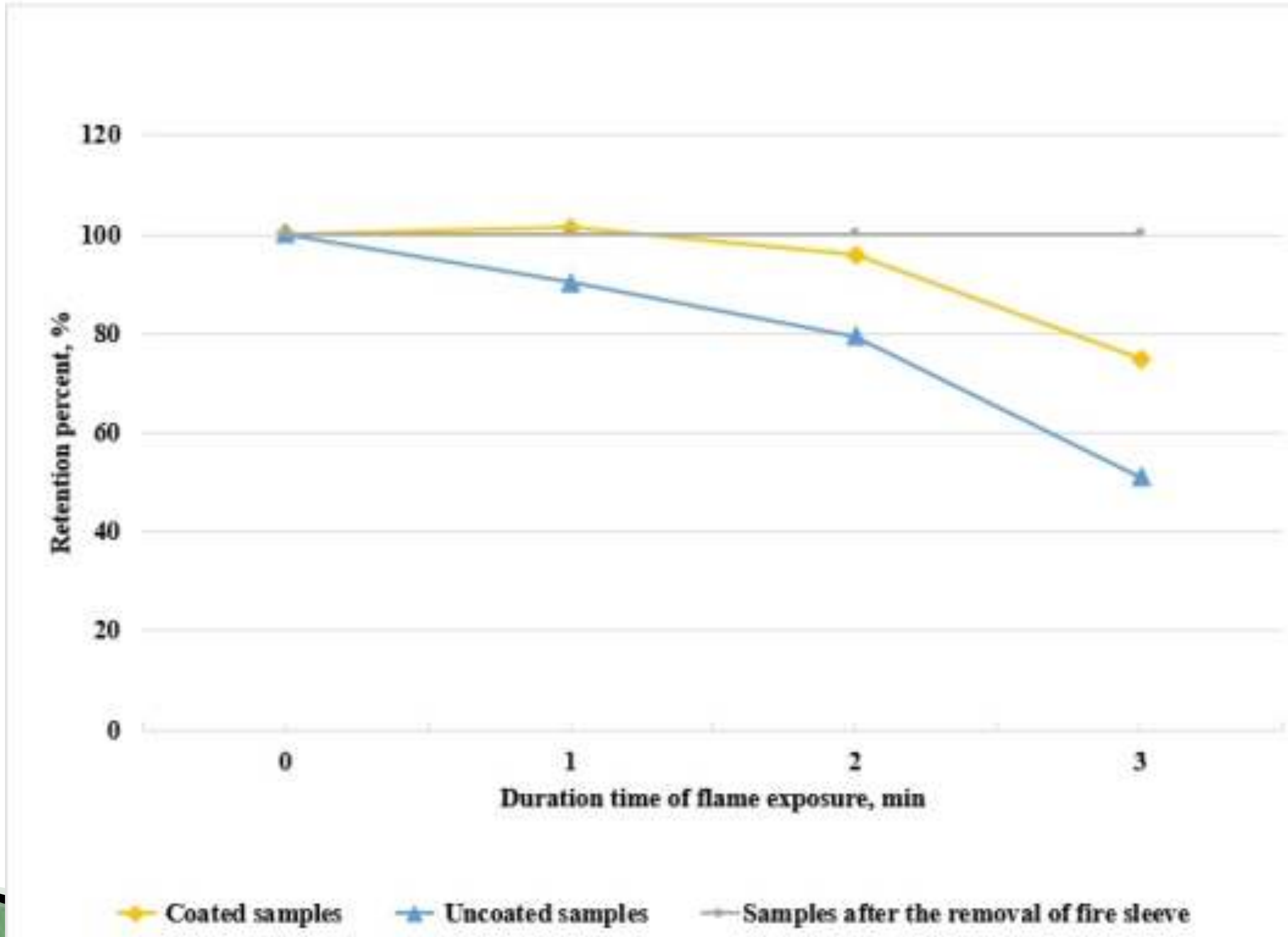

Comparison of short beam shear strength of uncoated vs coated vs sleeved CP composite pole

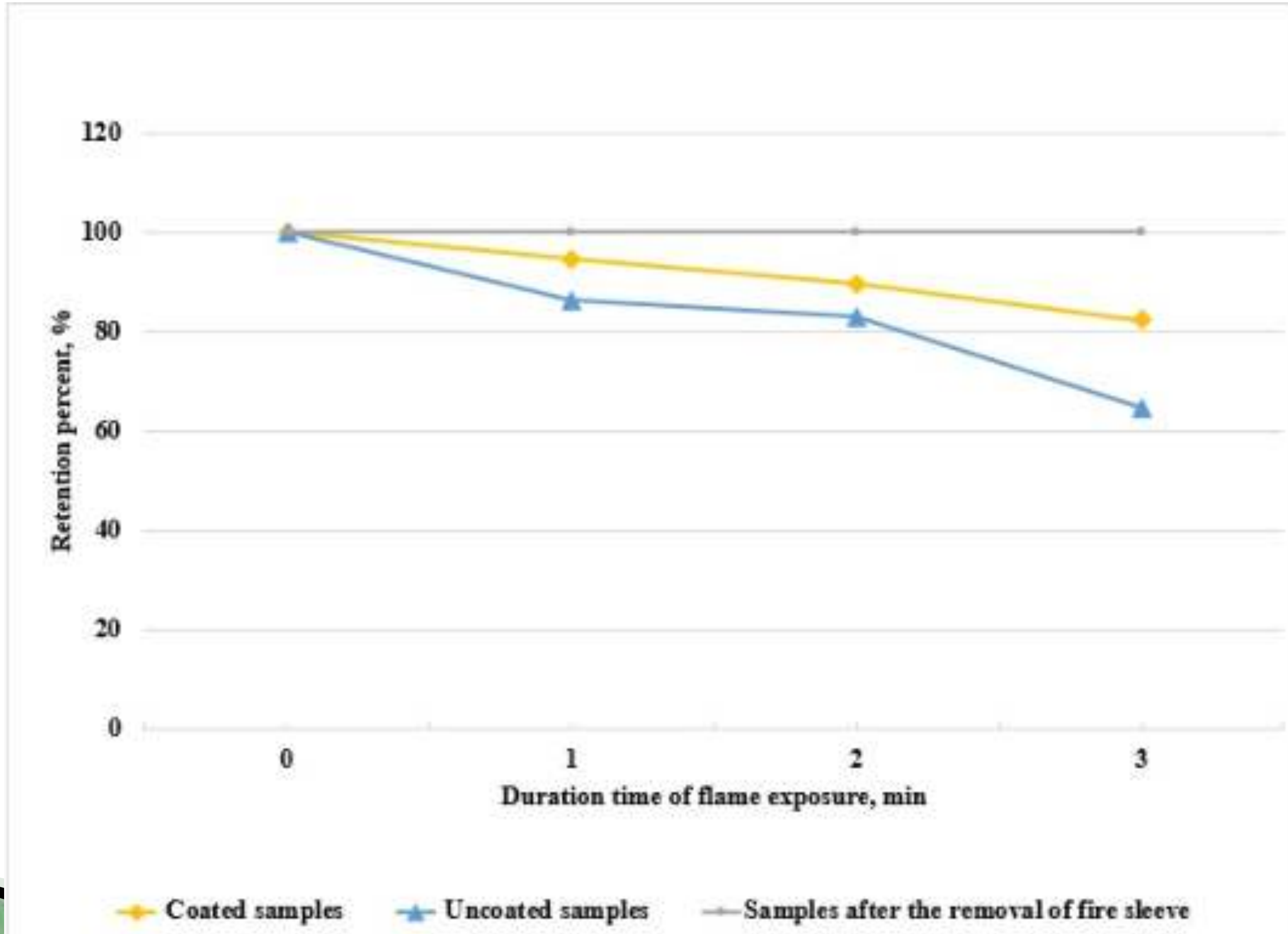

Effectiveness of Fire Protection Methods

Protection Method	Protection Effectiveness	Material Cost	Labor Cost	Notes
Intumescent Coating	Moderate to high	$1/ft $50 for 50 feet pole	$150 (automation)	Labor cost will be higher if NOT automated, $300
Sleeve	Full	30% additional per pole $1500 for 50 feet pole	$500	Protection sleeve only applicable to 1 feet below ground and 20 feet above ground

Conclusions

- FRP utility poles, especially with use of intumescent coatings at low cost, are able to survive from general wildfires. This conclusion will help utility industries to use FRP poles with confidence.

- FRP utility poles with protective sleeve offer the best protection again wildfire but at additional high cost.

Impact

- FRP utility poles, especially with use of intumescent coatings, are able to survive from general wildfires. This conclusion will help utility industries to use FRP poles with confidence.

- FRP wraps readily available can be used to retrofit the post-fire utility poles, if needed. This will further release potential concerns from utility industries.

Project Duration & Proposed Budget

Sponsor	Duration	Budget		Total, $	Progress Status
		Spent, $	Remaining, $		
EPRI	**2020.4-2023.12**	**75k**	**0k**	**75,000**	**Ongoing to Year 4**

Project Name: Responses of FRP Composite Utility Poles and Crossarms under Wildfires
Project Number: WVU-11

Courtesy of RS Technologies

Center for Integration of Composites into Infrastructure

Project # 12
Responses of Composite Structural Components and Systems

December 2023

Sponsor: Sports Imports & Bedford Reinforced Plastics, Inc.

Presented by: Maxwell Carey (GRA)
Jack Wykle (GRA)
Manish Adhikari (GRA)
Dr. Hota V.S.GangaRao

Constructed Facilities Center
Wadsworth Department of Civil and Environmental Engineering
Statler College of Engineering and Mineral Resources

Introduction to FRP Composite

Fiber Reinforced Polymers (FRP) Composites

- made of a polymer matrix reinforced with fibers

Use in Structural Engineering:

- 2 to 8 times stronger than steel based on fiber type on unit weight basis (specific strength)
- More flexible than steel, but some carbon composite are 3 times stiffer than steel
- Corrosion Resistance
- Thermal Conductivity/Resistance

Handrails, structural supports, ladders, columns, platforms, and grating

waterfront sheet piles

GFRP wicket gates

FRP Volleyball Poles

FRP components ⟷ FRP Structures

FRP Structural Components

- **Beams:** Experience bending under loads; composites can be designed to handle specific stress profiles.
- **Columns:** Support compressive loads; composite materials can be tailored for buckling resistance.
- **Plates and Sheet:** Form the flat or curved surfaces in structures like aircraft fuselages or boat hulls.
- **Joints and Connections:** Key to the integrity of composite structures; designed to manage loads without failure.

Beam

Column

Sheet

Joint

Composite Structural Systems: Integrated Responses

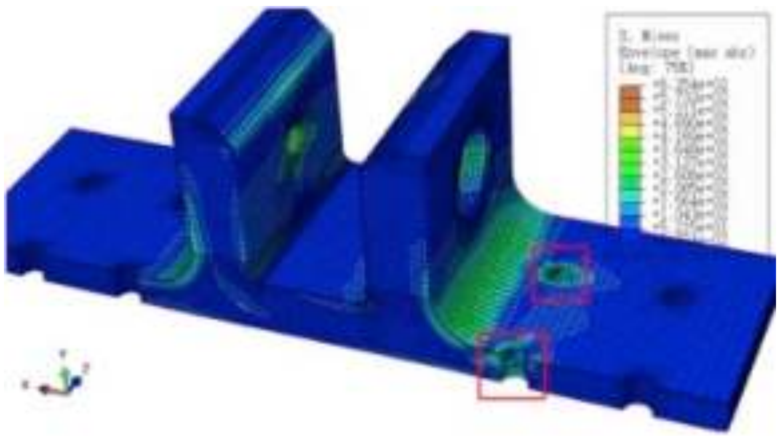

Stress Distribution: Composites often distribute loads differently due to their anisotropy.

Component Interaction: The synergy between different composite materials within a structure.

Redundancy and Load Paths: Ensuring structural integrity even if one component fails.

Objectives

- ✓ Assess the load-bearing capacity of composite elements, specifically carbon fiber poles, and composite structures, such as platforms, under actual loading conditions.
- ✓ Identify and analyze the modes and initiation points of failure within composite components and structures.
- ✓ Examine the influence of connections and joints, including the impact of torque levels and fixed conditions, on the structural integrity of fiber-reinforced polymer (FRP) systems.

FRP platform

Case 1 - Carbon fiber poles

To simulate the bending of volleyball poles caused by impacts from athletes or high-speed balls, and to establish safe load-bearing values. All specimen was test at women and men height.

Real-world scenario

Test in lab

Specimen name	Women's Height		Men's Height	
	Pin	Pulley	Pin	Pulley
FRP Composite	87.25"	89.25"	94.00"	96.00"
Aluminum Sample	86.50"	88.50"	93.75"	95.75"

Case 1 - Carbon fiber poles

FRP Composite

Aluminum Sample

•**Aluminum Sample** exhibits ductile failure, characterized by significant deformation before failure. **FRP Composite Sample** shows brittle failure, where the material breaks suddenly without substantial deformation.

•**Anisotropic Behavior of FRP Composite** leads to uneven deflection at tensile and compressive sides during bending, necessitating additional measurements.

Case 2 – GFRP Platform subjected to lateral load

To evaluate the resilience of FRP platforms against wind load, particularly focusing on their ability to withstand lateral forces.

Test Setup for loading in long direction (a) and short direction (b).

Experimental Variations:

- ❑ Angles thickness (used as platform-floor connections), yellow grating, torque Level,
- ❑ platform size Sizes: 3x3 ft, 3x6 ft, 3x9 ft platforms tested.
- ❑ Load Application: Along the long and short direction.

Case 2 – GFRP Platform subjected to lateral load

Platform-floor connections effect

3 by 8-inch Angle

½ inch Angle

½ inch Square Tube

3 by 8-inch Angle Connection: tension and tearing around bolt leading shear failure
1/2 inch Angle Connection : delamination and fracturing
1/2-inch Square Tube Connection : rupture damages near the bolt

Case 2 – GFRP Platform subjected to lateral load

Torque effect

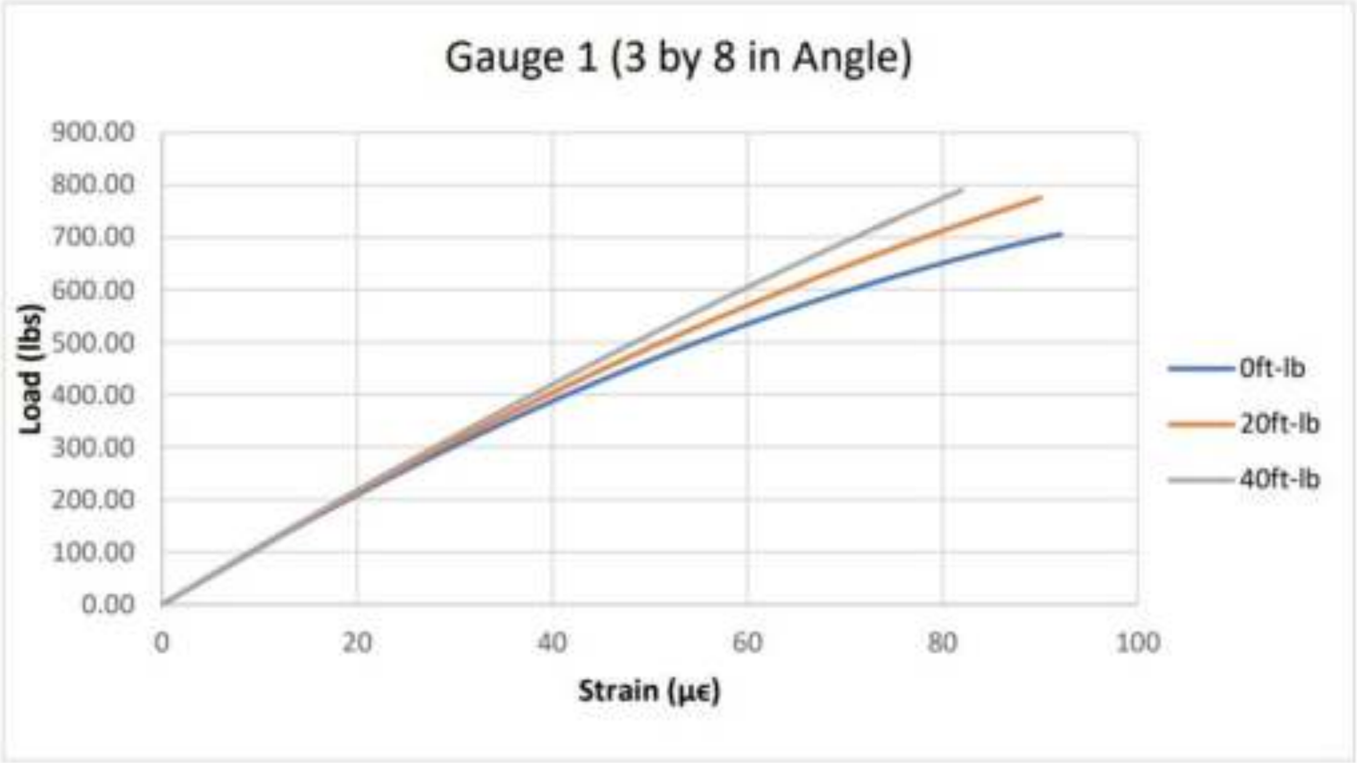

Increasing the torque level enhances the structure's resistance to lateral load

Case 2 – GFRP Platform subjected to lateral load

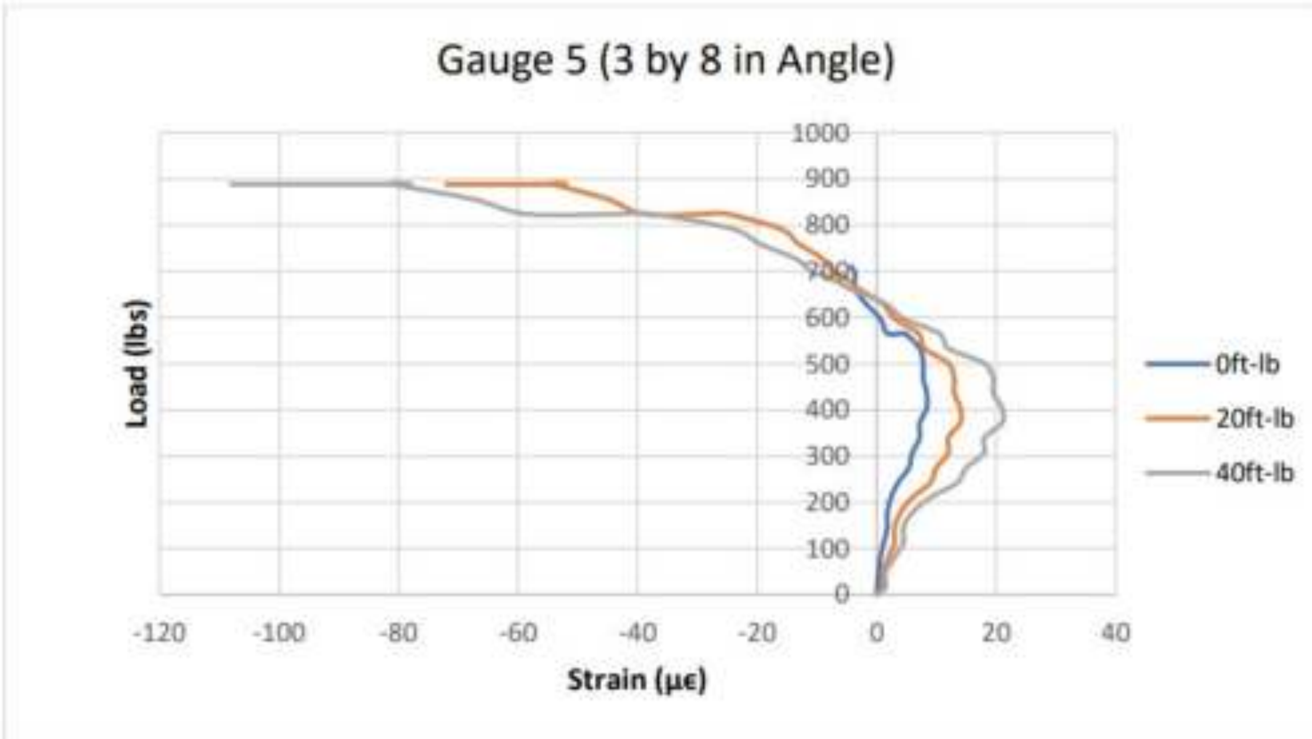

The initial change in the slope of the strain data indicates a gradual loosening at the connection.

Summary

Carbon Poles under Pulling Load

- Analysis of failure modes for volleyball poles design and safety

FRP Platform Joint Efficiency

- provides an understanding about failure modes and joint efficiency of bolted joints on the FRP platform under lateral load
- Identified the critical role of torque levels in maintaining joint integrity and overall structure safety in platform system.

Project Duration & Proposed Budget

Sponsor	Duration	Budget		Total, $	Progress Status
		Spent, $	Remaining, $		
Sports Imports & BRP	**2023.9-2023.12**	**20,000**	**2,000**	**18,000**	**95%**

Project Name: Responses of Composite Structural Components and Systems
Project Number: WVU 12

Thank you!

Center for Integration of Composites into Infrastructure

Industrial Advisory Board (IAB) Meeting

December 7, 2023

CICI-13

Design and Repair of Prestressed Concrete Dapped End Beams

Mohammad Qambar – PhD Student

PI: Gregory Lucier

Co-PI: Rudolf Seracino, Giorgio Proestos

Introduction

- Daps are a common end condition in thin-stemmed double-tee beams that allow for reduced floor-to-floor heights.
  - Repairs are sometimes needed due to fabrication errors, change in loading, or damage sustained in transit, during construction, or in service.

Previous Work

- Previous work on strengthening dapped ends in the literature and at NCSU, has led to insights on the viability of strengthening these members.
- Strengthening can be difficult in-situ as some common details are impractical (wrapping end of nib for example).

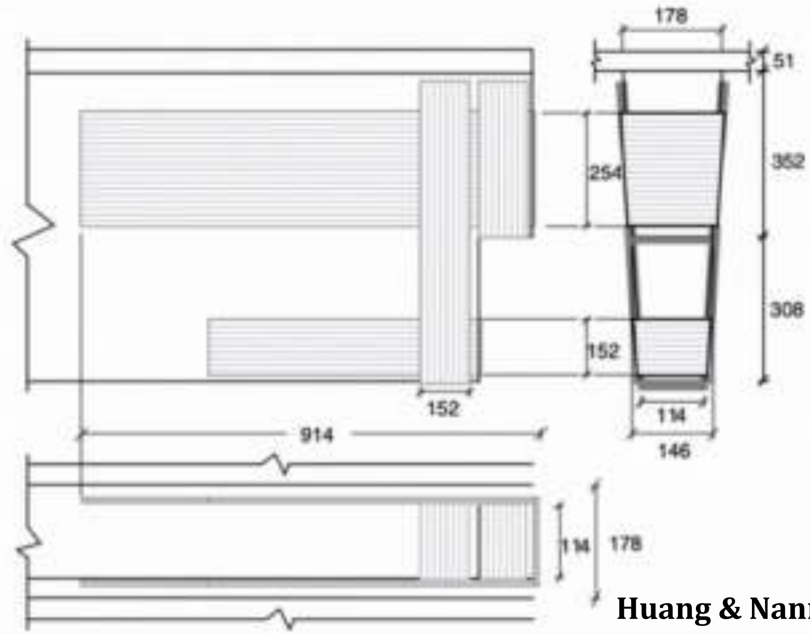

Huang & Nanni, 2006

Taher, 2005

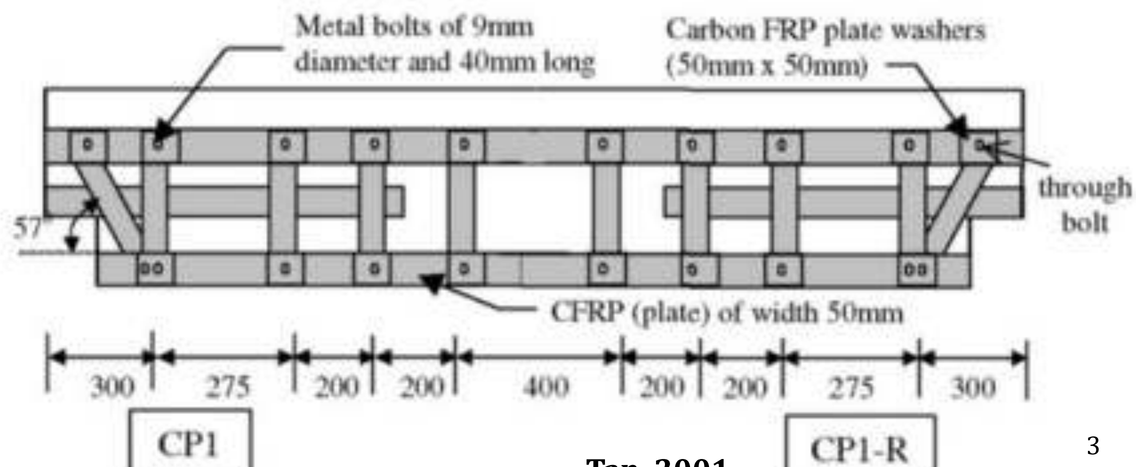

Tan, 2001

Project Goals and Objectives

- Goals of this project:
  - Develop an FRP strengthening technique for thin-stemmed prestressed double tees that may be readily applied in situ.
  - Investigate the applicability of strain compatibility between a bonded FRP plate and surrounding concrete (dapped ends are disturbed regions).

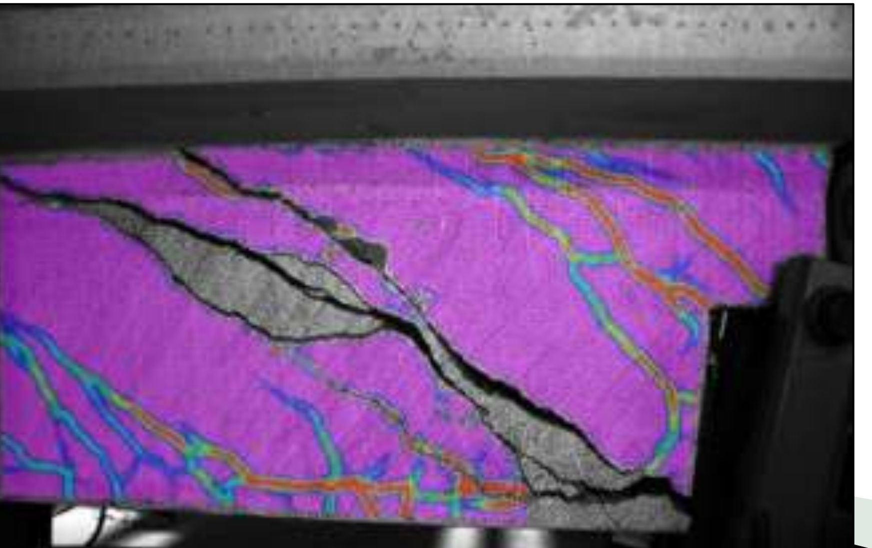

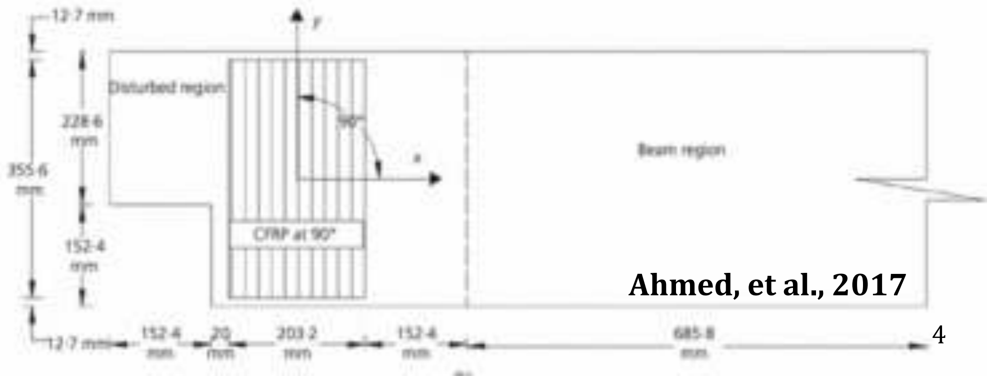

Ahmed, et al., 2017

Failure Modes

Shear in the Full Section

Shear in the Nib

Flexure-Shear/Splitting

Normal Weight Concrete Specimen Investigated

- NWC prestressed DT with (2) layers of W4 @ 8 in. stem mesh.
- Failure at an end reaction of 42.6 kips.

Test Setup to Directly Load the Nib

Testing Plan

- The current specimen will be a pilot test; Results will guide future strengthening.

- **Only** the nib strengthened and loaded in this pilot test, allowing for direct evaluation of GFRP plates (typical relatively low modulus) as a strengthening technique in shear.

- The ultimate goal is to achieve an observable increase in nib capacity (nib shear limits some designs).

Strengthening Configuration

- Pultruded GFRP plate
- Bi-directional strength, light weight, good availability, low cost, and ease of installation. Corrosion resistance a positive in many applications.
- Are the shear strains compatible? (GRFP has a relatively low modulus; will it provide capacity in shear at the right time?)
  - The plate needs anchoring in the nib since the bonded length is short and wrapping the end of the nib is often not practical.

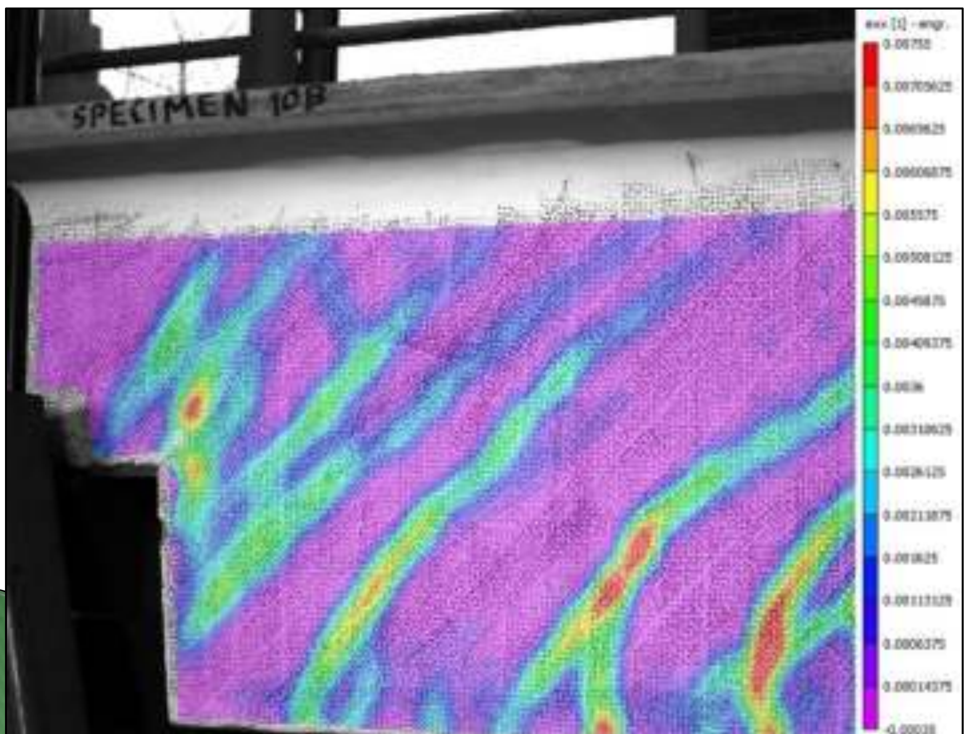

Strengthening Configuration

- GFRP Plate shear modulus = 0.425 x 10^6 psi.
- Conservative estimate of shear strain = 0.002
  - Precluding debonding, should nominally achieve a shear capacity increase of 6.8 kips.
- Mechanical fastening to develop required strains.

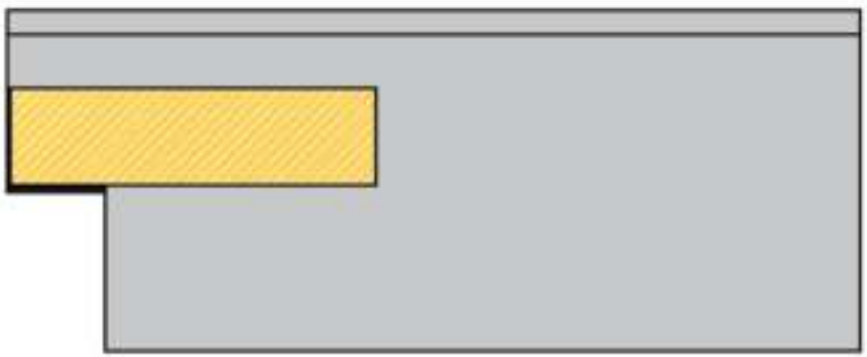

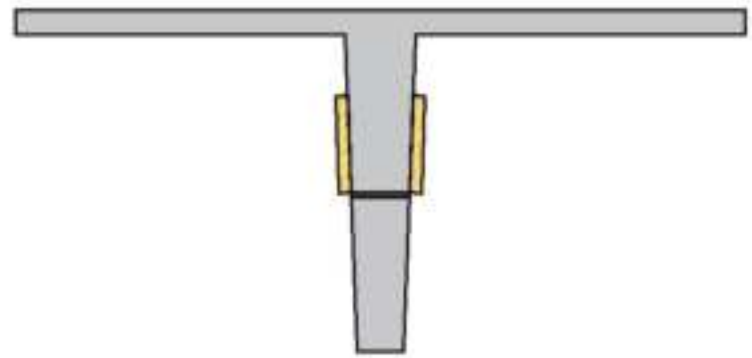

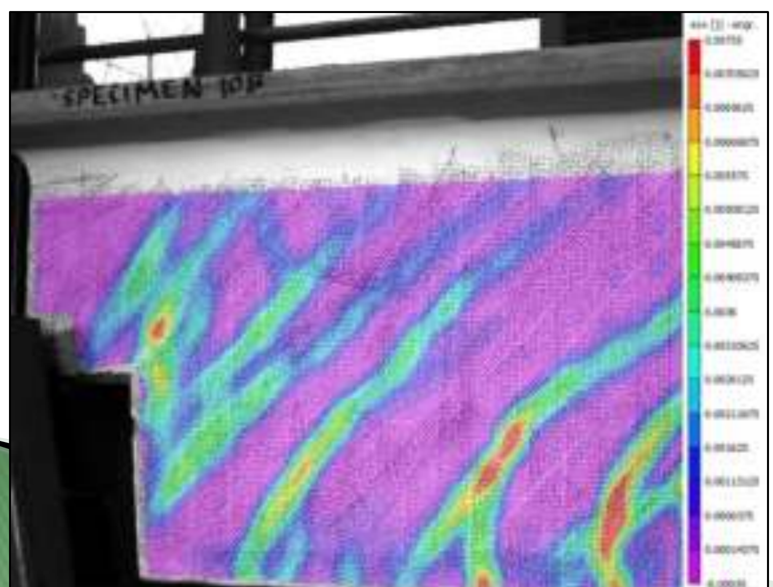

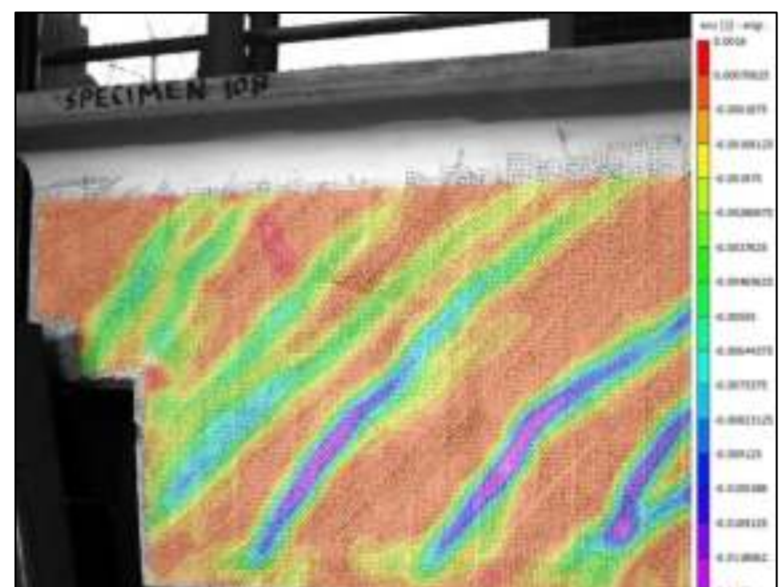

Strengthening Configuration

- Two 8” x 36” x 0.5” GFRP plates mechanically fastened by (12) 3/8” diameter stainless threaded rods.
- Plate designed using typical failure modes (section rupture, bolt shear, etc.), i.e., assuming various debonding modes would not govern due to the mechanical anchorage.

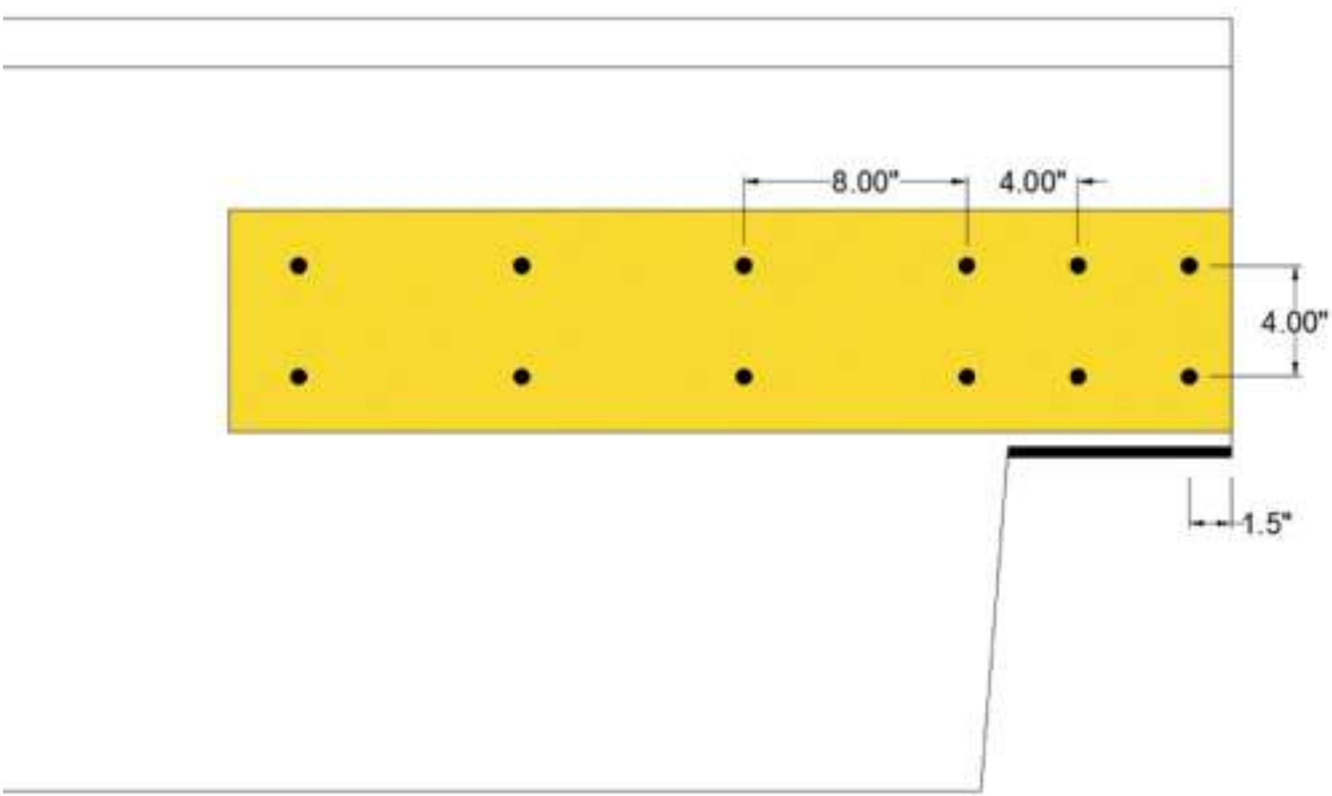

Application of Strengthening

Testing

- Test setup consisted of an applied load beneath the nib, a string potentiometer measuring nib displacement, and digital image correlation (DIC) to capture real-time strain data.

Testing

- Load-displacement data is shown below.
- Member achieved a peak reaction of 66 kips at a nib displacement of 1.25 in.
- Member ultimately experienced heavy flexural distress, at which point the test was unloaded.
- DIC Data was then used to determine whether utilization of the relatively low-modulus GFRP plate was achieved.

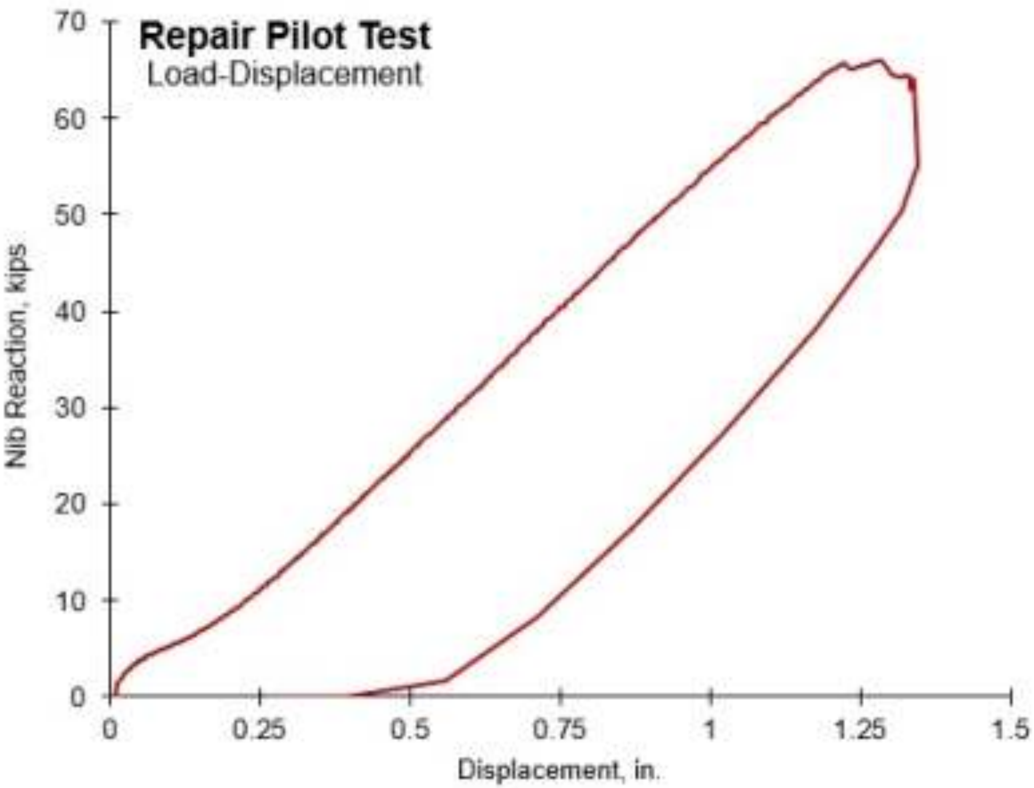

Testing

Shear Strains

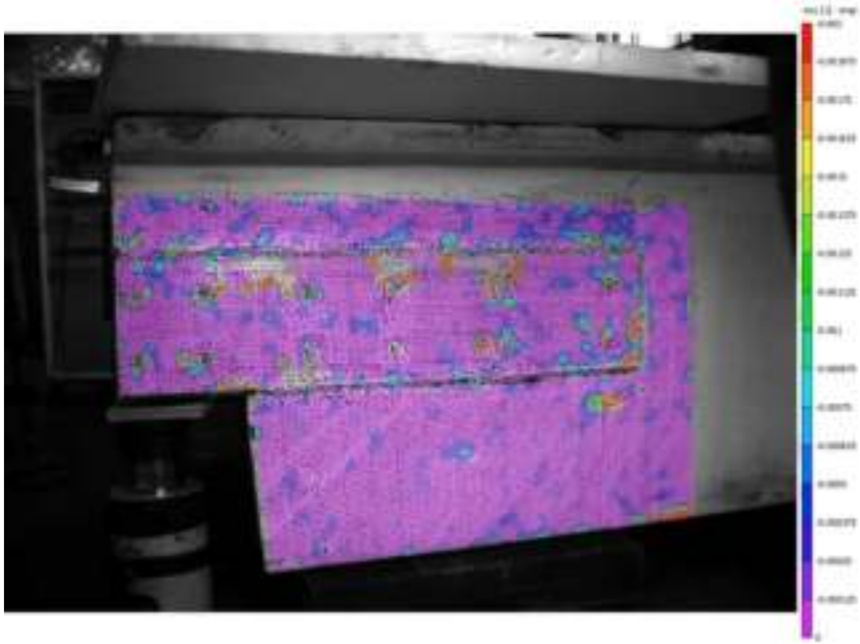

Principal Tensile Strains

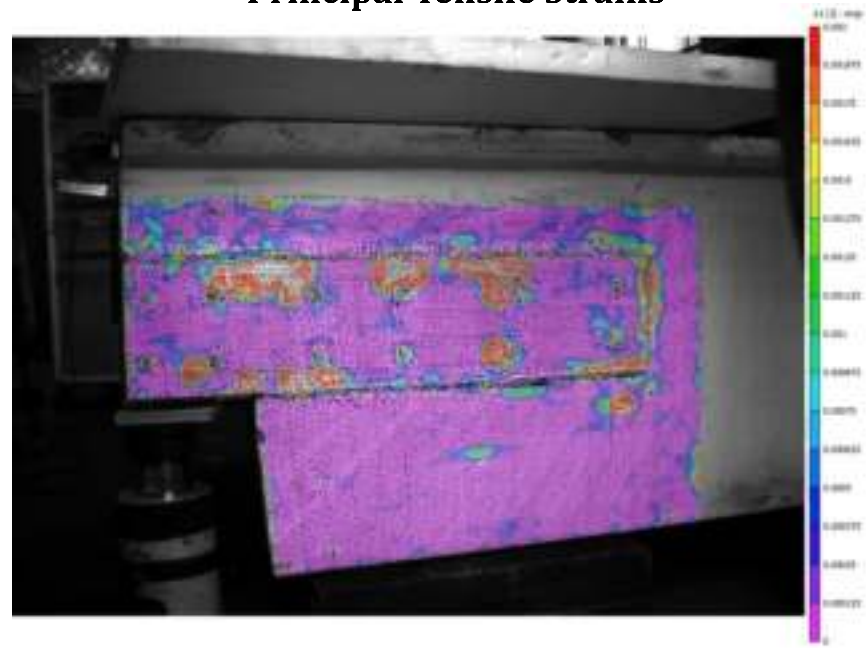

Ongoing / Future Work

Strain c
shear st
gives the

- Expa
  to the
  situ n
- Expa
  end n
  splitt

Thank you for your interest and questions

Project Name: Design and Repair of Prestressed Concrete Dapped End Beams

Project Number: CICI-13

Center for Integration of Composites into Infrastructure

Center for Integration of Composites into Infrastructure

Industrial Advisory Board (IAB) Meeting

December 7, 2023

CICI-14
Creep Behavior of CFRP Wythe Connectors

Gregory Lucier, Ph.D. – Research Associate Professor, NCSU
Francisco De Caso, Ph.D. – Research Associate Professor, UM

Need and Industrial Relevance (Reminder)

- Precast concrete sandwich wall panels are common structural elements that can provide high levels of thermal and structural efficiency.
- Performance depends on an efficient wythe connection that joins two layers of concrete through a rigid insulating core.

Need and Industrial Relevance (Reminder)

Typical Shear Mechanisms:

– Steel truss connectors
  - Thermally inefficient

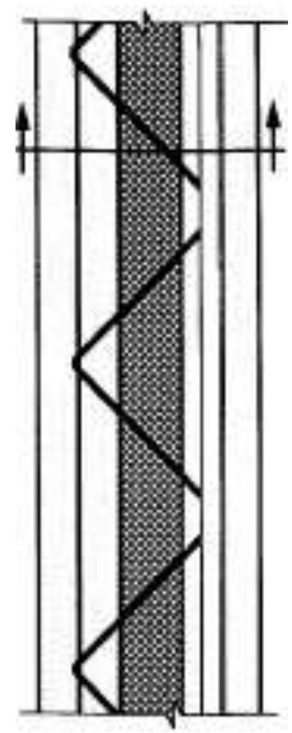

– Steel tie connectors
  - Thermally and structurally inefficient

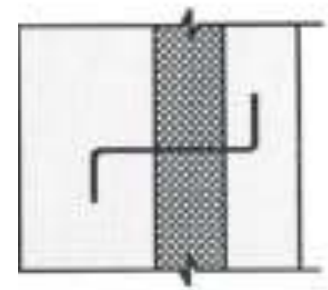

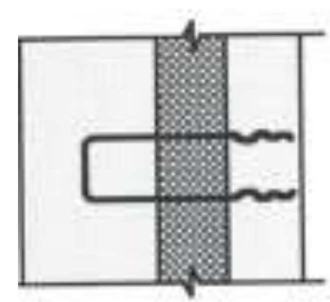

– Concrete solid zones
  - Thermally inefficient

Need and Industrial Relevance (Reminder)

CFRP Shear Grid

- Orthogonal CFRP Grid
- Cut at a 45-degees to develop a truss action
- Provides composite action
- Structurally and thermally efficient

Project Goals and Objectives (Reminder)

- Measure the creep performance of the CFRP grid connection using standard “push specimens” loaded for 1 year.
- Test loaded specimens to failure after 1 year of loading.
- Test control specimens to failure before and after the 1 year period.
- Determine the appropriate design values that should be considered to account for creep in service.

Work Progress to Date:

- Developed a testing matrix and test setup.
- Designed test specimens
- Fabricated specimens and prepared them for testing
- Designed test setup, procured components, and fabricated required parts and pieces
- Initial control samples tested
- Creep specimens underway (with long term controls sitting unloaded in the same environment)

Specimen Design:

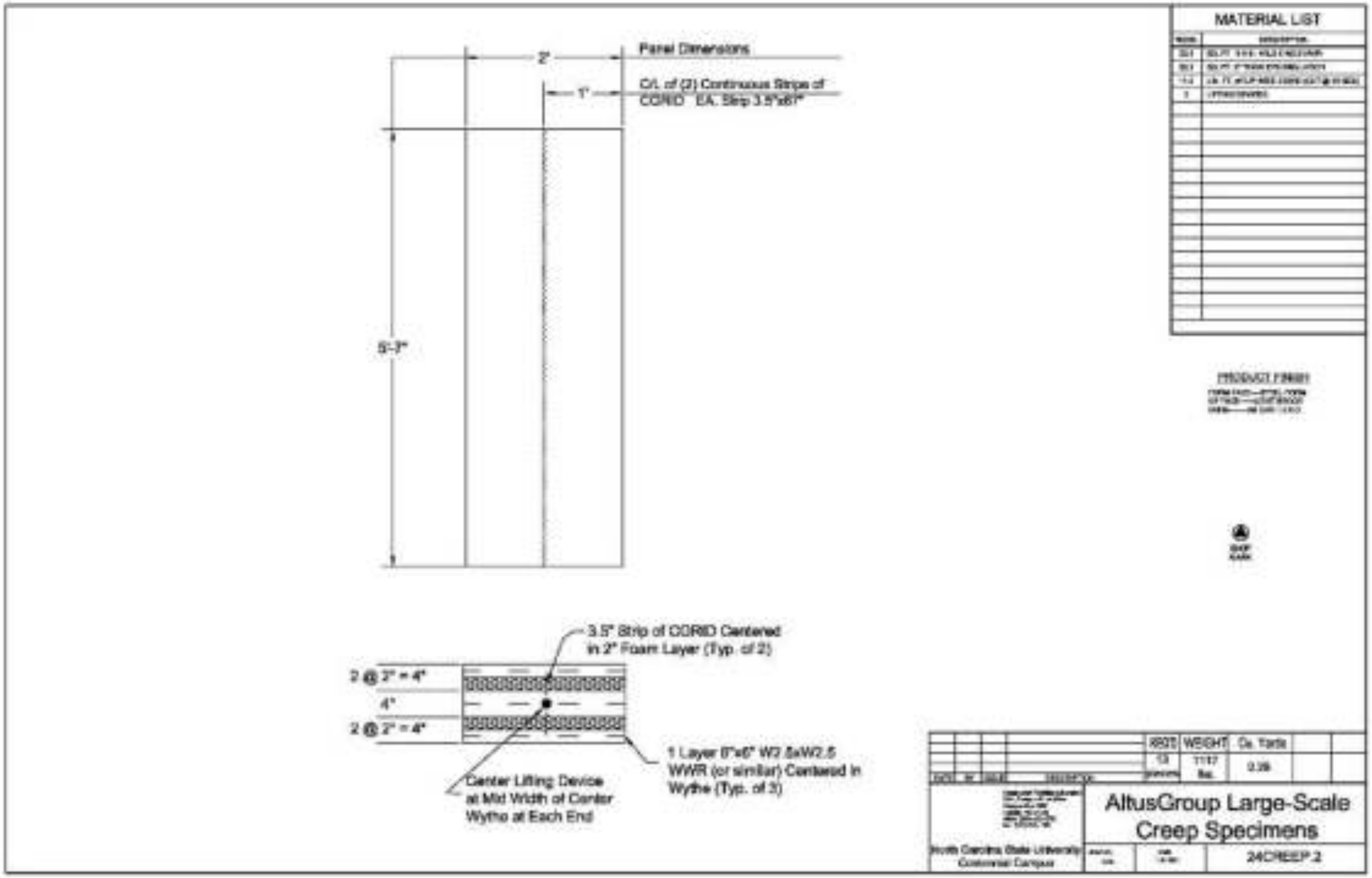

Control "Push Specimen" Tests:

60-ton Hydraulic Cylinder Loads Middle Wythe

Relative Wythe Slip Measured

2" Steel Bar, Supporting Outer Wythes

Creep Specimens Underway:

Creep Specimens Underway:

Walk Down Creep Specimen Aisle

Long Term Control Samples in Place:

Ongoing Work: Now with Data!!!

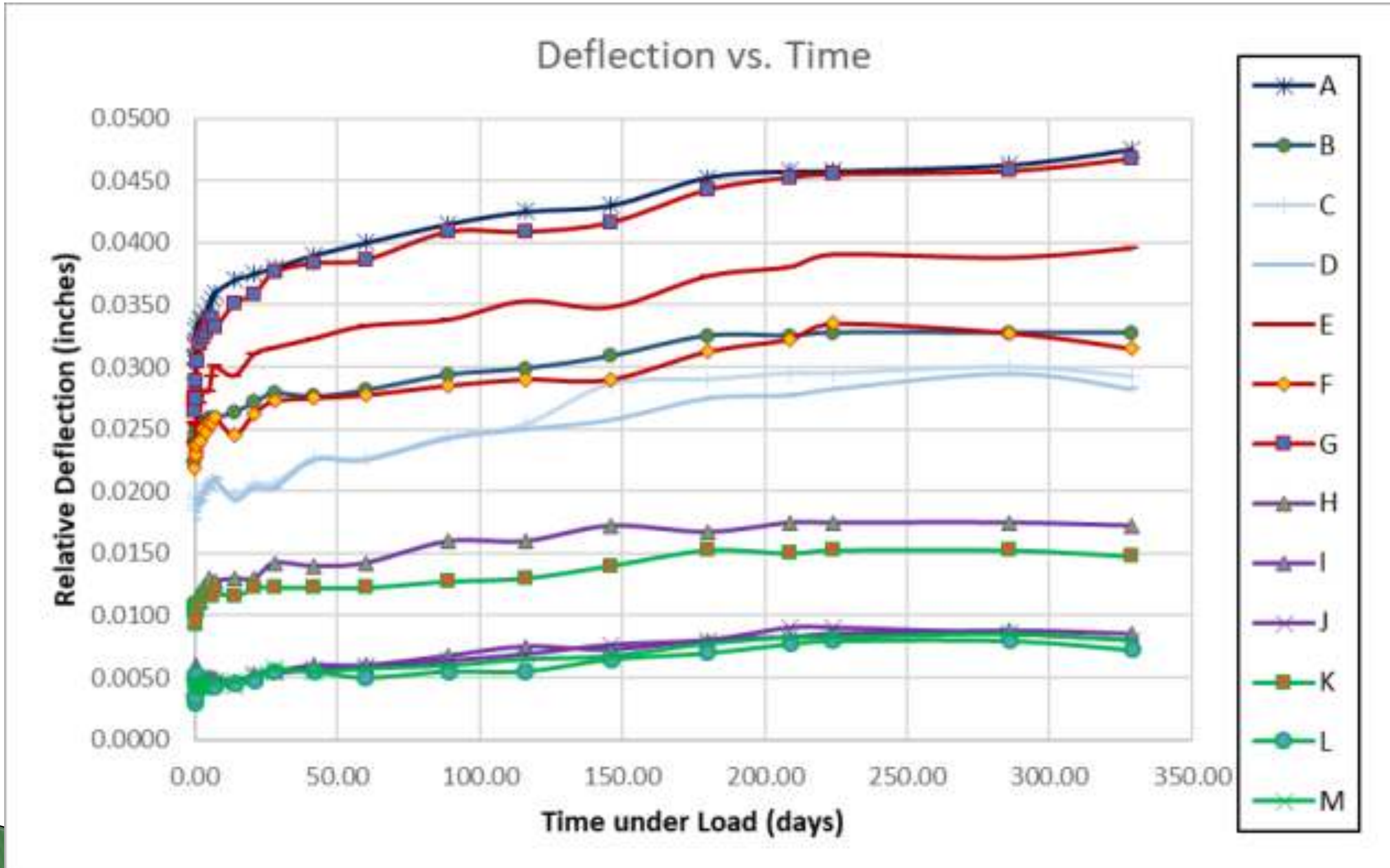

Ongoing Work:

- Continue loading panels in creep (6 more days).
- Final failure tests of all specimens after creep loading.
- The project will be wrapped up in Dec. 2023 (end of creep loading) and January 2024 (final push testing).

Thank you for your interest and questions

Project Name: Creep Behavior of CFRP Wythe Connectors

Project Number: CICI-14

Center for Integration of Composites into Infrastructure

Center for Integration of Composites into Infrastructure

Industrial Advisory Board (IAB) Meeting

December 7, 2023

CICI-15

Design and Assessment of Disturbed Regions Reinforced with FRP Bars

PI: Rudi Seracino

Co-PI: Giorgio Proestos

PhD Student: Taylor Brodbeck

Introduction

- **Deep Beams** are typically defined when the shear span-to-depth ratio is less than approximately 2.5
- This applies to many common elements in modern concrete infrastructure.
- In deep beams plane sections **do not** remain plane due to large shear stresses that develop in the "disturbed regions" resulting in a non-linear strain distribution through the depth.

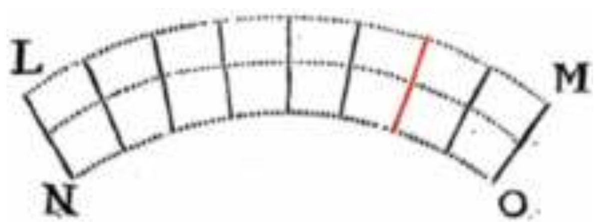

Robert Hooke's beam (1678)

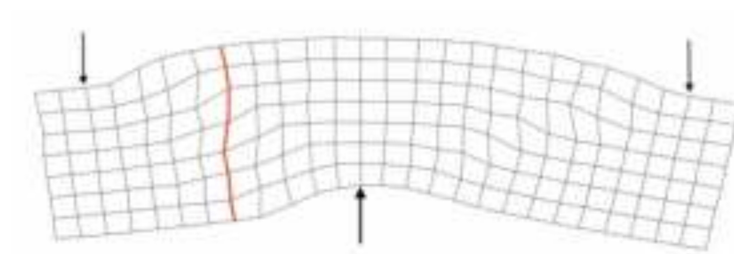

Experimental Data of a Deep Beam (x10 magnification)

Introduction

- Designing deep beams using standard sectional analysis techniques is overly conservative.
- Strut-and-tie methods provide a more realistic representation of the actual behavior of deep beams.

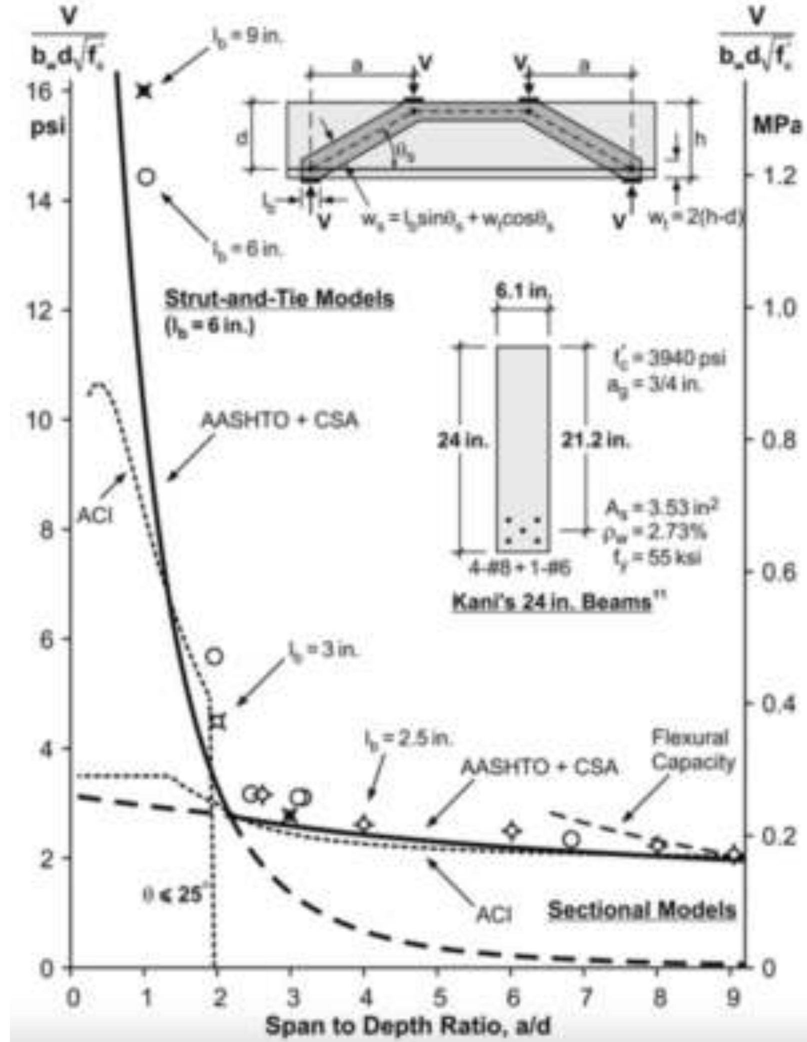

Introduction

- Strut-and-tie stress limits are empirical and based on tests of deep beams reinforced with steel bars.
- Little experimental data exists for deep beams reinforced with only FRP bars, and results are variable.

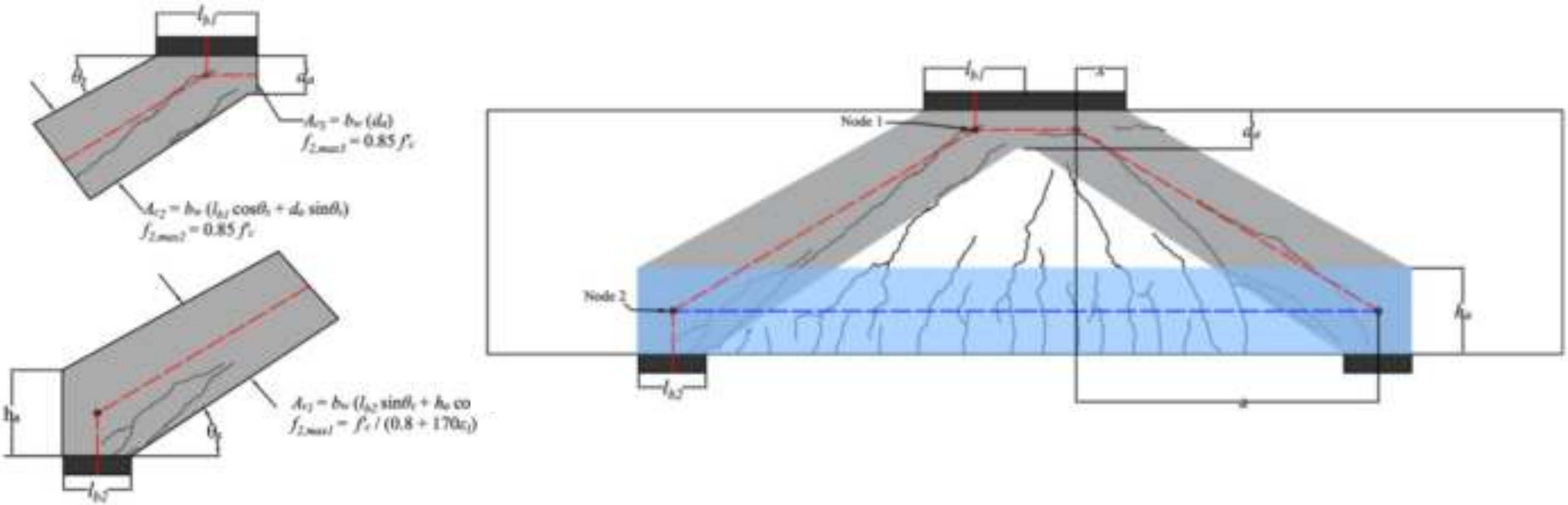

Comparison Between Strut-and-Tie and Published Experiments

- These beams had a/d ratios between 0.83 and 2.07 and longitudinal reinforcing ratios between 0.69 and 2.13%

- Using the factors directly from ACI 318 provides unconservative predictions of capacity for experiments published in the literature.

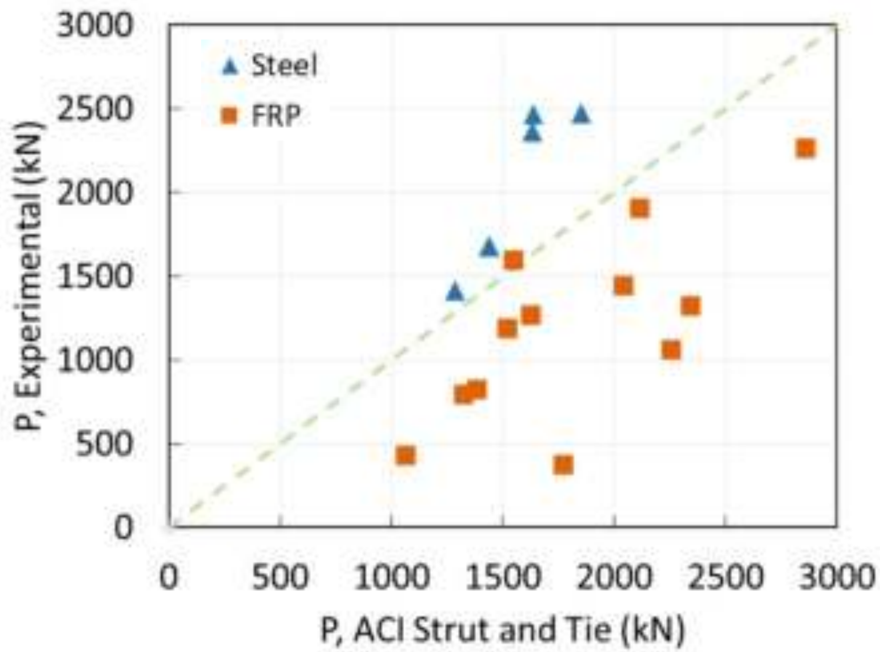

		ACI 318	CSA S806-12
Struts	Struts located in a tension zone	0.40	$\frac{1}{0.8 + 170\varepsilon_1}$
	Struts not located in a tension zone	0.75	0.85
Nodes	CCC node	1.00	0.85
	CCT node	0.80	0.75
	CTT node	0.60	0.65

Comparison Between Strut-and-Tie and Published Experiments

- These beams had a/d ratios between 0.83 and 2.07 and longitudinal reinforcing ratios between 0.69 and 2.13%

- Using the factors directly from ACI 318 provides unconservative predictions of capacity for experiments published in the literature.

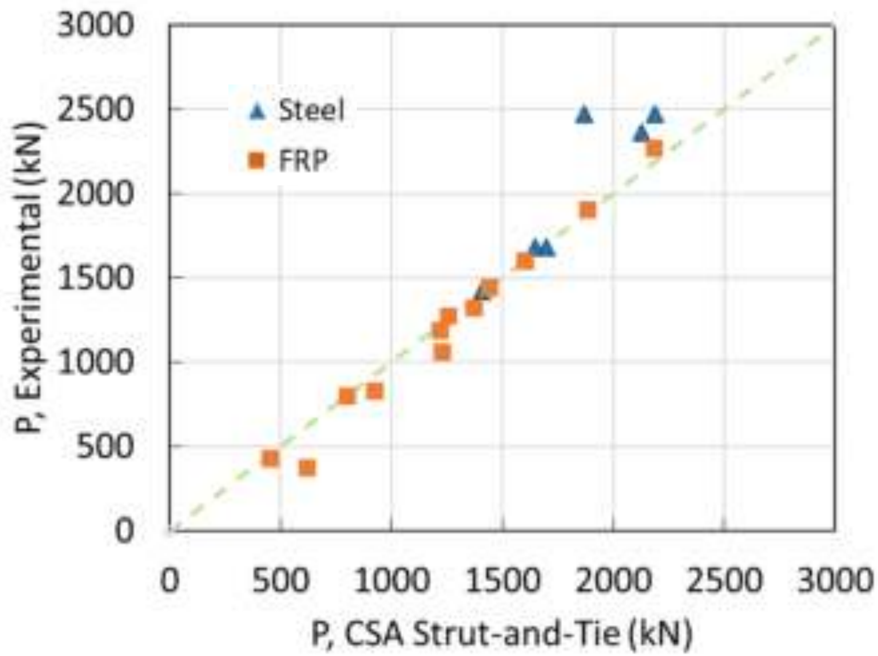

		ACI 318	CSA S806-12
Struts	Struts located in a tension zone	0.40	$\frac{1}{0.8 + 170\varepsilon_1}$
	Struts not located in a tension zone	0.75	0.85
Nodes	CCC node	1.00	0.85
	CCT node	0.80	0.75
	CTT node	0.60	0.65

Experimental Program

These beams were designed with an a/d ratio of 1.5 and longitudinal reinforcements of 0.4 and 0.8%.

b_w = 16 in. based on minimum stirrup width

Beam Name	Longitudinal Reinforcement	Transverse Reinforcement
FDB 1	6 No. 6	--
FDB 2	12 No. 6	--
FDB 3	6 No. 6	No. 4 @ 6 in.
FDB 4	12 No. 6	No. 4 @ 6 in.

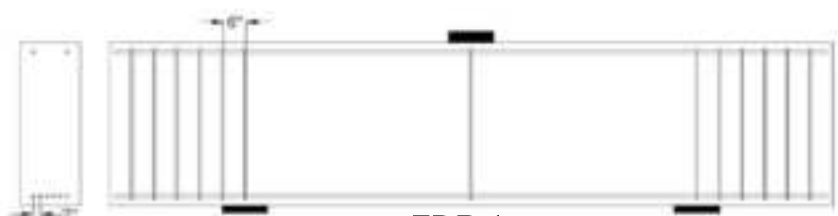

FDB 1

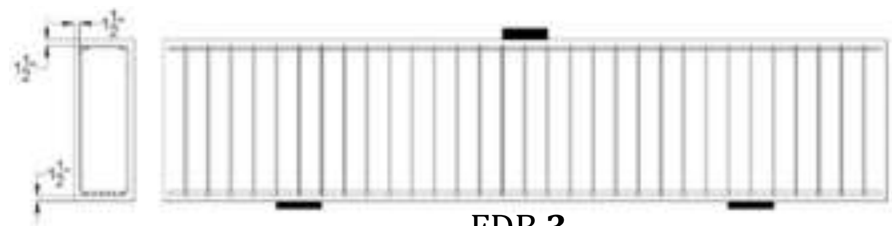

FDB **3**

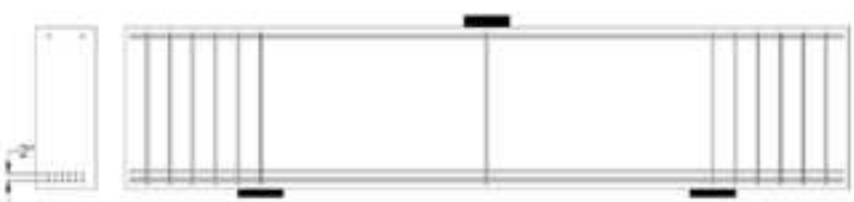

FDB 2

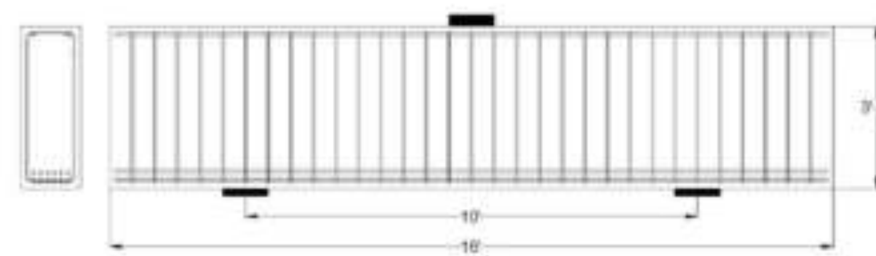

FDB 4

Experimental Program

Beam Name	Longitudinal Reinforcement	CSA Strut-and-Tie Prediction (kips)	ACI 318 Strut-and-Tie Prediction (kips)	VecTor2 Prediction (kips)
FDB 1	6 No. 6	180	367	175
FDB 2	12 No. 6	267	361	283
FDB 3	6 No. 6	180	367	175
FDB 4	12 No. 6	267	361	283

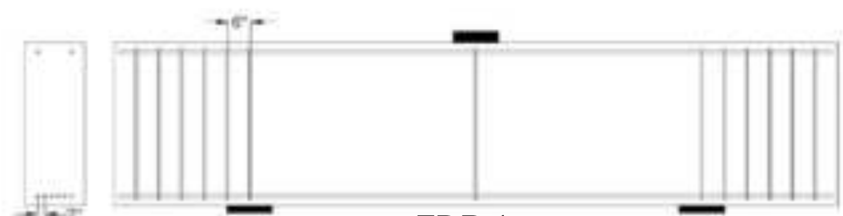

FDB 1

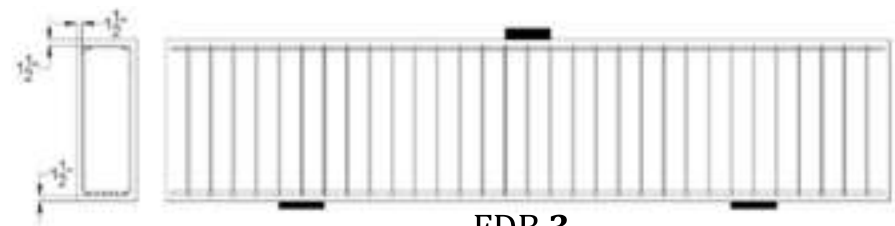

FDB **3**

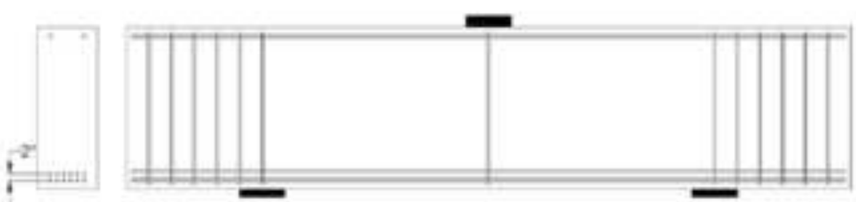

FDB 2

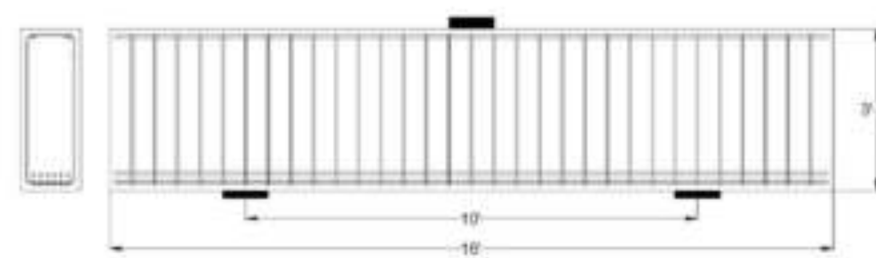

FDB 4

Experimental Set-up

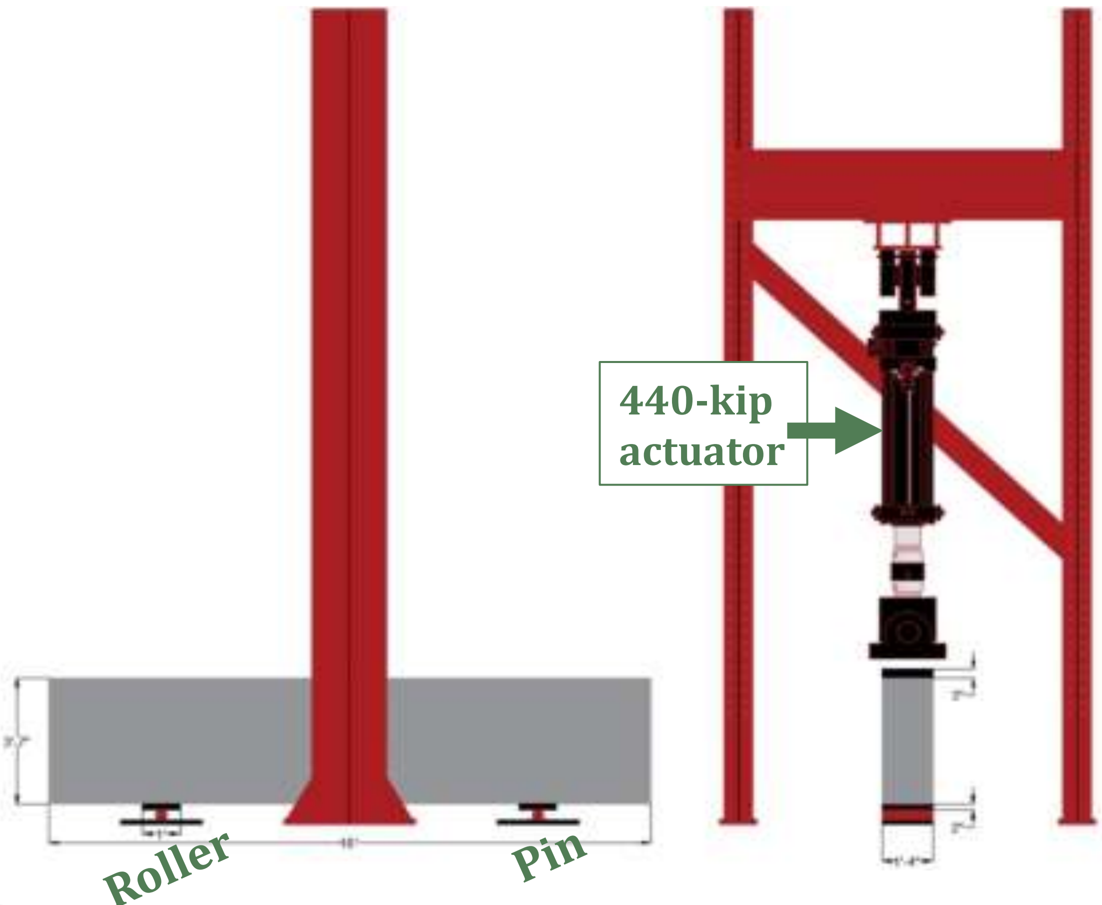

Preliminary Results

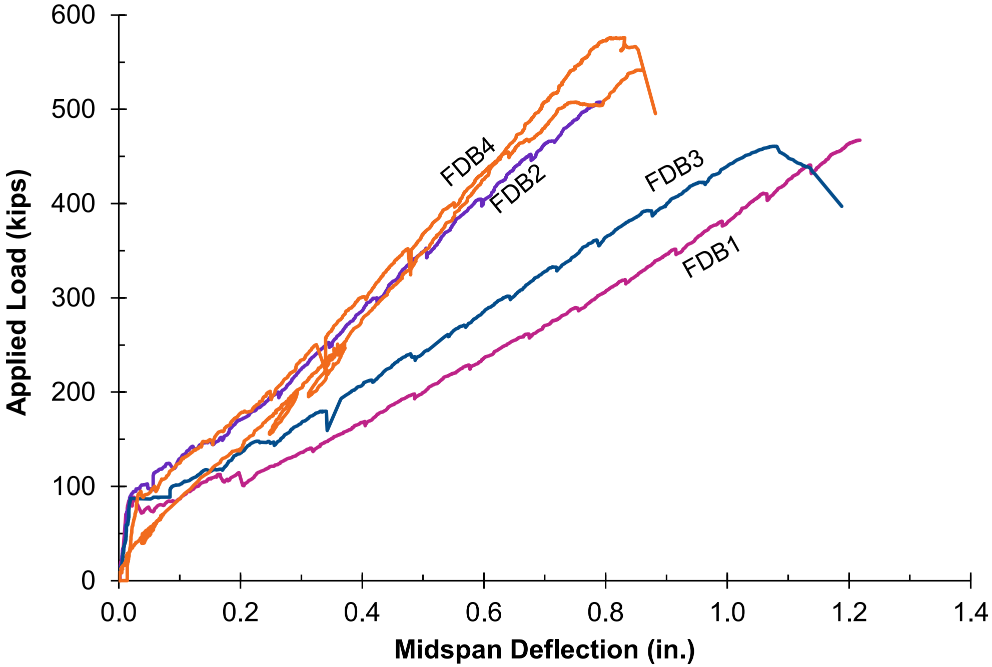

Beam Name	Longitudinal Reinforcement	Transverse Reinforcement
FDB 1	6 No. 6	--
FDB 2	12 No. 6	--
FDB 3	6 No. 6	No. 4 @ 6 in.
FDB 4	12 No. 6	No. 4 @ 6 in.

Beam Name	Peak Load (kips)	CSA T/P	ACI T/P	VT2 T/P
FDB 1	467	2.6	1.3	2.7
FDB 2	507	1.9	1.4	1.8
FDB 3	465	2.6	1.3	2.7
FDB 4	575	2.2	1.6	2.0

Beams at Failure



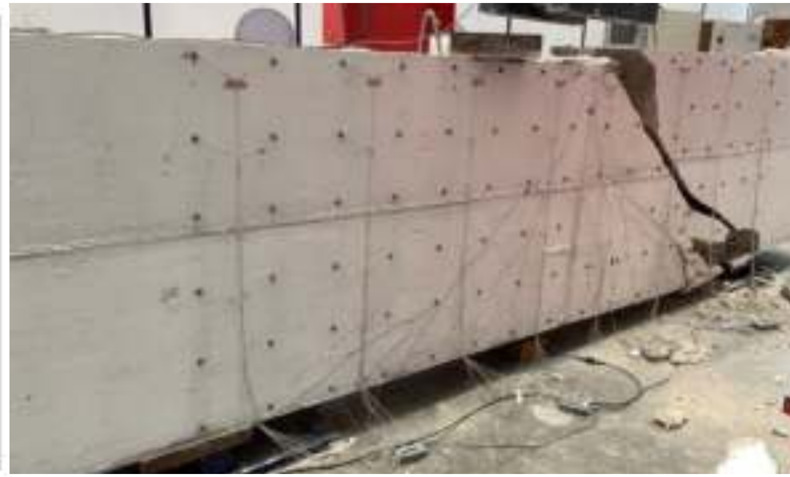




Failure Progression

These images show the moments immediately before and after the failure of FDB3.

DIC images were recorded at 2 Hz during the test and allow for detailed understanding of events throughout loading.

Just Before Peak Load

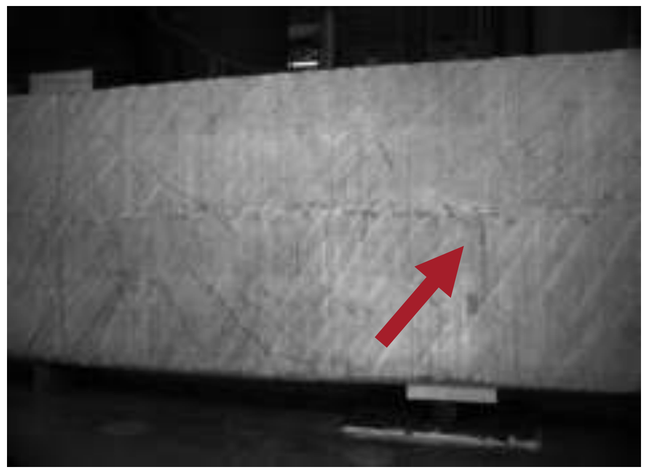

Peak Load
Formation of a new diagonal crack

Failure
Crushing of the top node and rupture of stirrups

For beams without stirrups, these events happened simultaneously

Impact of Bond on VecTor2

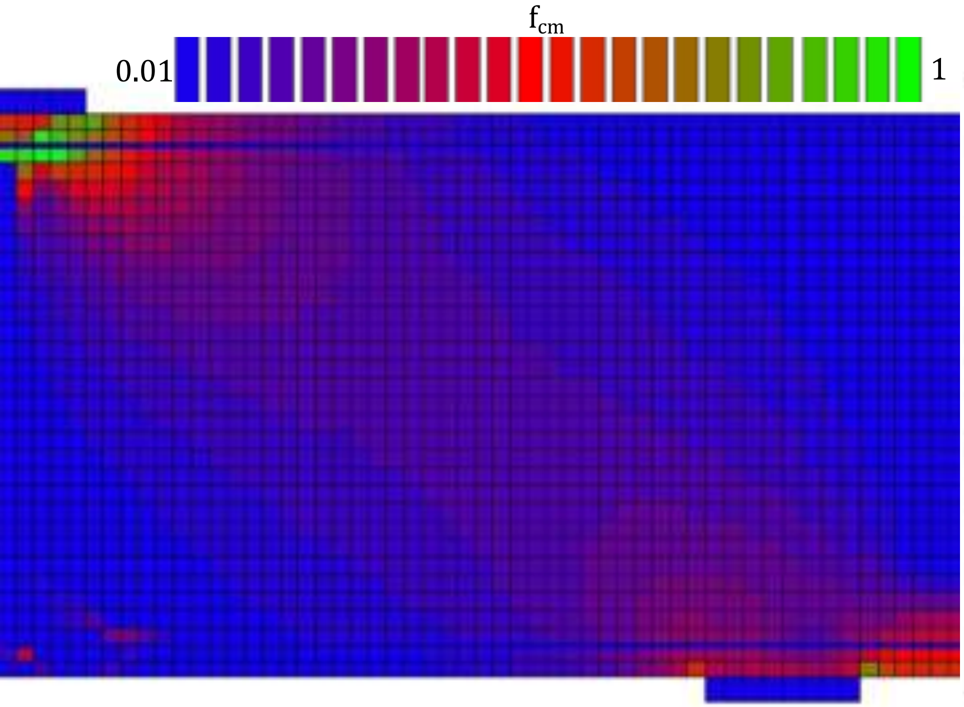

VecTor2 with bond model
400 kips
(previously ~175 kips)

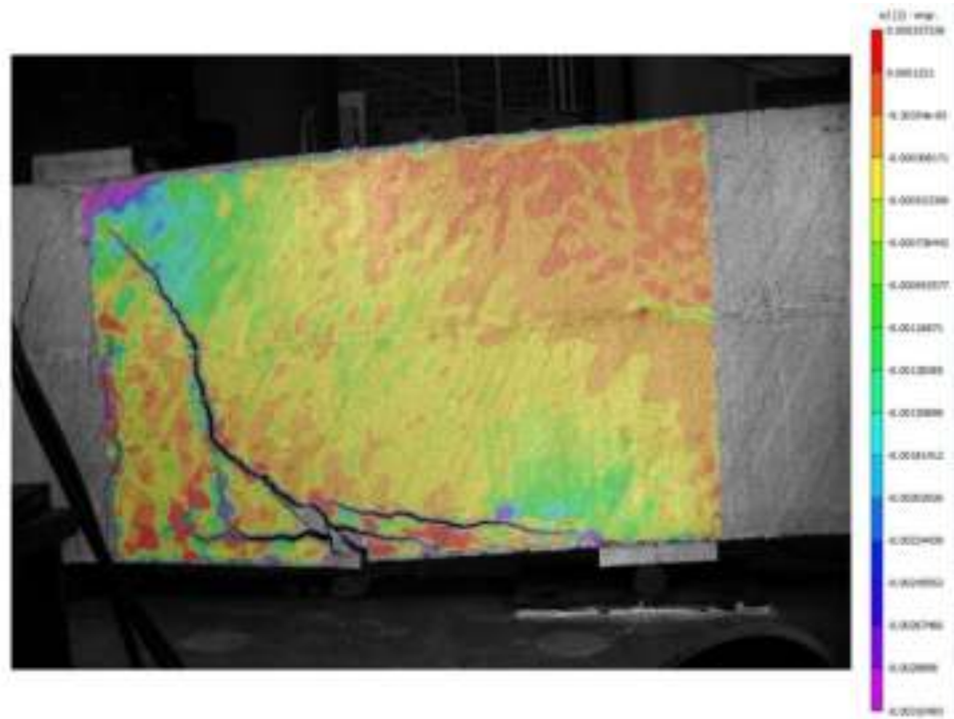

Experimental
467 kips

Impact of Bond on VecTor2

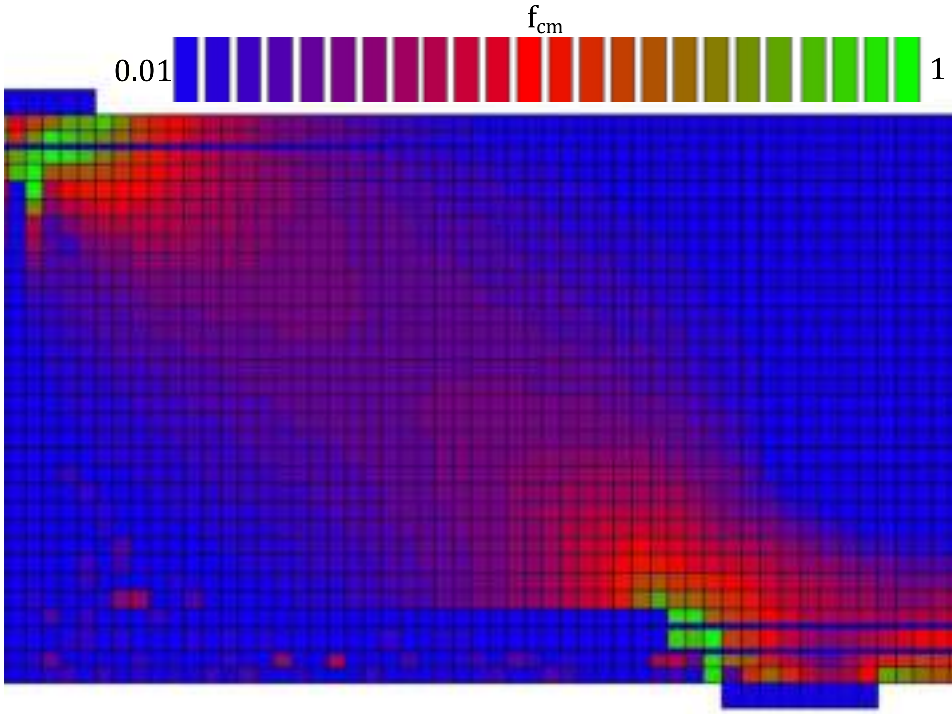

VecTor2 with bond model
450 kips
(previously ~283 kips)

Experimental
507 kips

Impact of Bond on Strut-and-Tie

In CSA S806, the compressive stress in the strut is limited to $\frac{f_c'}{0.8+170\varepsilon_1}$ and ε_1 is a function of the strain in the reinforcement.

Because of the splitting, the strains in the concrete are not the same as the strains in the reinforcement.

Using the ε_1 strains from DIC, the capacity of the strut is much larger.

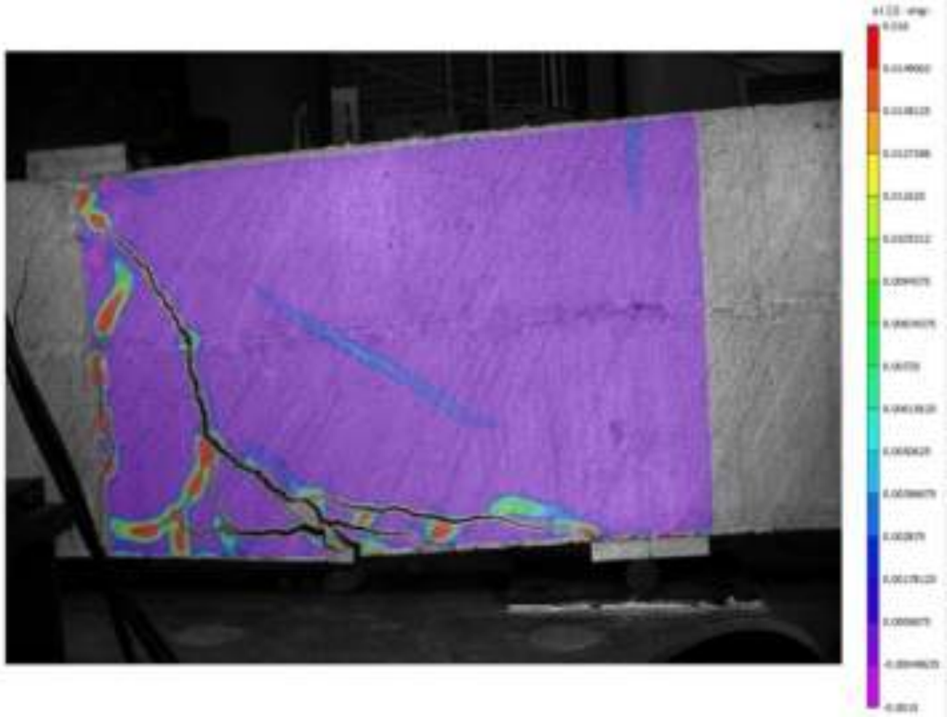

Future Work

Develop a second test series that:

- Explores the impact of bond, either with a different GFRP bar type or arrangement of bars
- Aims to exhibit different failure modes, leading to comprehensive design recommendations

Thank you for your interest and questions

Project Name: Design and Assessment of Disturbed Regions Reinforced with FRP bars

Project Number: CICI-15

Center for Integration of Composites into Infrastructure